

**For Reference**

---

**NOT TO BE TAKEN FROM THIS ROOM**

# For Reference

---

NOT TO BE TAKEN FROM THIS ROOM

Ex LIBRIS  
UNIVERSITATIS  
ALBERTAENSIS











Digitized by the Internet Archive  
in 2020 with funding from  
University of Alberta Libraries

<https://archive.org/details/Onions1969>



THE UNIVERSITY OF ALBERTA

GEOCHRONOLOGY OF THE BAMBLE SECTOR OF THE BALTIC SHIELD,  
SOUTH NORWAY.

by



ROBERT KEITH O'NIONS B.Sc.

A THESIS

SUBMITTED TO THE FACULTY OF GRADUATE STUDIES

IN PARTIAL FULFILLMENT OF THE REQUIREMENTS FOR THE DEGREE OF

DOCTOR OF PHILOSOPHY

DEPARTMENT OF GEOLOGY

EDMONTON, ALBERTA

FALL, 1969



UNIVERSITY OF ALBERTA  
FACULTY OF GRADUATE STUDIES

The undersigned certify that they have read, and recommend to the Faculty of Graduate Studies for acceptance, a thesis entitled "Geochronology of the Bamble Sector of the Baltic Shield, South Norway" submitted by Robert Keith O'Nions BSc. in partial fulfilment of the requirements for the degree of Doctor of Philosophy.





## ABSTRACT

K-Ar, U-Th-Pb and Rb-Sr methods of radiometric dating have been applied to a comparatively small part of the Bamble-sector of the Baltic Shield, in South Norway.

Apparent K-Ar ages of micas range from 1114 m.y. to 975 m.y. and have been interpreted in terms of a slow cooling history, whereby amphibole compositions near the pargasite end-member and coarse-grained biotites retained radiogenic argon from near the thermal maximum of the metamorphic episode. Other more Fe-rich amphibole compositions near the ferropargasite end-member and medium grained biotites did not quantitatively begin to retain radiogenic argon until considerably lower temperatures (approximately 250°C). The high apparent diffusion coefficients in Fe-rich amphiboles is thought to result from their ability to equilibrate with the ambient fluid composition to lower temperatures than Mg-rich amphiboles.

Zircons extracted from the Levang gneiss dome have undergone a polycyclic history. Some of these zircons appear to have, in part, recrystallised during the Sveconorwegian metamorphic episode and isotopically 'reset', whereas others show apparent U-Pb ages intermediate between the time of formation of the Levang gneiss dome as derived from whole rock Rb-Sr dating (1673 $\pm$ 24 m.y.) and the time of the Sveconorwegian metamorphic episode. This apparent enigma possibly results from superimposed periods of daughter loss and isotopically younger metamorphic and/or authigenic overgrowths on the zircons. A number of sphenes analysed from the Levang gneiss dome and various pegmatites within the area are much more concordant than the zircons and provide an independent estimate of the time of the metamorphic maximum of the Sveconorwegian metamorphic episode.

A Rb-Sr whole rock study of the banded Hovdefjell paragneisses



indicates that Sr isotopic homogenization occurred on the scale of only centimeters during the Sveconorwegian metamorphic episode. Rb-Sr whole rock results of the gabbros and metagabbros suggests that there may have been a post-intrusion alkali metasomatism in the neighbourhood of the Ødegaarden and Bjordammen gabbros. The time of this event may be estimated at 1030 m.y. based upon apparent K-Ar ages of amphiboles.

The folding and metamorphic episodes associated with the Sveconorwegian episode appear to have occurred in a time interval of less than 90 m.y. on the basis of U-Th-Pb dating. The thermal metamorphic maximum at approximately 1150 m.y. involved the reactivation of the Levang gneiss dome, which was formed during the Svecofennian orogeny. By approximately 975 m.y. sufficient uplift had occurred for the area to cool to the order of 200 to 250°C.



## ACKNOWLEDGEMENTS

The writer is particularly indebted to his research advisor Dr. R. D. Morton, who initially suggested the project and introduced him to the field area. His advice concerning the project is gratefully appreciated. Dr. H. Baadsgaard introduced the author to the techniques of isotope dilution analysis and his assistance in the laboratory has been invaluable. The writer was guided in the techniques of electron probe analysis by Dr. D.G.W. Smith and has benefitted greatly from numerous discussions with him.

Also discussions with faculty and graduate student members of the Geochemistry - Isotope - Petrology Seminars group have been of considerable benefit to the author.

Mass spectrometry facilities in the Department of Physics were kindly provided by Dr. G.L. Cumming and maintenance was carried out by Mr. H. Langer. Mr. A. Stelmach was of assistance in the chemical laboratory. Mrs. E. Vincze made most of the thin sections, and Mr. D. Tomlinson assisted with the electron probe analyses.

The writer is grateful to Dr. D.C. Green who collected additional specimens on the authors behalf in 1968 and to the Boreal Institute, of the University of Alberta for a grant to defray the field expenses. Financial assistance has been provided by Graduate Teaching Assistantships and a Postgraduate Scholarship from the National Research Council (1967-69). A grant from Norges Almenvitenskapelige Forskningsråd helped defray field expenses in the summer of 1966.

Acknowledgements are due to Mr. F. Dimitrov for his drafting services and Mrs. P. Lamothe, Miss J. Conklin and my wife for typing the various drafts of this thesis. Mr. B. W. Robinson kindly read and commented upon the first draft of this thesis.

Finally the writer would like to express his thanks to Fru Ingeborg





Ødegaarden and family for their hospitality during the field seasons of 1965 and 1966.



TABLE OF CONTENTS.

	Page
ABSTRACT .....	i
ACKNOWLEDGEMENTS .....	ii
<u>CHAPTER I.</u> INTRODUCTION .....	1
Geographical setting .....	1
Geological setting .....	3
Previous geochronology .....	5
Fundamentals of radiometric dating .....	6
<u>CHAPTER II.</u> GEOLOGY .....	7
Regional geological and tectonic setting .....	7
History of research in Bamble .....	9
Metasedimentary and metavolcanic rocks .....	10
Metamorphic facies .....	12
The gabbro - norite suite .....	17
Gabbros and norites .....	17
Albitite and apatite veins .....	20
The Levang gneiss dome .....	24
The Cataclastite belt .....	26
Pegmatites .....	27
Metalliferous ore deposits .....	29
The Oslo Graben .....	30
<u>CHAPTER III.</u> POTASSIUM-ARGON DATING .....	33
Analytical methods and errors .....	34
Argon diffusion in micas and amphiboles .....	36
Mica apparent ages .....	40
Amphibole apparent ages .....	47



<u>CHAPTER IV. CRYSTAL CHEMISTRY AND ARGON RETENTIVITY OF CALCIC AMPHIBOLES</u>	51
Introduction .....	51
Electron microprobe analyses .....	51
X-ray study .....	54
Crystal chemistry of calcic amphiboles .....	55
1. Crystal chemistry of dated amphiboles .....	61
2. Unit - cell parameter variation .....	67
Amphibole crystal chemistry and K-Ar apparent age .....	74
Summary .....	81
<u>CHAPTER V. URANIUM-THORIUM-LEAD DATING</u>	82
Introduction .....	82
Analytical techniques .....	83
Diffusion processes in uranium-lead systems .....	87
Results of zircon and sphene dating .....	94
1. Levang gneiss dome .....	98
2. Pegmatites .....	101
3. Th-Pb results .....	104
Electron probe investigation of Ødegaarden pegmatite zircon .....	107
Multiphase U-Th-Pb systems .....	109
Mechanisms of lead loss from zircons .....	112
<u>CHAPTER VI. RUBIDIUM-STRONTIUM DATING</u>	117
Introduction .....	117
Analytical techniques .....	118
Systematics of the whole rock isochron method .....	120
Levang gneiss dome .....	123
The Hovdefjell banded paragneiss .....	126
The gabbros and metagabbros .....	133





<u>CHAPTER VII.</u>	TECTONIC HISTORY OF THE BAMBLE AREA .....	137
	Provenance of Bamble metasediments .....	138
	Emplacement of gabbroic and associated rocks .....	139
	Development of the Levang gneiss dome .....	140
	Formation of metamorphic pegmatites .....	142
	The duration of the Sveconorwegian orogenic cycle .....	142
	Thermal history .....	143
	Evolution of the Oslo Graben .....	144
	Summary .....	145
<u>CHAPTER VIII.</u>	COMPARISON WITH OTHER AREAS .....	146
	Introduction .....	146
	Comparisons with Europe and Greenland .....	148
	Comparisons with the Grenville Province .....	150
SUMMARY AND CONCLUSIONS	.....	152
APPENDIX A.	DESCRIPTION AND LOCATION OF ANALYSED SPECIMENS .....	A-1
APPENDIX B.	CHEMICAL PROCEDURES FOR K, RB, SR AND PB .....	A-17
	Potassium .....	A-17
	Rubidium .....	A-18
	Strontium .....	A-18
	Lead .....	A-19
APPENDIX C.	CHEMICAL PROCEDURES FOR URANIUM AND THORIUM .....	A-22
APPENDIX D.	AMPHIBOLE X-RAY DATA .....	A-28
APPENDIX E.	COMPUTATIONS .....	A-44
	Potassium-argon .....	A-44
	Uranium-thorium-lead .....	A-45
	Rubidium-strontium .....	A-49



Monoclinic lattice parameters .....	A-53
Correction of microprobe data .....	A-54
Structural formulae .....	A-58



LIST OF FIGURES.

Figure 1:	Location map of the Bamble-sector of the Baltic Shield .....	2
Figure 2:	Geological sketch map of the Bamble-Risør area .....	4
Figure 3:	Zonal geochronological subdivisions of the Baltic Shield .....	8
Figure 4:	ACF and AKF diagrams .....	14
Figure 5:	Relationships between the stability fields of muscovite, the alumino-silicates, etc. ....	16
Figure 6:	Sketch of relationship of the apatite veins .....	22
Figure 7:	Gabbroic immiscibility .....	24
Figure 8:	Structure and mineral occurrences in Bamble .....	31
Figure 9:	K-Ar ages of micas .....	46
Figure 10:	K-Ar ages of amphiboles .....	48
Figure 11:	Crystal chemistry of the amphiboles .....	59
Figure 12:	Major element variation in amphiboles .....	62
Figure 13:	Plot of $Ti + (Na + K)$ versus $Al^{VI}$ .....	66
Figure 14:	Plot of mean $M_2$ cation radius (disordered) versus 'b' .....	69
Figure 15:	Plot of mean $M_2$ cation radius (ordered) versus 'b' .....	70
Figure 16:	Idealized deviations from linearity due to order-disorder .....	71
Figure 17:	Corrected 'b' versus mean $M_2$ cation radius .....	72
Figure 18:	$a.\sin$ versus mean cation radius of $M_2$ (disordered) .....	73
Figure 19:	$100(Mg^{2+} + Fe^{3+} + Al^{VI}) / (Mg^{2+} + Al^{VI} + Fe^{3+} + Fe^{2+})$ versus apparent K-Ar age of amphiboles .....	77
Figure 20:	Mean $M_2$ cation radius of (ordered and disordered) versus apparent K-Ar age .....	78
Figure 21:	Comparison of diffusion trajectories .....	92
Figure 22:	Comparison of pure Pb and pure U diffusion .....	93





Figure 23:	U-Pb data for the Levang gneiss dome .....	102
Figure 24:	U-Pb data for the pegmatites .....	103
Figure 25:	U-Th-Pb data .....	105
Figure 26:	Episodic parent and daughter loss in the U-Th-Pb system .....	111
Figure 27:	Plot of 'f' versus $U + eqTh$ .....	112a
Figure 28:	Plot of 'K' versus 'F' .....	112b
Figure 29:	Whole rock isochron for the Levang gneiss dome .....	125
Figure 30:	Sketch map of the Hovdefjell paragneiss .....	128
Figure 31:	Hovdefjell banded gneiss whole rocks .....	129
Figure 32:	Development of Rb and Sr in the Hovdefjell banded gneiss .....	131
Figure 33:	Whole rock isochron plot of the gabbros .....	135
Figure 34:	Column calibration for U, Th, Ce, and Ti .....	A-24
Figure 35:	Column calibration for zircon .....	A-25
Figure 36:	Stripping efficiency of $0.5M HNO_3$ .....	A-26
Figure 37:	Tectonic history of the Bamble-sector of the Shield .....	154.



LIST OF TABLES.

TABLE 1:	Apparent K-Ar ages of metasediments and metavolcanics .....	41-42
TABLE 2.	Apparent K-Ar ages of granites, gabbros and pegmatites .....	43-44
TABLE 3:	Analyses and structural formulae of amphiboles .....	53
TABLE 4:	Gravimetric and electron probe analyses of potassium .....	56
TABLE 5:	Unit cell parameters .....	57
TABLE 6:	Correlation coefficients of elements in amphiboles .....	65
TABLE 7:	Analysis of Equal Atom Lead and Broken Hill Lead .....	86
TABLE 8:	U-Th-Pb analytical data .....	95
TABLE 9:	U-Th-Pb apparent ages .....	96-97
TABLE 10:	Rb-Sr analytical data for the Levang gneiss dome .....	124
TABLE 11:	Rb-Sr analytical data for the Hovdefjell gneisses .....	127
TABLE 12:	Rb-Sr analytical data for the gabbros and metagabbros .....	134



LIST OF PLATES.

Plate 1. Opposite page 99

Plate 2. Opposite page 108

Plate 3. Opposite page 108



## CHAPTER I - INTRODUCTION

Radiometric dating may potentially yield important fundamental information concerning the nature, duration and extent of regional metamorphic episodes. All too often, however, methods of radiometric dating have been applied in insufficient detail to areas where extensive geological mapping and petrological investigations have already been carried out, or otherwise, only as reconnaissance tools in areas which are little understood geologically; very often precluding information of the above nature.

The Bamble sector of the Baltic Shield has been studied in considerable detail by a number of investigators and thus provides a sound cartographic and petrological basis to study certain temporal aspects of regional metamorphism and orogenesis using radiometric dating methods.

The author was introduced to the field-area by R.D. Morton in 1965 and samples for radiometric dating were collected by the author and R. D. Morton during the summer of 1966. Further samples were collected on the author's behalf by D.C. Green in the summer of 1968.

This thesis essentially embodies the results and interpretation of whole-rock Rb/Sr dating and K-Ar and U-Th-Pb dating of selected minerals from within the area. Certain aspects of the work have some bearing on the fundamental behaviour of the parent-daughter systems, under regional metamorphic conditions.

### Geographical Setting

The Bamble sector of the Baltic Shield is located within the Skagerrak coastal region of South Norway, southwest of Oslo (Fig 1). A representative but comparatively small part of the area designated the





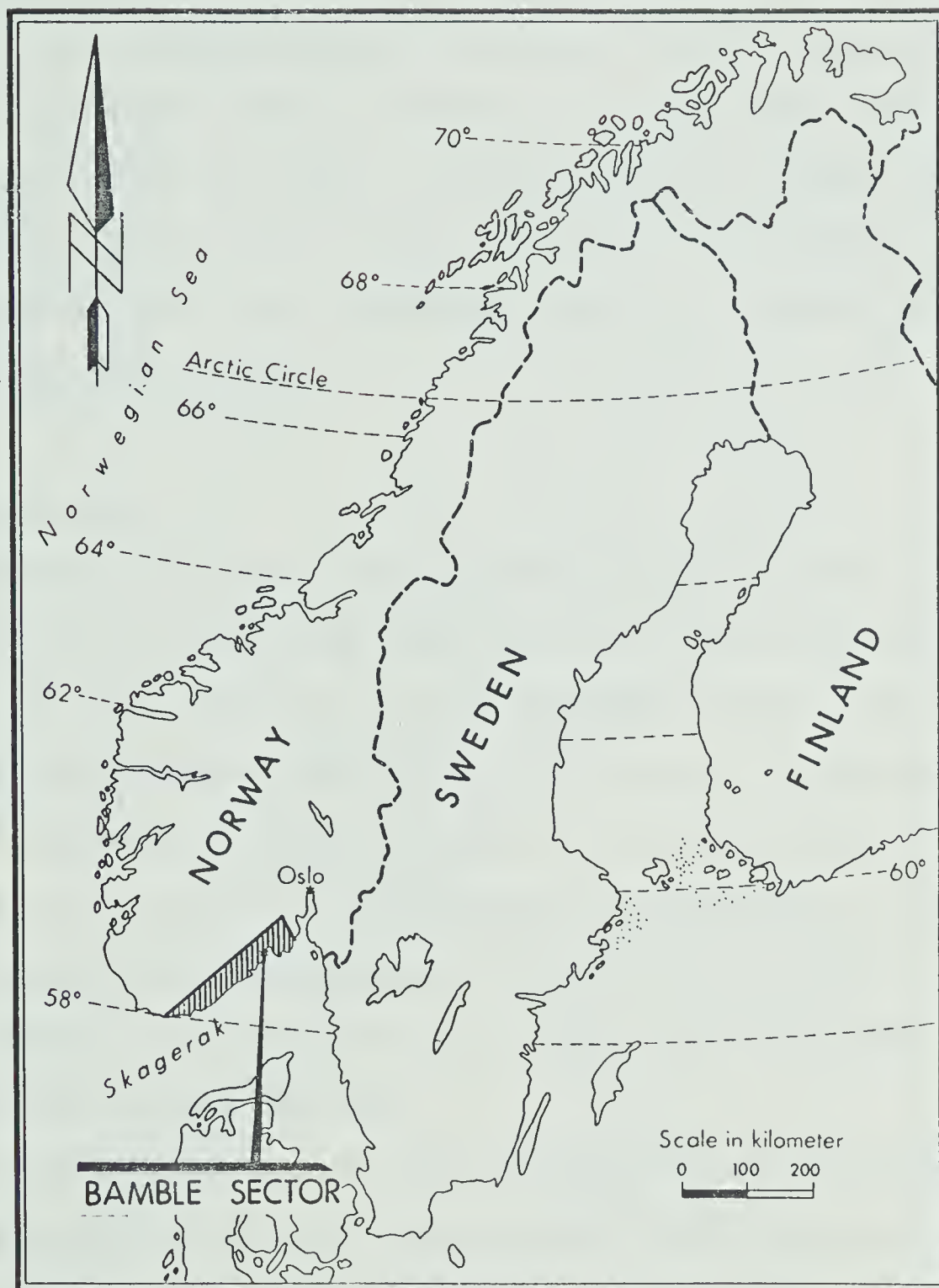


Fig.1. Location map of the Bamble-sector of the Baltic Shield.



Bamble sector has been studied (Fig 2); this extends approximately from Ødegaarden southwest to Risør. Topographically the area is a low, undulating, highly dissected plateau attaining a maximum elevation of around 200m above sea-level in the northern portion of the area. Detailed mapping is somewhat hampered by the rugged nature of the region and heavy forest cover, except in the arable and pastoral areas of the valley bottoms. Sample collecting for geochronological purposes, however, is greatly facilitated by recent road excavations, which have necessitated blasting to considerable depths below the weathered surface.

### Geological Setting

Sufficient radiometric age determinations have now been carried out to make an approximate zonal subdivision of the Baltic Shield possible (KRATZ et al. 1968, O'NIONS et al. 1969 and BURWASH, 1969). This subdivision recognises a Svecofennian zone (2300 m.y. to 1650 m.y.) corresponding to the Svecofennides of the central and western part of the Shield, a Saamokarelian zone (3600 m.y. to 1900 m.y.) corresponding to the Karelides in the eastern part of the Shield and a Sveconorwegian zone (1200 m.y. to 900 m.y.) in the southern part of the Shield consisting of the so called Pregothian, Gothian, Dalslandian and Telemark complexes.

The Bamble sector of the Baltic Shield is separated from the 'Telemark complex' proper by a major fault-zone extending from Porsgrunn to Kristiansand, referred to as the 'Great Friction Breccia' by BUGGE (1928). Following MORTON et al. (1969) this fault will be referred to as the Porsgrunn-Kristiansand fault in further mention. KRATZ et al. (1968) have not distinguished between the Telemark area proper to the north of the fault and the Bamble region, but it is felt that the Telemark complex may in part be around 1450 m.y. old and



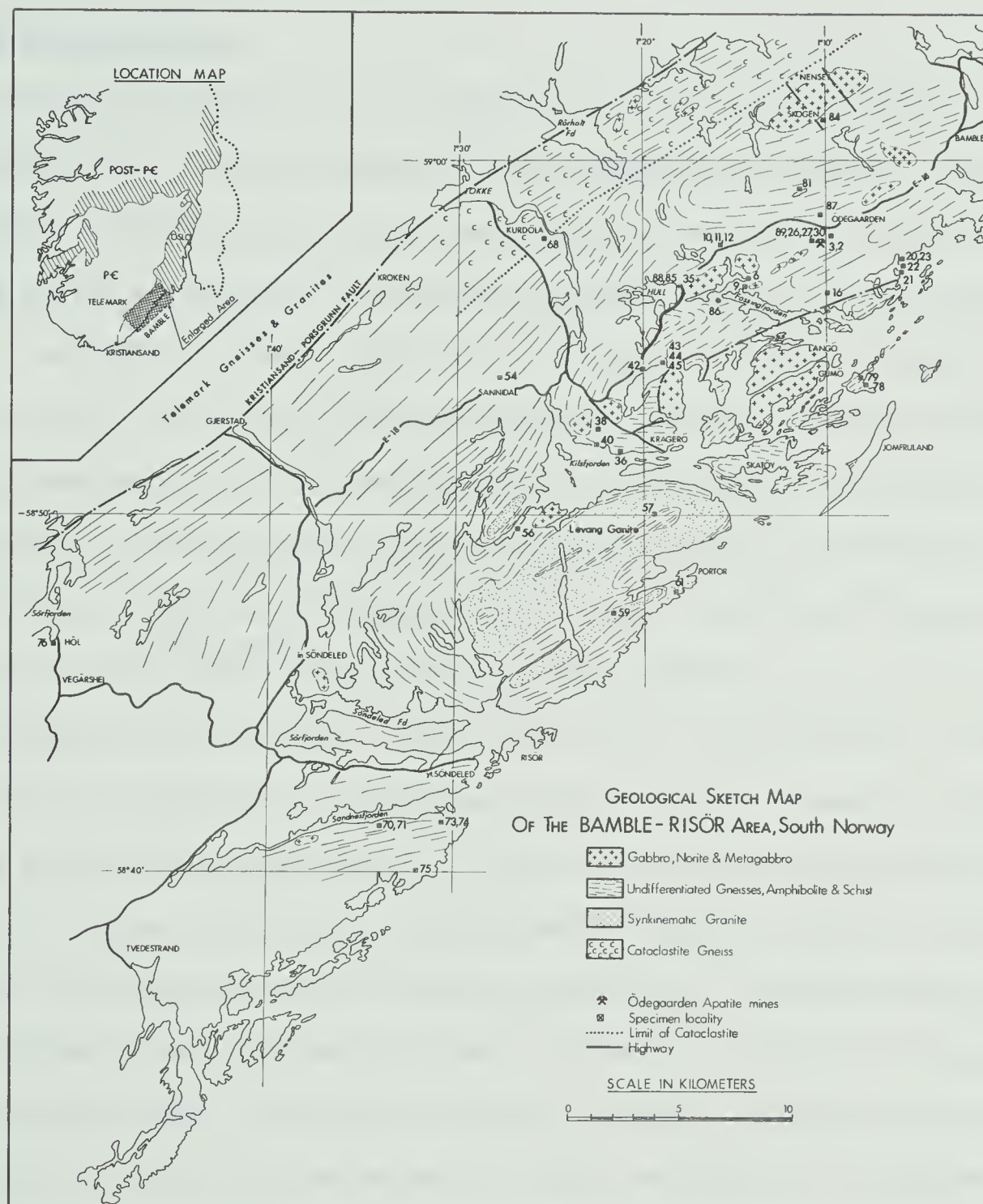


Fig. 2. Geological sketch map of the Bamble - Risør area.





may ultimately be correlated with the Elsonian of the Canadian Shield. To the east the Precambrian complex is overlain by sediments from Cambrian to Silurian in age.

### Previous Geochronology

Previous radiometric age determinations from South Norway published by NEUMANN (1960), KULP and NEUMANN (1961), POLKANOV and GERLING (1961) and BROCH (1964) have been principally concerned with apparent K-Ar ages of micas and have served to indicate a metamorphic episode which occurred between 1100 m.y. and 900 m.y. ago. Within the confines of the area forming the subject of this thesis, only one previous K-Ar apparent age and one Th-U-Pb age have been reported. KULP and NEUMANN (op.cit.) obtained an apparent age of 1080 m.y. for phlogopite from a productive vein at the Ødegaarden apatite mines and KULP and ECKLEMANN (1957) report a  $\text{Pb}^{207}/\text{Pb}^{206}$  age of 940 m.y. and a  $\text{Th}^{232}/\text{Pb}^{208}$  age of 980 m.y. for a euxinite sample from the Kalstad pegmatite near Kragerø. BROCH (loc. cit.) has summarized all age determinations carried out on Norwegian rocks up to 1964, however it should be noted that the K-Ar ages reported by Broch from the Leningrad laboratories are 5% to 6% higher than ages calculated using presently accepted decay constants and therefore are not directly comparable. Age determinations on lithologies between Arendal and Risør, southwest of the area forming the subject of this thesis, range from 1345 m.y. to 828 m.y. with a pronounced, but as will be pointed out subsequently, quite meaningless, histogrammic maximum at 900 m.y. This maximum has been termed the 'Sveconorwegian regeneration period' by Magnusson (1960).

Recently MICHOT and PASTEELS (1968) have published preliminary results of what is intended to be an extensive geochronological study of the southernmost Norwegian metamorphic basement. Their present data suggests a





metamorphism between 1000-1050 m.y. and a late-kinematic intrusion of mangerites at approximately 950 m.y.

### Fundamentals of Radiometric Dating

In view of the increasing number of geologists involved in some way with radiometric dating, it is not felt necessary to review the fundamentals of this subject. Rather, reference is made to recent comprehensive texts on the subject by BAADSGAARD (1965), HAMILTON (1966) and HAMILTON and FARQUHAR (1968) and SCHAEFFER and ZHRINGER (1966). However, the reader is reminded of one of the fundamental requirements for dating, "No gain or loss of either parent nuclide or daughter should occur after the phase (to be dated) has once formed a closed system." The importance of the recognition and evaluation of departures from closed system behaviour cannot be overemphasized, since such departures may in certain instances yield very useful ancillary information.



## CHAPTER II - GEOLOGY

Regional Geological and Tectonic Setting

The Baltic Shield, like the Canadian Shield, has been geochronologically subdivided into a number of zones or provinces on the basis of dating programs carried out by various laboratories (Fig 3). Although based in part upon very scanty information, it does serve to illustrate the currently recognizable broad divisions.

Subsequent to the work of BRÖGGER (1900) the term Bamble 'formation' has been applied to the Precambrian rocks of the Skagerrak coastal area of S. Norway between Langesund and Kristiansand. MORTON et al. (1969) propose that the erroneous usage of the term 'formation', in this context, should be discontinued and the preferable terminology of Bamble-sector is suggested. The Bamble-sector was regarded by BUGGE (1928, 1936) to be bounded to the north by a major NE-SW fault extending from Kristiansand on the coast, in the southwest to Porsgrunn in the northeast, designated by him the 'Great Friction Breccia'.

The almost geographical subdivision of this portion of the Shield into three provinces was recognized by BARTH (1933, 1947), who postulated that the Telemark and Bamble provinces were probably related portions of an homogeneous Precambrian complex. Support for this contention was later expressed by HOLTEDAHL (1945) who considered that the extensively migmatized rocks of the Telemark sector may merely represent deeper crustal levels than the less mobilized rocks of the Bamble sector.

Although BUGGE (1938) believed that the Bamble sector of the Shield represented an older and deeper group of rocks than those of Telemark, the converse is now accepted. Gravity studies carried out by SMITHSON (1963, 1965) have revealed the presence of a positive Bouguer anomaly increasing from the coast, which together with observations by SELMER OLSEN (1950) and ELDERS



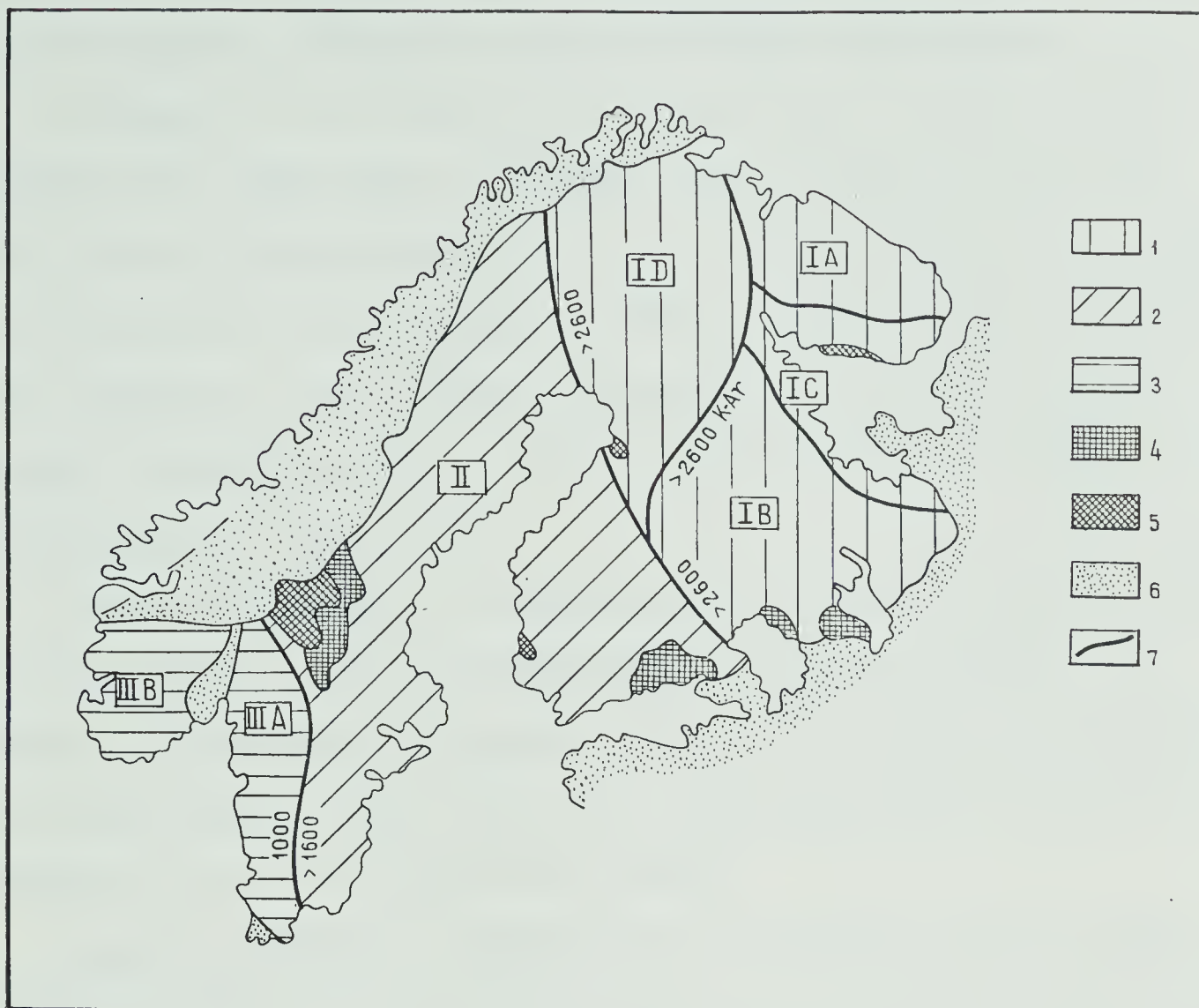


Fig. 3. Schematic geochronological map of the Baltic Shield. Geochronological zones: I = Saamokarelian; II = Svecofennian; and III = Sveconorwegian. Orogenic formations with age: 1 = 3600 - 1900 m.y.; 2 = 2300 - 1650 m.y.; and 3 = 1200 - 900 m.y. Platform formations with age: 4 = 1800 - 1600 m.y.; 5 = 1450 - 1000 m.y.; 6 = Eocambrian and Paleozoic; and 7 = boundaries of zones. (after KRATZ et al. 1968).





(1961, 1963) suggests that a wedge of denser Bamble rocks along the coastal region is underlain at depth by Telemark migmatites and granites.

The nature of the Porsgrunn-Kristiansand fault has been discussed by BUGGE (1928), BARTH (1947) and ELDERS (1963), of which the latter two authors have both suggested that the total relative movement was of a normal nature and the N.W. side was moved up relative to the S.E. side. SMITHSON (1963) calculated a minimum vertical displacement of 0.5 km on the basis of gravity measurements north of Herefoss, where granite and Telemark gneisses are faulted against Bamble rocks.

Recent investigations of MORTON et al. (loc.cit.) and MORTON (1969a) have suggested that the Porsgrunn-Kristiansand fault may represent the continuation of the Oslo fault graben; the southern boundary fault of which lies off the Skagerrak coast. The entire Bamble sector must, therefore, be considered as part of the Permian Oslo graben.

Various petrological investigations have revealed that the Bamble sector of the Shield is occupied by a series of metasedimentary and metavolcanic rocks in part migmatized and metasomatized and intruded by basic igneous rocks, pegmatites and both post- and synkinematic-granites. The grade of metamorphism has for many years been stated to be at a maximum in the Arendal district, where it attains hornblende granulite facies and decreases northwestwards to the upper amphibolite facies. TOURET (1961) however has described rocks of charnockitic affinity from the Vegarshei-Gjerstad region, suggesting a local attainment of the hornblende granulite facies in this area.

#### History of Research in Bamble

Although the literature concerning the geology of this portion of the Shield is quite voluminous, comparatively few systematic areal surveys have been carried out. BUGGE (1943) published a regional description of the whole





Bamble portion of the Shield, which has been enlarged upon and to some extent modified in recent publications by HOLTEDAHL (1960), BARTH and REITAN (1963) and BUGGE (1965).

More recently R.D. Morton, whilst at the University of Nottingham, initiated a new and detailed systematic study of the Bamble sector, commencing in the Langesund district and continuing, during the period 1960 to 1968, to the Tvedestrand district. Unpublished theses pertaining to the geology and petrology of Eastern Bamble have been produced by BATEY (1963) and RYAN (1966), of the Levang district by BURRELL (1964) and PETTERSSON (1964) and of the Risør area by STARMER (1967). An extensive study of Eastern Bamble has recently been published by MORTON, BATEY and O'NIONS (1969) and for a more detailed treatment of the petrological and structural aspects of Bamble than will be presented here, the reader is referred to this work.

#### Metasedimentary and Metavolcanic Rocks

Various workers in the Bamble region have discussed the possibilities of sedimentary or volcanic origins for many lithologies such as amphibolites, granite gneisses, nodular-sillimanite rocks and so on.

MORTON (1969b) has documented the occurrence of rocks of unmistakable sedimentary origin on the island of Arø and its neighbouring islets, where a sequence of cross-stratified intercalated quartz-arenites, quartz-pebble ortho- and para-conglomerates occur, which have been metamorphosed in the upper amphibolite facies. Stereographic rotation of the angular disposition of the foreset beds has indicated the derivation of the source material for these rocks from the N.W. In view of the difficulties inherent in evaluating the degree of flattening, fold style and orientation of kinematic axes in regional metamorphic terrains the above current direction is only considered to be approximate. On the island of Røsholmen MORTON (op.cit.) has described a



unique sequence, within the Bamble region, consisting of 2000 or more feet of what are thought to be metapyroclastic breccias of trondhjemitic affinity.

For the most part the Bamble sector of the Shield is composed of interbedded quartzites, biotite and hornblende-biotite schists (often graphite-bearing), amphibolites and granite, granodiorite and quartz-diorite gneisses. Of less frequent occurrence are marbles, calc-silicate rocks and anthophyllite cordierite rocks. These lithologies have been modified in places by metasomatism and granitization (*sensu lato*) processes, particularly in the Risør area (see, STARMER, 1969).

Amphibolites occur within the area mostly as conformable bands and boudins, however MORTON (*op.cit.*) has described discordant orthoamphibolites from Røsholmen. The chemistry of some amphibolite bodies reported by MORTON et al. (1969) from Eastern Bamble are most consistent with an igneous derivation in view of the similarity of their chemical variation with the Karoo dolerites differentiation trend. This interpretation is further substantiated by the frequent occurrence of apparently relict igneous textures in many amphibolite bodies. Ortho-amphibolites in Bamble may result from metamorphism of intrusive or extrusive basic volcanics or possibly, and more likely in some instances, by direct crystallization of a basic magma under high  $\text{PH}_2\text{O}$  conditions (GATES, 1967). However, it is not intended to infer that all of the amphibolite bodies have an igneous origin, since zircons extracted from sample SN-68-121 from Kjonnyøya are very rounded and obviously detrital.

Lithologies mapped as 'granitic' gneisses vary in bulk chemistry from granite through granodiorite to quartz-diorite. The chemical and mineralogical distinction of the gneisses in Eastern Bamble is in part related to their mode of occurrence (MORTON et al. *op.cit.*). The granite gneisses occur as lenticular or subrounded masses, which are poorly foliated and often possess an igneous texture. On the other hand, granodioritic gneisses are located marginal



to the granitic gneiss units where they are peripheral to the amphibolites or biotite schists. STARMER (1969) has described 'granitic' gneisses from the migmatite complex of the Risør area, apparently resulting from an extensive K-metasomatism accompanying upper amphibolite facies metamorphism.

Quartzites are common within the area and are frequently sillimanite bearing. With an increase of biotite, quartzites may grade laterally into biotite schist, or of K-feldspar and mica into granite gneiss. Biotite- and hornblende-biotite schists usually occur as small discontinuous bands and may grade laterally into amphibolite or quartzites etc.

MORTON et al. (loc.cit.) have described a local occurrence of hornblende-pyroxene gneisses south of the Skogen norite which are probably basic igneous (some possess a relict igneous texture) rocks metamorphosed under a local transition to the hornblende-granulite facies.

### Metamorphic Facies

On the basis of petrographic data of MORTON (et al., 1969) and RYAN (1966) the following diagnostic assemblages have been selected to infer the metamorphic conditions.

#### a. Pelitic rocks.

1. Quartz-muscovite-andesine-biotite-microcline.
2. Quartz-muscovite-biotite-plagioclase-sillimanite.
3. Quartz-muscovite-biotite.
4. Quartz-plagioclase-almandine-biotite.

#### b. Quartz-feldspathic rocks.

5. Quartz-microcline-biotite.
6. Quartz-microcline-plagioclase-biotite-sillimanite.
7. Quartz-microcline-plagioclase-biotite.





c. Basic rocks.

8. Plagioclase-hornblende-diopside.
9. Quartz-plagioclase-hornblende.
10. Quartz-plagioclase-hornblende-biotite.
11. Quartz-plagioclase-hornblende-biotite-garnet.
12. Quartz-hornblende-plagioclase-diopside.
13. Quartz-cordierite-anthophyllite-phlogopite.
14. Anthophyllite-cordierite-biotite (phlogopite).

d. Hornblende-Pyroxene Gneisses.

1. Plagioclase-diopside-hypersthene-hornblende-garnet.
2. Plagioclase-microcline-diopside-hypersthene-hornblende-garnet.

Some of the features of the metamorphic assemblages present are plotted in Fig 4 on the familiar ACF and AKF diagrams. Since chemical data is not presently available on many coexisting phases, all the phases are represented as ideal compositions. Of particular interest is the apparent equilibrium coexistence of muscovite and sillimanite in pelitic assemblages. This area may be compared to the sillimanite isograd studied in Maine by EVANS and GUIDOTTI (1966) where sillimanite, muscovite and orthoclase coexist over a zone approximately 10Km wide, and is in some respects similar to the sillimanite-muscovite zone of New Hampshire (TURNER, 1968). Insufficient work has been carried out at this time in order to ascertain at what point muscovite disappears either northwards to southwestwards towards the Arendal district; the paucity of pelitic assemblages towards the Kristiansand-Porsgrunn fault in eastern Bamble at least, renders it's identification difficult.

It is apparent from the above discussion that the P-T conditions for the metamorphism in Bamble must have been close to those for the univariant reaction of muscovite plus quartz to sillimanite plus orthoclase. The paucity





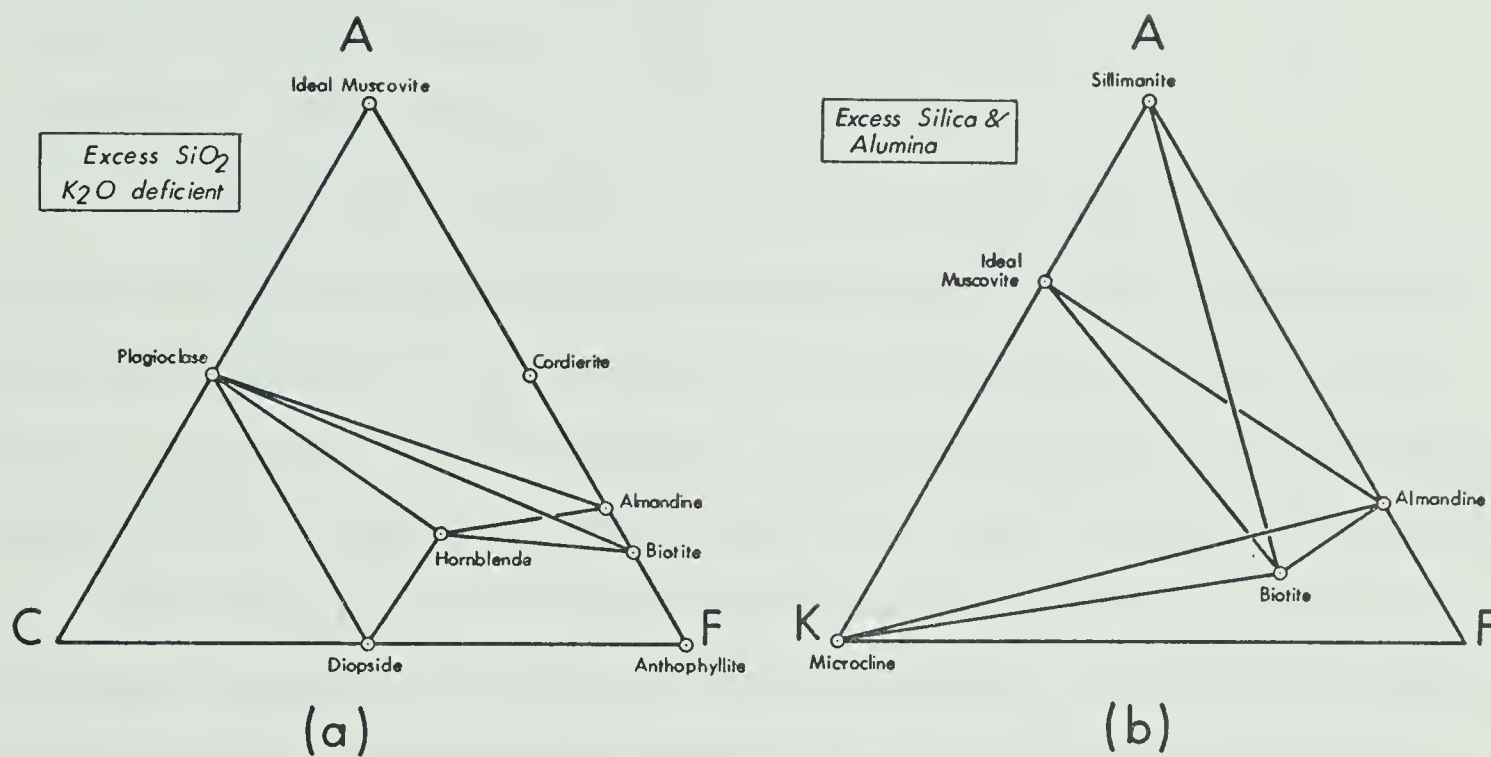
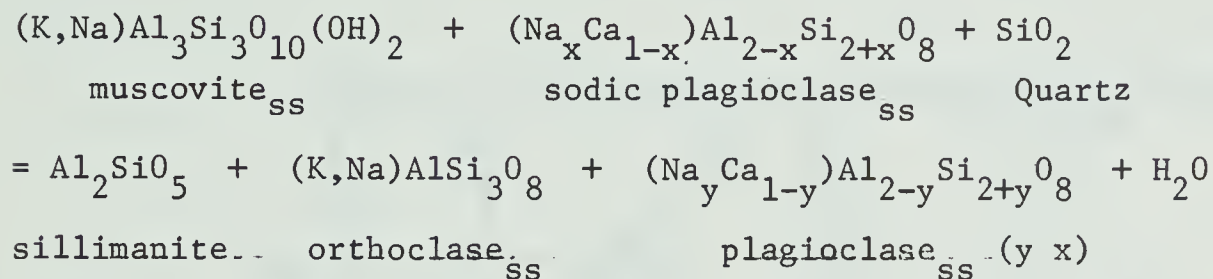


Fig.4. (a). ACF diagram based on descriptions given by MORTON, BATEY and O'NIONS (1969) and RYAN (1966) for rocks with excess  $\text{SiO}_2$  and deficient in  $\text{K}_2\text{O}$ . Quartz is in all cases an additional phase.  
 (b). AKF diagram based on descriptions of above authors for rocks with excess silica and alumina. Plagioclase is an additional phase in all assemblages.



of pelitic assemblages towards the Skogen area from where MORTON et al. have described hornblende-pyroxene gneisses has not as yet permitted the identification of a sillimanite-orthoclase isograd. GUIDOTTI (1963) suggests the following dehydration reaction for the formation of sillimanite-orthoclase assemblages in Maine;



The presence of andesine in most pelitic assemblages in Bamble suggests that this reaction is more applicable here than the simple muscovite plus quartz reaction. It is also possible that dehydration reactions will involve biotite in certain instances. From the above equation it is apparent that  $\mu_{\text{H}_2\text{O}}/\mu_{\text{SiO}_2}=1$  and also from Evans' (EVANS 1965) study of muscovite stability, it is clear that  $\mu_{\text{H}_2\text{O}}$  for the univariant reaction muscovite + quartz to orthoclase (sanidine) + sillimanite +  $\text{H}_2\text{O}$  is positive, therefore an increase in the chemical potential of water after metamorphism would tend to drive the equation to the left and an increase in temperature might initiate a drive to the right. The commonly observed replacement of sillimanite by muscovite may, therefore, result from a decrease in temperature or an increase in  $\mu_{\text{H}_2\text{O}}$ , the latter being most likely.

EVANS (op.cit.) has estimated that muscovite reacts with quartz to form sillimanite and orthoclase at  $T=655^\circ\text{C}$  to  $715^\circ$  in the pressure interval  $P_{\text{H}_2\text{O}} = 4$  to  $6$  kb. An independent temperature estimate for this univariant reaction may be made on the basis of  $^{18}\text{O}/^{16}\text{O}$  ratios in quartz-ilmenite pairs measured by GARLICK and EPSTEIN (1967) suggesting a temperature of around  $700^\circ\text{C}$  for the above reaction.



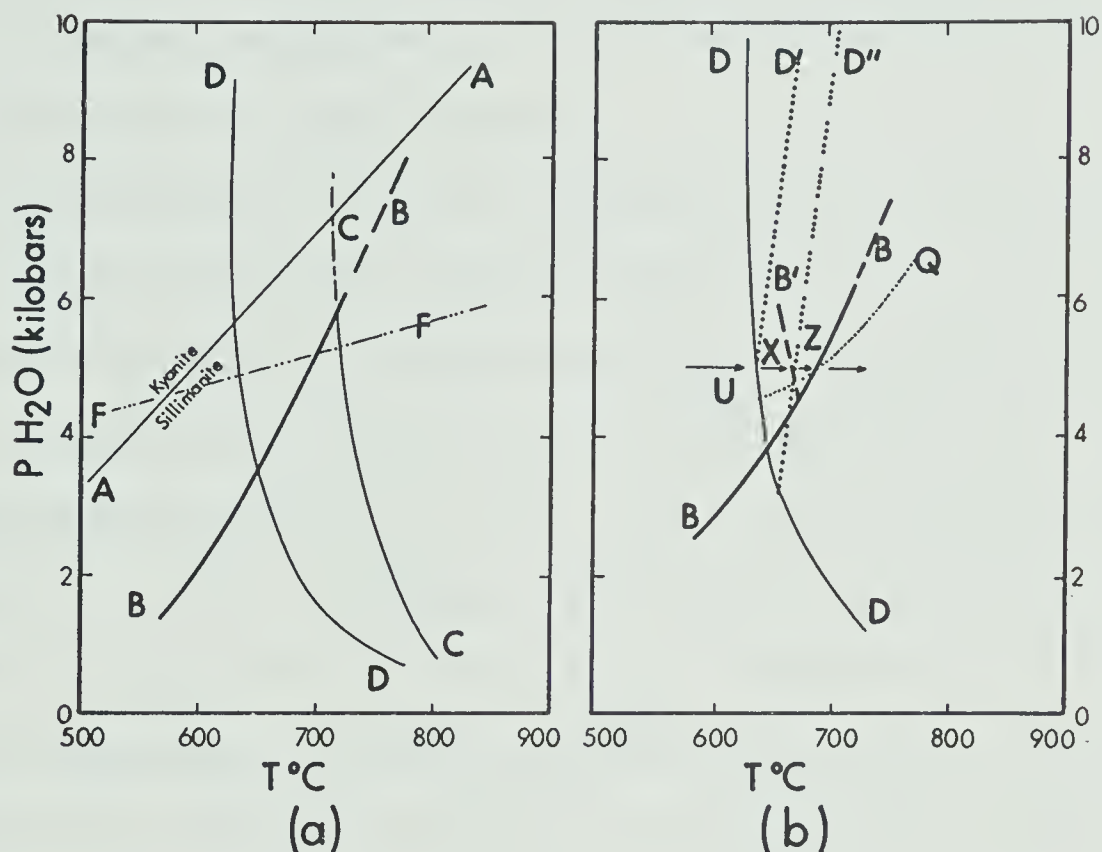


Fig.5. Relationships between the stability fields of muscovite and the aluminosilicates and the melting temperatures of quartz-feldspar mixtures (modified from LUNDGREN, 1966).

(a). Relationships where  $P_{H_2O} = P_{TOTAL}$  (i.e. aqueous phase present). A: kyanite to sillimanite inversion curve (FYFE, 1966). B: muscovite + quartz = sillimanite + orthoclase + water (EVANS, 1965). C: the four phase melting curve of sanidine - quartz - liquid - gas (SHAW, 1963). D: PT curve for the quaternary minimum in the system  $KAlSi_3O_8 - NaAlSi_3O_8 - SiO_2 - H_2O$  (LUTH, JAHNS and TUTTLE, 1964). F: Sillimanite (higher pressure) = mullite + quartz (lower pressure).

(b). Relationships when  $P_{H_2O} \neq P_{TOTAL}$ . Curves B and D as (a) above. Arrows indicate path of increasing temperature at 5 Kb. B': estimated position of muscovite + quartz boundary if  $P_{H_2O}$  fixed at 4.5 Kb. D': PT curve for complete melting of 'granite' containing approximately 11% water. D'': PT curve for complete melting of 'granite' containing approximately 8% water. Q: schematic PT curve for granite minimum when  $P_{H_2O}$  is fixed at 4.5 Kb.





In Fig 5 some pertinent reactions are plotted after LUNDGREN (1966). It is apparent that the muscovite plus quartz reaction boundary is intersected by the minimum melting curve for quartz-alkali feldspar mixtures around 655°C and 3.5Kb. Even allowing for solid solution of Na in muscovite it is apparent that melting should generally accompany the muscovite plus quartz reaction. Since the amount of melting which can take place will be dependent on the amount of water available, melting will probably be restricted to grain boundaries.

At total pressures in excess of approximately 4Kb the muscovite plus quartz reaction will precede partial melting only if  $P_{H_2O}$  is less than  $P_{total}$ , since both B and D are a function of  $P_{H_2O}$ . If  $P_{H_2O}$  were less than  $P_{total}$  then the muscovite plus quartz reaction might commence at (X in Fig 5b) a lower temperature than when  $P_{H_2O} = P_{total}$  (z) and the beginning of melting may take place at a higher temperature. Since  $H_2O$  is released in the muscovite + quartz reaction,  $P_{H_2O}$  must be equal to  $P_{total}$ , therefore the consequence of the reaction is apparently to produce sillimanite plus a melt. Water released by the reaction will therefore be 'fixed' by the small amount of melt. If at a higher temperature larger scale melting involving biotite also occurs, producing undersaturated melts, these may be able to rise into the lower temperature zones as long as water is available. Water derived from such reactions as discussed above may be released, absorbed by the melt and enable granite pegmatites, lit par lit gneisses and ever larger granitic bodies to form.

#### The Gabbro-Norite Suite

##### Gabbros and Norites

Rocks of gabbroic composition occur throughout the area as lensoid





masses, concordant with the foliation of the surrounding metasediments and metavolcanics. Petrographically the rocks are divisible into gabbro (*sensu stricto*), norite and olivine norite and chemically vary from nepheline to quartz normative compositions (MORTON et al. loc. cit.). The term hyperite has frequently been used by Scandinavian geologists (BUGGE, 1943, HOLTEDAHL, 1960) to include all Precambrian gabbroic rocks and their metamorphosed equivalents (i.e. orthoamphibolites).

Corona structures, principally around olivine, are evident in the majority of the gabbros in the area and are one of their most characteristic features. Commonly olivine, where in contact with plagioclase, is surrounded by an inner corona of orthopyroxene and occasionally minor clinopyroxene and a second corona of hornblende and spinel. On occasions a third corona of garnet plus clinozoisite may be present. Magnetite also is frequently surrounded by an inner corona of biotite and an outer corona of hornblende with spinel.

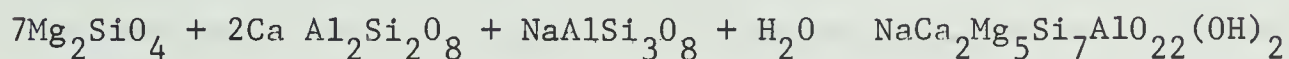
The presence of amphibolitized margins to the gabbroic bodies is typical; often only the central portions of the mass contain relatively unaltered gabbro and in some instances the transition from gabbro to amphibolite is complete. In the case of the gabbro at Ødegaardens-verk, with the associated famous chlorapatite veins, the alteration of the gabbro has involved both amphibolitization and scapolitization (BUGGE, 1943, BUGGE, 1965, MORTON, 1960, RYAN, 1966) and will be further discussed shortly.

The Bjordammen intrusion described by RYAN (1966) is composed of lower pyroxenite phases overlain by coronite gabbro. Primary cumulate hypersthene (see the petrographic description of sample SN-35) is replaced by a fibrous amphibole, compositionally approaching edenite. For more extensive petrographic descriptions of the gabbros and norites the reader is referred to the work of the aforementioned authors and petrographic descriptions of some of the



mentioned rocks in Appendix A (see samples SN-41, Sn-28, SN-26, SN-35, SN-47).

The presence of corona structures in the gabbros of south Norway and indeed other parts of the world is generally agreed upon to be a metamorphic phenomenon. However the nature of the reactions taking place are still a subject of controversy. Various theories of petrogenesis have been discussed by BROGGER (1935), GJELSVIK (1952) and RYAN (1966). Recently FRODESEN (1968a,b) has described coronas from the Hiåsen gabbro, Bamble, which he feels result from a combination of deuteritic effects (orthopyroxene-hornblende corona) and metamorphic effects (garnet corona). REYNOLDS and FREDRICKSON (1962) have discussed the necessity for the addition of  $\text{SiO}_2$  (up to 10wt%) to the rock for the necessary reactions to occur. A simpler and more likely reaction has been proposed by MORTON et al. (1969) for the reaction between olivine and plagioclase:



forsterite                  plagioclase<sub>ss</sub>                  edenite



hypersthene          spinel

involving only the addition of  $\text{H}_2\text{O}$  as an extra component.

The investigations of anhydrous reactions in undersaturated alkali-olivine basalts and olivine tholeiites by GREEN and RINGWOOD (1967) are pertinent to the present discussion. Reactions between olivine and plagioclase were found to be important at about 7Kb and 1100°C, yielding pyroxene and spinel in starting compositions with 100Mg/(Mg+Fe<sup>2+</sup>) between 60-70. Garnet appeared at a lower pressure in more iron-rich starting compositions. The compositional control of the appearance of garnet may have been operative during the formation of the Bamble coronites.

The corona mineralogy is considered to be a function of the ambient





$P_{H_2O}$ -T conditions, which in this instance apparently characterize the hornblende-granulite facies. The coronite gabbros create somewhat of an enigma in terms of their metamorphic facies, since the country rock and the amphibolitized margins of the gabbros have parageneses characteristic of the upper almandine amphibolite facies, whereas the coronite gabbros exhibit parageneses diagnostic of a higher grade hornblende granulite facies. Firstly, since the gabbro to amphibolite transition is often more complete at the margin of a gabbroic body than at the centre, and secondly water is a necessary additional component for the reactions, a gradient in  $\mu_{H_2O}$  must have existed within the gabbroic bodies during the formation of the corona structures. The muscovite plus quartz reaction was shown to be dependant on  $\mu_{H_2O}$ , therefore at a given temperature the country rock might exhibit a different, lower grade facies than the coronites. Conversely if the gabbros had not cooled to the temperature of the host rock, the different parageneses exhibited may have been a function of temperature differences. It is most likely, however, that differences in  $\mu_{H_2O}$  within the area were primarily responsible for the local transitions into the hornblende-granulite facies and that temperature gradients were of less importance.

The absence of chilled margins to the gabbroic bodies and their concordant relationships with the country rocks lends support to the concept of syntectonic or slightly pre-tectonic emplacement.

#### Albitite and Apatite Veins

Associated with gabbro and metagabbro in particular at Ødegaardens-verk and probably genetically related to them, are a series of apatite and albitite veins.

Most of the chlorapatite occurrences within the area occur as 'dykes' dipping between  $28^\circ$  and  $40^\circ$ , within the elongate metagabbro body at Ødegaardens-





verk. Commonly the veins are seen to be zoned, containing apatite at the centre and flanked by enstatite (largely pseudomorphed by talc) and phlogopite (BUGGE, 1965). The intruded gabbro proximal to the apatite veins may be altered to an enstatite-phlogopite-scapolite-rutile-ilmenite rock (Fig 6), called 'sand-rock' by the old miners in view of its friable aspect (see petrographic description of SN-27, Appendix A). Further away from the veins the gabbro is extensively scapolitized and amphibolitized.

The apatite is of two types at Ødegaarden, a fresh clear golden-yellow chlorapatite and a white to yellow-white hydroxy-apatite. Small quantities of other phosphates are found associated with the apatites such as xenotime, woodhouseite and whitlockite (described by MORTON, 1961). Other small occurrences of apatite have been mapped within the area (MORTON, personal communication) but only the major Ødegaarden deposit has been studied from a geochronological viewpoint.

Albitites, rocks composed essentially of Na-plagioclase and minor quartz (usually less than 10%) and occasionally rutile and sphene, occur throughout the area in close association with gabbro and metagabbro. BRØGGER (1935) proposed the term Kragerøite for rutile-bearing varieties occurring in the Kragerø district. Rutile may be partially or completely replaced by sphene in some albitites (see petrographic description of SN-92, Appendix A) consistent with the view of sphene being the stable Ti-phase under upper amphibolite facies conditions.

Larger bodies of albitite are often concordant with the foliation, for example those west of Valle (RYAN, 1966), whereas smaller veins are usually discordant frequently exhibiting 'diffuse' contacts with their host amphibolites. Small patches of albitite with sphene occur in the metagabbro at Ødegaarden and are now well exposed in the Road Metal Quarry at the Ødegaarden Apatite Mines.





Scapolite-hornblende meta-gabbro  
"Ødegårdite"

45 cm. altered green gabbro "Sand Rock"  
fine phlogopite

25 cm. apatite with phlogopite pseudomorph.  
after enstatite

variable width, phlogopite

8 cm. sand rock

15 cm. vein of medium grained phlogopite  
with apatite stringers

diffuse contact  
15 cm. sand rock

45 cm. normal Ødegårdite

30 cm. sand rock

fine phlogopite

coarse phlogopite

18 cm. apatite with phlogopite pseudomorphs  
coarse phlogopite after enstatite

fine phlogopite, diffuse contact

15 cm. sand rock

normal Ødegårdite

Fig.6. Sketch map showing a typical example of the contact relationships between the metagabbro and the chlorapatite veins at the Ødegården apatite mines. (after MORTON, pers. comm.)





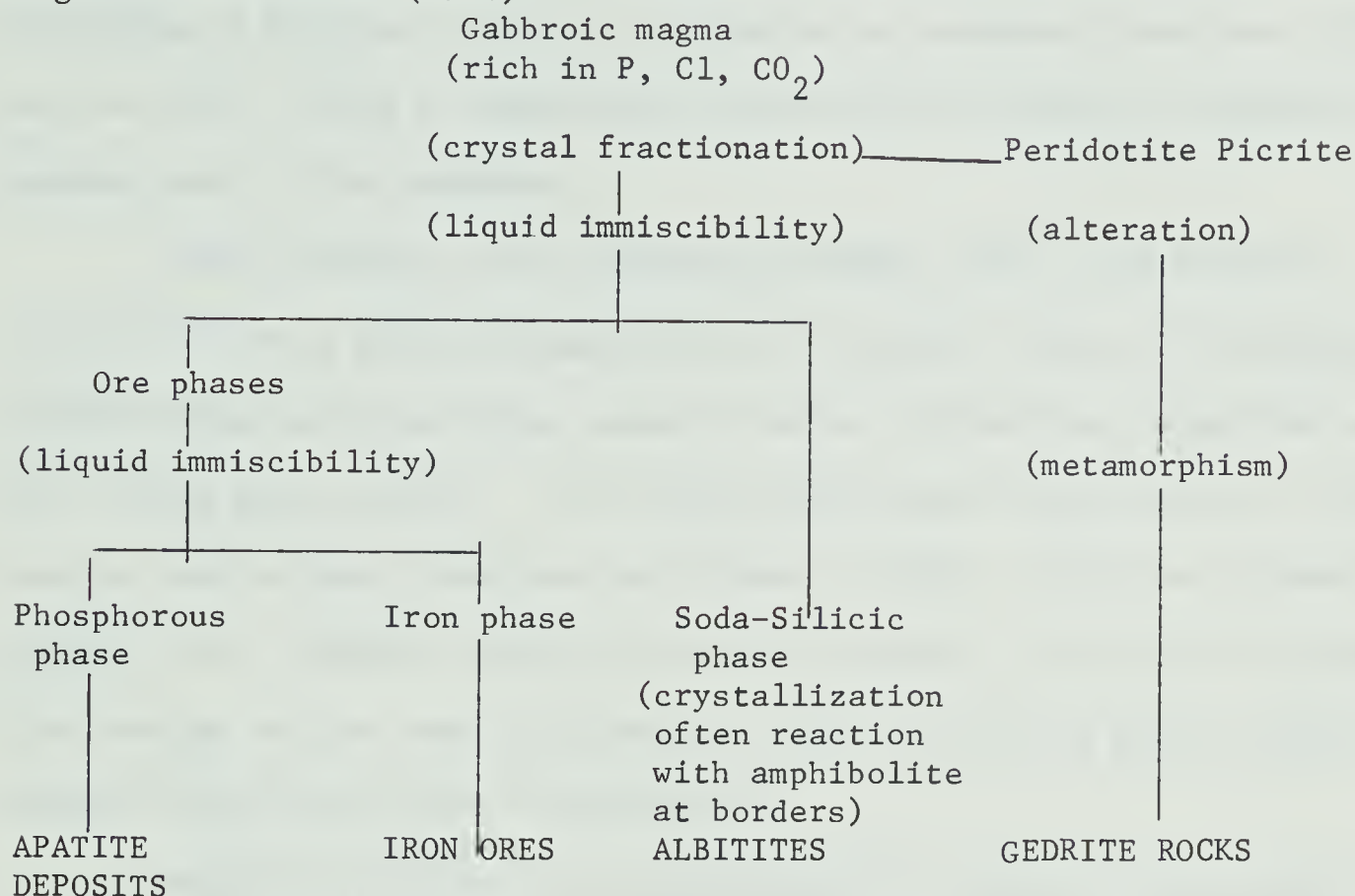
The various theories for the origin of the albitite deposits fall broadly into two categories; those proposing a primary genetic connection with the magmatic stage of the gabbros, and those proposing subsequent metamorphic and metasomatic origins. The hypothesis of 'pneumatolytic differentiation' (BRÜGGER, 1935) would belong to the first category; the hypothesis of partial melting of amphibolite under upper amphibolite facies metamorphism (ELLIOT, 1966) and the metasomatic alteration of amphibolite (GREEN, 1956) belong to the second category. More recently BODART (1968) has proposed a mechanism genetically relating the gabbros, albitites and apatite deposits via a process of liquid immiscibility. Our understanding of apatite-magnetite immiscibility largely derives from the work of PHILPOTTS (1964): Bodart's scheme is essentially an extension of these ideas, whereby a gabbroic magma rich in P, Cl, and  $\text{CO}_2$  forms three immiscible phases, a gabbroic phase, a soda-silicic phase and an apatite-Fe oxide phase. The soda-silicic phase separates and crystallizes as albitite and the apatite-Fe oxide phase forms two additional immiscible phases; an apatite and an oxide phase (see Fig 7, below). Bodart's scheme appears to be the most plausible currently proposed scheme, being consistent with the observed spatial relationships of albitite, apatite and gabbro and explains some of the chemical difficulties inherent in the other schemes outlined above.

The writer, however, would take exception to Bodart's proposal of an early peridotite-picrite crystal differentiate being the precursor of the gedrite lithologies in all instances. This may in part be the case for some gedritic rocks spatially related to the gabbros, however other cordierite-gedrite rocks in the area possibly owe their origin to low-grade alteration and subsequent isochemical metamorphism of other mafic lithologies within the 'normal' metasedimentary-metavolcanic sequence. VALLANCE (1966) has shown that low-grade mafic rock alteration may produce an assemblage chemically



equivalent to Mg-chlorite plus quartz, which may be converted to the cordierite plus anthophyllite paragenesis upon metamorphism.

Fig 7. after BODART (1968)



Scapolitization of amphibolites is quite a widespread phenomenon in the Ødegaarden-Kragerø region. The observation by RYAN (1966) of scapolite forming an outer corona in some coronite metagabbros at Ødegaardens-verk suggests that scapolitization in this instance is a metamorphic phenomenon; the chlorine probably being derived from the partial chlorapatite to hydroxy-apatite conversion during metamorphism. We may thus infer that the gabbro-apatite-albitite paragenesis at Ødegaardens-verk at least, is pre-or synmetamorphic.

#### The Levang Granite Gneiss Dome

The Levang peninsula, south of Kragerø, has been described by HOFSETH (1942), BROGGER (1933) and BUGGE (1965) as composed in the main of a red,





medium-grained granite, normally a biotite granite, composed of microcline, oligoclase, quartz, biotite and magnetite, with accessory green hornblende, epidote, allanite, zircon and apatite. The granite was described as possessing a foliated structure and forming an elongated mass about 15Km long and 4Km wide, having a predominantly NE-SW strike, veering to ENE-WSW in the eastern part of the peninsula.

Recent mapping of the peninsula (ELDERS, 1964), has shown the 'granite' to be a crude, elongated dome structure, flanked by metasediments, metavolcanics and other minor granite bodies. Elders has termed the structure the 'Levang gneiss dome'. The Levang gneiss dome differs from the classic mantled gneiss domes described in Finland by ESKOLA (1949) and in Maryland (BRODEL, 1937, HOPSON, 1964) in that the 'mantling' strata are of apparently the same age as the dome rocks and the term is used in a purely descriptive context without any genetic implications.

Samples collected for geochronological purposes in the present study are petrographically consistent with Brøgger's above description (see description of samples SN-68, 157, 158; SN-68, 104, 105, SN-59 and 61, Appendix A) except for the identification of sphene in some samples (SN-59, SN-61, SN-68-159). BURRELL (1964) has mapped the western side of the Levang peninsula between Øysang and Kjølebrond and some pertinent observations made by him are listed below:

1. Foliated granite predominates over granodiorite. Occasionally granite may grade laterally into granodiorite.
2. Granite is bounded principally by amphibolite and boundaries are sharp and distinct. The writer's observations further east on the peninsula reveal that quartzite, graphite-biotite schist and biotite-plagioclase gneisses may flank the gneiss-dome.
3. Intrusive, discordant relationships are not seen, and there is no



diminution in grain size at the margins of the granite.

4. The bulk mineralogy is typically granite and modal quartz-albite-orthoclase plots show a concentration near the ternary minimum of TUTTLE and BOWEN (1958).

Any theory for the origin of this foliated granite must be consistent with the above observations. In addition zircons separated from a number of granite specimens in this study exhibit morphological peculiarities which are pertinent to the present discussion (see Chapter V). Most of the zircons appear to have been detrital in nature, showing metamorphic overgrowths in many instances. These will be further discussed in relation to the geochronology.

On the basis of field relationships and the presumed metamorphic conditions, an origin for the Levang gneiss dome by partial anatexis seems the most probable. The possibility of granite forming at high temperatures under fairly anhydrous conditions and rising upwards with an increase of  $P_{H_2O}$  to lower temperature regions has been discussed previously in the section concerned with metamorphism. In view of the observed concordant field relationships it would appear that the process was one of essentially 'in situ' partial anatexis.

#### The Cataclastic Belt

In E. Bamble, and indeed all parts of the Bamble sector so far investigated by the Nottingham group (MORTON, personal communication) a zone, 4 to 4.5Km wide, of predominantly cataclastic rocks have been recognised on the SE side of the Porsgrunn-Kristiansand fault. Because of the general increase in intensity of deformation toward the Porsgrunn-Kristiansand fault, the southern boundary has been somewhat arbitrarily defined (Fig 2).

The cataclastites are characteristically fine to very fine-grained, well-foliated rocks often possessing a very strong lineation. Compositionally





rocks in the cataclastite belt have been found to include all the lithological variations previously described. In addition, however, in Eastern Bamble augen granite gneisses and granite gneisses with a rapakivi texture have been recognised (MORTON et al., loc. cit.). Since geochronological studies have not been undertaken in the cataclastite belt to date, no further mention of the lithologies will be made here.

The intense deformation characterising the cataclastite belt does not appear to continue into the Vegårshei-Gjerstad region (TOURET, 1962, 1967, 1968), where the metamorphic grade appears to be in the hornblende-granulite facies.

### Pegmatites

Pegmatite occurrences in Bamble may be broadly divided into two groups:

1. A sykinematic and synmetamorphic group of predominantly plagioclase (An 20-30) pegmatites, usually concordant with the foliation of the country rocks. Smaller plagioclase pegmatites however may occupy shears and gashes with consistent orientations (REITAN, 1959).

2. A postkinematic, postmetamorphic group of predominantly K-feldspar pegmatites usually discordant with the foliation of the country rocks.

Foliation is normally lacking in the pegmatite bodies, but mapping, by the author and R.D. Morton in 1965, of the island of Øterøy revealed relict foliation in some of the plagioclase pegmatites. The plagioclase pegmatites are mineralogically simple consisting usually of quartz, plagioclase and biotite, however occasionally sphene, rutile diopside and allanite may be present. K-feldspar pegmatites, on the other hand, consist of quartz, microcline, biotite or muscovite. In addition they often show enrichments in U, Th, Zr, Nb, Ta and Ce, revealed by the presence of allanite and fergusonite (e.g. the Engevann pegmatite), zircon, anatase sphene (e.g. the Ødegaarden pegmatite), euxinite





(e.g. the Kalstad pegmatite, Kragerø). HEIER and TAYLOR (1959) and HEIER et al. (1967) have investigated the geochemistry of a number of alkali feldspars in South Norway. Of particular interest here are the very low Pb contents (less than 9ppm) in the Kragerø and Arendal pegmatites, possibly indicative of higher grades of metamorphism in this region compared with Telemark, where Pb contents of the K-feldspars are much higher.

The concordant plagioclase pegmatites have most probably formed in situ by metamorphic differentiation involving local partial anatexis. The later K-feldspar pegmatites may result from mobilized partial anatectic material formed elsewhere in the metamorphic complex

### Structure

The Bamble sector of the Shield is separated from the Telemark sector by the Porsgrunn-Kristiansand fault, which appears to be of normal character with a minimum normal vertical displacement of 0.5Km (SMITHSON, 1963); the north side being the upthrown side.

In Eastern Bamble the first recognizable phase of folding (MORTON et al., loc. cit.) was the formation of NE-SW shear folds of a similar style, which tend to be open near the coast plunging between 20° and 30°, and become strongly isoclinal northwards. In the Cataclastite belt the deformation was sufficiently intense to shear many folds along their axes, leaving a series of parallel banded lithologies often without any recognisable fold structures, but with a very strong, presumably 'b', lineation. In the subjacent area north and west of Ødegaardens-verk MORTON (personal communication) has found evidence for a second phase of N-S folding. No evidence has been found for this second phase in Eastern Bamble and it appears to increase in intensity towards Aust Agder where the structural history is considerably more complex.

STARMER (1969) has recognised four phases of folding in the migmatite



area of the Risør peninsula as follows:

1.  $F_1$ : formed both major and minor isoclinal structures and a marked foliation along NE-SW axes. Accompanied by upper amphibolite facies metamorphism.
2.  $F_2$ : intense isoclinal folding, producing structures with sub-vertical axes and NE-SW trending axial planes. Accompanied by a second upper amphibolite facies metamorphism involving granitization.
3.  $F_3$ : formation of major and minor open concentric folds and occasionally tighter similar folds. The fold axes were inclined sub-horizontally and the axial planes sub-vertically. The trend of the folds was mainly E-W but was in places deflected by basic plutons intruded in the interval  $F_2$ - $F_3$ .
4.  $F_4$ : formation of minor, concentric folds, with sub-vertical axial planes and sub-horizontal N-S axes. In places they definitely post-date  $F_3$  structures, but at other localities are apparently broadly contemporaneous with  $F_3$ .

In Eastern Bamble (MORTON et al., loc, cit.) have recognised two fault sets; an early NE-SW set subparallel to the Porsgrunn-Kristiansand fault and frequently associated with zones of brecciation and mylonitization, and a younger set oriented NNW-SSE. The similarity in orientation of the NE-SW faults and the Porsgrunn-Kristiansand fault suggests that they may be genetically related. Horizontal slickensides have been observed at a number of places along the younger NNW-SSE group of faults suggesting that the last movement was of a strike-slip nature.

#### Metalliferous Ore Deposits

As no geochronological investigations of metalliferous ore deposits in the area have been undertaken by the author, only a brief reference will be made to these here.



During the late 19th century and early 20th centuries the Bamble region was a site of active mining and quarrying operations. MORTON et al. (loc.cit.) have discussed the ore deposits in Eastern Bamble in some detail, (see Fig 8) in terms of Precambrian and Permian met allogenic provinces, as follows:

#### Precambrian Metallogenic Province:

Ores belonging to this province fall into two distinct groupings:

1. Fe, Ni, Cu ores associated with gabbros, norites and metagabbros.

In Eastern Bamble ores belonging to this category are located around the SE portion of the Skogen norite and the Nystein and Vissestad gabbros, and have been partially exploited.

2. Fe, Ti, Cu and Mo ores associated with the metamorphic suite.

These occur as disseminated ilmenite and rutile associated with albitites, pegmatites and metagabbros, and as disseminated molybdenite in pegmatites.

#### Permian Metallogenic Province:

Vein type occurrences of Pb, Zn, Cu and Fe sulphides associated with younger faults are present in Eastern Bamble. The only workings of any significance are those at Traak (pyrite, sphalerite, galena, chalcopryrite and pyrite), Styggedalen and Asdalvann, (sphalerite and galena).

MOORBATH and VOKES (1963) have analyzed a number of galenas from South Norway, all of which were found to be 'J' - type leads. Ordinary leads associated with the Permian province lie on a 250 m.y. isochron. The best-fit anomalous lead line through the 'J' - type leads suggests a maximum age of  $1110 \pm 200$  m.y. for the source of the reaiogenic lead.

#### The Oslo Graben

MORTON et al. (loc. cit.) and MORTON (1969b) have offered a reinterpretation of the position of the extension of the Oslo graben beyond





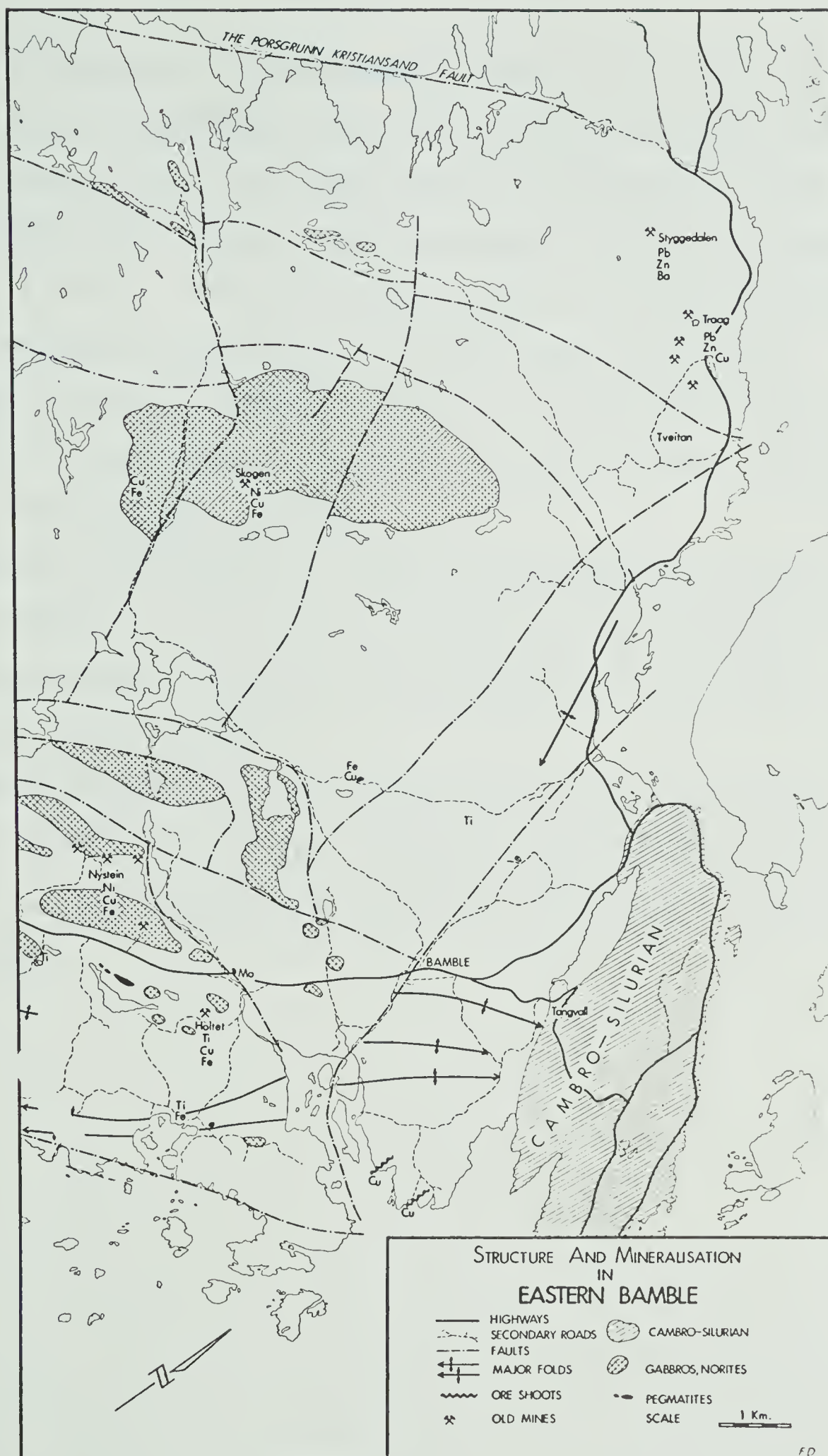


Fig.8. Structure and mineral occurrences in Eastern Bamble.  
(after MORTON et al., 1969).





Oslo. Field investigations in the Stokkevang area in Eastern Bamble and the borehole data of HENNINGSMOEN (1946) do not reveal the presence of any major fault along the line of the Cambro-Silurian escarpment near Brevik. Similarly SMITHSON (1964) did not find any gravimetric evidence to support the presence of a fault. It has been suggested that the Porsgrunn-Kristiansand fault is the northwest bounding fault of the Oslo graben, the southern boundary fault of which lies offshore southeast of the Skaergård islands. The Bamble sector of the Shield is therefore considered to form a southwestern extension of the Oslo graben structure.

Abundant evidence exists, at least in Eastern Bamble, of Permian activity. In addition to the Permian ore deposits at Traak, and Styggedal mentioned above, numerous explosion breccias presumably of Permian age, have been recognised in Eastern Bamble.

Numerous syenite and dolerite dykes occur throughout the area and have a preferred NNW-SSE orientation. To the author's knowledge, none of these have as yet been radiometrically dated and a Permian age for them can only be inferred.



## CHAPTER III - POTASSIUM-ARGON DATING

Potassium consists of three isotopes,  $K^{39}$ ,  $K^{40}$  and  $K^{41}$  of which  $K^{40}$  is naturally radioactive and decays to two daughter products,  $Ca^{40}$  and  $Ar^{40}$  by a branched decay scheme, in which 89 percent of the disintegrating nuclei go to  $Ca^{40}$  by  $\beta$  emission and 11 per cent to  $Ar^{40}$  by K-electron capture. A potassium-argon age may be calculated from the relationship:

$$\frac{Ar^{40}}{K^{40}} = \frac{\lambda_k}{\lambda_\beta + \lambda_k} (e^{(\lambda_k + \lambda_\beta)t} - 1) \quad (1)$$

where  $\lambda_k$  is the decay constant for K-electron capture,  $\lambda_\beta$  is the decay constant for decay by  $\beta$  emission, and  $t$  the age of the K-Ar system.

Potassium-argon dating has been, and still is, the most extensively applied method of radiometric dating. Its usefulness as a method stems not only from the favourable magnitude of the  $K^{40}$  half-life, but from the abundance in the upper crust of K-bearing mineral phases together with the fact that only small volumes of 'contaminant' argon are incorporated into many minerals upon crystallization. It is the latter condition which severely limits the utility of the method in the case of geologically young materials, since errors are made in correcting for both the amount of argon initially incorporated in the phase, and in some instances its isotopic compositions.

In the case of Precambrian K-Ar systems the above problem is not usually, or at least has not been shown to be significant with minerals containing more than about 0.5%  $K_2O$  (i.e. hornblendes and micas). Even if the decay constants are well known and the amounts of  $Ar^{40}$  and  $K^{40}$  determined accurately, the  $Ar^{40}/K^{40}$  ratio can only yield an apparent age for the system, until closed system behaviour can be demonstrated for the phase concerned; this often being difficult in practice, unless additional information is available. Since different minerals often show different degrees of departure



from closed-system behaviour under geological conditions, and some of the above-mentioned problems are greatly enhanced in the minerals of low K-content, the present investigation has been restricted to micas and amphiboles. Hopefully, micas and amphiboles representative of all the aforementioned metamorphic and intrusive phases in the Bamble region have been selected.

### Analytical Methods and Errors

All samples to be used for dating were initially collected on the basis of their 'freshness'. Prior to mineral separation they were examined petrographically and samples showing any signs of weathering were discarded. Samples were crushed to -60+120 mesh and the micas and amphiboles separated by conventional magnetic (Franz isodynamic separator) and heavy liquid techniques (tetrabromoethane and methylene iodide). The use of a centrifuge was found to be particularly valuable in the final purification stages of hornblende concentrates. Since mineral impurities having negligible potassium contents only act as dilutants of the K-Ar system and do not affect the  $\text{Ar}^{40}/\text{K}^{40}$  ratio, their presence is not critical. However it should be emphasized that 5% of biotite in a hornblende separate may contribute 25% to 50% of the total radiogenic argon. The mineral concentrates analysed here were usually greater than, or equal to, 98% pure (Appendix A) and in all instances any impurity present is not considered to significantly affect the  $\text{Ar}^{40}/\text{K}^{40}$  ratio obtained.

Potassium determinations of both micas and amphiboles were performed by precipitation of  $\text{Kb}(\text{C}_6\text{H}_5)_4$ . This method has been employed for a number of years in the University of Alberta laboratory and duplicate determinations yield a standard deviation of about 1% (see University of Alberta analysis of P-207 standard muscovite, LANPHERE and DALRYMPLE, 1967). In order to assess the precision of the method for low potassium minerals, nine replicate





determinations were performed over a period of a few months on the hornblende sample SN-88, which yielded a mean value of 0.52%  $K_2O$  and a standard deviation of 2.8%; it may be expected that amphiboles with higher  $K_2O$  contents than SN-88 will be more precise than this. All the hornblendes were also analyzed for  $K_2O$  by electron microprobe, which yielded results in very close agreement with the values obtained by  $KB(C_6H_5)_4$ ; for example a  $K_2O$  content of 0.53% was obtained for SN-88 (see comparisons of gravimetric and electron probe analyses in Chapter IV).

Argon was extracted from the samples using an NaOH flux-fusion technique similar to that described by GOLDICH et al. (1961). Individually prepared and calibrated  $Ar^{38}$  spikes (99.9% pure  $Ar^{38}$  isotope dilutant) were added to the samples during fusion, prior to the final purification.

Argon was isotopically analyzed on an A.E.I. M.S.-10, 180° mass spectrometer, modified to the requirements of the Laboratory by H. Baadsgaard. Vacuum requirements are met by an oil diffusion pump and a Varian VacIon getter pump, and ion currents are amplified by a Cary vibrating reed amplifier. Argon was measured dynamically and mass discrimination effects were monitored before and after the analyses by measuring purified air argon introduced into the mass spectrometer under the same pressure conditions.  $Ar^{40}/Ar^{36}$  ratios obtained for air argon were usually around 305 and all analyses were normalized to Nier's value of 295.5 (NIER, 1950).

Contaminant argon corrections, based on the measured amount of  $Ar^{36}$ , assuming an  $Ar^{40}/Ar^{36}$  ratio of 295.5, were usually small (Tables 1 and 2). Corrections to the measured ratios were also carried out for residual argon in the mass spectrometer, measured before the introduction of each sample. The precision of duplicate argon determinations is about 1% (BAADSGAARD, 1965).

Ages were calculated using the following decay constants (ALDRICH and WETHERILL, 1958) for  $K^{40}$  and isotopic abundance of  $K^{40}$  decay (Nier, 1950).



$$\lambda\beta = 4.72 \times 10^{-10} \text{ yr}^{-1}$$

$$\lambda k = 0.585 \times 10^{-10} \text{ yr}^{-1}$$

$$K^{40}/K = 0.0119 \text{ atomic per cent.}$$

Analytical errors were calculated assuming standard deviations of 1% for  $Ar^{40}$  and  $K^{40}$  determinations respectively for micas and 1% and 3% respectively for amphiboles. Errors were calculated on the basis of the following error equation (Kirsten, 1966).

$$\frac{\Delta t}{t} = \frac{\Delta \lambda}{\lambda} + \frac{1 - e^{-\lambda t}}{\lambda t} \cdot \frac{\Delta(Ar^{40}/K^{40})}{(Ar^{40}/K^{40})} + \frac{(1 - e^{-\lambda t})}{\lambda t} \cdot \frac{\lambda\beta(\Delta\lambda k/\lambda k - \Delta\lambda\beta/\lambda\beta)}{\lambda} \quad (2)$$

In practice the contribution from the last term is negligible. Since the error in  $Ar^{40}/K^{40}$  depends on  $1 - e^{-\lambda t}$  which is a function of  $t$ , the error in the apparent age increases as  $t$  increases. The total uncertainty in the apparent ages, taking into consideration errors in the decay constants, is approximately  $\pm 60$  m.y. and  $\pm 80$  m.y. for biotites and amphiboles respectively.

#### Argon Diffusion in Micas and Amphiboles

It is becoming increasingly more apparent that K-Ar mineral ages from regional metamorphic terrains do not relate to any specific geological event, but are 'cooling' ages related to the time at which specific minerals became closed systems to the diffusion of radiogenic argon during post-metamorphic uplift and cooling (ARMSTRONG, 1966; ARMSTRONG and HILLS, 1967; HARPER, 1967a, 1967b; MOORBATH, 1967; DAMON, 1968 and O'NIONS et al., 1969). Since the time of 'closure' of different potassium bearing minerals is related to the argon diffusion characteristics of that mineral some features of argon diffusion in micas and amphiboles will be briefly reviewed.

The diffusion coefficient of radiogenic argon is empirically related to the activation energy by the following relationships:





$$D = D_0 \exp (-E/RT) \quad (3)$$

or

$$D/a^2 = D_0/a^2 \exp (-E/RT) \quad (4)$$

where

$D$  = diffusion coefficient at some temperature  $T$ .

$D_0$  = rate constant

$a$  = effective radius of the sphere of argon diffusion

$E$  = activation energy

$R$  = gas constant

$T$  = absolute temperature

$D_0$  may be thought of as a function of the lattice

characteristics of a given material, and there is no reason to suppose that this is identical within a given solid solution series. The effective radius of the sphere of argon diffusion may vary from mineral to mineral and is not always a known quantity, therefore the diffusion parameter of (4) is the most useful (HART, 1960). FECHTIG and KALBITZER (1966) and MOORBATH (op. cit.) have recently reviewed the more reliable determinations of  $D$  or  $D/a^2$  for a number of minerals.

Experimentally determined activation energies, for the liberation of argon from biotite, range from 33kcal/mole to 86kcal/mole. GERLING et al. (1963) report activation energies of 33, 48 and 69kcal/mole for a biotite; each related to energetically different 'reservoirs' of argon in the mineral. The low activation energies probably result from non-volume, low temperature diffusion of loosely bound argon in structural defects. Reported activation energies for muscovites, on the other hand, are slightly higher, ranging from 56 kcal/mole. DENISENKO (1965) found three distinct activation energies for the liberation of argon from muscovite, 38, 52 and 83kcal/mole. It is interesting to note that geological estimates of diffusion parameters and activation energies are lower than experimental values. For example HURLEY et al (1962) give a geological estimate of  $E = 27$ kcal/mole for a biotite and WESTCOTT (1966) estimates





$E = 40\text{kcal/mole}$  also for a biotite. The reason for higher experimental values may result in part from violation of boundary conditions (i.e. samples may have lost argon at time of experiment) and incorrectly estimated thermal models for the geological conditions. HANSON and GAST (1967) in a very interesting piece of work, have estimated activation energies for argon liberation from biotite, K-feldspar, muscovite and hornblende from the aureole of the Snowbank stock, Minnesota, and biotite and hornblende from amphibolite near the contact with a quartz dolerite dyke in the Beartooth Mountains, Wyoming. They have interpreted their results assuming volume diffusion and zero and first order chemical reaction rate models. Note, the equation for the reaction rate of order  $n$  is given by:

$$\frac{dC}{dT} = -KC^n \quad (5)$$

in which  $n$  is the order of the reaction,  $C$  is the concentration of the species of interest,  $t$  is the time and  $K$  is a rate constant. The loss of radiogenic argon from biotite, assuming volume diffusion, was estimated at between 50 and 75kcal/mole, for a zero order model ( $n=0$  in equation 5) 25kcal/mole, and for a first order model about 50kcal/mole. Their estimates are more in keeping with experimentally determined values, but as yet insufficient cases have been studied to demonstrate which model is most applicable (i.e. volume diffusion or recrystallization).

The actual temperatures at which minerals become closed systems to the diffusion of radiogenic argon is not certain, but is probably around 200 to 300°C for muscovite and 150° to 200°C for biotite. There does appear to be a qualitative agreement between experimental studies concerning the probable relative 'closure' temperatures of micas and field studies. For example (HARPER (1967a) found muscovite from the Scottish Caledonides to be consistently 10 m.y. older than coexisting biotites.



Comparatively few reliable determinations of  $E$  and  $D/a^2$  have been made for amphiboles. GERLING et al. (1965) report activation energies ranging from 110 kcal/mole to over 200 kcal/mole for five amphiboles ranging in composition from riebeckite to pargasite, and note an inverse correlation between increasing total iron content and decreasing experimental activation energy. Investigations by HART (1961 and 1964) and STEIGER (1964) indicate that amphiboles may frequently yield older apparent ages than coexisting micas, as may be expected from the determined activation energies. Results obtained by HANSON and GAST (op.cit.) for hornblende, apparently varied from 75 - 100 kcal/mole in one situation, to around 200 kcal/mole in another. The authors suggested that a compositional influence may be the cause of the discrepancy, but had no chemical data on hand.

Argon liberation from minerals may be controlled by different factors during cooling from the temperature of crystallization and during reheating (HEIER, 1964, HARPER, 1967a). During cooling  $D_t/a^2$  will be the rate controlling step, whereas during updating or reheating of a mineral the activation energy will be the controlling step. In mineralogical terms this would mean that a phase, which has remained a closed-system and accumulated radiogenic argon since its formation, would upon an elevation of temperature retain argon until it had sufficient energy to surmount the potential barrier and move into a vacant or interstitial position, i.e. its removal would be dependent on the activation energy ( $E$ ). On the other hand during cooling the argon will have sufficient energy to surmount the potential barrier and its loss will merely depend upon the relative rates of argon production and its removal,  $\lambda$  and  $\lambda_d$ , where  $\lambda_d$  is the diffusion rate.

DAMON (1968) has given an equation which expresses the behaviour of the K-Ar system in minerals as it is presently understood after crystallization.





$$\frac{(Ar^{40}/K^{40})}{Ar_o^{40}/K^{40} \exp(-\lambda_d t_B)} = \exp(\lambda t_c) [\exp(-\lambda t_B) - \exp(-\lambda_d t_B)] + \frac{\lambda k}{\lambda} \exp(\lambda t_R - 1) + \quad (6)$$

where  $Ar_o^{40}$  = initial concentration of  $Ar^{40}$  in the system prior to radiogenic accumulation.

$\lambda_d$  = diffusion rate of  $Ar^{40}$

$t_c$  = time of crystallization

$t_B$  = time between crystallization and refrigeration

$t_R$  = time of refrigeration of argon in system.

The first term is for the period of accumulation with diffusional leakage ( $D_t/a^2$ ) controlling argon loss); the second term is for accumulation without leakage ('closure' to present); the third term is for excess  $Ar^{40}$  entering the mineral post-crystallization an improbable situation.

### Mica Apparent Ages

Some thirty-three K-Ar age determinations of micas have been carried out to include most of the datable lithologies in the area (Tables 1 and 2). From the foregoing discussion it should be clear that the apparent ages of micas are related to the time at which they became closed systems to the diffusion of radiogenic argon upon post-metamorphic uplift and cooling, or in the terms of ARMSTRONG (1966) passed through the 'metamorphic veil'.

The apparent ages of medium-grained micas from metasediments and metavolcanics in Bamble range from 1038 m.y. to 966 m.y. and are graphically presented in Fig 9 in terms of a numerical frequency diagram. The spread of apparent biotite ages would appear to be larger than expected from probable experimental errors and is most likely related to geological parameters. Consideration of Fig 2 does not reveal any logical geographical variation of





TABLE 1

Apparent K-Ar ages of metasediments and metavolcanics.

Number	Sample *	K <sup>40</sup> ppm.	Ar <sup>40</sup> /K <sup>40</sup>	%rad. Ar <sup>40</sup>	App. age m.y.
a) Micas.					
SN-36	Marble (P)	9.50	0.09092	99.6	1038 $\pm$ 16
SN-21	Biotite amphibolite (B)	6.83	0.08020	99.2	1030 $\pm$ 16
SN-23	Nodular Sillimanite gneiss (M)	11.05	0.08008	98.9	1029 $\pm$ 16
SN-20	Biotite schist (B)	8.96	0.07982	99.6	1027 $\pm$ 16
SN-10	Orthoamphibolite (B)	8.52	0.07977	99.4	1026 $\pm$ 16
SN-73	Amphibolite (B)	7.64	0.07816	99.9	1010 $\pm$ 16
SN-11	Granite gneiss (B)	9.28	0.07776	99.8	1006 $\pm$ 15
SN-79	Metaconglomerate (M)	10.53	0.07761	98.8	1005 $\pm$ 15
SN-56	Quartzite (B)	8.85	0.07769	99.9	1005 $\pm$ 16
SN-74	Augen gneiss (B)	7.46	0.07712	99.6	1000 $\pm$ 16
SN-75	Augen Gneiss (B)	8.42	0.07651	99.1	993 $\pm$ 15
SN-78	Quartzite (B)	9.21	0.07646	99.7	993 $\pm$ 15
SN-6	Graphitic gneiss (B)	8.79	0.07622	99.6	991 $\pm$ 15
SN-68	Garnet-biotite schist (B)	9.29	0.07581	99.6	986 $\pm$ 15
SN-3	Biotite schist (B)	8.01	0.07575	99.5	986 $\pm$ 15
SN-16	Graphitic schist (B)	8.51	0.07520	99.9	980 $\pm$ 15
SN-40	Biotite gneiss (B)	7.84	0.07469	99.3	975 $\pm$ 15
SN-54	Biotite gneiss (B)	7.36	0.07385	99.7	966 $\pm$ 15
SN-44	Granite gneiss (B)	7.95	0.06950	98.7	921 $\pm$ 14
SN-76	Augen gneiss (B)	6.86	0.06355	98.9	860 $\pm$ 14



TABLE 1 (Cont.)

## b) Amphiboles

SN-2	Amphibolite	0.59	0.08839	98.8	1110 $\pm$ 34
SN-9	Garnet amphibolite	0.60	0.08788	99.7	1105 $\pm$ 33
SN-10	Orthoamphibolite	1.64	0.08661	99.9	1093 $\pm$ 33
SN-22	Amphibolite	0.56	0.08492	97.9	1077 $\pm$ 33
SN-45	Amphibolite	0.65	0.08224	90.7	1050 $\pm$ 32
SN-16	Graphitic schist	1.35	0.08218	99.7	1050 $\pm$ 32
SN-21	Amphibolite	0.61	0.08193	92.4	1047 $\pm$ 32
SN-73	Amphibolite	1.02	0.08177	98.9	1046 $\pm$ 32
SN-38	Amphibolite	1.35	0.07913	95.5	1020 $\pm$ 31
SN-74	Augen Gneiss	1.88	0.07728	98.9	1001 $\pm$ 31
SN-70	Amphibolite	0.96	0.07652	99.2	994 $\pm$ 31
SN-71	Metagabbro	0.76	0.07419	90.5	970 $\pm$ 30

\* B=Biotite; M=Muscovite; P=Phlogopite



TABLE 2

Apparent K-Ar ages of gabbros, granites and pegmatites

Number	Sample *	K <sup>40</sup> ppm.	Ar <sup>40</sup> /K <sup>40</sup>	% rad. Ar <sup>40</sup>	App. age m.y.
a) Levang synkinematic 'granite'					
SN-57	Foliated Granite (B)	6.48	0.07729	99.9	1001±15
SN-61	Porphyritic granite (B)	7.62	0.07586	99.7	987±15
SN-59	Gneissic granite (B)	8.59	0.07528	99.5	981±15
SN-61	Porphyritic granite (H)	1.76	0.08285	94.3	1056±32
b) Ödegaarden apatite mines					
SN-26	Ödegaardite (H)	0.47	0.08887	98.5	1114±32
SN-89	Hornblende (massive)	0.82	0.08057	98.3	1034±32
SN-30	Phlogopite (apatite vein)	8.23	0.08043	92.3	1033±16
SN-27	Wall rock (P)	7.64	0.07894	99.3	1020±16
c) Gabbros					
SN-35	Pyroxenite (H)	0.54	0.07830	97.6	1012±31
SN-88	Massive hornblende	0.53	0.08065	96.1	1035±32
SN-35	Pyroxenite (P)	7.91	0.07582	99.2	987±15
d) Pegmatites and coarse grained metavolcanics					
SN-43	Plag. pegmatite (B)	8.65	0.08871	96.5	1112±17
SN-84	K-feld. pegmatite (M)	10.38	0.08641	94.7	1091±17
SN-85	Plag. pegmatite (B)	8.36	0.08452	96.2	1073±16
SN-42	Plag. pegmatite (B)	8.23	0.08390	95.3	1067±16





TABLE 2 (Cont.)

SN-86	Cordierite-anthophyllite rock (B)	8.26	0.08374	94.2	1065 $\pm$ 16
SN-12	Plag. pegmatite (B)	9.65	0.08120	93.3	1040 $\pm$ 16
SN-81	K-feld. pegmatite (B)	9.39	0.07893	91.3	1017 $\pm$ 16
SN-87	K-feld. pegmatite (B)	9.61	0.07790	94.9	1008 $\pm$ 16

\* B=Biotite; H=Hornblende; M=Muscovite; P=Phlogopite



apparent ages and it is unlikely that the spread can be related to simple thermal gradients at the time of cooling (cf HARPER, 1967b). From equation (3) it may be seen that the diffusion coefficient ( $D_t/a^2$ ) is inversely dependent upon the square of the radius of the sphere of argon diffusion and may potentially exert considerable control on the argon diffusion characteristics of a mineral. Studies of micas of variable grain size HART (1964) and ROSLER and PILOT (1967) indicate that, up to a limit, the actual physical grain size influences the retentivity of the mica, coarse-grained micas being more retentive than fine-grained micas. Since all samples were crushed to -60+120 mesh, grain size effects are difficult to evaluate but are undoubtedly present to some degree. In addition it may be expected that departures from ideal trioctahedral compositions (see FOSTER, 1960) together with polytypic variations could influence the argon retentivity of the biotites. GERLING, MOROZOVA and KURBATOV (1961) have demonstrated some effects of structural changes of micas on their argon retentivity. The relative influence of these parameters on the argon retentivity of the biotites cannot be evaluated on the basis of the present data. However, a detailed investigation in an area such as this, to include a large number of grain size fractions, and determinations of chemical compositions and structural state of the biotites, would undoubtedly prove exceedingly fruitful.

Only two medium-grained muscovite samples have been dated and it is not possible to draw any conclusions concerning their argon retentivity relative to biotite. Coarse-grained pegmatitic muscovites and biotites are as a group older than their enclosing metasediments and metavolcanics. They range in age from 1112 m.y. to 1008 m.y. and their distribution is indicated in Fig 9. O'NIONS et al. (1969) considered that grain size and compositional factors alone were not capable of explaining the dis-



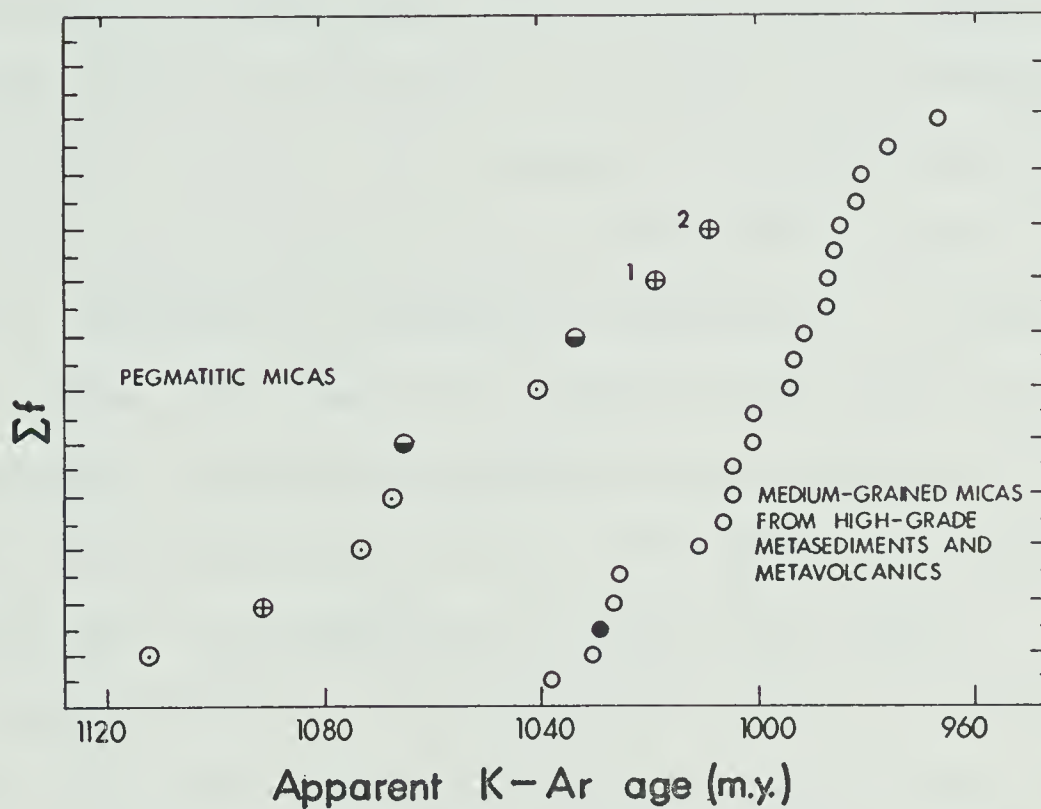


Fig.9. Cumulative frequency distribution of mica apparent ages. Small circles: medium-grained biotites (open circles) and muscovite (solid circles) from upper amphibolite facies metasedimentary and metavolcanic rocks. Dotted circles: coarse-grained biotites from concordant plagioclase pegmatites. Crossed circles: micas from discordant K-feldspar pegmatites (1 and 2 seen to be younger than the apatite deposits at Ødegaardens-verk.). Upper-half solid circles: biotite from cordierite-anthophyllite rock (included with the pegmatites in view of its coarse grain size). Lower half solid circles: phlogopite associated with chlorapatite at the Ødegaarden apatite mines.





tribution of apparent ages; for the most coarse-grained sample (SN-81) which was in excess of 19 cm. in diameter is considerably younger (1008 m.y.) than other finer-grained samples. It was therefore concluded that some of the discordant K-feldspar pegmatites, at least, were 1010 m.y. to 1020 m.y. old. This conclusion has not been validated by subsequent U-Pb dating (Chapter V) which suggests that the K-feldspar pegmatites are younger than the plagioclase pegmatites, but appear to be approximately 1100 m.y. old by U-Pb dating. It is doubtful if this difference between apparent K-Ar and U-Pb is entirely due to uncertainties in decay constants, and it seems to illustrate our incomplete understanding of the argon retentivity of micas. The plagioclase pegmatites which appear to be syn-kinematic from field observations have apparent ages ranging up to 1112 m.y. The muscovite apparent age of sample SN-84 ( $1091 \pm 17$ ) is very close to the apparent age of the pegmatites obtained by U-Pb dating.

The apparent K-Ar ages of the pegmatites provide an excellent illustration of grain size effects on the apparent ages of micas, but also demonstrates that other geological factors, at present little understood, may predominate over them. It would appear that the thermal maximum of the metamorphic event was obtained in excess of 1112 m.y. and that by 975 m.y. uplift had been sufficient to cool the area to around  $150^{\circ} - 200^{\circ}\text{C}$ .

The apparent ages of SN-44 and SN-76 do not fit into the general scheme of apparent ages. It is possible that they have been affected by a later thermal event. In the Arendal-Kristiansand district, post-kinematic granites (eg. Herefoss granite) have yielded apparent ages around 860 m.y.; however, field studies in the Kragerø district have not as yet revealed a possible cause for this updating. Also to be considered are the possibilities of parochial effects during the Permian period.



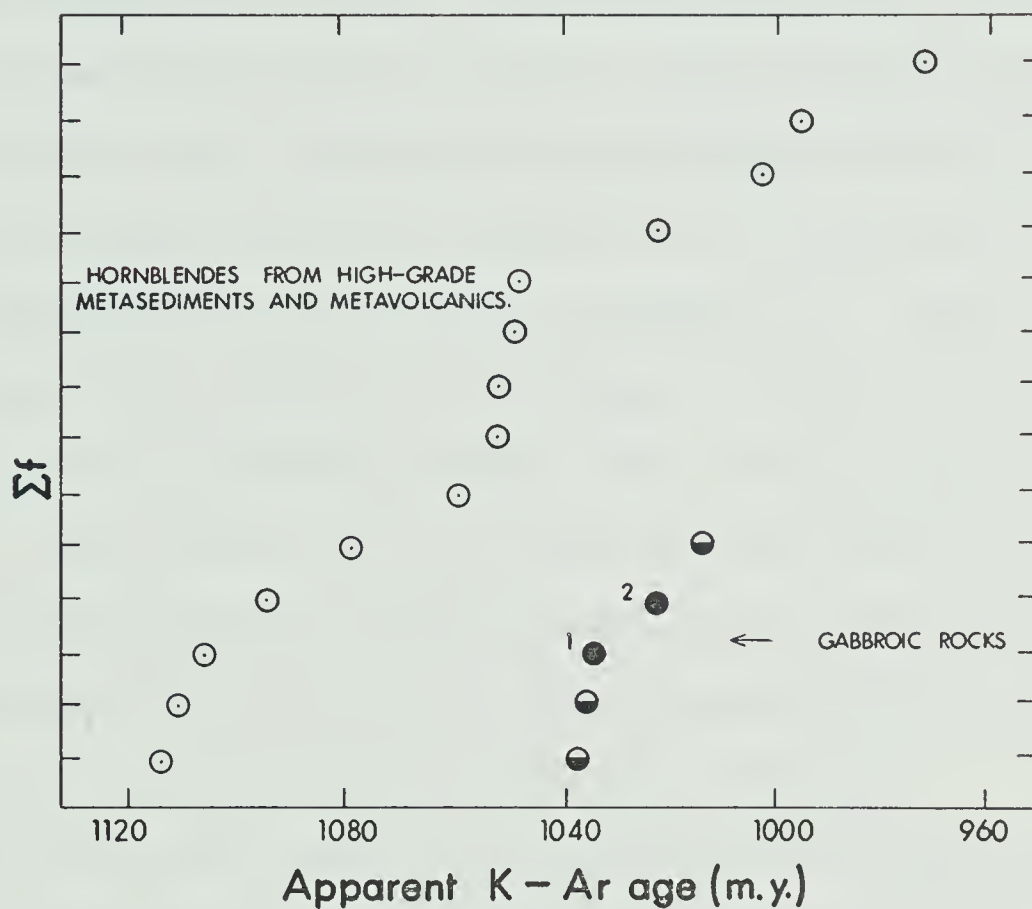


Fig.10. Cumulative frequency distribution of amphibole apparent ages from upper amphibolite facies metasedimentary and metavolcanic rocks together with apparent ages of late kinematic gabbroic rocks. Dotted circles: hornblendes from upper amphibolite facies rocks. Solid circles: coarse grained phlogopite from wall rock (2) at Ødergaarden Apatite Mines. Lower half-solid circles: amphiboles associated with late-kinematic gabbroic rocks.



### Amphibole Apparent Ages

Recent studies, such as those by STEIGER (1964), HART (1964) and BAADSGAARD and GODFREY (1967) support the contention of hornblendes having greater argon retentivities than micas. In the present study amphiboles have been analyzed from gneisses, amphibolites, granitic and gabbroic rocks and associated veins. Amphibole apparent ages (Tables 1 and 2) from metasediments and metavolcanics cover the same time span as do the mica apparent ages; a rather surprising result in view of the much higher experimental activation energies for  $\text{Ar}^{40}$  liberation from amphiboles, compared with micas obtained by GERLING et al. (1965) and the high argon retentivities exhibited by amphiboles in contact metamorphic environments (HART, 1964; HANSON and GAST, 1967, see also discussions by DAMON, 1968). This observation is not unique however, WEBB and McDOUGALL (1968) have recently reported on Permo-Triassic ages of amphiboles from Eastern Queensland, which appear to have had argon retentivities similar to biotites under zeolite facies metamorphic conditions.

One may infer that under certain conditions the diffusion constant is sufficiently high in some amphiboles to permit the loss of radiogenic argon at comparatively low temperatures ( $\sim 200^{\circ}\text{C}$ ). For the amphiboles from South Norway this appears to have occurred in high Fe-amphiboles. The following section is entirely devoted to a discussion of the amphiboles' apparent ages in the light of their crystal chemistry and thus further reference to compositional influences on the argon retentivity of amphiboles will not be made here.

Amphiboles associated with gabbroic intrusions, SN-88, SN-89, and SN-35 have apparent ages of 1034, 1035 and 1012 m.y. respectively. Analyses presented in the next section show them all to be high-Mg amphiboles and supposedly very retentive. Coarse-grained phlogopite from a productive





apatite vein at Ødegaardens-verk (SN-30) and medium-grained phlogopite from the wall rock (SN-27) have apparent ages of 1033 and 1020 m.y. respectively. These apparent ages may indicate a parochial event in the neighbourhood of the Ødegaardens-verk gabbro and the Bjordammen gabbro at 1030 m.y., the nature of which is not at all clear at present.

Further reference will be made to the K-Ar apparent ages after discussion of the U-Th-Pb results and Rb-Sr results, when all this data will be discussed in terms of a metamorphic and tectonic history.



## CHAPTER IV CRYSTAL CHEMISTRY AND ARGON RETENTIVITY OF CALCIC AMPHIBOLES

Introduction

From the discussion of the amphibole apparent ages in the previous section, it will be recalled that the amphiboles from metasediments and metavolcanics range in apparent age from 1114( $\pm 32$ ) m.y. to 970( $\pm 30$ ) m.y.; a spread which covers the same time-span as the mica apparent ages and is in excess of probable experimental error. Such results may appear surprising in view of the much greater apparent argon retentivity exhibited by amphiboles, compared with micas, where studied in contact metamorphic environments, and the high activation energies required to produce volume diffusion of  $\text{Ar}^{40}$  in laboratory experiments. (KOTLOVSKAYA, 1964, GERLING, et al. 1965).

HARPER (1967b) has related apparent K-Ar ages of biotites from metasediments and metavolcanics in the Grenville Province (ranging in age from 1125 m.y. to 860 m.y.), to differential uplift of the Grenville cratonic block through a single isothermal surface. Such a relationship would not appear to hold for the amphiboles from the Bamble-Risør area, as there is no obvious systematic geographical variation of apparent ages, as might be expected to result from such circumstances.

Since the radius of the effective sphere of argon diffusion in amphiboles is likely to be less than the physical grain size considered (approximately 30 microns as compared with more than 1000 microns, HART, 1960) the apparent ages of the amphiboles would appear to be related to features of their crystal chemistry.

Electron Microprobe Analyses

Separated amphibole grains ( $-60+120$  mesh) were mounted in an epoxy-resin and polished for electron probe analysis. An Applied Research Lab-



oratories 'EMX' microprobe equipped with a light element channel and two normal channels was utilized for the analysis of F, Na, Mg, Si, Al, Cl, K, Ca, Ti, Mn, and Fe. Peaks and backgrounds were counted for 50 sec. periods, while randomly traversing individual grains; a minimum of ten grains being counted for each sample. The samples were counted versus a biotite standard (EP/S12-2) for the analysis of Si, K, Ti, a second biotite standard (EP/S12-1) for the analysis of Cl and Mn, a clinopyroxene (EP/S6-13) for Ca and Na and a garnet (EP/S12-4) for the analysis of Fe and Mg. In order to monitor drift effects the standards were measured at the beginning and end of each 'batch' of samples.

All the amphiboles were found to be apparently homogeneous, within experimental error, with respect to the analyzed elements. Corrections were applied to the apparent concentrations of each element except fluorine, for atomic number, absorption and fluorescence effects employing an APL-360 program written by D.G.W. Smith and M.C. Tomlinson. The atomic number correction employed, utilized the stopping power and back-scattering coefficients of DUNCUMB and REED (1967). The absorption correction was applied by a method similar to that given by HEINRICH (1967), using the mass absorption coefficients of HEINRICH (1966). The fluorescence correction used was a modification of the original Castaing formula for possible K-L, L-K, and L-L excitations by REED (1965).

Analyses of the sixteen amphiboles considered in Chapter III are given in Table 3 together with structural formulae calculated on the basis of twenty-three oxygens. Values for  $\text{Fe}_2\text{O}_3$  were obtained by difference between the electron probe total iron analyses and wet chemical determinations of ferrous iron performed on further purified amphibole separates. The procedure used for ferrous iron determinations is identical to the  $\text{KMnO}_4$  titration method employed in the Rock Analyses





TABLE 3

Electron probe analyses of amphiboles and mineral structural formulas on the basis of 23 oxygens.  
(Note: FeO determined by wet chemical analysis.)

Amphiboles from metasediments, metavolcanics													Amphiboles associated with gabbros		
Sample	SN-22	SN-45	SN-26	SN-2	SN-21	SN-38	SN-16	SN-73	SN-10	SN-74	SN-71	SN-70	SN-88	SN-89	SN-35
SiO <sub>2</sub>	42.50	44.07	45.03	43.32	42.56	42.48	42.50	43.24	41.69	39.50	43.30	42.92	44.50	45.13	42.45
TiO <sub>2</sub>	1.08	1.46	3.07	1.24	1.07	1.73	1.69	1.90	2.53	2.09	1.94	1.94	1.70	2.14	0.71
Al <sub>2</sub> O <sub>3</sub>	13.70	13.04	11.31	13.23	13.58	11.91	12.77	10.48	11.79	12.03	12.14	11.93	11.58	9.07	15.66
Fe <sub>2</sub> O <sub>3</sub>	3.76	2.70	1.78	4.79	4.86	1.49	2.75	3.63	4.26	5.66	6.89	1.89	2.33	3.10	2.83
FeO	11.68	12.08	6.08	12.72	13.44	15.48	14.55	15.08	16.67	19.06	18.88	20.35	8.72	12.00	7.67
MnO	0.30	0.30	0.22	0.27	0.27	0.31	0.28	0.32	0.31	0.36	0.37	0.36	0.18	0.26	0.23
MgO	12.13	12.21	16.78	11.21	10.38	10.28	9.33	10.33	8.34	5.59	5.08	7.42	15.21	12.97	15.27
CaO	10.92	10.42	11.47	10.27	10.51	11.28	11.20	11.01	10.85	10.73	10.25	10.16	10.80	10.63	10.23
Na <sub>2</sub> O	1.72	1.73	3.15	1.85	1.88	1.91	1.47	1.91	1.90	1.87	2.02	1.93	2.26	2.70	3.45
K <sub>2</sub> O	0.57	0.61	0.52	0.62	0.59	1.38	1.40	1.08	1.59	1.95	0.78	0.99	0.54	0.80	0.52
F	*	0.06	0.04	0.18	*	0.08	0.20	*	*	0.10	*	*	0.09	0.24	0.03
Cl	0.19	0.21	0.52	0.03	0.08	0.52	0.28	0.17	0.13	1.01	0.03	0.04	0.85	0.62	1.01
-O≡F	-	0.03	0.02	0.08	-	0.03	0.08	-	-	0.04	-	-	0.04	0.10	0.01
-O≡Cl	0.04	0.05	0.12	0.01	0.02	0.12	0.06	0.04	0.03	0.23	0.01	0.01	0.19	0.14	0.23
Total	98.81	98.81	99.83	99.64	99.20	98.70	98.28	99.11	100.3	99.68	101.67	99.92	98.53	99.42	99.32
Structural formula on the basis of 23 oxygens															
Si	6.229	6.406	6.368	6.303	6.250	6.359	6.353	6.434	6.228	6.100	6.389	6.420	6.442	6.606	6.070
Al	1.771	1.594	1.632	1.697	1.750	1.641	1.647	1.566	1.772	1.900	1.611	1.580	1.558	1.394	1.930
Σ tetra-hedral	8.000	8.000	8.000	8.000	8.000	8.000	8.000	8.000	8.000	8.000	8.000	8.000	8.000	8.000	8.000
Al	0.596	0.640	0.253	0.572	0.601	0.461	0.603	0.272	0.340	0.290	0.501	0.524	0.418	0.171	0.709
Ti	0.119	0.160	0.327	0.136	0.118	0.195	0.190	0.213	0.284	0.243	0.215	0.218	0.185	0.236	0.076
Fe <sup>3+</sup>	0.415	0.295	0.189	0.524	0.532	0.168	0.309	0.406	0.479	0.658	0.765	0.213	0.254	0.341	0.304
Fe <sup>2+</sup>	1.432	1.469	0.719	1.548	1.651	1.938	1.819	1.876	2.083	2.462	2.330	2.546	1.056	1.469	0.917
Mn	0.037	0.037	0.026	0.033	0.034	0.039	0.035	0.040	0.039	0.047	0.046	0.056	0.022	0.032	0.028
Mg	2.650	2.645	3.536	2.431	2.272	2.293	2.079	2.291	1.856	1.286	1.117	1.654	3.281	2.830	3.254
Σ octa-hedral	5.249	5.246	5.050	5.244	5.213	5.094	5.035	5.098	5.046	4.987	4.974	5.201	5.216	5.079	5.288
Ca	1.715	1.623	1.738	1.601	1.654	1.809	1.794	1.755	1.737	1.775	1.621	1.628	1.675	1.667	1.567
Na	0.489	0.488	0.864	0.522	0.535	0.554	0.426	0.551	0.550	0.560	0.578	0.560	0.634	0.766	0.956
K	0.107	0.113	0.094	0.115	0.111	0.264	0.267	0.205	0.303	0.384	0.147	0.189	0.100	0.149	0.095
Σ large	2.311	2.224	2.996	2.238	2.300	2.627	2.487	2.511	2.590	2.719	2.346	2.377	2.409	2.582	2.618
Mean M <sub>2</sub> ordered	0.6111	0.6089	0.6390	0.6118	0.6095	0.6238	0.6115	0.6354	0.6324	0.6316	0.6148	0.6185	0.6261	0.6437	0.6037
Mean M <sub>2</sub> disordered	0.6660	0.6659	0.6661	0.6679	0.6686	0.6796	0.6728	0.6833	0.6850	0.6923	0.6833	0.6870	0.6653	0.6798	0.6547

\* Undetected



Laboratory of the Dept. of Geology, University of Alberta.  $\text{H}_2\text{O}^+$  was not determined in any of the samples, due to the difficulty in obtaining reliable values by standard techniques. It is apparent, however, that the totals are somewhat high even allowing for only a small amount of water. Some systematic error in the garnet standard (EP/S12-4) is suspected to be the cause of the high totals, but efforts to locate this have been unsuccessful up to the time of writing. Some check on the accuracy of the electron probe K-determinations is provided by the analyses of the separates by KTPB precipitation (Table 4). One would expect the small amounts of impurity undoubtedly present to produce slightly lower values for the KTPB analyses compared with the electron probe analyses and this is generally the case.

#### X-Ray Study

A Norelco X-Ray Diffractometer was employed to obtain diffractograms for all of the amphiboles in the range of  $10^\circ$  to  $70^\circ$   $2\theta$ . Sodium fluoride mixed in a ratio of approximately 3:1 with finely ground sample was used as an internal standard in each instance. The measured d-spacings for each of the amphiboles are listed in Appendix D. The unit cell parameters a, b, c, and  $\beta$  were determined using a least-squares unit cell refinement program, employing variable-indexing options, written by EVANS, APPLEMAN and HANDWERKER (1963). A modified FORTRAN IV version of this program was supplied to the author by J.J. Papike.

The criteria imposed by the program for acceptance of a given reflection in a current least-squares solution for a fixed-indexed line is:-

$$| \theta_{\text{obs}} - \theta_{\text{calc}} | \times (\text{weight})^{1/2} \leq T\theta L$$

where the weight and tolerance limits ( $T\theta L$ ) are selected by the operator. For non-fixed indexing the theoretical reflection generated by the program with the closest value of interplanar spacing to the observed d-spacing is



chosen for further consideration and to be accepted in a current least-squares solution must satisfy the following relationship:

$$\begin{aligned} & |\theta_{\text{obs}} - \theta_{\text{calc}}| \times (\text{weight})^{1/2} > T\sigma_L && \text{(preceding observation)} \\ \text{and} \quad & |\theta_{\text{obs}} - \theta_{\text{calc}}| \times (\text{weight})^{1/2} > T\sigma_L && \text{(following observation)} \end{aligned}$$

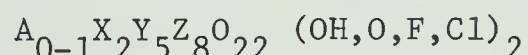
It is usual to adjust the 'weight' factor according to the observed intensity of the reflection.

Unit cell parameters were calculated taking into consideration only those reflections compatible with C2/m symmetry (Table 5). Since there are four unknowns, a minimum of four d-spacings are required for the determination of a, b, c and  $\beta$  and these results would obviously have the maximum possible errors. Therefore it is desirable that at least ten d-spacings should be accepted in the final least-squares refinement cycle, in order to obtain reasonable estimates of the unit cell parameters and meaningful quoted errors.

### Crystal Chemistry of Calcic Amphiboles

Recent reviews and discussions of the crystal chemistry of amphiboles have been published by DEER, HOWIE and ZUSSMAN (1962), COLVILLE et al. (1966) and ERNST (1968). LEAKE (1965) and KOSTYUK and SOBOLEV (1969) have more specifically discussed in some detail the chemistry of metamorphic calcic amphiboles. Features of the crystal chemistry of calcic amphiboles pertinent to the present discussion of their argon retentivities will be briefly reviewed and for more extensive treatments the reader is referred to the literature cited above.

A generalized structural formula for amphiboles may be written as:-



The coördination of the cations is, A=10, X=6-8, Y=6 and Z=4.

In the amphibole unit there are fourteen non-equivalent structural sites. Three of the anion sites ( $O_5, O_6$  and  $O_7$ ) each share two Z-cations and three ( $O_1, O_2$  and  $O_4$ ) are each bound to one Z-cation and one X or Y-cation; the anion site ( $O_3$ ) containing OH, F, or Cl lies at the apex of a squat, pseudo-





TABLE 4

Comparisons of gravimetric and electron probe analyses of potassium  
in amphiboles.

<u>Sample</u>	<u>K<sub>2</sub>O(KTPB)%</u>	<u>K<sub>2</sub>O (Probe)%</u>
SN-22	0.55	0.57
SN-45	0.64	0.61
SN-26	0.47	0.52
SN-2	0.58	0.62
SN-21	0.60	0.59
SN-38	1.34	1.38
SN-16	1.34	1.40
SN-73	1.01	1.08
SN-10	1.62	1.59
SN-74	1.86	1.95
SN-71	0.75	0.78
SN-70	0.95	0.99
SN-88	0.52*	0.54
SN-89	0.81	0.80
SN-35	0.51	0.52

\*Average of nine analyses.



TABLE 5

UNIT CELL PARAMETERS.

Sample	a(Å)	b(Å)	c(Å)	$\beta^\circ$	V(Å <sup>3</sup> )
SN-22	9.875±0.007	18.07±0.002	5.355±0.02	105°29'	920.9
SN-45	9.842±0.022	18.100±0.004	5.294±0.001	104°50'	911.2
SN-26	9.772±0.007	18.07±0.02	5.364±0.020	103°0.5'	923.2
SN-2	9.850±0.04	18.110±0.01	5.296±0.005	103°37'	918.2
SN-21	9.847±0.012	18.093±0.002	5.255±0.005	105°16'	902.2
SN-38	9.899±0.010	18.135±0.009	5.333±0.005	105°8'	924.4
SN-16	9.909±0.010	18.118±0.009	5.301±0.001	104°27'	921.6
SN-73	9.873±0.004	18.161±0.006	5.266±0.002	105°10'	911.4
SN-10	9.884±0.003	18.201±0.010	5.283±0.006	104°43'	919.4
SN-74	9.874±0.005	18.205±0.007	5.271±0.003	104°11'	918.7
SN-71	9.834±0.019	18.102±0.014	5.387±0.027	102°48'	935.2
SN-70	9.918±0.035	18.136±0.027	5.326±0.04	104°46'	926.6
SN-88	9.836±0.002	18.072±0.015	5.316±0.001	104°50'	913.5
SN-89	9.812±0.005	18.093±0.010	5.380±0.006	102°45'	931.5
SN-35	9.864±0.016	18.049±0.010	5.302±0.002	104°58'	911.8

Note: Unit cell parameters are calculated for CuK $\alpha$  radiation ( $\lambda = 1.5405 \text{ Å}$ ).

NaF used as an internal standard.



trigonal pyramid, the base of which is formed by three bivalent cations, two of which are in crystallographically equivalent  $M_1$  positions (GHOSE, 1961). Of the remaining seven cation sites, two are tetrahedral sites ( $Si_I$  and  $Si_{II}$ ), three are octahedral sites ( $M_1$ ,  $M_2$  and  $M_3$ ), one is a site of eight-fold coordination ( $M_4$ ) and one is a site of ten-fold coordination (A). The octahedral sites  $M_1$ ,  $M_2$  and  $M_3$  are occupied by Y-cations and  $M_4$  is occupied by X-cations. In calcic amphiboles  $Ca+Na$  is usually greater than two cations per twenty-four anions, therefore the 'excess' Na and K is usually assigned to the A-site. Natural calcic amphiboles may contain a variety of cations in  $M_1$ ,  $M_2$  and  $M_3$  including (DEER, HOWIE and ZUSSMAN, op. cit.) Mg,  $Fe^{2+}$ ,  $Fe^{3+}$ , Al, Ti, Ni, Al, Cr, Sn, and Co however, Mg,  $Fe^{2+}$ ,  $Fe^{3+}$  and Al are by far the most common. It should be noted that in calcic amphiboles the  $Si_I$  and  $Si_{II}$  sites are partially occupied by Al in tetrahedral coordination ( $Al^{IV}$ ) and are not entirely occupied by Si.

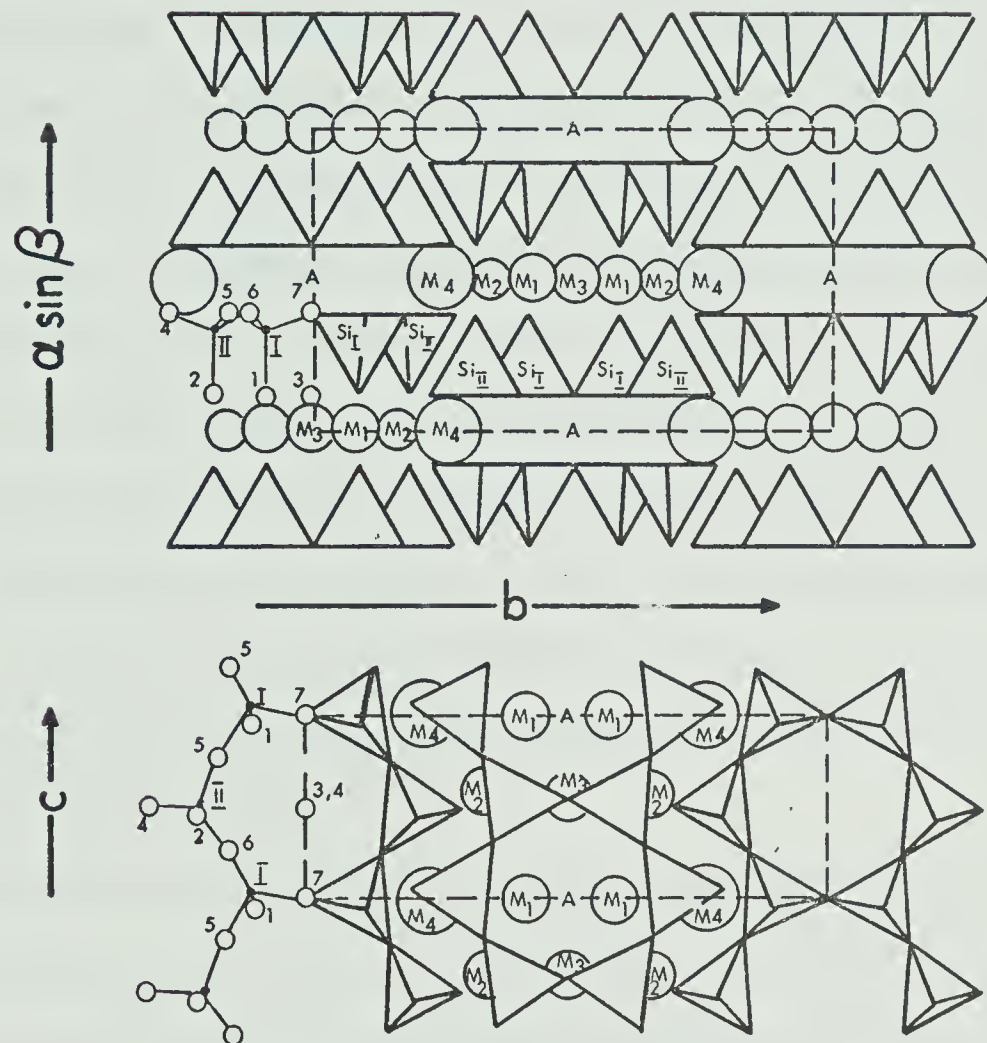
Order-disorder relationships in amphiboles are currently topics of considerable interest to mineralogists, but investigations are still very much in their infancy. Structural refinements on crocidolite (magnesioriebeckite) by WHITTAKER (1949) suggested that  $Fe^{2+}$  and Mg are equally distributed amongst the slightly larger  $M_1$  and  $M_3$  sites, with the smaller  $Fe^{3+}$  and  $Al^{VI}$  concentrated in  $M_2$ . Subsequent structural refinements of cummingtonite, grunerite and alkali amphiboles by a number of workers (see review by ERNST, 1968) have demonstrated partial ordering amongst the Y-cations as follows:

1.  $M_4$  usually contains the largest proportion of X-cations.
2. Y-cations of intermediate size are distributed between  $M_1$  and  $M_3$ , with a possible preference for the larger in  $M_3$ .
3. Smallest Y-cations tend to be concentrated in  $M_2$ .

Infrared absorption studies of amphiboles by STRENS (1966) and BURNS and STRENS (1966) together with Mossbauer spectral studies of BANCROFT, BURNS,







## CRYSTAL CHEMISTRY OF THE AMPHIBOLES

Fig.11. Generalised crystal chemistry of the amphiboles. Note the location of the  $M_1$ ,  $M_2$ , and  $M_3$  sites within the amphibole structure.(after ERNST,1968).



and MADDOCK (1967) have also indicated this site preference.

The relative influence of differences in the occupancy of the identified sites in the amphibole structure on their unit cell dimensions is largely derived from a knowledge of synthetic and natural end-member amphibole compositions. A measure of the double-chain width in amphiboles is given by the normal distance from the  $\text{Si}_{\text{II}}$  site to the a-c plane, parallel to the 'b' axis (Fig 11b). For tremolite, Colville et al. (op.cit.) have calculated the  $\text{Si}_{\text{II}}$ -b distance as 3.07Å and for actinolite the same authors have calculated an  $\text{Si}_{\text{II}}$ -b distance of 3.08Å. The chain width parallel to 'b' would appear to be quite insensitive to compositional variations. In the a.sin  $\beta$  direction, the chain thickness is fairly constant, as is the c-repeat distance. Variations in the double-chain width are small and the double chains appear to be fairly inflexible units of the amphibole structure. Since the size of the A-site is controlled by the double chain dimensions, this also may be assumed to be invariable in clinoamphiboles.

All but variations in 'Y' -occupancy have been eliminated as causing significant variations in the unit cell parameters. In calcic amphiboles variations in 'b' are the most significant and since  $M_1$  and  $M_3$  are well within the double chains (Fig 11), variation in their occupancy can only be reflected in the value of a.sin  $\beta$ . The chain linking cations  $M_2$  and  $M_4$  on the margins of the chains must, therefore, be primarily responsible for variations in the 'b' unit cell dimensions, and since in any one particular series of calcic amphiboles the occupancy  $M_4$  is almost invariant, the occupancy of  $M_2$  must be primarily responsible.

Normally the 'b' axis length is seen to increase at about four times the computed mean atomic radius increment of the  $M_2$  site, indicating a one to one correlation between ionic size and unit cell dimension (only two  $M_2$  sites are intersected in one 'b' unit repeat.). The a. sin dimension (which is the





projected length of the a-axis normal to the b-c plane) increases as the mean  $M_2$  or Y-cation radius increases.

From the data of ERNST (op. cit) it can be seen that the relationship between the mean cation radius of the  $M_2$  site and the b-axis length is more nearly linear assuming that the  $M_2$  site is disordered. This is in some ways predictable, since synthetic studies have generally indicated that high-temperature, low-pressure minerals show less order than high-pressure, low-temperature minerals. COLVILLE et al. (1966) have shown the glaucophane II polymorph to be approximately 50% more ordered than high temperature glaucophane I. By analogy with Al-rich and Al-deficient synthetic amphiboles it is probable that, at least in high-temperature and low-pressure amphiboles, ordering of Y-cations is not as important as is usually assumed (ERNST, op.cit.).

### Crystal Chemistry of Dated Amphiboles

#### 1. Compositional Variations.

The major element variations of the analysed calcic amphiboles are plotted in Fig 12, in terms of the following four end-members: pargasite + magnesiohastingsite  $[\text{NaCa}_2\text{Mg}_4(\text{Al}, \text{Fe}^{3+})\text{Si}_6\text{Al}_2\text{O}_{22}(\text{OH})_2]$ , ferropargasite + hastingsite  $[\text{NaCa}_2\text{Fe}_4^{2+}(\text{Al}, \text{Fe}^{3+})\text{Si}_6\text{Al}_2\text{O}_{22}(\text{OH})_2]$ , tremolite  $[\text{oCa}_2\text{Mg}_5\text{Si}_8\text{O}_{22}(\text{OH})_2]$  and ferrotremolite  $[\text{oCa}_2\text{Fe}_5^{2+}\text{Si}_8\text{O}_{22}(\text{OH})_2]$  after the method of COLVILLE et al. (op.cit.). It is apparent that a considerable compositional range is represented from near the ferropargasite + hastingsite composition to near the pargasite + magnesiohastingsite composition.

Recently KOSTYUK and SOBOLEV (1969) have compiled some 550 reliable analyses of metamorphic calcic amphiboles and have attempted to relate, in a quantitative manner, the amphibole composition to metamorphic grade and host rock composition. The amphibole analyses reported here are comparable to the averages of calcic amphibole analyses given by Kostyuk and Sobolev from similar grades





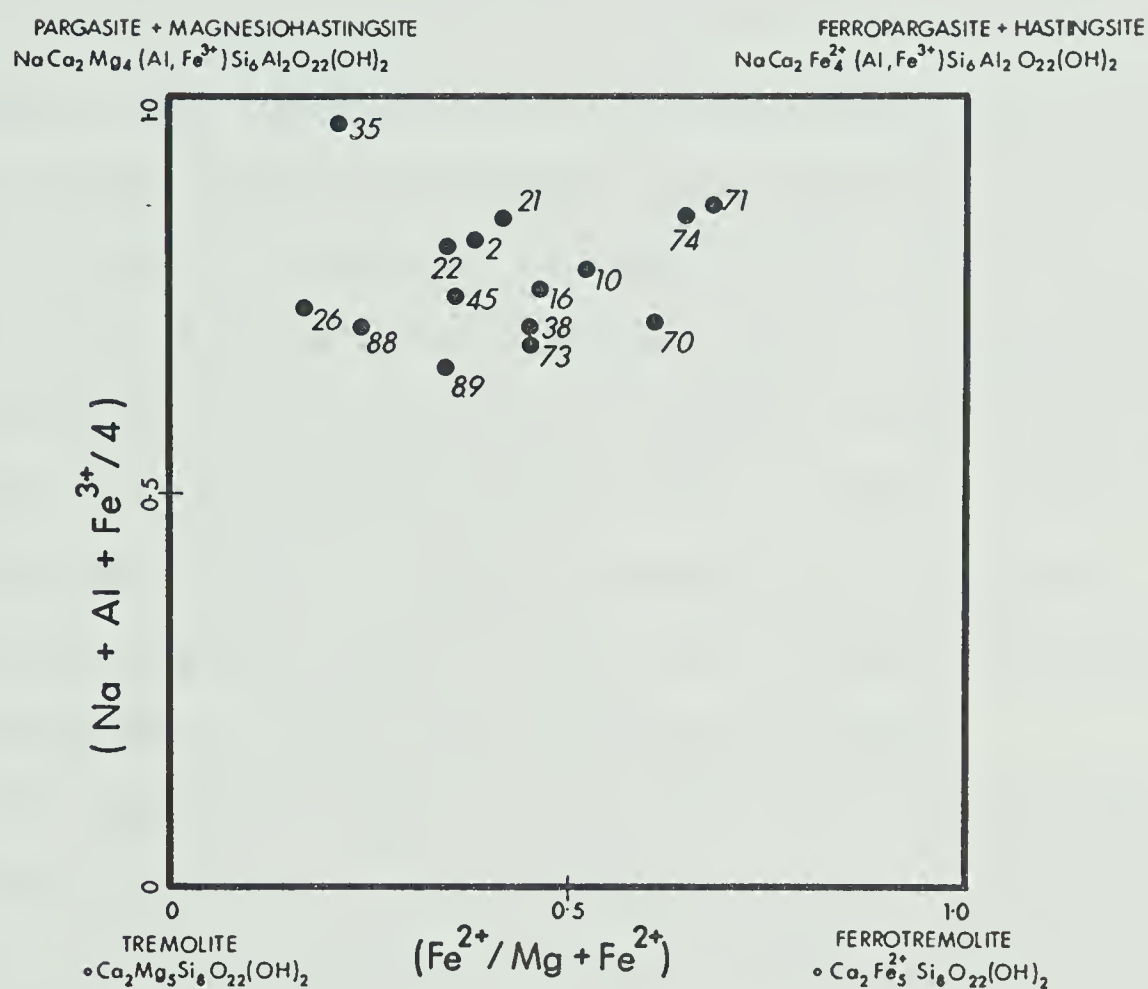


Fig.12. Element variation in the Bamble metamorphic calcic amphiboles in terms of the end-members pargasite+magnesiohastingsite, ferropargasite+hastingsite, tremolite and ferrotremolite.



of metamorphism and lithologies, in terms of their  $\text{Al}^{\text{IV}}$  and  $\text{Al}^{\text{VI}}$  contents.

As a result of the complex chemistry of calcic amphiboles the various possible atomic substitutional variations, particularly coupled substitutions, are little understood. When considering the possibilities, one must attempt to evaluate the effects of temperature, pressure and host rock composition, in addition to the partitioning effects of various elements with coexisting phases. LEAKE (1966) has shown that higher temperatures tend to favour higher titanium contents, since igneous calcic amphiboles have higher Ti contents for a given Si content than metamorphic calcic amphiboles, and ENGEL and ENGEL (1962) studying calcic amphiboles from the Adirondacks have shown that total alkalis and titanium tend to increase in passing from the upper amphibolite facies to the hornblende granulite facies. ENGEL and HAVENS (1964) have demonstrated the influence of host rock chemistry on the amphibole composition particularly with respect to their alkali contents, in addition to the partitioning effects of sodium with coexisting plagioclase.

The calcic amphiboles sampled in this study are all from the upper amphibolite facies and, as far as can be ascertained, close to the conditions characterising the univariant reaction from close to muscovite plus quartz to sillimanite plus orthoclase.

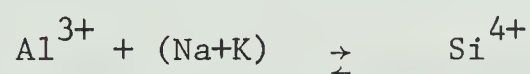
It cannot, however, be claimed that they are an isothermal-isobaric suite of amphiboles, but it might be expected that variations due to metamorphic grade are subordinate compared with variations due to the composition of coexisting phases and therefore host rock chemistry.

Some insight as to the nature of possible substitutions in a given atomic-substitution (or solid-solution) series may be obtained from calculated correlation coefficients between elements. The high degree of variation in  $\text{Fe}^{2+}$  and Mg in the analysed amphiboles is obvious from a mere cursory examination of the analyses, but it is not possible to evaluate other more complex, possibly



coupled, substitutions without a closer statistical examination.

The substitution of  $\text{Al}^{\text{IV}}$  for Si in tetrahedrally coordinated  $\text{Si}_{\text{I}}$  and  $\text{Si}_{\text{II}}$  produces a charge deficiency, which could be compensated for by extra alkali cations in the A sites. KOSTYUK and SOBOLEV (op.cit.) note a positive correlation between  $\text{Al}^{\text{IV}}$  and Na+K in their study; suggesting to them that the following substitution may be possible:



The positive correlation coefficient of 0.265 between Na+K and  $\text{Al}^{\text{IV}}$  (Table 6) obtained for the amphiboles in this study is not significant and suggests that the variations in  $\text{Al}^{\text{IV}}$  are small, as might be expected under fairly constant total pressure-temperature conditions. The high degree of correlation (Table 6) between  $\text{Fe}^{2+}$  and Mg is predictable; the best-fit straight line through the data having a negative slope of 1.2.

Of particular interest is the strong positive correlation (0.778) between (Na + K) and Ti and the strong negative correlation (0.734) between  $\text{Al}^{\text{VI}}$  and Ti. The slope of the best-fit line, through the data points in a plot of (Na + K) versus Ti, is 1.64, suggesting that for an increase of one Ti atom, there is a concomitant increase of approximately 1.6 atoms of total alkali; whereas a similar plot of  $\text{Al}^{\text{VI}}$  versus Ti has a negative slope of 1.9 suggesting a decrease of approximately two  $\text{Al}^{\text{VI}}$  atoms for an increase of one Ti atom. As far as the author is aware this is the first time this feature has been noted in metamorphic calcic amphiboles, although similar correlations may be noted in the table of correlation coefficients presented by KOSTYUK and SOBOLEV (op. cit.). It is of interest to inquire how these two features may be related. A coupled substitution of the following type is suggested:



In this case, charge neutrality might be maintained in the structure by the location of additional alkali atoms in vacant A sites. A plot of  $\text{Ti} + 2 (\text{Na}+\text{K})$





TABLE 6

## CORRELATION COEFFICIENTS BETWEEN ELEMENTS IN CALCIC AMPHIBOLES.

	Si	Ti	Al <sup><u>iv</u></sup>	Al <sup><u>vi</u></sup>	Fe <sup>3+</sup>	Fe <sup>2+</sup>	Mn	Mg	Ca	Na	K	Na+K
Na+K	<u>0.265</u>	(0.778) <u>0.335</u>	0.265	0.484	<u>0.129</u>	<u>0.025</u>	<u>0.070</u>	0.147	0.172	<u>0.755</u>		
K	<u>0.305</u>	0.317	0.305	<u>0.429</u>	0.235	<u>0.734</u>	<u>0.600</u>	<u>0.661</u>	<u>0.744</u>	0.387		
Na	<u>0.058</u>	0.110	0.058	<u>0.177</u>	<u>0.289</u>	<u>0.600</u>	<u>0.478</u>	<u>0.600</u>	<u>0.341</u>			
Ca	<u>0.075</u>	0.392	0.075	<u>0.385</u>	<u>0.101</u>	0.323	<u>0.220</u>	<u>0.230</u>				
Mg	0.173	0.136	<u>0.173</u>	0.064	<u>0.653</u>	<u>0.958</u>	<u>0.861</u>					
Mn	<u>0.109</u>	0.118	0.109	<u>0.097</u>	0.336	<u>0.927</u>						
Fe <sup>2+</sup>	<u>0.083</u>	0.164	0.083	<u>0.169</u>	0.466							
Fe <sup>3+</sup>	<u>0.334</u>	<u>0.068</u>	0.334	<u>0.036</u>								
Al <sup><u>vi</u></sup>	<u>0.321</u>	<u>0.734</u>	0.320									
Al <sup><u>iv</u></sup>	<u>1.000</u>	<u>0.357</u>										
Ti	0.357											
Si												

n= 16

 $r_{\text{(signif)}} \geq 0.49$ 

at 95% confidence limits.

Note: The correlation coefficient in parentheses between Na+K and Ti is for all samples except SN-35. Significant correlations are underlined.



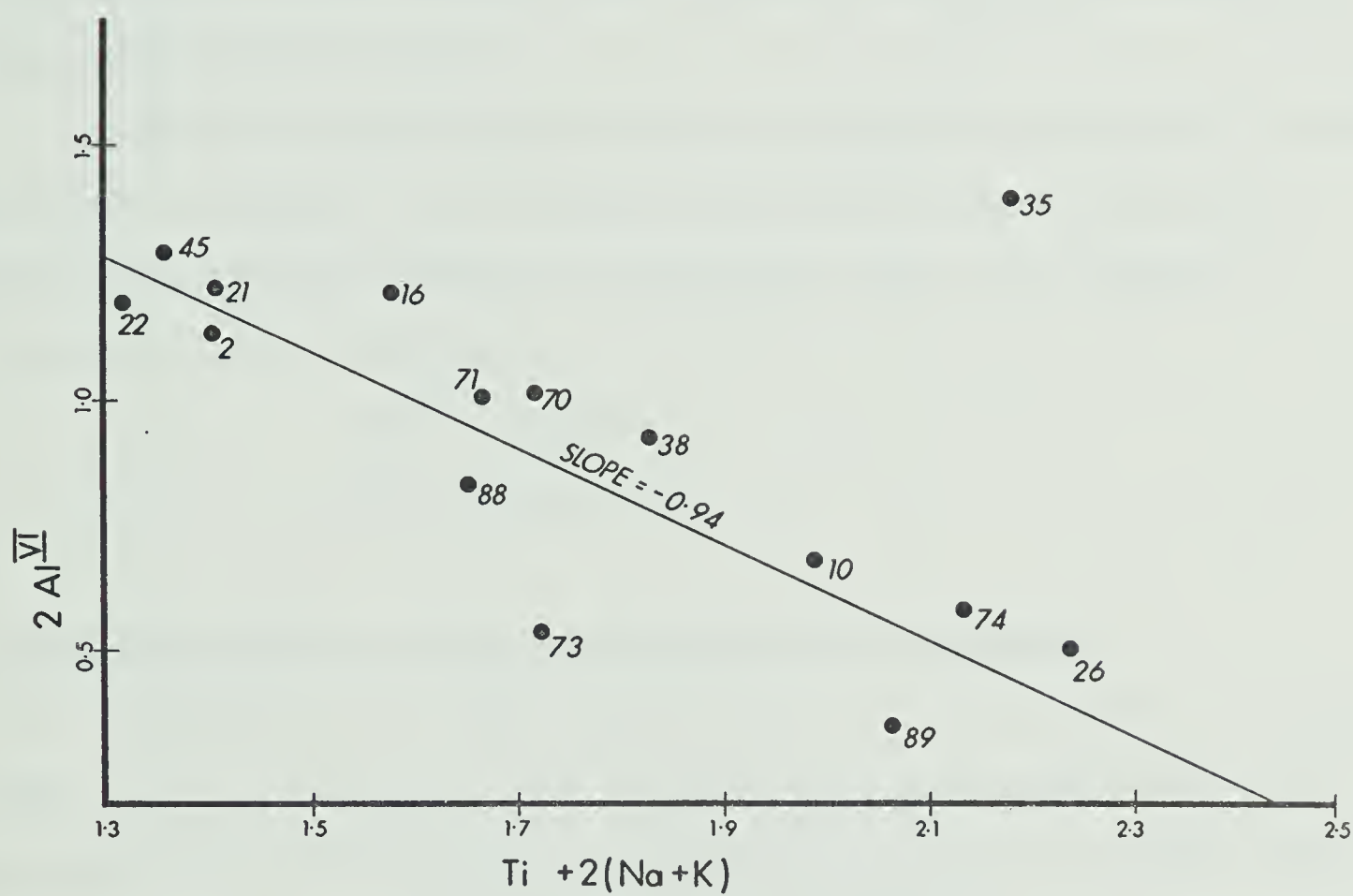
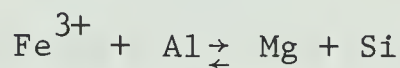
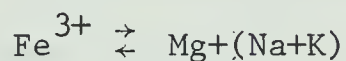


Fig.13. Plot of  $Ti + 2(Na + K)$  versus  $2Al^{VI}$  for the Bamble metamorphic calcic amphiboles. SN-35 was not included in the least - squares fitting of the line shown.



versus  $2Al^{VI}$  (Fig 13) has a best-fit straight line slope of -0.9 suggesting that this coupled substitution might in part be operative. Whether the above substitution results from the influence of the host rock chemistry (this would be a simultaneous enrichment in alkali and Ti in the lithologies concerned), or whether it is merely a function of the partitioning of Ti between the phases, must await additional analyses of other phases coexisting with amphiboles. It is interesting to note the high alkali content of SN-35 and the absence of plagioclase in the host rock.

Other more complex substitutions are obviously possible, but are very difficult to evaluate. From the correlation coefficients of Kostyuk and Sobolev, the following additional substitutions appear to be feasible in metamorphic calcic amphiboles.



## 2. Unit Cell Parameter Variation: Order-Disorder Relationships

COLVILLE et al. (1966) have shown that for the assumption of ordering of the Y-cations in natural calcic amphiboles the relationship between the mean ionic radius of the cations occupying the  $M_2$  site and the b-axis length is approximately linear. In synthetic amphiboles (ERNST, 1968) the assumption of disordering of Y-cations produces a more linear relationship between the 'b' unit cell length and the mean cation radius of  $M_2$ , than does the assumption of ordering.

In order to assess the influence of unit cell size and possibly order-disorder relationships on the argon retentivity of the amphiboles, the unit cell parameters (a,b,c and  $\beta$ ) were calculated for each of the amphibole samples analysed.

In Figs 14 and 15, the b-axis lengths of the sixteen amphiboles have





been plotted versus the mean cation radius of  $M_2$ , assuming complete disordering of the Y-cations and an ordering preference by the smallest Y-cations for the  $M_2$  site. The mean  $M_2$  cation radius for the assumption of an ordered structure was calculated by summing the products of  $Al^{VI}$ ,  $Fe^{3+}$ ,  $Mg^{2+}$ ,  $Ti^{4+}$  and  $Fe^{2+}$  and their ionic radii to two cations per 24 anions, using ionic radii of 0.51, 0.64, 0.66, 0.68 and 0.74 Å respectively. The relationship between the b-axis length and the mean  $M_2$  cation radius is more linear assuming disordering than ordering. This, however, does not necessarily imply complete disorder of  $M_2$ , since with the exception of samples SN 26, 88 and 89, there is a good linear relationship for the assumption of an ordered structure. These relationships are worthy of further consideration.

Fig 16 shows an idealized relationship between the mean  $M_2$  cation radius and the b-unit cell length, when the  $M_2$  site is 100% ordered. If this requirement is not fulfilled and the site is x% disordered, then each point (A,B,C and D) will be moved parallel to the ordinate by  $x/100$  multiplied by the difference between the mean  $M_2$  cation radius (ordered) and the mean  $M_2$  cation radius (disordered) multiplied by four (since 'b' increases at four times the mean  $M_2$  radius) upon disordering. It has been assumed for compositions A,B and D that the difference between the mean  $M_2$  cation radius (ordered) and the mean  $M_2$  cation radius (disordered) is approximately the same; upon which they will fall on a straight line suggesting apparent ordering. Only if the mean  $M_2$  radius (ordered) - the mean  $M_2$  radius (disordered) is different, for example in the case of C, which will be displaced to  $C^1$ , will the relationship be destroyed. Similar reasoning applies to the case of 100% disorder, where  $C-C^1$  is greater than  $A-A^1$ ,  $B-B^1$  and  $D-D^1$ , because the mean  $M_2$  radius (disordered) - the mean  $M_2$  radius (ordered) is larger for C than A,B and D. Thus, a linear relationship does not necessarily imply the assumption of ordering or disordering to be correct.



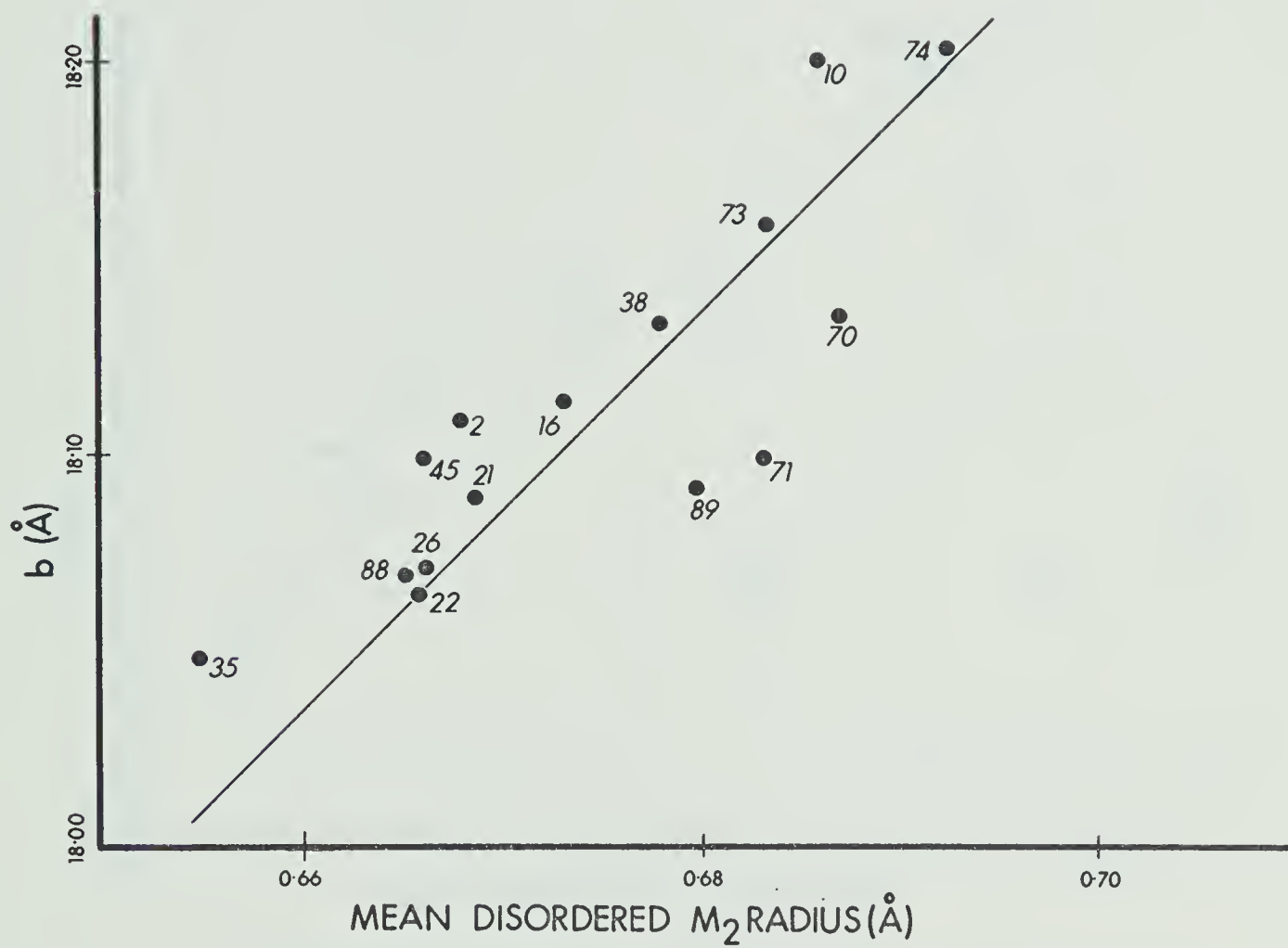


Fig.14. Plot of the b-unit cell lengths versus the mean cation radius of the  $M_2$  site assuming 100% disordering of the 'Y'-cations.



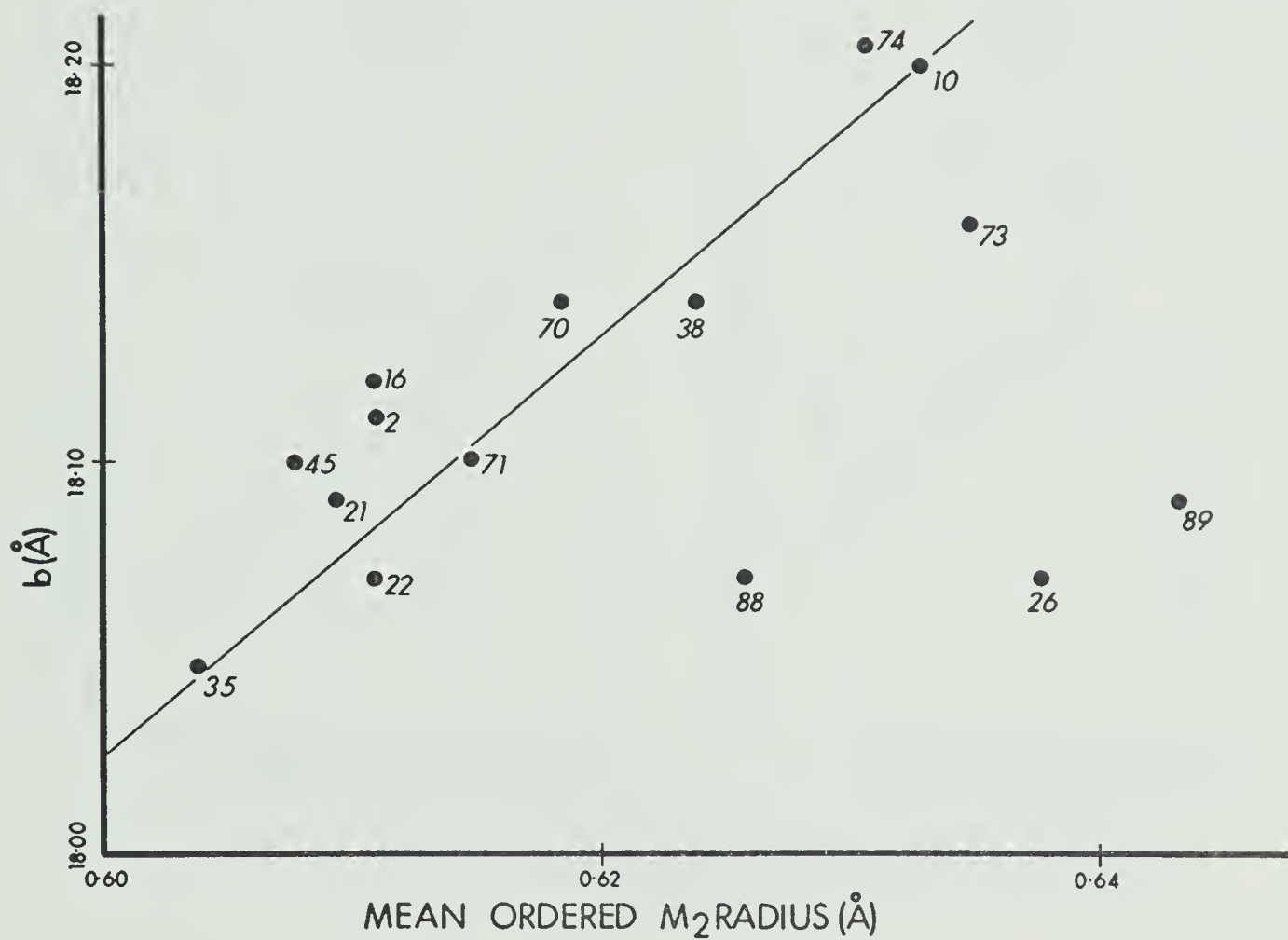


Fig.15. Plot of the b-unit cell lengths versus the mean cation radius of the  $M_2$  site assuming 100% ordering.





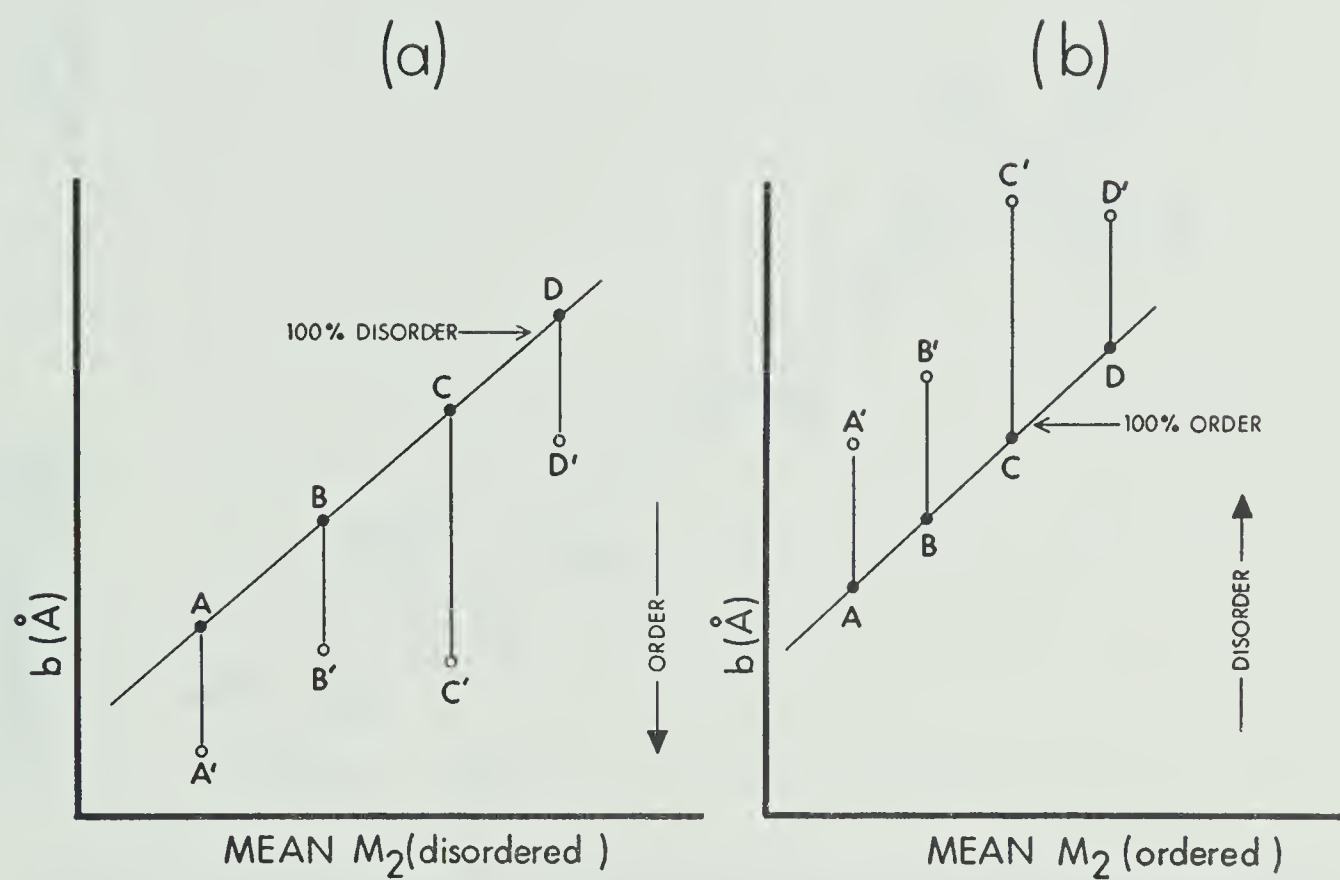


Fig. 16. *Idealized Deviations from Linearity due to Order-Disorder in  $M_2$*



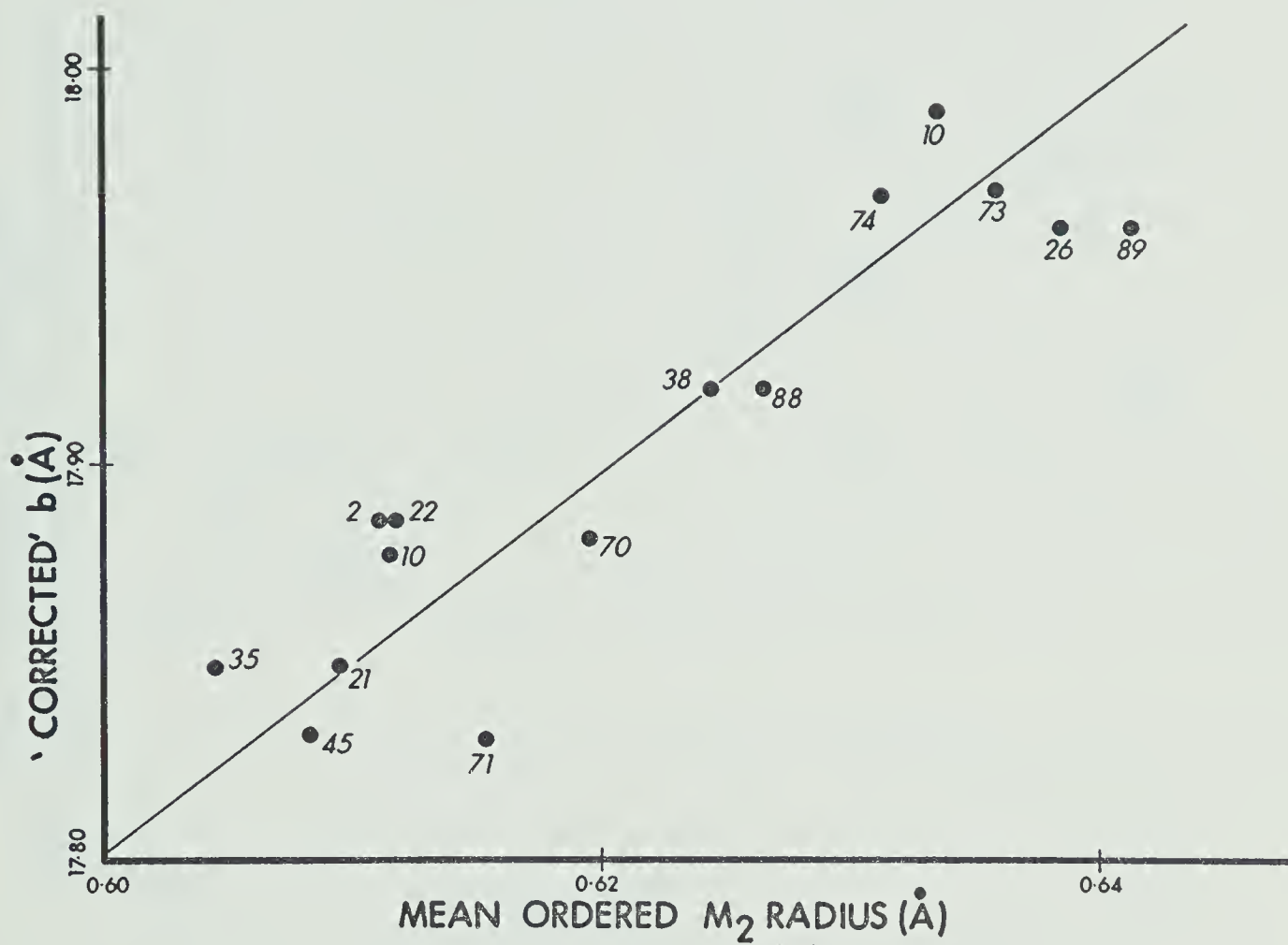


Fig.17. 'Corrected' b-unit cell lengths of the Bamble metamorphic calcic amphiboles to the ordered positions they would occupy if they were in fact 100% disordered. Each point has been moved parallel to the ordinate by 4 times the difference between the mean cation radii of M<sub>2</sub> assuming order and disorder in M<sub>2</sub>.



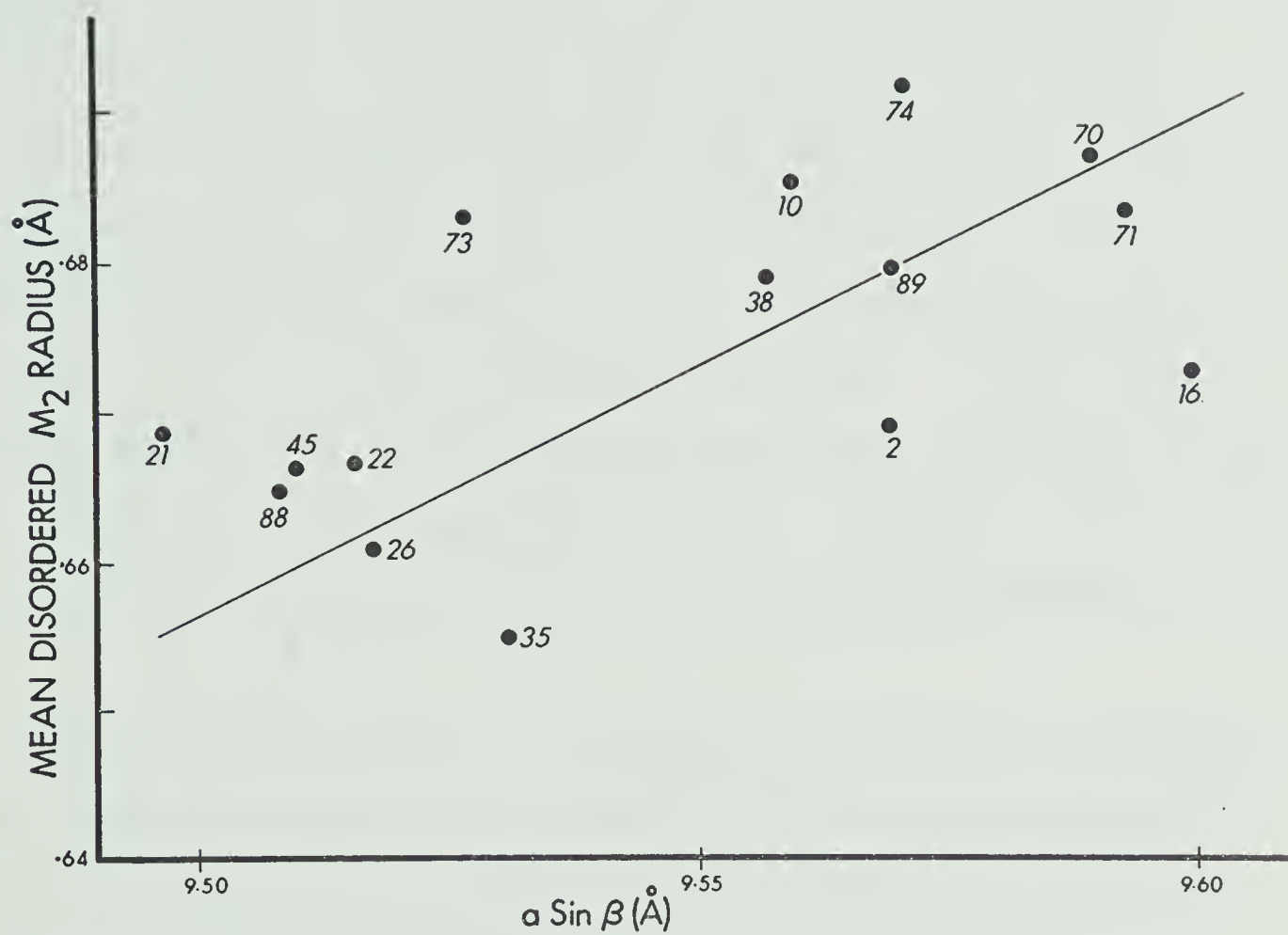


Fig.18. Plot of  $a \sin \beta$  versus the mean cation radius of  $M_2$  assuming disordering of the 'Y'-cations.





In an attempt to evaluate the order-disorder relationships in the analysed calcic amphiboles, it has been assumed that the amphiboles are 100% disordered. The b-unit cell lengths in Fig 17 have been 'adjusted' parallel to the ordinate, taking the initial assumption of order to be incorrect, to the positions they would occupy if the  $M_2$  site was in fact 100% ordered. This is achieved by moving each point by four times the mean  $M_2$  radius (ordered) - the mean  $M_2$  radius (disordered) in a negative sense parallel to the ordinate. It can be seen that a much more linear relationship is attained and SN-88, SN-26 and SN-89 now lie on the line. If there was much more than approximately 10% ordering of the  $M_2$  site, the relationship in (Fig 17) would be somewhat less linear. It may, thus, be tentatively concluded that under high-grade metamorphic conditions (probably 650°C to 700°C for the upper amphibolite facies) the  $M_2$  site is less than 10% ordered, and Y-cations are essentially randomly distributed between  $M_1$ ,  $M_2$  and  $M_3$ .

There should be a tendency for the  $a \cdot \sin \beta$  parameter to increase as the mean radius of the Y-cations increases. A plot of  $a \cdot \sin \beta$  versus the mean  $M_2$  cation radius for the amphiboles (Fig 18) shows that this is most certainly the case for the amphiboles under consideration here.

#### Amphibole Crystal Chemistry and K-Ar Apparent Age

Recent linear heating experiments of GERLING et al. (1965) and KOTLOVSKAYA (1964) have indicated the greater argon retentivity of amphiboles relative to micas (see discussion of argon diffusion in potassic minerals in Chapter 3). GERLING et al. (op. cit.) found that the activation energy for the liberation of radiogenic argon from five amphiboles ranging in composition from pargasite ( $\text{NaCa}_2\text{Mg}_4\text{Al}(\text{Si}_6\text{Al}_2)\text{O}_{22}(\text{OH})_2$ ) to riebeckite ( $\text{Na}_2\text{Fe}_3^{2+}\text{Si}_8\text{O}_{22}(\text{OH})_2$ ) varied from more than 200kcal/mol for pargasite to 110kcal/mol for riebeckite; all in



excess of reported activation energies for argon liberation from micas. At the same time, Gerling and his coworkers demonstrated a relationship between increasing Fe content in the amphibole and decreasing experimental activation energy. In view of the very high activation energies (higher than one would normally associate with diffusional processes) it would at first appear improbable that one would observe any compositional dependence of apparent K-Ar age in regional metamorphic terrains.

The following geological factors are considered to be of potential importance in producing variations in apparent K-Ar ages of calcic amphiboles and are worthy of further consideration:

1. Thermal gradients within a particular area during uplift and cooling (cf. HARPER, 1967).
2. Grain size effects.
3. Amphibole chemical composition.
4. Variable amounts of excess radiogenic argon resulting from differing external partial pressures of argon during crystallization.
5. Loss of 'loosely bound' argon having low activation energies for its removal.
6. Unit cell size variations.
7. Order-disorder relationships.

The lack of any apparent, logical geographical variations of apparent age renders the first possibility of simple thermal gradients across the area during cooling unlikely. Indications are that the radius of the effective sphere of argon diffusion in amphiboles is much less than the physical grain size usually considered (HART, 1960) and is not likely to be an important factor as it is in micas. There is always a possibility of a certain amount of excess radiogenic argon in amphiboles, but as yet there is no reliable documented evidence of this. In the present case, if the spread in apparent ages resulted



from excess radiogenic argon the oldest ages would presumably contain the most excess  $\text{Ar}^{40}$ ; an unlikely possibility because the oldest ages agree with the apparent time of the thermal metamorphic maximum derived from U-Th-Pb datings of zircons and sphenes (Chapter V). GERLING et al. (1965) have not found any evidence, during their linear heating experiments, for argon in a site within the amphibole lattice requiring a low activation energy for its removal, although it may be claimed that this has already been removed, thus violating the assumed boundary conditions for the experiment. The b-unit cell lengths of the amphiboles do not show a linear relationship with their apparent K-Ar ages and a simple relationship between unit cell size and argon retentivity does not appear to exist. The influence of order-disorder relationships are difficult to evaluate on the basis of the information presently available. However, as far as the  $M_2$  site is concerned the degree of ordering appears to be consistently low, as might be expected under high-grade metamorphic conditions. Only features of the amphibole chemical composition and their influence on the argon retentivity of the amphiboles remain to be discussed out of the seven possibilities listed above.

In Fig 19 the apparent ages for twelve amphiboles (the high Mg amphiboles associated with gabbros are excluded) are plotted versus  $100 (\text{Mg}^{2+} + \text{Al}^{\text{VI}} + \text{Fe}^{3+}) / (\text{Mg}^{2+} + \text{Al}^{\text{VI}} + \text{Fe}^{3+} + \text{Fe}^{2+})$  based on the structural formulae; essentially an expression of small octahedrally coordinated cations in  $M_1$ ,  $M_2$  and  $M_3$  versus the larger cations in these sites. With the exception of SN-10 these show a strong positive correlation. This relationship may be expressed differently by calculating the mean cation radius of the  $M_2$  site assuming that the  $M_2$  site is completely ordered and completely disordered (Fig 20): it was shown earlier that the  $M_2$  occupancy was likely to have the largest effect on the 'b' unit cell parameters. It is interesting to note that the relationship between the mean  $M_2$  cation radius and the apparent K-Ar age is more nearly linear





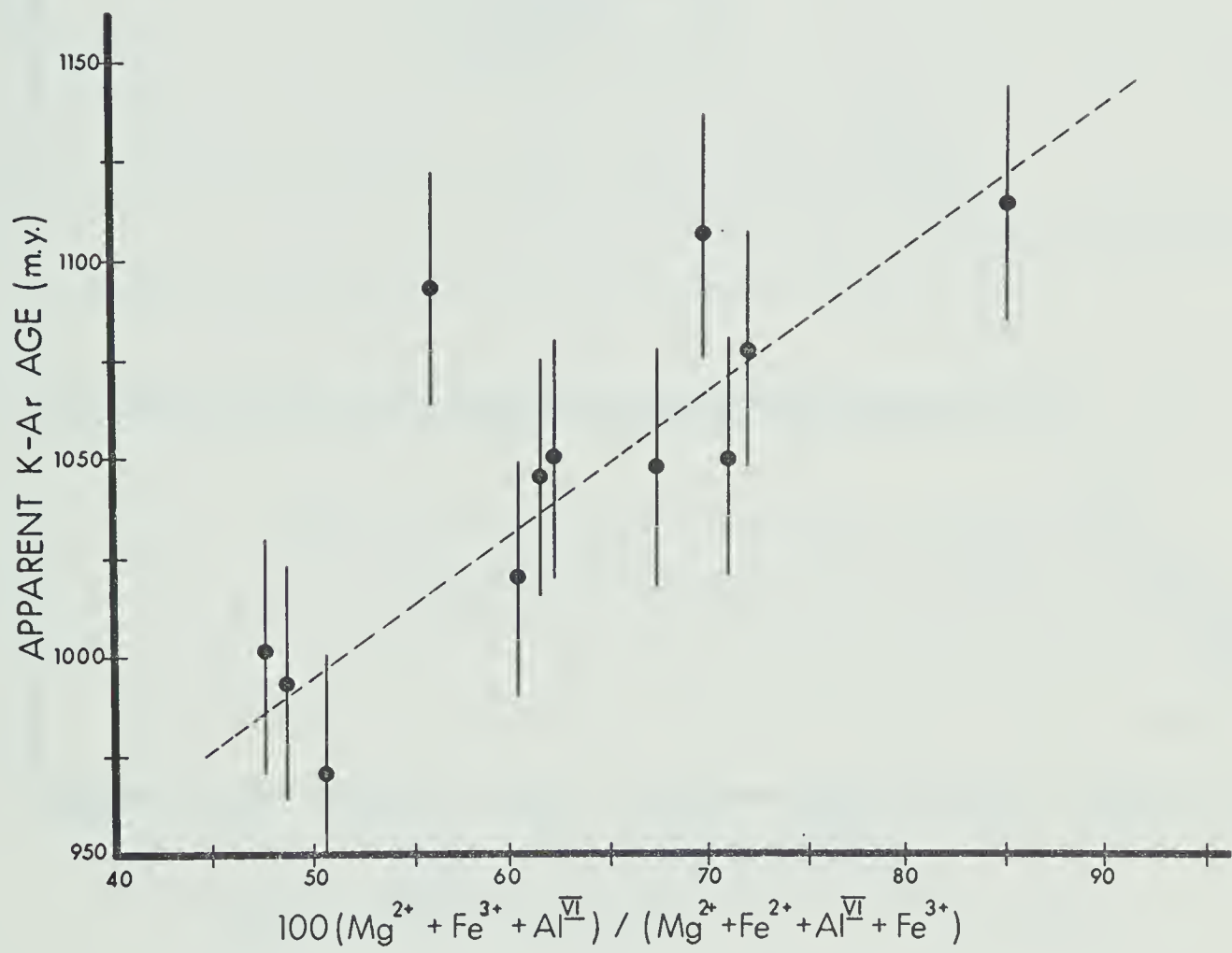


Fig.19. Plot of apparent K-Ar age versus  $100(\text{Mg}^{2+} + \text{Fe}^{3+} + \text{Al}^{\text{VI}}) / (\text{Mg}^{2+} + \text{Fe}^{2+} + \text{Al}^{\text{VI}} + \text{Fe}^{3+})$  based on the structural formulae.



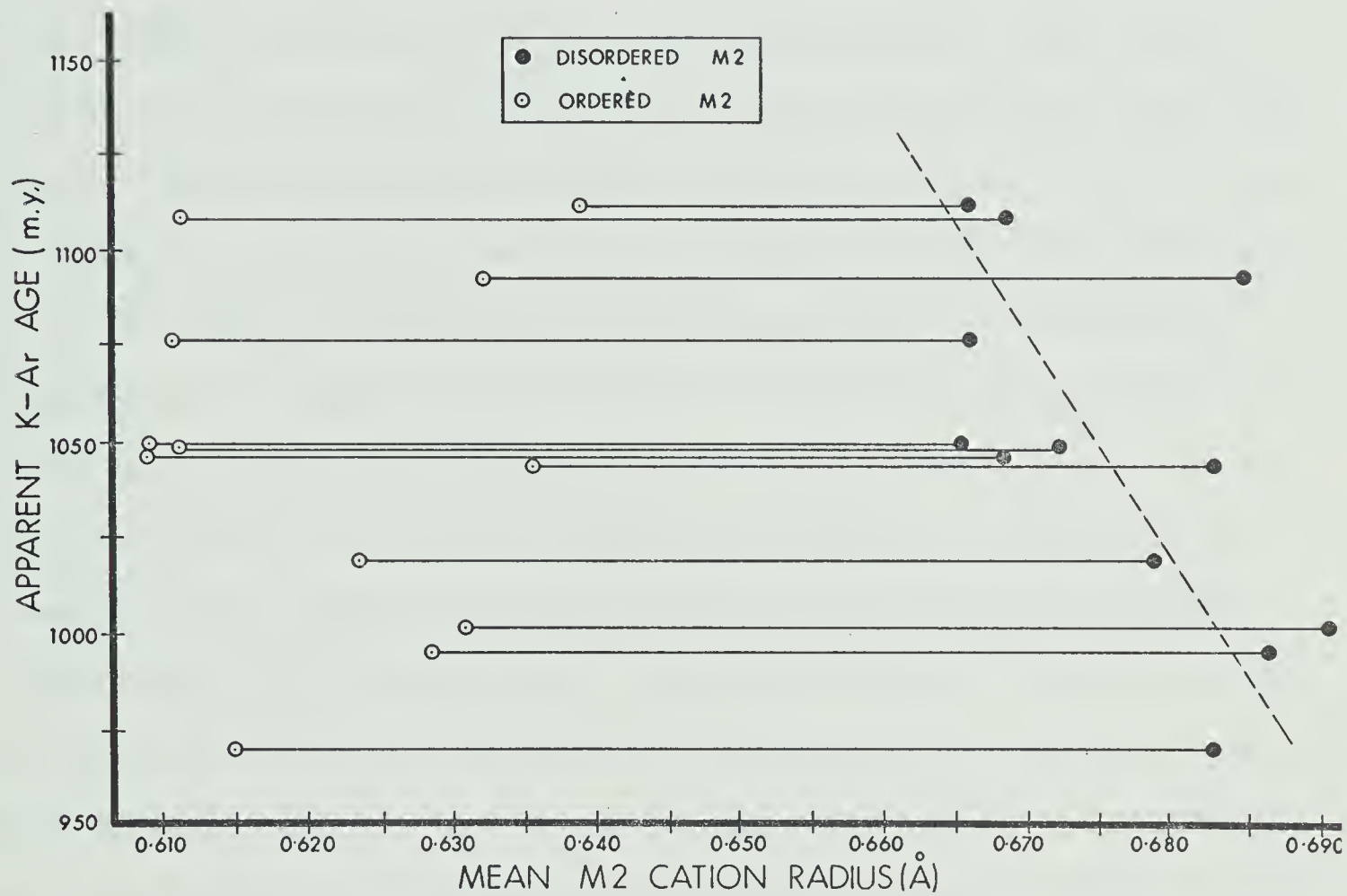


Fig.20. Plot of apparent K-Ar ages versus mean  $M_2$  cation radius assuming a completely ordered and a completely disordered structure.



assuming a disordered structure, as might well be expected in view of the apparent low degree of ordering noted for these amphiboles.

The above relationships suggest that under certain conditions of slow cooling high Fe-amphiboles may lose radiogenic argon until the time of 'closure' of medium-grained biotites to  $\text{Ar}^{40}$  diffusion. This temperature may be estimated at 250°C or even lower (HURLEY et al. 1962). GERLING et al. (1965) estimated from their experimental work that argon would be retained in the amphibole lattice for  $10^9$  years at temperatures below 500°C. However, recently DAMON (1968) has estimated that complete argon loss from an amphibole could be achieved in 600,000 years at a maintained temperature of 475°C; basing his estimate on the experimental work on phlogopite of EVERNDEN et al. (1960) and the observed stability relationship of K-minerals in the contact metamorphic zone of the Eldora stock (HART, 1964). At this point the important distinction between the heating of a mineral in the laboratory and the post-metamorphic slow cooling of a mineral from high temperatures should be emphasized. During the heating of a mineral in the laboratory or in a contact metamorphic environment, the activation energy for argon diffusion will be the rate controlling step since it is a function of the energy which must be supplied to the system in order to enable the argon to surmount the potential barrier and 'jump' into a lattice vacancy or interstitial position within the lattice in order to start a lattice or volume diffusion process. On the other hand, during cooling from elevated temperatures, the retention of radiogenic argon may be related to the diffusion rate constant ( $D_0/a^2$ ) and not to the activation energy. It is, therefore, useful to consider a mechanism or some mechanisms whereby during cooling the diffusion rate constant may be enhanced in some amphiboles compositions.

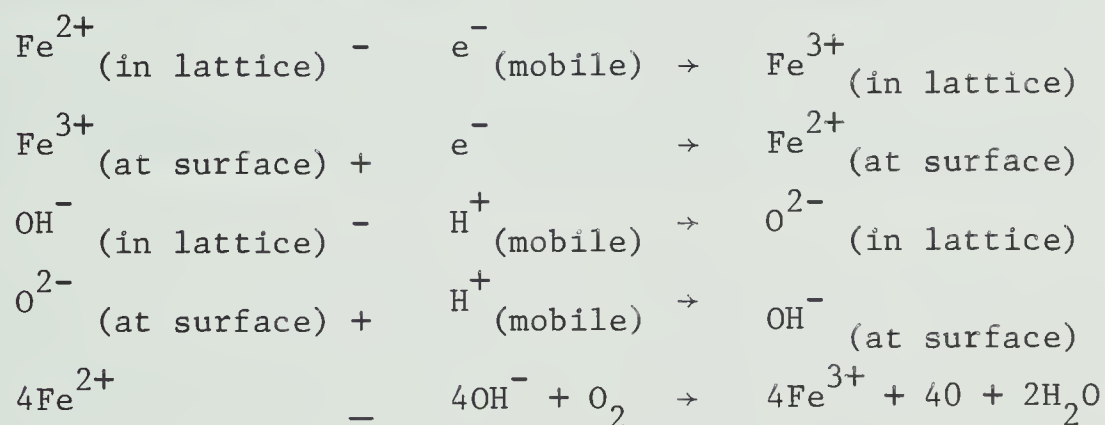
KOTLOVSKAYA (1964) has suggested that the loss of argon from amphiboles is closely related to their dehydration. However subsequent experiments by





GERLING et al. (1966) have shown that unlike biotites, the loss of radiogenic argon from amphiboles does not occur until they are almost entirely dehydrated; the dehydration energies ranging from 40kcal/mol to 100kcal/mol, some two or three times less than the activation energy for  $\text{Ar}^{40}$  diffusion. A compositional dependence of dehydration energy was noted; Mg-rich amphiboles having higher activation energies than Fe-rich amphiboles. Upon cooling from temperatures characteristic of the upper amphibolite facies of regional metamorphism it is, thus, possible that  $\text{O}_3$  anions (predominantly OH) are capable of re-equilibration with the ambient  $f\text{O}_2$  and  $f\text{H}_2$  conditions to lower temperatures in Fe-rich compositions than Mg-rich compositions. Although the precise mechanism and diffusion paths, by which such a process could occur, remain obscure, dehydroxylation experiments (ADDISON et al. 1962, 1968) on crocidolites (magnesioriebeckite) do shed some light on the problem.

ADDISON et al. (1962) list the following reactions as being operative in the dehydroxylation process.



In this process  $\text{Fe}^{2+}$  in the lattice is envisaged to release an electron, which travels along the cation ribbons to the surface of the crystal by changes in the oxidation state of Fe. At the surface,  $\text{Fe}^{2+}$  reacts with  $\text{OH}^{-}$  and  $\text{O}_2$  to produce water and O and hence dehydroxylate the amphibole. Should the above process of dehydroxylation and a converse hydroxylation process continue after the crystallization of the amphibole it would likely enhance  $D_o/a^2$ .



Since electrons must migrate along cation 'ribbons' in the above processes and two Mg atoms in a 'ribbon' will 'block' the process of electron migration between them, the process may be expected to continue to lower temperatures in high Fe-amphiboles, near the ferropargasite end-member. Such a process is dependent upon the ability of  $H^+$  and electrons to migrate through the amphibole lattice.

### Summary

Amphibole compositions near the ferropargasite end-member apparently do not begin to quantitatively retain radiogenic argon until quite low temperatures (approximately 250°C) upon cooling from temperatures characteristic of the upper amphibolite facies of regional metamorphism, whereas compositions near the pargasite end-member retain argon from considerably higher temperatures. It is possible that the high values of  $D_0/a^2$  required to produce sufficiently high values of the diffusion coefficient at low temperatures in the Fe-rich compositions are a result of the minerals ability to re-equilibrate with the external fluid composition.



## CHAPTER V - URANIUM-THORIUM-LEAD DATING

Introduction

With some information concerning the time of the thermal maximum of the metamorphism and the subsequent cooling history of the Bamble area obtained from the K-Ar dating of micas and amphiboles, certain lithologies were selected for U-Th-Pb dating, with respect to the following problems.

1. The age and possible origin of the Levang gneiss dome
2. The age of the Ødegaarden apatite deposits and their relationship to the metamorphism.
3. The age of the post-kinematic K-feldspar pegmatites.
4. An independent estimate of the time of the thermal maximum of metamorphism.
5. The provenance of the metasediments.

The U-Th-Pb method of dating has proven to be particularly valuable for obtaining information of the above kind. Detrital zircons, for example, have in a number of instances been shown to retain their ages of crystallization even when subjected to high-grade metamorphism (see reviews by BAADSGAARD, 1965, HAMILTON, 1966, MOORBATH, 1967 and CATANZARO, 1968). However many zircons do appear to be susceptible to lead-loss at low temperatures, especially if the lattice has suffered extensive radiation damage. With these features in mind, zircons were separated from various lithologies in the Levang gneiss dome, from a sample of the Arø metaconglomerate and a paramphibolite from Kjønnøya.

Early attempts to date sphenes by the U-Th-Pb method (TILTON et al., 1955) were not particularly successful, however more encouraging results have recently been obtained by TILTON and GRUNENFELDER (1968) on sphenes ranging in age from 1.0 b.y. to 2.75 b.y. All of the samples analyzed by Tilton and Grunenfelter were found to be concordant or nearly concordant, with a maximum difference between the  $\text{Pb}^{206}$ - $\text{U}^{238}$  and  $\text{Pb}^{207}$ - $\text{U}^{235}$  ages of 10 percent. With a





view to obtaining an independent estimate of the time of metamorphism and examining their discordance patterns relative to zircons, sphenes were separated from three granite gneiss samples from the Levang gneiss dome, four pegmatites, an albitite and an orthoamphibolite specimen. Only the sphene from the orthoamphibolite (SN-38) had too little radiogenic lead to provide a useful apparent age.

In addition to the above zircons and sphenes, a sample of xenotime, cognetic with the Ødegaarden chlorapatite deposits and an allanite from the Engevann K-feldspar pegmatite were also analyzed.

### Analytical Techniques

#### 1. Mineral separations.

In the case of pegmatitic minerals, samples to be used for dating were merely ground to -150 to +250 mesh and purified by conventional magnetic and heavy liquid techniques. For other mineral concentrates rock samples between 50 and 150 lbs. were crushed in a rotary plate mill and fed onto a Wilfley table, from which heavy mineral concentrates were obtained. Zircon and sphene were concentrated from the Wilfley 'heavies' and were purified by magnetic separation, sinking in methylene iodide and finally by a float-sink procedure in hot clerici solution. Zircons were washed for 90 minutes and sphenes for 20 minutes in warm (60°C) redistilled 8M HNO<sub>3</sub> immediately prior to analysis. Wherever possible zircon populations were split into different gravity fractions.

#### 2. Lead extraction and mass spectrometry.

Zircon samples between 0.2 and 0.8 gms., and sphene samples of about 1.5 gms. were fused in a platinum crucible with purified sodium tetraborate. The fused sample was dissolved in redistilled 1.5M HCL, with constant stirring (in this way silica remained in solution) and the solution stored in volumetric flasks sealed with 'Parafilm'. In the case of sphenes, 3M HCL was often found



more effective in retaining the silica in solution.

All reagents employed in the extraction of lead were specially cleaned for this purpose (see Appendix B). For the measurement of isotope ratios, lead was recovered from an aliquot of the sample solution by extraction with 0.01% diphenylthiocarbozone (dithizone) first in the presence of ammonium citrate and then in the presence of potassium cyanide at a pH of 9.0 (TILTON et al. 1957). In each case lead was back-extracted with 2%  $\text{HNO}_3$  and washed with chloroform. Finally lead was precipitated as  $\text{PbS}$  with  $\text{H}_2\text{S}$  and loaded on a single oxidized Ta filament for isotope analyses. The procedure for the 'spiked' aliquot (for the determination of the Pb concentration) is identical to the above, except for the addition of  $\text{Pb}^{208}$  isotope dilutant (or  $\text{Pb}^{206}$  isotope dilutant in the case of the allanite and xenotime) prior to the first dithizone extraction. A more complete description of the method, together with details of reagent preparation and blank is given in Appendix B.

Lead was isotopically analyzed using a 12" radius of curvature,  $60^\circ$  sector, single focussing mass-spectrometer designed and built by Dr. G.L. Cumming of the Dept. of Physics, University of Alberta. This mass-spectrometer is equipped with facilities for switching between preset magnet positions, vibrating-reed amplification and a digital voltmeter. Normal operating conditions were 4.5 KV accelerating voltage and a  $10^{11}$  ohm leak resistor on a Cary amplifier. A Keithley amplifier with a  $10^{10}$  ohm resistor was used for some of the analyses. Lead emission commenced at a filament current of 1.8 amps from which point it was slowly built up to a total ion current of 1 to  $2 \times 10^{-10}$  amps. The  $\text{Pb}^{207} / \text{Pb}^{206}$  and  $\text{Pb}^{208} / \text{Pb}^{206}$  ratios were measured by switching between preset magnet current positions for masses 206, 207 and 208 and taking digital output. The  $\text{Pb}^{206} / \text{Pb}^{204}$  ratio was adequately measured from chart-scans. Normally the 208, 207, 206 masses were resolved and only very occasionally were small tail-corrections necessary. Measurement of National Bureau of Standards





Equal Atom Lead (NBS-982) performed by the author and H. Baadsgaard and D.C. Green in the period 1967-1969 are listed in Table 7. Since the results do not reveal any obvious mass discrimination, mass discrimination corrections have not been applied to the measured isotope ratios. Measurement precision of the  $\text{Pb}^{207} / \text{Pb}^{206}$  and  $\text{Pb}^{208} / \text{Pb}^{206}$  ratios was normally plus or minus 0.1% (1 standard deviation) and the  $\text{Pb}^{206} / \text{Pb}^{204}$  normally plus or minus 2% or better. Since the common lead corrections were small in most instances, it was not necessary to measure the  $\text{Pb}^{206} / \text{Pb}^{204}$  ratio more accurately.

Uranium and thorium were extracted from a double-spiked aliquot of sample solution by an anion exchange method. The technique developed during the course of this study is directly applicable to zircon, sphene, monazite, allanite, xenotime etc. and with some modification probably to whole rocks, although none have been attempted as yet.  $\text{U}^{235}$  and  $\text{Th}^{230}$  isotope dilutants were added directly to aliquots of sample solutions proportioned so that the  $\text{U}^{238} / \text{U}^{235}$  and  $\text{Th}^{232} / \text{Th}^{230}$  ratios were approximately unity. Uranium and thorium were coprecipitated from solution as hydroxides with  $\text{NH}_4\text{OH}$ . The centrifuged precipitate was dissolved in 10ml of 6M  $\text{HNO}_3$  and added to a 14 x 1.2 cm(o.d) Dowex 1-X8 anion exchange column from which uranium was eluted with redistilled 6M  $\text{HNO}_3$ . Thorium forms a very strongly retained anion complex with 6M  $\text{HNO}_3$  and is removed from the column by stripping with 0.5M  $\text{HNO}_3$ . Uranium and thorium were recombined and loaded as nitrates on a single Ta filament. A complete description of the anion exchange method is given in Appendix C.

Uranium and thorium were isotopically analyzed on the same 12" mass-spectrometer as described above for lead. During the calibration of the  $\text{U}^{235}$  and  $\text{Th}^{230}$  spikes, a number of different methods of sample loading were examined. These were as follows:

(a) A common method of loading combined U and Th as nitrates and oxidizing in air before analysis was found to be quite unsatisfactory using





TABLE 7.

Analyses of N.B.S. - 982 (Equal Atom Lead) Standard.

<u>208/206</u>	<u>Date of Analysis</u>	<u>Analyst *</u>
$1.0001 \pm 0.0008$	Nov. 1967	D.C.G.
$1.0001 \pm 0.0005$	Nov. 1967	H.B.
$0.9989 \pm 0.0012$	Jan. 9th 1969	R.K.O.
$1.0000 \pm .0012$	Jan. 9th 1969	R.K.O.
$0.9991 \pm 0.0014$	Jan. 9th 1969	R.K.O.
$0.9984 \pm 0.0009$	Feb. 16th 1969	R.K.O.
$0.9996 \pm 0.0010$	Feb. 16th 1969	R.K.O.
$1.0053 \pm 0.0011$	March 6th 1969	R.K.O.
$1.0063 \pm 0.0010$	March 6th 1969	R.K.O.

Average value =  $1.0008 \pm 0.0029$

Standard value =  $1.0002 \pm 0.0004$   
(CATANZARO et al., 1968)

Broken Hill Galena

(2nd. Feb. 1969 R.K.O.)

(STACEY et al., 1969)

 $206/204 = 16.057 \pm 0.016$  $16.007 \pm 0.010$  $207/206 = 0.9628 \pm 0.0006$  $0.96187 \pm 0.054$  $208/206 = 2.2325 \pm 0.0015$  $2.2286 \pm 0.0013$ 

\*D.C.G.: D.C.Green; H.B.: H. Baadsgaard; R.K.O.: R. K. O'Nions



a single Ta filament. Uranium emission as  $UO^{2+}$  and  $UO^+$  at higher filament currents, was usually strong (ion currents upto  $1 \times 10^{-10}$  amps were normally obtained) but very unstable. Thorium emission as  $ThO^+$  however was much more stable, but only produced ion currents of  $10^{-12}$  amps.

(b) In an attempt to produce  $U^+$  and  $Th^+$  ions, the combined uranium and thorium nitrates were mixed with a small amount of finely ground, spectroscopically pure graphite and glowed in air before analysis. This also proved to be unsatisfactory, since emission of  $U^+$  was poor, and required very high filament currents (3.7 amps).

(c) Thirdly a U-Th- $B_2O_3$  load was attempted.  $H_3BO_3$  was added to the filament and evaporated to dryness and converted to a  $B_2O_3$  bead before analysis by glowing the filament in air. Uranium emission was found to be reduced compared with (a) above, but much more stable. Emission of uranium, as  $UO^{2+}$  commenced at about 2.70 amps and was increased very slowly to an ion current of  $10^{-11}$  amps, at which point digital data was obtained by switching between preset magnet positions for masses 235 and 238. When the  $UO^{2+}$  emission decreased, the filament current was increased to between 3.1 and 3.3 amps and  $ThO^+$  measured digitally. Ion currents were very poor and usually no greater than  $5 \times 10^{-13}$  amps, but could be measured digitally using a  $10^{12}$  ohm leak resistor on the Keithley amplifier, and a peak-switching interval of 15 secs between masses 232 and 230 in order to overcome the time constant. Occasionally data was measured from the chart output on poor runs. The measurement precision of uranium isotope analyses is between 0.5% and 1%.

#### Diffusion Processes in Uranium-Lead Systems

If a given U, Th, Pb-bearing phase has remained a closed-system from a time  $t$  until present, then four values may be obtained for  $t$  as follows:



$$\text{Pb}^{206} = \text{U}^{238} (e^{\lambda^{238}t} - 1)$$

$$\text{Pb}^{207} = \text{U}^{235} (e^{\lambda^{235}t} - 1)$$

$$\text{Pb}^{208} = \text{Th}^{232} (e^{\lambda^{232}t} - 1)$$

$$\begin{aligned} \text{and } \frac{\text{Pb}^{207}}{\text{Pb}^{206}} &= \frac{\text{U}^{238}}{137.8 \text{ U}^{238}} \cdot \frac{(e^{\lambda^{235}t} - 1)}{(e^{\lambda^{238}t} - 1)} \\ &= \frac{1}{137.8} \cdot \frac{(e^{\lambda^{235}t} - 1)}{(e^{\lambda^{238}t} - 1)} \end{aligned}$$

providing a  $\text{U}^{238}\text{-Pb}^{206}(t_{206})$ ,  $\text{U}^{235}\text{-Pb}^{207}(t_{207})$ ,  $\text{Th}^{232}\text{-Pb}^{208}(t_{208})$  and a  $\text{Pb}^{207}\text{-Pb}^{206}(t_{207/206})$  age.

The U-Pb system of zircons, the most commonly utilized mineral for U-Th-Pb dating, frequently departs from ideal closed system behaviour such that  $t_{206} < t_{207} < t_{207/206}$ . This pattern of discordance is usually interpreted in terms of a lead loss model (see BAADSGAARD, 1965 for review). Reversed sequences to the above i.e.  $t_{206} > t_{207} > t_{208}$  may be observed in monazites (TILTON and NICOLAYSEN, 1957), suggesting a predominance of uranium loss over lead loss. The  $t_{208}$  ages of zircons are most commonly less than their  $t_{206}$  ages, but occasionally  $t_{208}$  ages much greater than the  $t_{207/206}$  ages have been reported (c.f. ALDRICH et al, 1965). Unfortunately the tendency has arisen to ignore Th-Pb ages of zircons unless they concord with U-Pb ages, as a consequence of which the literature is probably biased in favour of  $t_{208}$  ages, which are in agreement with U-Pb ages.

WETHERILL (1965) showed that the measured ratios in the U-Pb system of cogenetic zircons plotted on a  $\text{Pb}^{206}/\text{U}^{238} - \text{Pb}^{207}/\text{U}^{235}$  diagram (this will be referred to as an  $r_{238} - r_{235}$  diagram in future discussions) lie on a straight line, which intersects the concordia (locus of points for which  $t_{207} = t_{206}$ ) at the 'true age' of the system and at a lower point on the concordia; this lower point may or may not temporally correspond to an episode of daughter loss.

It is by now apparent that for an adequate understanding of discordancy





patterns of zircons and other U-Th-Pb bearing minerals, one must examine closely the effects and possible causes of open system behaviour in the U-Th-Pb system. Diffusion in lead-uranium systems has been discussed at considerable length by NICOLAYSEN (1957), TILTON (1960), WETHERILL (1963) and WASSERBURG (1963) and only a brief summary will be presented here.

### 1. Pure Daughter Loss (Constant $D/a^2$ )

The flux ( $J$ ) of a diffusing species (e.g. lead in a zircon) is related to the diffusion coefficient ( $D$ ) by Fick's first law:

$$\bar{J} = -D \text{ grad } C = -D \nabla C \quad (1)$$

where  $\nabla C$  is the concentration gradient.

Fick's second law relates the rate of change of concentration to the divergence of  $\bar{J}$

$$-\frac{\partial C}{\partial t} = \text{div } \bar{J} = D \nabla^2 C \quad (2)$$

which simplifies to

$$\frac{\partial C}{\partial t} = \frac{D d^2 C}{dx^2} \quad (3)$$

for diffusion in say the  $x$  direction only

The time varying concentration of daughter is described by

$$\frac{\partial C_D}{\partial t} = D \nabla^2 C_D + \lambda N_o e^{-\lambda t} \quad (4)$$

Adopting the boundary conditions  $C = C_o$ ,  $t = 0$  and  $r = a$  (radius of sphere of diffusion), the solution of the equation for spherical diffusion is (TILTON, 1960)

$$\frac{\bar{C}}{C_o} = \frac{6}{\pi^2} \sum_{n=1}^{\infty} \frac{e^{-n^2 \pi^2 D t / a^2}}{n^2} \quad (5)$$

where  $C_o$  is the initial concentration and  $\bar{C}$  the average concentration of daughter product after an elapsed time  $t$ .

If one now includes the simultaneous generation of daughter with the loss of daughter at a rate of  $Dt/a^2$ , the relationship between the average



concentration of daughter product relative to parent is given by (TILTON, op cit.):

$$\frac{C}{N} = \frac{6}{\pi^2} \sum_{n=1}^{\infty} \frac{\lambda(e^{\lambda t} - n^2 \pi^2 D t / a^2 - 1)}{n^2 (\lambda - n^2 \pi^2 D / a^2)} \quad (6)$$

NICOLAYSEN (1957) published tables of solutions to (6) above for values of  $\ln(1 + \frac{C}{N})$  and  $D/a^2$  from which diffusion ages and diffusion trajectories in the  $r_{\lambda 238} - r_{\lambda 235}$  diagram may be calculated.

TILTON (op. cit.) showed that the line, joining points of different  $D/a^2$  for a single age, on a  $r_{\lambda 235}$  diagram is linear over most of its length, but at small values of  $r_{\lambda 238}$  and  $r_{\lambda 235}$  curves down to the origin (Fig 21). In this way Tilton suggested that the apparent event at approximately 500 m.y. ago in many parts of the world where zircon ages in excess of 2500 m.y. had been analyzed, could be explained by a general process of lead diffusion with particular values of  $D/a^2$  for particular zircons. Although one cannot invoke processes of continuous diffusion to explain all cases of discordant ages, it is now established that in some instances a general process of low temperature, apparently continuous, lead loss does operate.

Solutions of the diffusion equation by Tilton for cylindrical diffusion and diffusion from an infinite plate do not significantly change the diffusion trajectories in an  $r_{\lambda 238} - r_{\lambda 235}$  diagram.

## 2. Pure Daughter Loss ( $D(t) = D_1 T$ )

A variant of the Nicolaysen-Tilton treatment has been developed by WASSERBURG (1963), assuming that to a first approximation the diffusion coefficient is a time varying function of the integrated radiation damage received by a lattice, rather than a constant 'saturation' value due to a saturated radiation damage condition in the Tilton model.

The total radiation damage received by a grain over a period of time due to the decay of uranium and thorium is of the form (after WASSERBURG,





loc.cit.).

$$AU^{238}(T) (\exp^{\lambda^{238}T} - 1) + BU^{235}(T) (\exp^{\lambda^{235}T} - 1) + C Th^{232}(T) (\exp^{\lambda^{232}T} - 1)$$

Since  $\alpha$  particle bombardment is the most probable source of lattice damage, and  $\alpha$  particles are probably of similar energy in the three decay schemes then, A : B : C are approximately in the ratio 8 : 7 : 6.

The ratio of daughter product to parent ( $r_\lambda$ ) at time T on a volume V is:

$$r_\lambda = \int_V C_\lambda(r,t) \cdot dV / \int_V U_\lambda(r,t) \cdot dV$$

where  $C_\lambda$  is the daughter product concentration, a function of time (T) and  $r_\lambda$  the radius of the sphere of diffusion. WASSERBURG (loc.cit.) has given solutions to the above equation for a variety of geometries and these need not be repeated here.

In Fig 21 the  $D = D_0$  (a constant) diffusion trajectory is compared with that for  $D = D_1 T$  ( $D_1$  a constant) and the best straight line fitted to the linear region. For losses of lead up to 73%, from a 1.8 b.y. old U-Pb system, the diffusion trajectory is essentially linear in the  $D = D_1 T$  model of Wasserburg. The extrapolated linear portion of the  $D = D_1 T$  trajectory is 370 m.y. compared with 530 m.y. for the  $D = D_0$  trajectory.

### 3. Combined Parent and Daughter Loss

For the case involving both parent and daughter loss from a U-Pb system, the following generalized equations apply. (WETHERILL, 1963):

In the case of daughter diffusion:

$$\frac{\partial C_D}{\partial t} = D_D(t) \nabla^2 C_D + \lambda C_P(r,t)$$

and parent diffusion:

$$\frac{\partial C_P}{\partial t} = D_P(t) \nabla^2 C_P - \lambda C_P(r,t)$$

where  $C_D$  and  $C_P$  refer to the concentrations of daughter and parent respectively.

For the case where  $D_D = D_P$ , solutions to the equations by WETHERILL (op.cit.) simplify to the equation  $\frac{C_D}{C_P} = e^{\lambda t} - 1$ , the familiar case for no





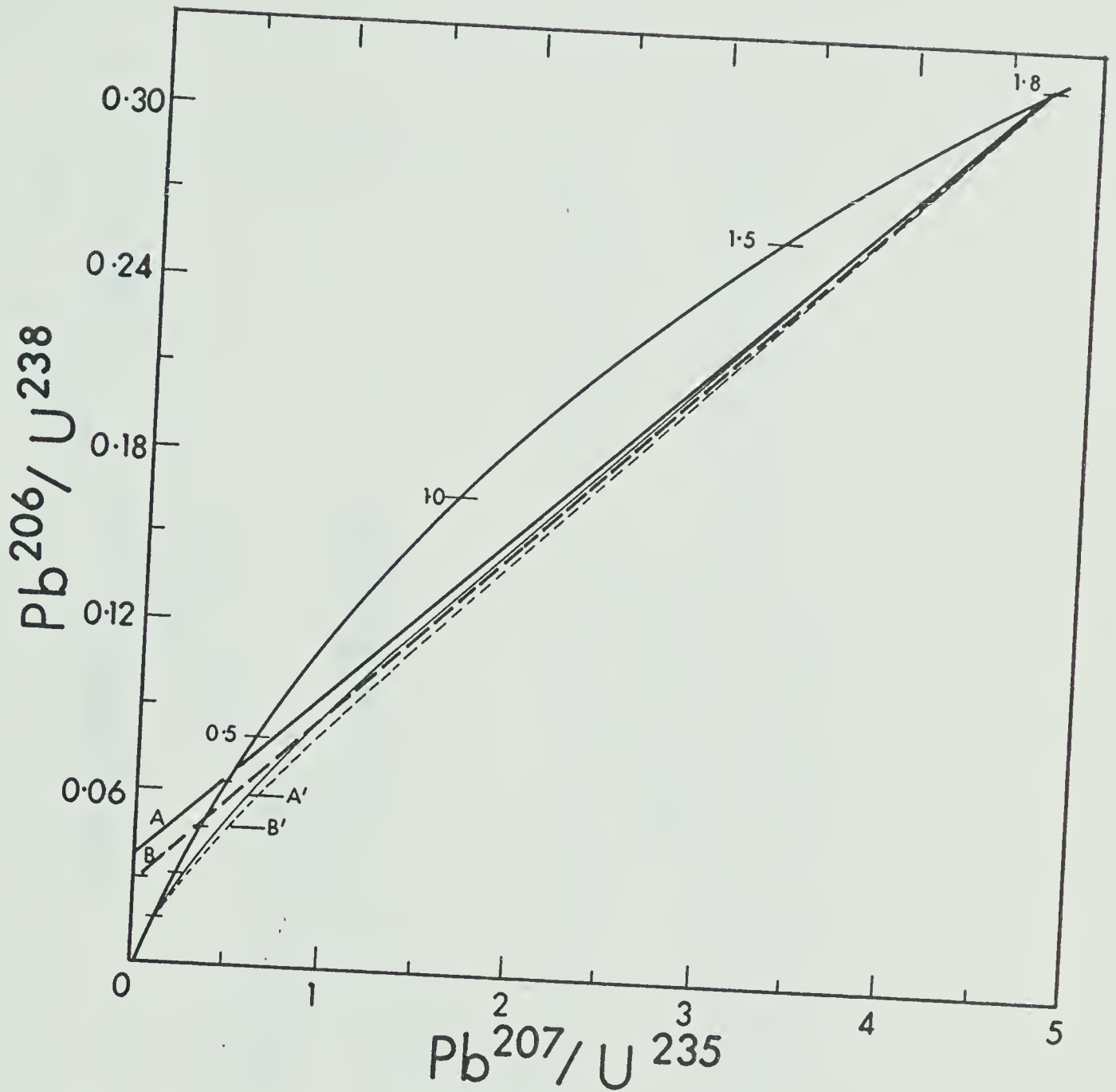


Fig.21. Comparison of the continuous diffusion trajectories for  $D(\tau) = D_0$  (a constant) [curve A'] and  $D(\tau) = D_1 \tau$  ( $D_1$  a constant) [curve B'] for a primary age of 1800m.y. Lines A and B are the extrapolated tangents to A' and B' drawn at the intersection of the diffusion trajectories and the concordia curve. (after WASSERBURG, 1963).



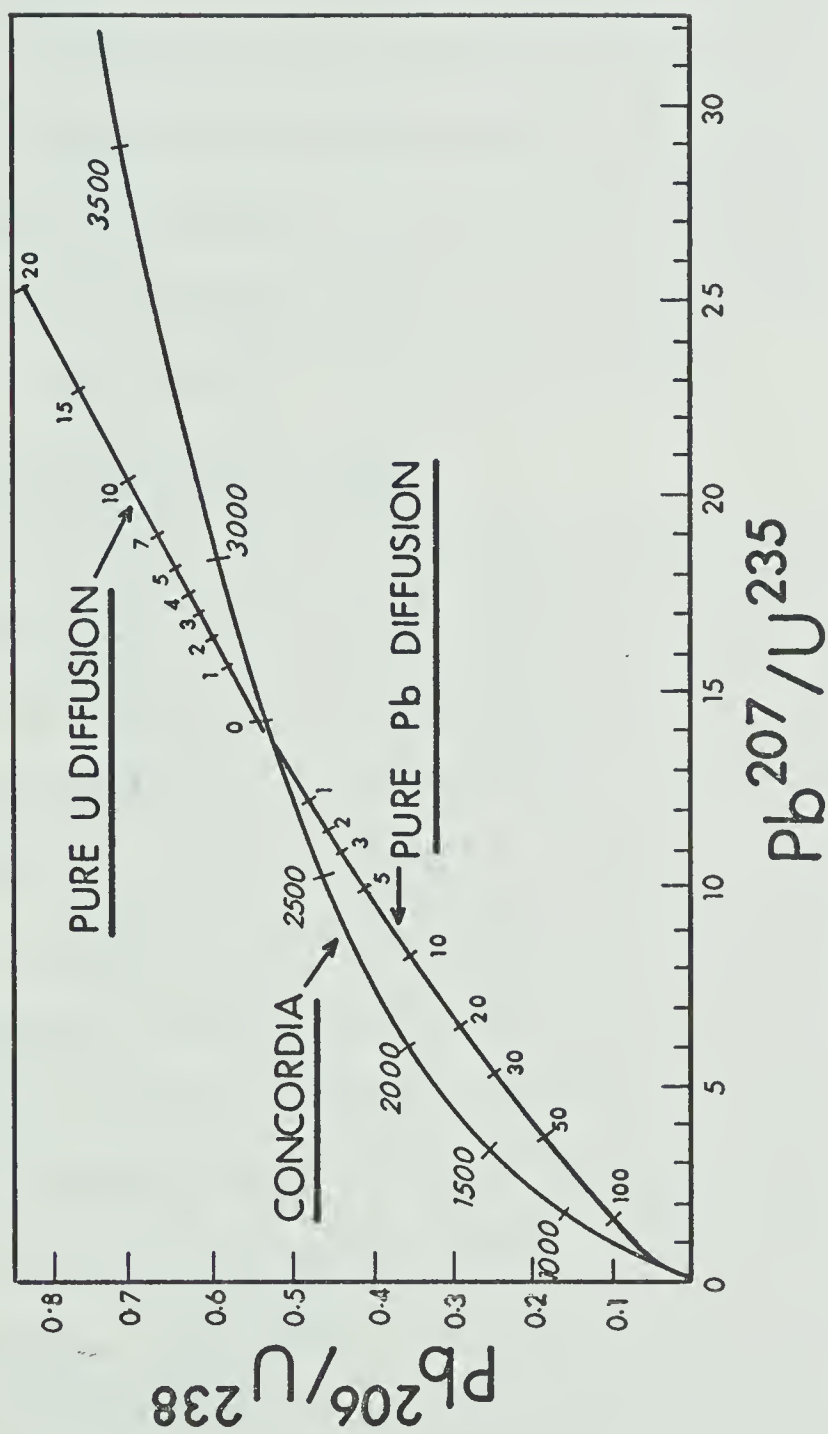


Fig.22. Comparison of pure Pb with pure U diffusion. The figures along the concordia curves represent the values of the diffusion parameter  $D/a^2$  in units of  $10^{-12} \text{ yr}^{-1}$ . (after WETHERILL, 1963.).



diffusion. Thus so long as uranium and lead diffuse out of a U-Pb system with the same diffusion coefficient, concordant ages will be maintained. A comparison of diffusion trajectories for pure U and pure Pb diffusion in Fig 22, shows the lower slope of the U diffusion trajectory compared with Pb diffusion trajectory. It is obviously extremely difficult in some situations to differentiate between episodic lead loss, lead loss by one of the continuous diffusion models and the added complexity of small amounts of parent loss.

An attempt to evaluate the usefulness of the proposed models in the interpretation of discordance patterns will be made later in this Chapter, in the light of data obtained in the present study.

#### Results of Zircon and Sphene Dating

Uranium, thorium and lead isotopic data for the various zircon fractions, sphenes, the allanite and the xenotime are presented in Table 8, and their calculated U-Pb, Th-Pb and Pb-Pb ages in Table 9.

The reproducibility of the  $\text{Pb}^{207}/\text{Pb}^{206}$  and  $\text{Pb}^{208}/\text{Pb}^{206}$  isotope ratios may be assessed from replicate analyses of N.B.S. - 982 (Equal Atom Lead) lead isotope reference standard performed in this Laboratory, which have yielded a standard deviation in the 208/206 ratio of less than 0.3% for analyses of variable quality. A number of calibration analyses of the  $\text{U}^{235}$  and  $\text{Th}^{230}$  isotope dilutants used in this study, by H. Baadsgaard and the author, enable an estimate of the reproducibility of  $\text{U}^{238}/\text{U}^{235}$  and  $\text{Th}^{230}$  isotope ratios to be made. The  $\text{U}^{238}/\text{U}^{235}$  ratio had a reproducibility of 0.5%, and that of the  $\text{Th}^{232}/\text{Th}^{230}$  ratio was similar, where good quality data (i.e. digital output) was obtainable. Assigned errors in the measured U-Pb ratios of  $\pm 1.5\%$  are therefore considered to be reasonable in instances where the common lead correction is small. Where the common lead correction is larger, then proportionately larger errors have been assigned.





TABLE 8

Concentrations - ppm.      Atomic Abundances  
Relative to Pb<sup>204</sup>

Sample	Mineral	U <sup>238</sup>	Th	Pb <sup>206</sup>	Pb <sup>204</sup>	Pb <sup>206</sup>	Pb <sup>207</sup>	Pb <sup>208</sup>
Levang Gneiss Dome								
SN-68-161	Zircon	483	110	64.7	1	850.4	64.69	63.74
SN-68-159(A)	Zircon	440	130	61.3	1	1042	80.04	107.2
SN-68-159(B)	Zircon	691	214	73.8	1	356.8	26.57	46.41
SN-59	Zircon	421	141	51.1	1	1461	113.3	151.3
SN-59	Sphene	113	45.0	17.8	1	583.7	45.96	63.89
SN-68-159	Sphene	132	36.9	21.2	1	743.2	57.41	68.05
SN-68-161	Sphene	114	26.6	18.4	1	462.5	35.19	48.82
SN-68-157(B)	Zircon	1547	297	188.6	1	1036	85.76	106.3
SN-68-157(C)	Zircon	2133	426	214.9	1	145.8	11.47	63.63
SN-68-158(A)	Zircon	1529	318	147.2	1	589.9	47.43	74.2
SN-68-158(B)	Zircon	2106	395	198.3	1	358.2	28.45	62.63
SN-68-158(D)	Zircon	2912	626	237.1	1	105.5	13.50	52.60
Metasediments								
SN-68-121	Zircon	436	68.8	65.5	1	2041	176.4	120.2
SN-79	Zircon	647	115	99.0	1	1436	127.4	81.15
Late Pegmatites (K-Feldspar)								
SN-97(A)	Zircon	1293	490	138.8	1	1432	105.1	239.2
SN-97(B)	Zircon	1310	476	138.4	1	1782	129.2	303.9
SN-97(C)	Zircon	1959	683	132.7	1	326.7	21.70	122.2
SN-81	Allanite	3888	54102	587.7	1	1399	105.8	6081
Other Pegmatites (Sphenes)								
SN-90	Sphene	90.2	53.3	14.3	1	1438	108.8	262.6
SN-91	Sphene	83.0	431	12.7	1	380.8	29.27	613.2
SN-96	Sphene	48.8	41.1	7.62	1	491.6	38.83	126.6
SN-92	Sphene	235	28.9	37.1	1	1826	140.7	66.47
SN-65	Sphene	62.0	267	9.64	1	360.9	27.82	504.3
Apatite Deposits (Ödegaarden)								
SN-94	Xenotime	269	3635	42.5	1	2226	175.3	9272



TABLE 9

## U - Th - Pb Apparent Ages (m.y.)

Sample	Mineral	Pb <sup>206</sup> /U <sup>238</sup>	Pb <sup>207</sup> /U <sup>235</sup>	Pb <sup>207</sup> /Pb <sup>206</sup>	Pb <sup>208</sup> /Th <sup>232</sup>
Levang Gneiss Dome					
SN-68-161	Zircon	936	984	1116	973
SN-68-159(A)	Zircon	970	1014	1136	1061
SN-68-159(B)	Zircon	757	834	1074	986
SN-59	Zircon	852	933	1156	826
SN-68-159	Sphene	1109	1114	1152	1148
SN-59	Sphene	1090	1115	1186	952
SN-68-161	Sphene	1112	1106	1117	1584
SN-68-157(B)	Zircon	857	978	1286	1419
SN-68-157(C)	Zircon	716	775	1183	4439
SN-68-158(A)	Zircon	687	819	1228	1274
SN-68-158(B)	Zircon	672	799	1204	1887
SN-68-158(D)	Zircon	584	997	2105	3864
Metasediments					
SN-68-121	Zircon	1044	1146	1370	1228
SN-79	Zircon	1060	1188	1422	1071
Late Pegmatites (K-Feldspar)					
SN-97(A)	Zircon	761	829	1044	1039
SN-97(B)	Zircon	750	813	1020	1088
SN-97(C)	Zircon	490	550	836	1576
SN-81	Allanite	1048	1058	1120	1038
Other Pegmatites (Sphenes)					
SN-90	Sphene	1094	1090	1106	1076
SN-91	Sphene	1056	1075	1138	1041
SN-96	Sphene	1078	1108	1192	1048



TABLE 9 (Cont.)

SN-92	Sphene	1092	1100	1142	1028
SN -65	Sphene	1075	1090	1143	1109
Ödegaarden Apatite Deposits					
SN-94	Xenotime	1090	1114	1187	1069

---

Note: Isotope values were corrected for contaminant lead according to the lead isotope ratios for conformable leads appropriate to the measured 207/206 ages, with the exception of SN-97(C), which has a 207/206 age of 830 m.y.; in this case the ratios appropriate to SN-97(A) were used: Blank lead isotope composition 1:23.8:15.9:49.6.





### 1. The Levang gneiss dome

Uranium-lead results from zircon and sphene analyses are plotted on a conventional  $^{238}\text{U} - ^{235}\text{U}$  diagram in Fig 23. Two straight lines have been fitted to the data points as shown in the figure. One of these discordia lines has an upper intercept with the concordia at 1160 m.y. and a lower intercept at 260 m.y.: the sphene sample SN-68-161 was excluded from the least-squares fitting of this line because of the uncertainty in the common lead correction. With the exception of the 'D'-fraction of SN-68-158, the remaining zircons were fitted to a line forced through the lower discordia-concordia intercept of the above data at 260 m.y.; this line has an upper intercept with the concordia at 1400 m.y. For purposes of comparison with the above episodic lead loss interpretation, a diffusion trajectory for the continuous radiation damage model ( $D(t) = D_1 T$ ) of a 1400 m.y. old U-Pb system has been plotted (WASSERBURG, 1963). This model is considered by the author to be more realistic in terms of zircon crystal chemistry than the saturation radiation damage model described by  $D(t) = D_0(\text{constant})$ . It is quite apparent that it is impossible to distinguish between an episodic and a continuous radiation damage model of daughter loss for this data, or indeed between the two continuous diffusion models. The significance of the lower 260 m.y. (Permian) intercept is debatable, since the extrapolated linear portion of the plotted diffusion trajectory would give essentially the same intercept. However, it was mentioned earlier in this thesis that this particular area is part of the Permian Oslo Graben and has most certainly been affected to some degree by activity associated with the Permian Oslo Igneous Province. This activity was not of sufficient intensity to cause significant argon leakage from the dated micas discussed earlier, but some degree of episodic lead loss in the Permian does seem possible.

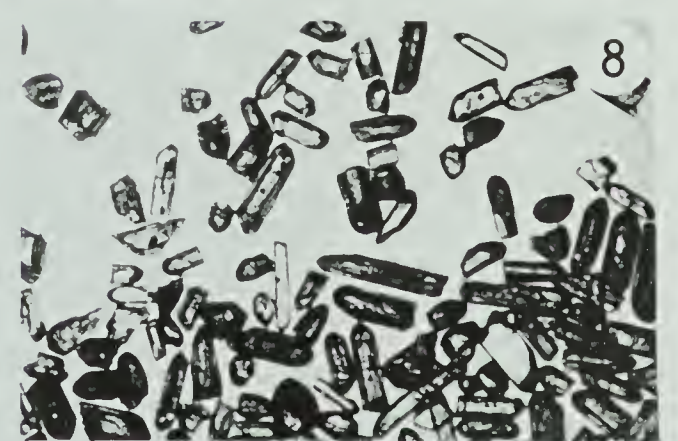
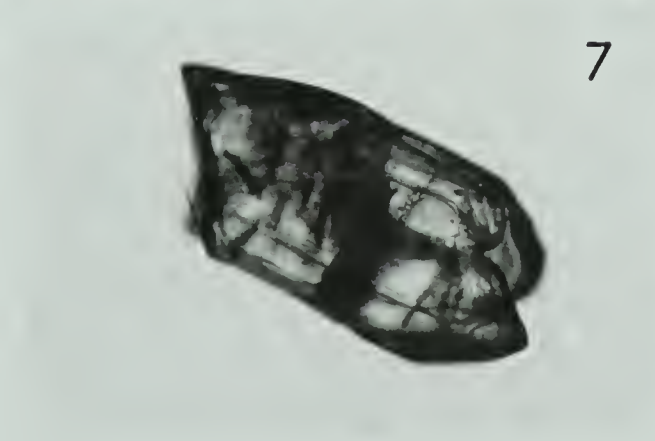
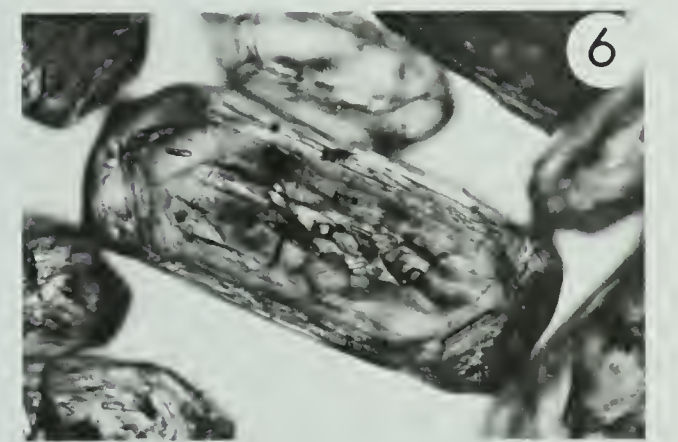
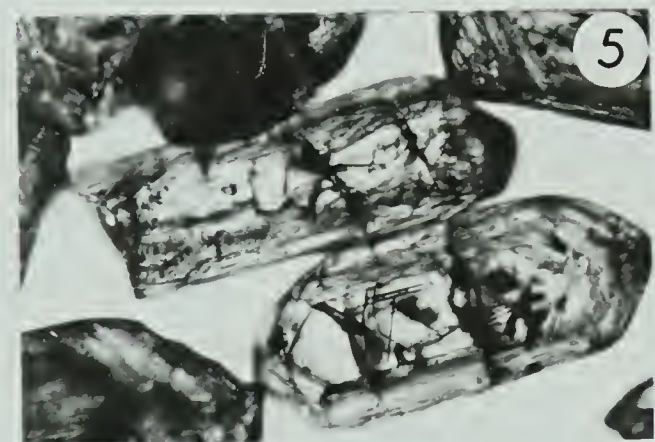
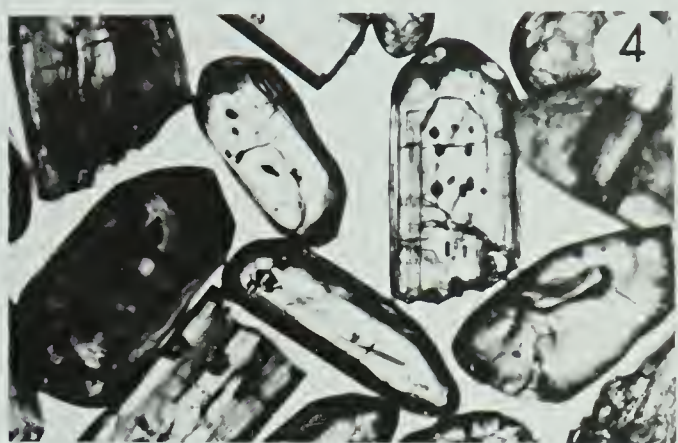
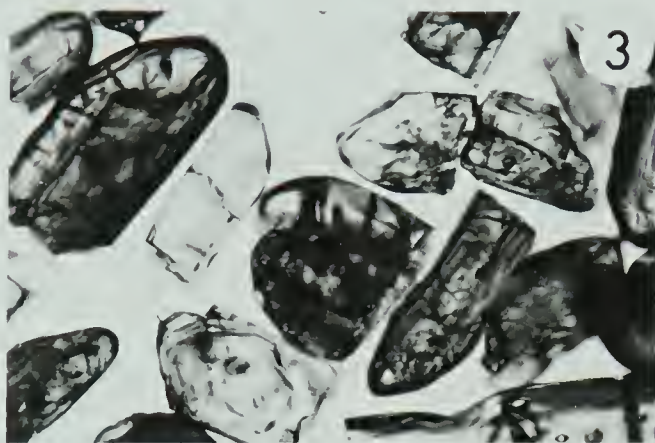
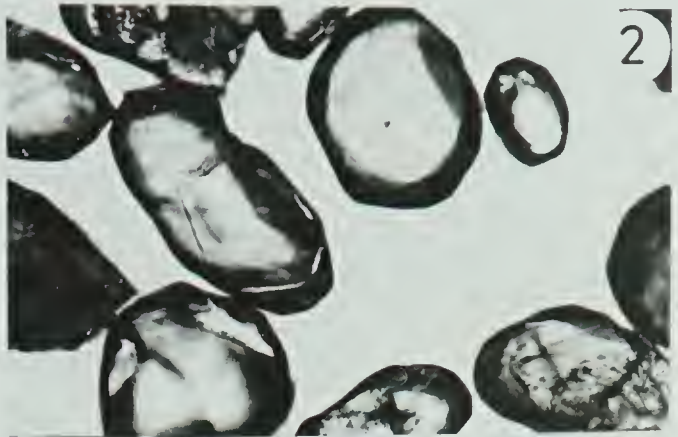
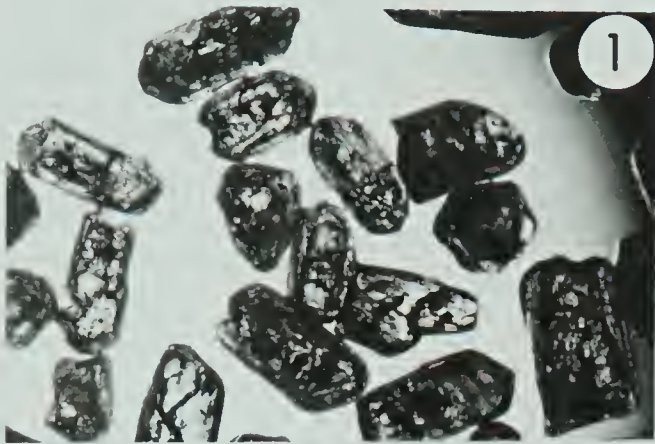
Concordia-discordia intercepts of 1160 m.y. and 1400 m.y. obtained above,

PLATE 1.

1. Zircons from granitic gneiss from the Levang gneiss dome (SN-68-157).  
Note the abundance of cracks and their clouded appearance. Outgrowths are visible on some of the grains. Plane light x100.
2. Rounded detrital zircons from the Kjonndøya para-amphibolite. x110.
3. Zircons from granite gneiss from the Levang gneiss dome (SN-68-159).  
Note the subrounded appearance and the overgrowths on some of the grains. x200.
4. Same sample as above. Note the more translucent appearance than (1) above and the fewer number of cracks. x200.
5. Same sample as above showing detrital cores and the abundant acicular inclusions. x250.
6. As above, but different grain. x250.
7. Same sample as above showing distinct zircon overgrowths. x250.
8. Sample SN-59, showing sample purity. Note the tendency towards more euhedral forms than in (1) above. x80.



PLATE I.





above, leave us with the apparent enigma of petrographically indistinguishable granitic gneisses from the Levang gneiss dome containing zircons with apparent ages of approximately 1400 m.y. and 1160 m.y.. It is thus, pertinent to consider the petrogenetic implications of these results.

The various zircon fractions from SN-68-157 and SN-68-158 are morphologically similar (Plate 1). The grains vary from distinctly rounded, anhedral forms to almost euhedral forms possessing slightly rounded terminations; all of which are distinctly zoned and have a yellow-brown colour and a clouded appearance in transmitted light. Frequently the grains contain acicular inclusions, which on the basis of the Becke lines appear to be of much lower refractive index than the enclosing zircon. In some instances distinct unzoned overgrowths are visible on the zircons.

Zircon fractions from samples SN-68-159, SN-68-161 and SN-59, lying on the 1160 m.y. discordia are quite different from the aforementioned zircons. In external morphology the differences are quite small, the only difference being a tendency towards more near-euhedral forms than in the above. They are distinctly clearer, more translucent in transmitted light, possess fewer inclusions and have a pale hyacinth colour. In most instances outgrowths are visible and the detrital cores appear to be unzoned or only slightly zoned. The overgrown material is in all instances optically unzoned.

Zircons have been extensively used in the past to infer the origins and evolution of various lithologies; their stability under conditions of weathering, transportation and metamorphism being noted (POLDERVAART, 1950, 1955, 1956). SAXENA (1966) has discussed the following origins of zircons:

1. Zircons crystallized from a magma.
2. Zircons formed authigenically in sediments.
3. Zircons formed under metamorphic conditions.
4. Zircons of authigenic origin transformed during metamorphism.





5. Zircons of all types recrystallized under high grade metamorphism.

The first three categories above represent genetic types, each of which may have overlapping characteristics. In view of the possibility of metamorphic and authigenic modification of zircon morphology, considerable care must be exercised when making petrogenetic inferences on the basis of zircon morphology. As a generalization however, one may expect magmatic zircons to be more euhedral and zoned than metamorphic and authigenic zircons, and detrital zircons to depart even more from euhedral forms. Metamorphic processes may lead to crystallization and recrystallization of zircons (e.g., TAUBENECK, 1957, DAVIS et al., 1968), producing euhedral forms.

The Levang gneiss dome zircons which lie on the 1400 m.y. discordia and exhibit strong zonation, were most probably derived from a source a minimum of 1400 m.y. old. Their zonation most likely results from successive peripheral additions of zircon throughout the crystallization of the magma (GOTTFRIED, et al., 1959, SILVER and DEUTSCH, 1963). The small overgrowths noted on some of the zircons may be of metamorphic and/or of authigenic origin; in either case these would tend to produce ages less than the age of the source material, and may be contributory to the displacement of zircons off the 1400 m.y. discordia. The 1400 m.y. apparent age must therefore be considered as a minimum age for the detrital zircons.

In view of the obviously detrital nature of the zircons now lying on the 1160 m.y. discordia, it is simplest, but not necessarily accurate, to infer that these were derived from a similar, older source and were much more extensively modified by metamorphic and possibly authigenic processes resulting in the formation of 'new'  $\text{ZrSiO}_4$  and recrystallization of the detrital zircon destroying much of the zonation, which it may have originally possessed. In some zircons no evidence could be found for a detrital origin and these may be essentially metamorphic zircons.



In considering possible explanations for the different behaviour of zircons under what appear to be very similar conditions, experiments of MUMPTON & ROY (1961) on natural zircons are pertinent. At approximately 4Kb and 500°C metamict zircons were found to recrystallize and produce good diffraction patterns. SAXENA (1966) has also managed to recrystallize a cyrtolite at 600°C and 2Kb in seven days. It is possible that the analyzed zircon populations from the Levang gneiss dome responded differently to metamorphic conditions, as a result of differing degrees of metamictization. Certainly quite large variations in the degree of metamictization can be found within a single zircon population (SILVER and DEUTSCH, 1961). It is however, very interesting to note the possibility of zircons actually being recrystallized and isotopically 'reset' under high grade metamorphic conditions.

Confirmatory evidence for the approximately 1160 m.y. zircon population being of metamorphic origin is obtained from the sphene results which also lie on the 1160 m.y. discordia and are undoubtedly metamorphic minerals.

The zircon samples SN-68-121 and SN-79 from an orthoamphibolite and metaconglomerate respectively are also seen to lie approximately on the 1400 m.y. discordia, indicating that, at least in part, the provenance of the Bamble series was from a 1400 m.y. or older source area.

## 2. Pegmatites

Sphenes, zircon and allanite were sampled from pegmatites in an attempt to isotopically differentiate between the two predominant groups of pegmatites in the area, i.e. the synkinematic plagioclase pegmatites and the post-kinematic discordant K-feldspar pegmatites. The U-Pb data for the pegmatite minerals is plotted on a  $^{238}\text{R} - ^{235}\text{R}$  diagram in Fig 24.

The K-feldspar Ødegaarden pegmatite contains large, zoned zircon crystals, up to 1 cm. in length, a few of which were crushed, purified and separated into three density fractions. A regression line has been fitted





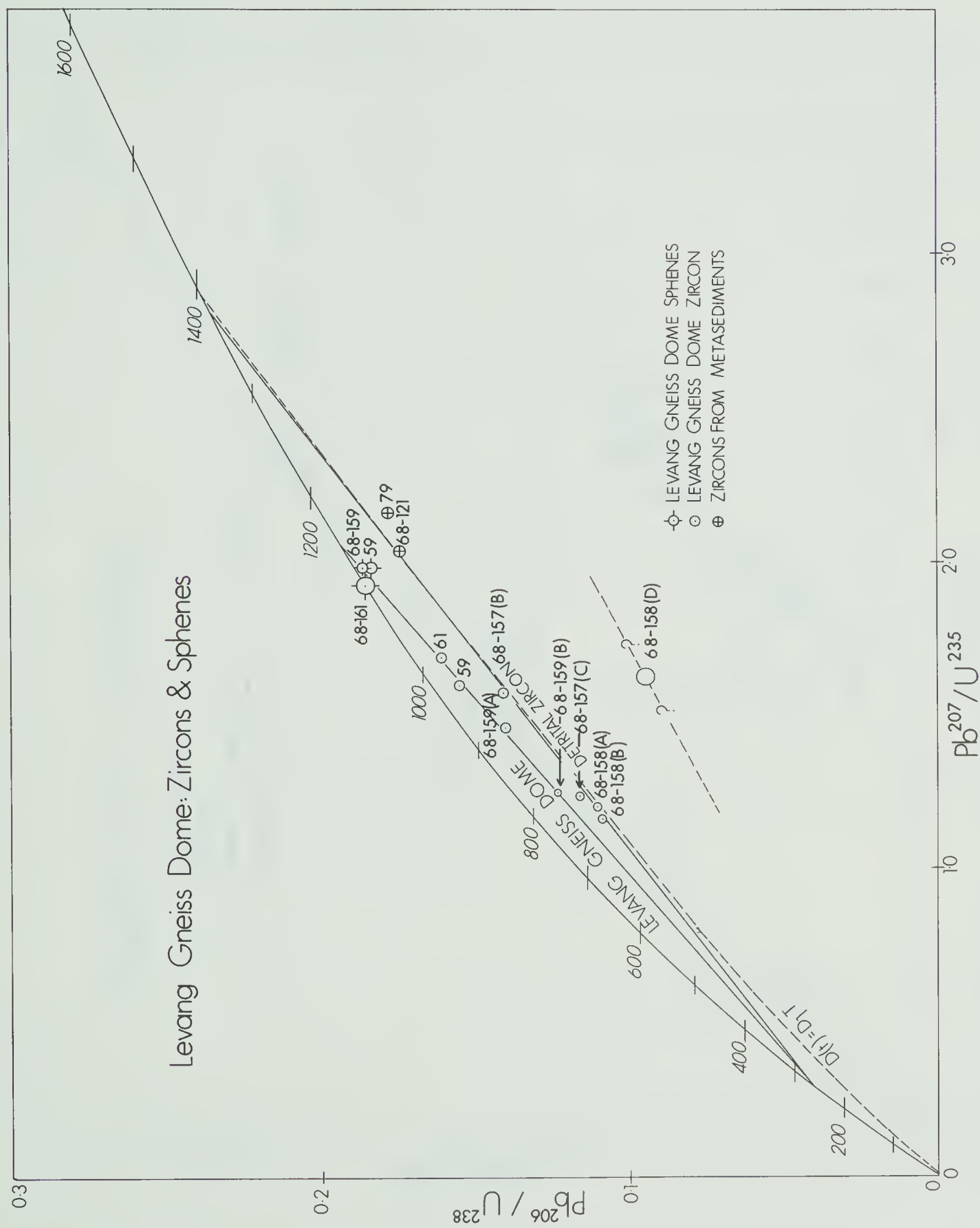
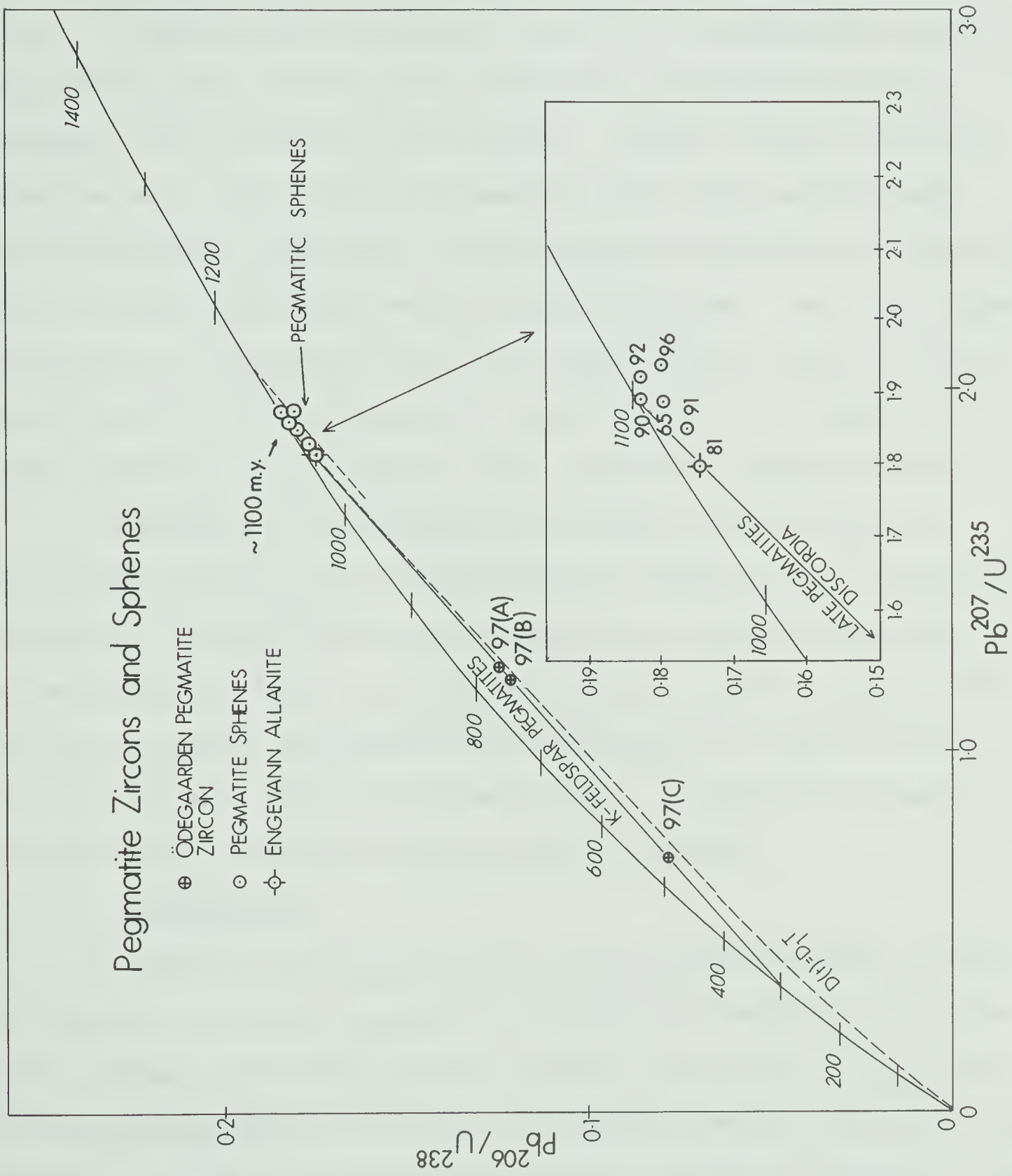


Fig. 23.  $Pb^{206}/U^{238}$  -  $Pb^{207}/U^{235}$  diagram for Levang gneiss dome zircons and sphenes.









through the three data points (for these zircon fractions) and the allanite (SN-81) from the Engevann K-feldspar pegmatite, which is seen to have an upper intercept with the concordia at 1100 m.y. and a lower intercept at 290 m.y. Sphene contained in xenolithic patches of the Ødegaarden pegmatite appears to be older than the zircon contained in the pegmatite proper, in accordance with the observed field relations. Sphenes analyzed from other pegmatites and a rutile albitite (kragerøite) yield older apparent ages than the K-feldspar pegmatites; it must, however, be emphasized that none of these are statistically older at two standard deviations. Due to the larger uncertainty in the analysis of the sphene sample SN-68-161 from the Levang gneiss dome, the K-feldspar pegmatites cannot be shown to be significantly younger than the Levang gneiss dome within reasonable confidence limits.

For purposes of comparison with the Permian episodic lead loss interpretation offered above for the Ødegaarden pegmatite zircon fractions, an 1100 m.y. diffusion trajectory for Wasserburg's radiation damage model has been plotted in Fig 24. Although the episodic loss model appears to fit the data from samples with greater than approximately 40% lead loss better than this particular continuous diffusion model, a unequivocal statement as to the mechanism of lead loss cannot be made at this time.

### 3. Th-Pb Results

In addition to the  $t_{206}$ ,  $t_{207}$ , and  $t_{207/206}$  ages obtainable from the U-Pb system, an unrelated  $t_{208}$  age is obtainable from the Th-Pb system. The tendency amongst many workers has been to make little mention of  $t_{208}$  ages of zircons unless they are concordant with results from the U-Pb system. The apparent  $t_{208}$  ages of zircons reported here are certainly no exception to the frequently observed discordance between the U-Pb and Th-Pb systems. It is felt, however, that there is much to be learned of parent daughter loss relationships, especially in multiphase systems, by a consideration of these









discordant data.

In principle two concordia-type diagrams can be constructed in the U-Th-Pb system; these being an  $r\lambda_{232} - r\lambda_{235}$  and an  $r\lambda_{232} - r\lambda_{238}$  diagram. However, it is only really practical to make use of the  $r\lambda_{232} - r\lambda_{235}$  diagram because of the small curvature of the concordia in the  $r\lambda_{232} - r\lambda_{238}$  diagram. All the U-Th-Pb data are shown on an  $r\lambda_{232} - r\lambda_{235}$  diagram in Fig 25. Since linear relationships are not present in Fig 25, the use of such a diagram for the data presently under consideration is somewhat unusual, however it is a very convenient method of graphically presenting such data. Approximate error circles have not been assigned to the plotted analyses in Fig 25, but the measured  $\text{Th}^{232}/\text{Pb}^{208}$  ratios are probably no more than  $\pm 2\%$  in error.

Consideration of Fig 25 reveals the following points:

1. The sphenes, with the exception of sample SN-68-161, are much more concordant than the zircons grouping close to the concordia near their 'true' age.
2. Zircons which plot on the 1160 m.y. discordia in the  $r\lambda_{238} - r\lambda_{235}$  diagram show considerably less scatter than the older zircons, but do not exhibit linear relationships.
3. The 1400 m.y. old zircons have apparent  $t_{208}$  ages ranging from near their 'true' age to greater than 4.0 b.y., which to a first approximation appears to correlate with their U + eq. Th contents and the degree of apparent lead loss in the U- Pb system.
4. The zircon fractions from the Ødegaarden pegmatite do show a linear relationship, falling on a line almost normal to the concordia and intersecting it at a value less than their apparent age as observed from the U-Pb system.

Some limiting lines for various types of parent-daughter loss have been plotted in Fig 24. AA' is the limiting line for pure  $\text{Pb}^{207}$  loss from an 1100 m.y. old multiphase U-Th-Pb system, and similarly BB' is the same for a 1400 m.y. old



system. Points lying above these lines cannot be explained in terms of daughter loss only from a single or multiphase U-Th-Pb system. A'C' and B'D' are the trajectories for pure Th loss from 1100 m.y. and 1400 m.y. old systems respectively, and AC'' the approximate trajectory for non-fractionating lead loss from a single phase U-Th-Pb system. A'A'' is the line for pure Pb<sup>208</sup> loss from a multiphase system. A more extensive treatment of U-Th-Pb systems will be made in a subsequent section.

#### Electron Probe Investigation of Ødegaarden Pegmatite Zircon

Recent electron probe analytical traverses of some zircon grains by STEIGER & WASSERBURG (1966) and DAVIS et al. (1968) have demonstrated an irregularity in the distribution of U and Th in some zircon crystals. When dealing with U-Th-Pb systems it is of course important to know whether the analyzed material is to be treated as a single or multiphase system. The Ødegaarden pegmatite zircon was selected for investigation because one can be reasonably sure that the three analyzed gravity fractions are cogenetic.

Sectioned crystals of the zircon are megascopically zoned, in part fractured and seen to contain secondary iron oxides along these fractures. Their pale grey colouration is suggestive of a metamict condition; evidence for which is derived from the rather weak x-ray diffraction pattern obtained from this mineral.

Initially it was considered likely that the different zones of the zircon crystal would have different uranium and thorium contents, as has been observed in 'stripping' experiments of SILVER & DEUTSCH (1963), therefore three outer zones of a zircon crystal were examined by counting for 50 seconds at 3 micron intervals across the zones. This procedure did not reveal detectable variations in uranium content in the particular zones examined, and the method was therefore abandoned. Using an electron-beam scanning technique it was possible to locate phases in the above zircon



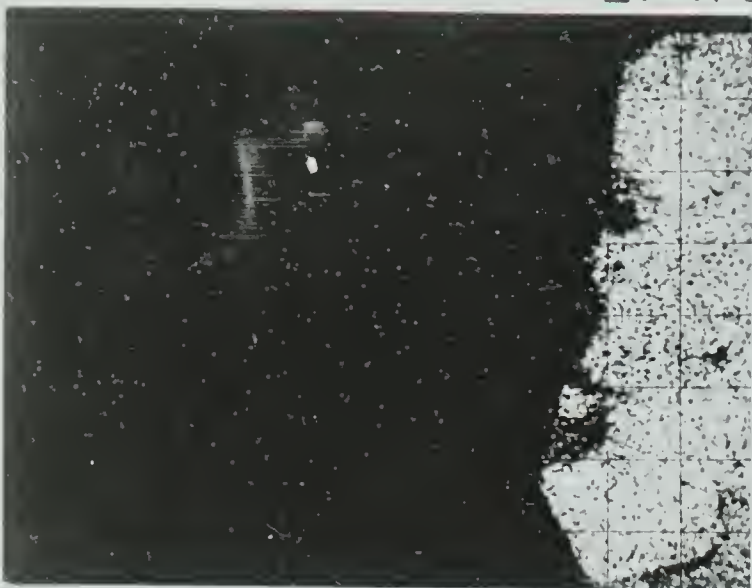




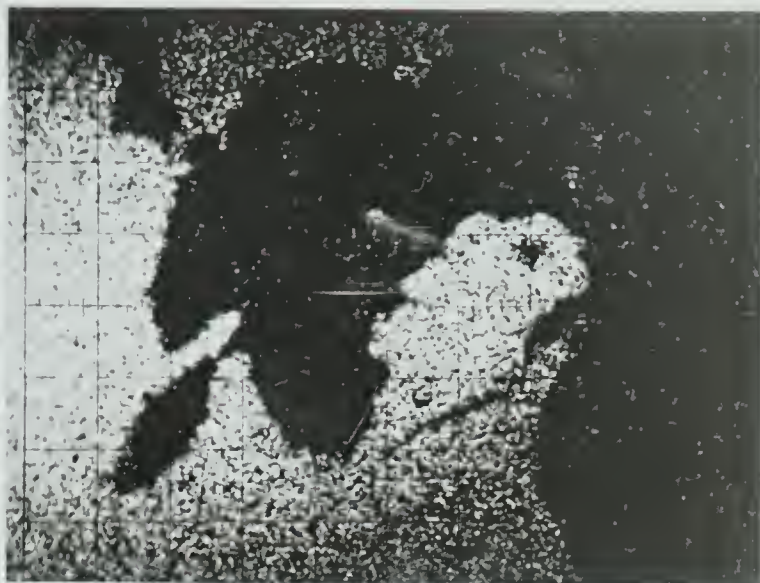
PLATE II.

X - ray scanning images of Zr, Al, K, Si, Pb, and C showing the location of K-feldspar and silica at the margin of the Ødegaarden pegmatite zircon. Note the location of Pb and C along the grain boundaries. Each photograph represents about 600 microns in the long dimension . As each photograph represents different lengths of exposure only a qualitative interpretation is possible.

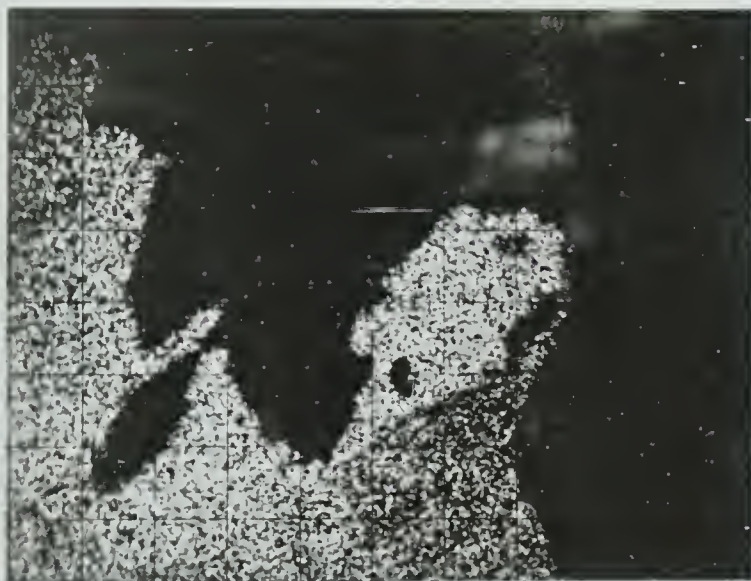
# PLATE II.



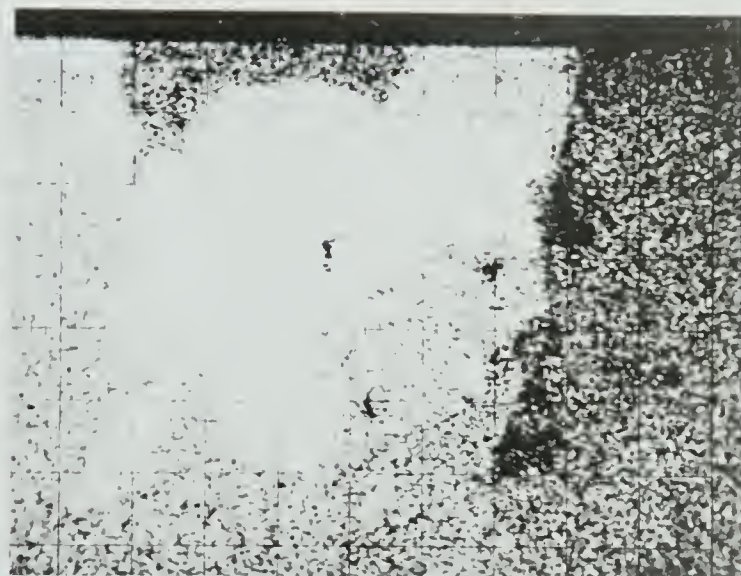
Zr



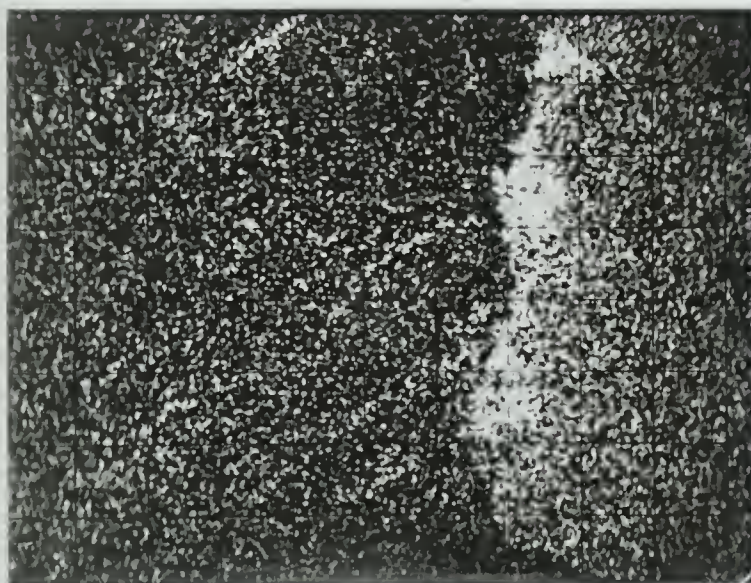
Al



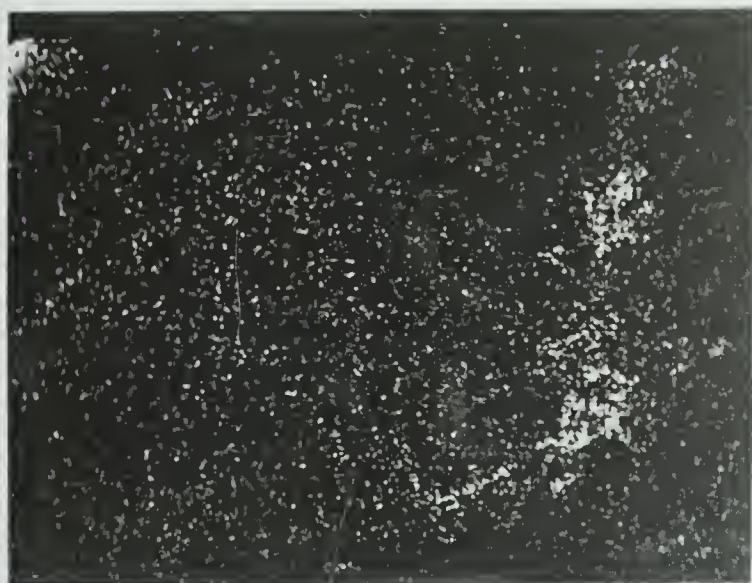
K



Si



Pb



C



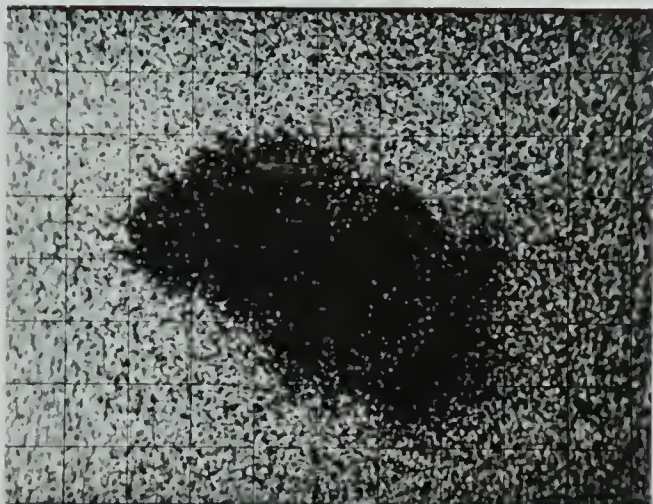


PLATE III.

X-ray scanning images for a high-Th phase located within the  
Ödegaarden pegmatite zircon for Zr, U, Si, Th, Al, and O. The size of the  
high-Th phase is about 60 microns. Note: since each of the photographs  
represent different lengths of exposure only a qualitative interpretation is  
possible.



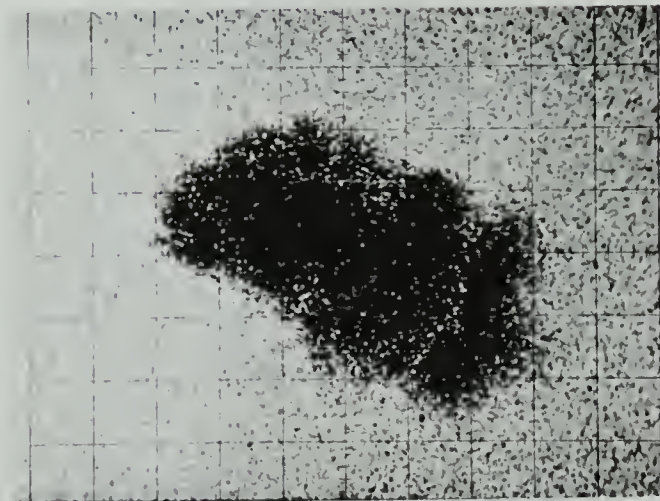
PLATE III.



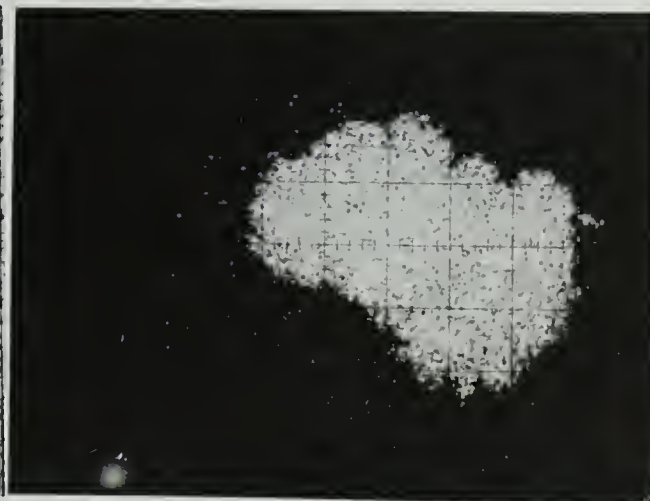
Zr



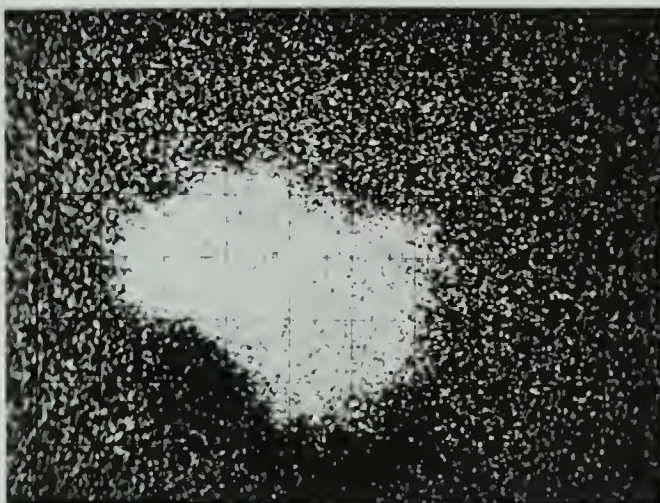
U



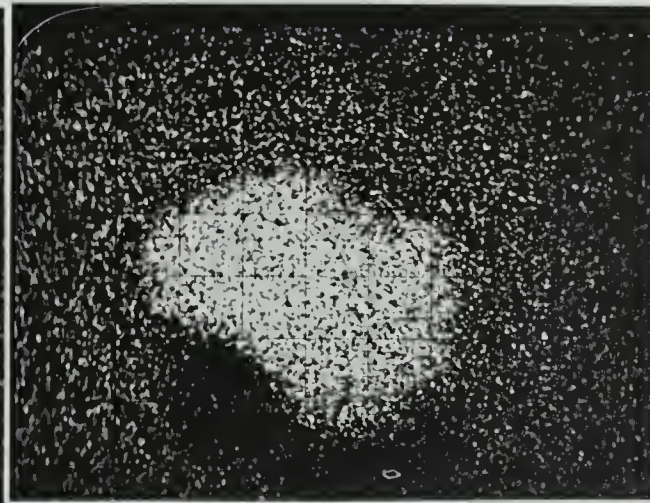
Si



Th



Al



O





crystal with U and Th concentrations considerably greater than the enclosing zircon.

One of the phases investigated is particularly high in thorium. Scanning x-ray image photographs for U, Th, Al, Zr, Si and O are shown for the area in which the phase was located in Plate 2: the diameter of the Th-rich phase is approximately 20 microns. Since the scanning x-ray image photographs were obtained using considerably different lengths of exposure, the intensities cannot be even semi-quantitatively related to concentrations and must only be interpreted on a 'present or absent' basis. At the time of analysis, however, it was apparent that the concentration of Th was far in excess of that of U and that only a small amount of Al was present. No elements, including rare earths, other than those in Plate 2 were detected in the phase, thus it appears to be similar to thorianite in composition, although Al has not been recorded to the author's knowledge in thorianites (e.g. MAKAROV and LIPOVA 1962). The apparent concentration of zircon in the centre of the phase is probably due to excitation of zirconium in the zircon beneath the grain. Within the particular zircon crystal investigated, no other thorium-rich phases were located.

At the margin of the zircon crystal adjacent phases were investigated using the same scanning technique described above. Scanning x-ray image photographs for Al, Si, K, Zr, Pb and C are shown in Plate 3. Again the same variations in exposure time apply here, and only qualitative interpretations are possible. Neither thorium nor uranium were detectable in either the zircon or K-rich phase. The two phases present are most likely K-feldspar and quartz. Also noteworthy is the concentration of lead at the left extremity of the zircon grain and along other phase boundaries and its association with carbon, indicating that it may be fixed along the grain boundaries as a carbonate. It would, of course, be very interesting to know if



this was radiogenic lead derived from the zircon or common lead from the K-feldspar in the pegmatite. The presence of this phase probably results from low temperature alteration or weathering of both the zircon and the K-feldspar; the susceptibility of zircon to weathering and alteration in alkaline environments has been noted by SAXENA (1966). High concentrations of Fe (probably as a hematite) were detected along some of the cracks throughout the zircon crystal.

The secondary Pb-bearing phase is probably dissolved during acid washing of the zircon prior to analysis and isotopically does not enter into a consideration of the discordancy patterns. This would not, however, apply to the high Th phases within the zircon crystal and these must be considered in any discussion of discordance in the U-Th-Pb system of this sample.

#### Multiphase: U-Th-Pb Systems

STEIGER and WASSERBURG (1966) in their discussion of the Sandia Mountains zircons have made an important contribution to our understanding of open U-Th-Pb systems. They have discussed in considerable detail various trajectories in the  $r\lambda_{232} - r\lambda_{235}$  diagram, which may result from two phase U-Th-Pb systems. ALLEGRE (1966) has also discussed some discordance patterns in the  $r\lambda_{232} - r\lambda_{235}$  systems.

The electron probe investigation of the Ødegaarden pegmatite zircon has demonstrated that the sample may be treated as a two phase system, to a first approximation at least, assuming that the secondary minerals are completely dissolved during acid washing. In the ensuing discussion the high Th and comparatively high U phase will be designated as phase  $\alpha$ , and the zircon as phase  $\beta$ .

Of particular pertinence to the  $r\lambda_{232}$  and  $r\lambda_{235}$  results for the Ødegaarden pegmatite zircon is Steiger and Wasserburg's treatment of episodic departure of a two phase U-Th-Pb system from closed-system conditions:



$$r\lambda_{232}(t) = [(1 - m_{208}^{\alpha}) T_B^{\alpha} + (1 - m_{208}^{\beta}) T_B^{\beta}] [\exp. \lambda_{232}t - \exp. \lambda_{232}t_1] / \\ [T_B^{\alpha}(1 - m_{232}^{\alpha}) + T_B^{\beta}(1 - m_{232}^{\beta})] + (\exp. \lambda_{232}t_1 - 1)$$

$$r\lambda_{235}(t) = [(1 - m_{207}^{\alpha}) U_B^{\alpha} + (1 - m_{207}^{\beta}) U_B^{\beta}] \cdot [\exp. \lambda_{235}t - \exp. \lambda_{235}t_1] / \\ [U_B^{\alpha}(1 - m_{235}^{\alpha}) + U_B^{\beta}(1 - m_{235}^{\beta})] + (\exp. \lambda_{235}t_1 - 1)$$

where  $m_{208}^{\alpha}$  is the mole fraction of  $Pb^{208}$  remaining in phase  $\alpha$  after the episodic disturbance of a system of age  $t$ , at  $t_1$ . Likewise  $m_{207}^{\beta}$  is correspondingly the remaining mole fraction of  $Pb^{207}$  in phase  $\beta$  after the disturbance etc.  $T_B^{\alpha}$ ,  $T_B^{\beta}$ ,  $U_B^{\alpha}$ ,  $U_B^{\beta}$ , are the initial thorium and uranium concentration in phases  $\alpha$  and  $\beta$  respectively,  $t_1$  is the time of episodic disturbance.

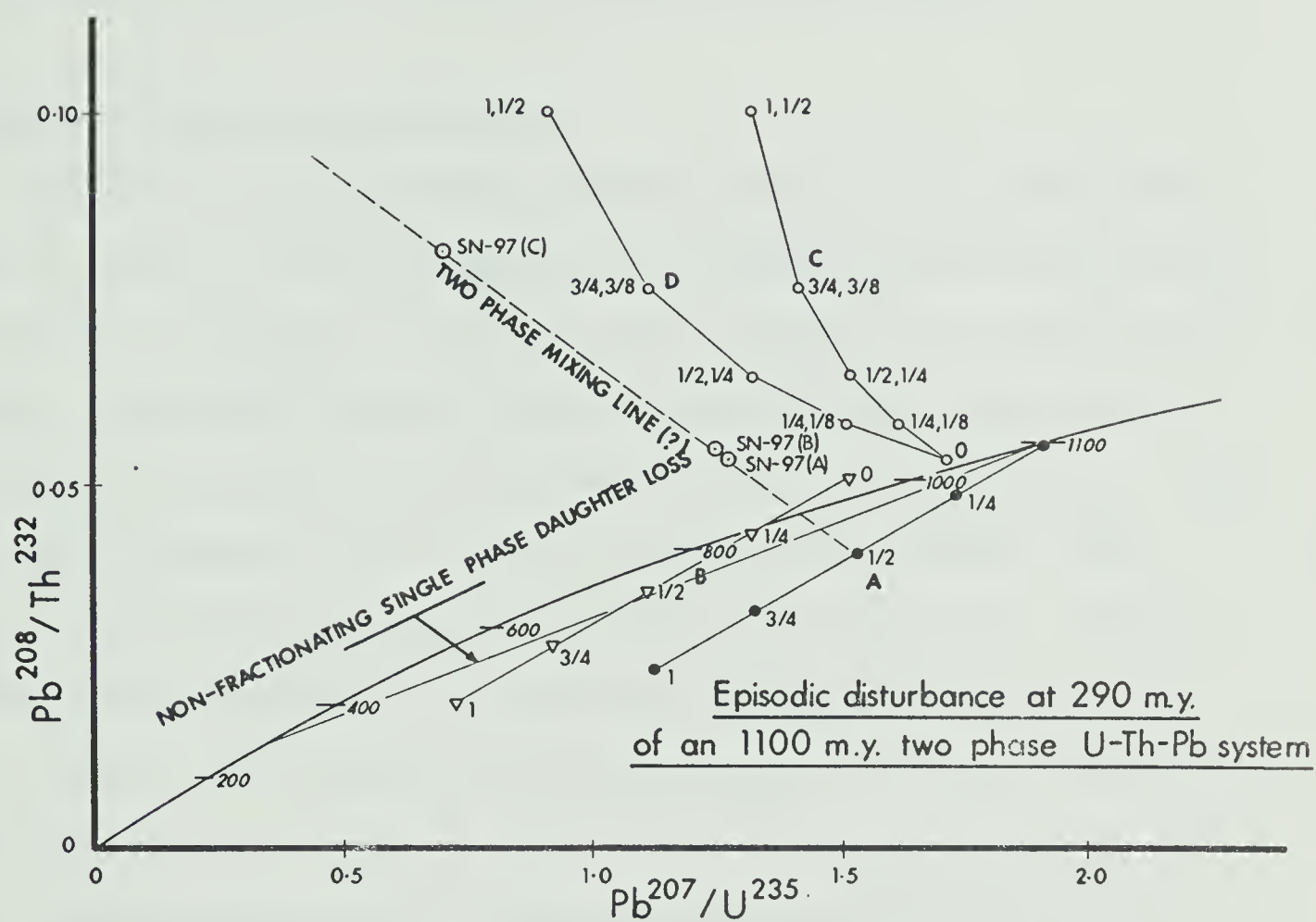
The values of  $t$  and  $t_1$  for the Ødegaarden pegmatite zircon are taken as 1100 m.y. and 290 m.y. respectively, as derived from the  $r\lambda_{238} - r\lambda_{235}$  diagram and the above equations have been solved for the following cases:

1. Non-fractionating lead loss from  $\beta$  only with  $T_B^{\beta} = 0.75$  and  $U_B^{\beta} = 0.5$ .
2. Lead loss from both  $\alpha$  and  $\beta$  with  $T_B^{\beta}$  and  $U_B^{\beta}$  as above and  $T_B^{\alpha} = 0.25$  and  $U_B^{\alpha} = 0.5$ , but with 50% of the daughter lost from  $\alpha$ .
3. Similar to above, but for lead loss from  $\alpha$  and  $\beta$  at half the rate of Th loss from  $\beta$ .
4. As for case (3), but lead loss from  $\alpha$  at twice the rate of lead loss from  $\beta$  and Th loss from  $\beta$  equal to the rate of lead loss from  $\alpha$ .

The results of these calculations together with the analytical data for the Ødegaarden pegmatite are plotted in Fig 26. In terms of a two phase U-Th-Pb system the Ødegaarden zircons could be explained as mixtures of two end components, one of which has undergone parent loss as well as daughter loss. The loss of parent may be a continuous or episodic diffusional loss, or else due to recent weathering or acid washing in the laboratory. The observed  $r\lambda_{232} - r\lambda_{235}$  relationship may result from a contin-









uous diffusion of  $\text{Pb}^{208}$  out of the high Th phase into the zircon, rather than Th-loss, where it remained comparatively unaffected by weathering or laboratory acid wash treatment. Obviously the actual situation may be much more complex than this, but this is one simple interpretation considering the sample to be composed of only two U-Th-Pb bearing phases.

#### Mechanisms of Lead Loss from Zircons

Difficulty in distinguishing between continuous and episodic mechanisms of lead loss from U-Pb systems is encountered in many geochronological studies of zircons. For example, data obtained in the present investigation, and by BANKS and CAIN (1969) and GREEN (1968) appear to be compatible with both episodic and continuous diffusion interpretations. Data of SILVER and DEUTSCH (1961), DAVID et al (1962) and CATANZARO (1963), however, are most consistent with an episodic lead loss model. Normally episodic lead loss models are favoured over continuous diffusion models, where there is other geological or geochronological evidence of an event at the apparent time of episodic lead loss as derived from the lower concordia-discordia intersection. Since geological evidence does exist in South Norway for a Carboniferous-Permian event one may favour an episodic lead loss interpretation over a continuous diffusion interpretation. In view of the fact that some zircons separated from xenoliths in a granodiorite have shown only slight lead loss (KUOVO and TILTON, 1966), whereas others apparently have lost lead at low temperatures, it is necessary to examine the mechanisms whereby lead may be lost from zircons, before further pursuing the present discussion of episodic versus continuous losses of lead.

Silver's observation (SILVER, 1961) that the amount of discordance in the U-Pb system of cogenetic zircons from the Johnny Lyon granodiorite



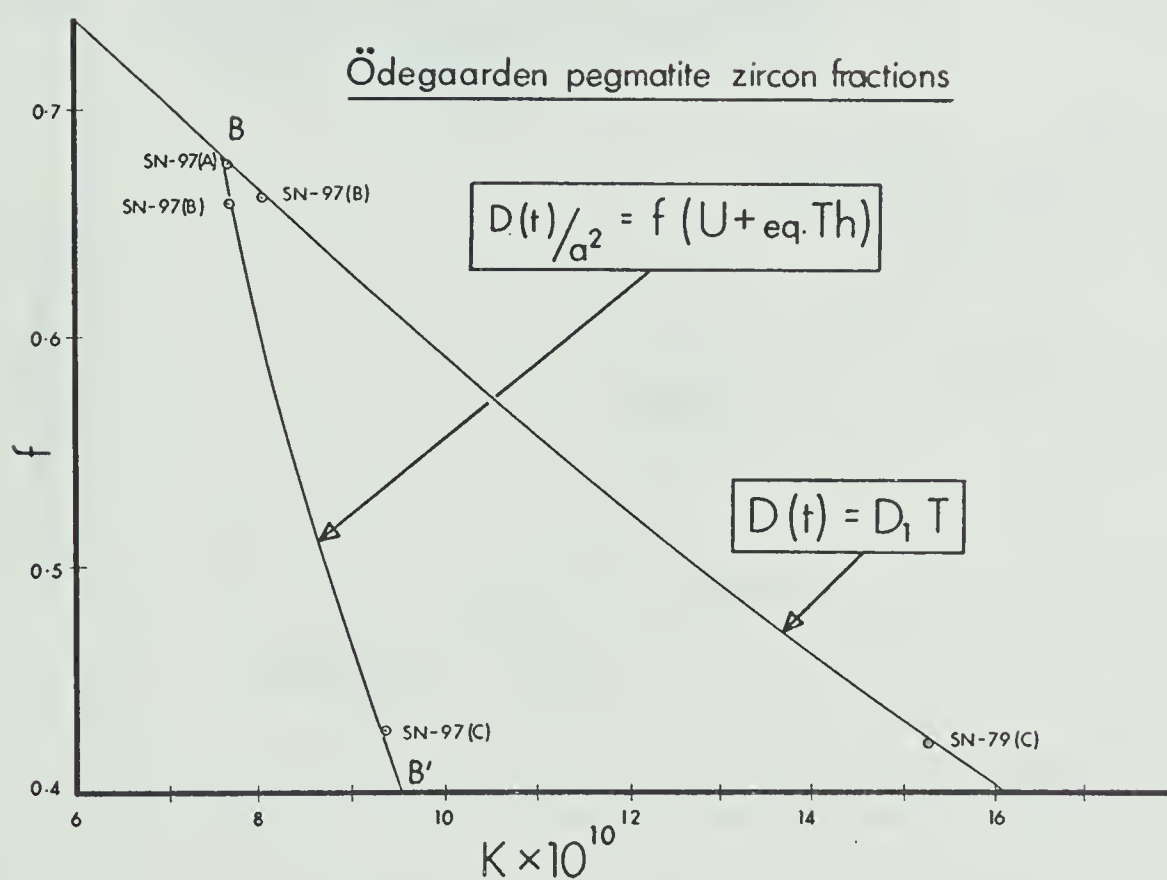


Fig.28. Plot of  $f'[(^{206}\text{Pb}/^{238}\text{U})/(e^{\lambda t}-1)]$  versus  $'K'(\pi\sqrt{2D_1}/a)$  for the Wasserburg continuous radiation model. Upper curve is plotted for the three fractions of the Ödegaarden pegmatite zircon assuming values of  $'K'$  proportional to  $'f'$  for the Wasserburg model. The lower curve assumes that  $D/a^2$  for the three fractions is proportional to their  $U + eq.Th$  contents. SN-97(A) is arbitrarily fixed on the upper curve.





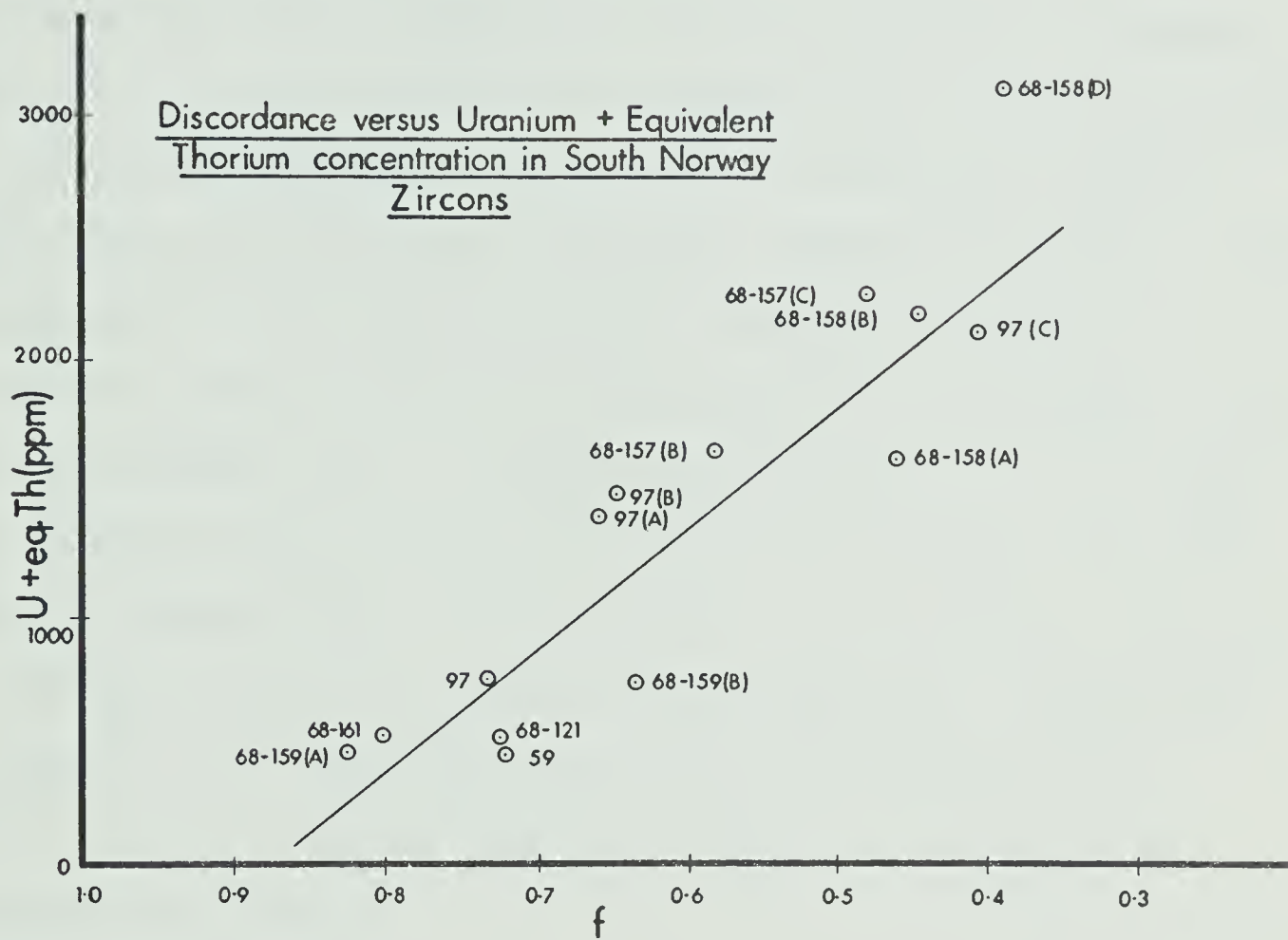


Fig.27. Plot of uranium plus equivalent thorium concentrations versus 'f'  $[(\text{Pb}^{206}/\text{U}^{238})/(e^{\lambda_{238}t} - 1)]$  in the South Norwegian zircons.



is related to the total radioactive bombardment received by the samples, is an important contribution to our understanding of zircon discordance. In Fig 27, the U+eq. Th concentrations in all the zircons analyzed are plotted versus  $f[(\text{Pb}^{206}/\text{U}^{238}) / (e^{\lambda^{238}t} - 1)]$ , and support the general functional relationship between discordance and total radioactivity received by zircons, noted by Silver.

The total radiation received by a zircon lattice since its formation is the sum of  $\alpha$ ,  $\beta$  and  $\gamma$  radiation from U and Th, and the contributions from recoil nuclei and spontaneous fission of  $\text{U}^{238}$ . Contributions from outside the lattice are in most cases negligible. HOLLAND and GOTTFRIED, (1965) have suggested that the progressive radiation damage and breakdown of a zircon lattice primarily results from the formation of displacements. LIPOVA (1966) has calculated that one  $\alpha$  particle from the decay of a  $\text{U}^{238}$  nucleus, with an energy of 4 Mev can displace 239 atoms and the recoil of the  $\text{U}^{234}$  nucleus will displace 1370, in close agreement with the estimate of HOLLAND and GOTTFRIED (loc.cit.) of around 1500 displacements per  $\alpha$ -decay event. On the basis of x-ray diffraction studies and density determinations, Holland and Gottfried suggested that the breakdown of the Ceylon zircon took place in three phases:

- a. Zircon lattice becomes saturated with displacements.
- b. Formation of ordered crystallites of zircon.
- c. Finally, transformation to a lower density phase.

A somewhat different view of the zircon metamictization process has been expressed by LIPOVA et al. (1965) and LIPOVA (1966). Using x-ray phase analyses of zirconite performed at successively higher temperatures, these authors have identified cubic  $\text{ZrO}_2$  and from the increase in  $\text{ZrSiO}_4$  lines at temperatures in excess of  $700^\circ\text{C}$  and the exothermic D.T.A. peak at  $870^\circ\text{C}$ , have inferred the presence of amorphous  $\text{SiO}_2$ , which is thought to



recombine with  $\text{ZrO}_2$  at higher temperatures. Metamictization in zircons is considered to proceed, with the concomitant formation of dispersed  $\text{SiO}_2$  and  $\text{ZrO}_2$  phases within the original  $\text{ZrSiO}_4$  phase.

The resulting micro-inhomogeneity in the zircon crystals, revealed by electron diffraction studies (LIPOVA, 1966), may have important effects on the subsequent behaviour of the U, Th and Pb in the zircon lattice. It is conceivable that separate thorium bearing phases (thorianite, thorite or uranothorite etc.) may form together with  $\text{ZrO}_2$  and  $\text{SiO}_2$  phases. Uranium will most likely enter into solid solution with  $\text{ZrO}_2$  (AHRENS, 1965, FRONDELL and COLETTE, 1957) or  $\text{ThO}_2$  or  $\text{ThSiO}_4$  as the case may be. Lead, however, is likely to be unstably located as a result of these processes, and as the metamictization process proceeds increasing amounts of lead may be available for comparatively easy removal. Admittedly such reasoning is entirely conjectural, but nevertheless may serve as a working hypothesis in future considerations of lead loss.

Of the two continuous diffusion models which have been proposed, the continuous radiation damage model of Wasserburg (WASSERBURG, 1963) is considered to be the more feasible since it attempts to relate the amount of lead loss to the radiation received. However some further comment is necessary. Inherent in Wasserburg's model is the assumption that the diffusion coefficient ( $D/a^2$ ) is proportional to the integrated radiation damage, and therefore to the uranium and equivalent thorium concentrations. STEIGER and WASSERBURG (1966) found the data from the Sandia Mountain zircons to be inconsistent with this simple proportionality relationship. For purposes of comparison with Steiger and Wasserburg's data, the relationship has been tested for the three fractions of the Ødegarden pegmatite zircon (Fig 28). Values of 'f' for the three zircon fractions have been plotted versus K (where  $K = 2D_1/a$ ) for the theoretical relationship  $D(t) = D_1 t$  ( $D_1 = \text{constant}$ ).





Also they have been plotted assuming constant 'a' and a proportional relationship between  $D/a^2$  and  $U + eq. Th$ , arbitrarily fixing fraction A on the theoretical curve and calculating  $D/a^2$  for that fraction. The result is qualitatively the same as that found by STEIGER and WASSERBURG (loc.cit.) namely that  $D/a^2$  increases at a rate faster than the proportionality relationship predicts. In the case of the fraction SN-97(C),  $(D/a^2)_{calc.} = 1/6 (D/a^2)_{theoretical}$ , which might imply that as radiation damage proceeds the radius of the sphere of diffusion is simultaneously decreased by  $1/\sqrt{6}$  i.e. approximately 1/2. In terms of zircon crystal chemistry this may reflect the coalescence of domains in the lattice which have a high proportion of displacement damage. Rather than thinking in terms of a decrease in the diffusion dimension it may be more realistic to consider that larger parts of the lattice are 'available' to hydrothermal effects.

Of some pertinence to the present discussion are the results of hydrothermal experiments of PIDGEON et al. (1966) on the metamict 500 m.y. old Ceylon zircon, since their experimental conditions approximate geological conditions. The zircon was maintained at a temperature of  $500^{\circ}\text{C}$  and 1000 bars pressure for times of up to 300 hours, which succeeded in removing approximately 50% of the lead present, without any measureable isotopic fractionation. However, the kinetic loss of lead from the zircon was not directly proportional to time; a large part of the lead might be located in two different positions within the zircon. This may correspond to lead located in  $\text{ZrSiO}_4$ , and lead released during the formation of  $\text{ZrO}_2$  and  $\text{SiO}_2$  phases upon metamictization. BRANDT and PERMINOV (1968) have attempted to evaluate the effect of pressure on the diffusion coefficient for the conditions of the above experiments ( $500^{\circ}\text{C}$ , 1Kb, 2M NaCl). Brandt and Perminov derive the following formula:



$$D/a^2 (T,P) = D_0/a^2 (1 + kp) e^{-E/RT}$$

where  $k$  is a phenomenological constant, which is a function of the fluid phase chemistry and may be greater or less than one. It is interesting to note that  $k$  and  $p$  only affect the pre-exponential term of the above equation i.e. the lattice characteristics, and not  $E$  (activation energy). Using in vacuo data for the liberation of lead from pitchblende (BRANDT et al., 1963)  $E=50$  kcal/mole,  $D/a^2 = 1$ , Brandt and Perminov have estimated  $k$  at  $0.6 \text{ atm}^{-1}$ , Since pitchblende and zircon are not directly comparable, this can only be considered to be an approximate value for  $k$ . For the conditions of 2M NaCl therefore, it is apparent that a small increase in pressure will greatly increase  $D/a^2$ . However departures from these values must be expected for natural solutions. Under certain hydrothermal conditions it may be expected that lead will be removed in an apparently continuous manner. At the same time, however, although exactly the same radiation damage processes may be operative within the zircon, P,T or C (fluid composition) differences may result in the retention of lead in the sample, which may or may not subsequently be removed as a result of change in P,T and C (i.e. episodic loss).

The distinction between episodic and continuous diffusion losses may therefore not necessarily derive from different processes operative within the zircon, nor solely from the thermal regime, but from combinations of the following:

- a. The degree of radiation damage in the crystal, and the resulting location of radiogenic lead.
- b. The subsequent thermal history of the zircon relative to the condition of (a) above.
- c. The chemistry of those hydrothermal solutions which may affect the zircon continuously or at an episode or episodes, temperature, i.e. depth of burial and the geothermal gradient.





## CHAPTER VI - RUBIDIUM-STRONTIUM DATING

Introduction

Natural rubidium consists of two isotopes with masses of 85 and 87, of which  $\text{Rb}^{87}$  decays by  $\beta$ -particle emission to  $\text{Sr}^{87}$ , at a rate which renders the  $\text{Rb}^{87}$ - $\text{Sr}^{87}$  decay scheme amenable to the radiometric dating of some geological materials.

Considerable uncertainty, however, still surrounds the magnitude of the  $\text{Rb}^{87}$  decay constant. For example, FLYNN and GLENDENIN (1959) counted the specific activity of natural rubidium by dissolving an organic rubidium salt in a liquid scintillation counter and determined a decay constant of  $\lambda^{87} = 1.47 \times 10^{-11} \text{ yr}^{-1}$ . ALDRICH et al. (1958) on the other hand, calculated a decay constant of  $\lambda^{87} = 1.39 \times 10^{-11} \text{ yr}^{-1}$  by the comparison of  $\text{Rb}^{87}/\text{Sr}^{87}$  ratios of pegmatitic minerals with U-Pb data for cogenetic uraninites. Many additional attempts have been made to determine the  $\text{Rb}^{87}$  half-life physically, a recent review of which has been given by HAMILTON (1966). The actual value of the half-life, although still uncertain, undoubtedly lies between 4.7 and 5.3 b.y. The decay constant of  $\lambda^{87} = 1.39 \times 10^{-11} \text{ yr}^{-1}$  is currently adopted at the University of Alberta and appears to give more consistent results with U-Pb and K-Ar results (see for example GREEN, 1968). CUMMING (1969) has recently reviewed and re-assessed some of the available Pb,Rb-Sr and K-Ar data for meteorites, from which he suggests that a decay constant of  $\lambda^{87} = 1.436 \times 10^{-11} \text{ yr}^{-1}$  intermediate between the currently used physical and geological estimates, may in fact be optimum.

It is the large half-life of rubidium which severely limits the application of the rubidium-strontium method to geologically young materials, with the analytical precision presently obtainable by most





laboratories. However, in favourable circumstances high-Rb, low common Sr phases as young as 12 m.y. may be successfully dated (c.f. JÄGER, 1966).

The whole rock method of rubidium-strontium dating is probably the singularly most powerful tool currently available to the geochronologist, since it appears that hand sized specimens of rocks may remain closed systems with respect to rubidium and strontium even when subjected to high grade metamorphism. Analyses of a series of cogenetic whole rock samples with differing Rb/Sr ratios are capable of providing a test for closed system behaviour (COMPSTON, 1961). It is, therefore, possible to define a whole rock in an isotopic sense, as the smallest sample size of the complete mode of a rock for which closed system behaviour may be demonstrated.

Whole rock Rb-Sr studies have been undertaken as part of this investigation primarily to examine the scale on which whole rock behaviour was maintained under conditions of high grade regional metamorphism in S. Norway, and to provide additional information concerning the age of the Levang gneiss dome and the gabbroic rocks of the Bamble sector.

### Analytical Techniques

In order to select rocks most suitable for Rb-Sr dating, preliminary X.R.F.S. analyses for rubidium and strontium were made on finely ground, whole rock samples. Any rocks showing signs of weathering were discarded.

For the isotope dilution analysis of strontium, 2 micrograms of an enriched  $\text{Sr}^{84}$  isotope dilutant were added to whole rock samples, containing approximately 20 micrograms of strontium, prior to their decomposition (in this way the measured  $\text{Sr}^{86}/\text{Sr}^{84}$  ratio is approximately one). Samples were decomposed in a mixture of HF and  $\text{HNO}_3$  and evaporated to dryness. HF was removed by adding additional  $\text{HNO}_3$  and evaporating to dryness and finally by adding HCl and again evaporating to dryness. Samples were dissolved in approximately 1 ml of 2.5 M HCl and added



directly to a Dowex 50W-X8(200-400 mesh) cation exchange column. Strontium was eluted with 2.5M HCl and evaporated to dryness. The strontium sample was redissolved in a small amount of demineralized water and loaded on to a single, outgassed Ta filament for mass spectrometric analysis.

The decomposition of the samples for the isotope dilution analysis of rubidium is similar to that described for the determination of potassium. Whole rock samples containing approximately 20 micrograms of rubidium were decomposed in a mixture of HF and  $\text{H}_2\text{SO}_4$  and evaporated to dryness. Approximately 20 micrograms of enriched  $\text{Rb}^{87}$  isotope dilutant in HCl was added to the decomposed sample, which was again evaporated to dryness.  $\text{SO}_3$  was fumed off and the samples ignited over a Meker burner. Rubidium was leached with 1 ml of demineralized water and loaded into a single Ta filament for mass spectrometry. A more complete description of the analytical techniques employed for the determination of rubidium and strontium are given in Appendix E.

The isotopic analyses of rubidium and strontium were performed on a 6 inch radius,  $60^\circ$  sector, single focussing mass spectrometer designed and built by Dr. G.L. Cumming of the Dept. of Physics, University of Alberta. Ion beams were produced by surface ionization from a single Ta filament and amplified directly, using a Cary 31 vibrating reed amplifier with a 10" ohm resistor. For the analysis of strontium, the mass ratios 88/86, 87/86 and 86/84 were measured by rapid peak switching between preset magnet current settings and recording the signals from digital voltmeter output. A slow scan of the strontium spectrum was used for making baseline and tailing corrections. Similarly rubidium was isotopically analyzed by switching between masses 87 and 85 and measuring the isotopic ratio from chart output. It has been the experience in this laboratory (H. Baadsgaard, pers. comm.) that the initial data obtained whilst the rubidium ion currents are slowly increasing is usually the least fractionated, therefore the 87/85 ratios were measured from the first obtainable data.





The measurement precision of  $\text{Sr}^{88}/\text{Sr}^{86}$ ,  $\text{Sr}^{87}/\text{Sr}^{86}$  and  $\text{Sr}^{86}/\text{Sr}^{84}$  is normally 0.1% or better; however the overall reproducibility is normally a factor of two or more greater than this.  $\text{Rb}^{87}/\text{Rb}^{85}$  ratios are usually measurable to within 0.5%, but the additional possibility of fractionation reduces the reliability to 1% or 2%.

### Systematics of the Whole Rock Isochron Method

Consider a phase (in this case a whole rock phase) which contained common strontium at the time of its formation and has accumulated radiogenic strontium for a time  $t$ , where  $t$  is the age of the Rb-Sr system, then:

$$\text{Sr}_p^{87} = \text{Sr}_o^{87} + \text{Rb}^{87} (e^{\lambda t} - 1) \quad (1)$$

where the subscripts  $o$  and  $p$  refer to the initial time of formation and the present time respectively. Dividing equation (1) by  $\text{Sr}^{86}$  we have:

$$\frac{\text{Sr}_p^{87}}{\text{Sr}^{86}} = \frac{\text{Sr}_o^{87}}{\text{Sr}^{86}} + \frac{\text{Rb}^{87}}{\text{Sr}^{86}} (e^{\lambda t} - 1) \quad (2)$$

Equation (2) is the equation of a straight line of the form  $y = a + bx$ , where  $y = \frac{\text{Sr}_p^{87}}{\text{Sr}^{86}}$ ;  $a = \frac{\text{Sr}_o^{87}}{\text{Sr}^{86}}$ ;

$$x = \frac{\text{Rb}^{87}}{\text{Sr}^{86}} \text{ and } b = (e^{\lambda t} - 1) \simeq \lambda t.$$

A plot of  $y$  versus  $x$  i.e.  $\text{Sr}_p^{87}/\text{Sr}^{86}$  versus  $\text{Rb}^{87}/\text{Sr}^{86}$

series of related whole rock samples will yield a straight line of approximate slope  $\lambda t$ . This is essentially a description of Nicolaysen's (NICOLAYSEN, 1961) treatment of the isochron method. More extensive reviews of the Rb-Sr isochron method have been given recently by BAADSGAARD (1965), MOORBATH (1965) and HAMILTON (1966).





It is customary to infer closed system behaviour of whole rock Rb-Sr systems from linear arrays on an isochron diagram, which approximate a straight line within analytical error. Since the present investigation involves rocks which have been subjected to high grade regional metamorphism and potentially might show some departures from closed-system behaviour it is pertinent at this point to consider mechanisms whereby anomalous isochrons may result from partial open-system behaviour. Some of these problems together with the problem of primary isochrons have been recently discussed by LONG (1964), LANPHERE et al. (1964) and KROGH and HURLEY (1968) and the following discussion is in part based upon comments made by these authors.

#### 1. Primary Isochrons and Initial Strontium Ratios

If at the time of formation of a group of related whole rock systems the slope of the isochron was not zero, but rather slightly positive, then the measured isochron age will at all times be in excess of the true age of formation and the projected initial strontium ratio too low. As an example the study of recent volcanics from Arabia by DICKINSON et al. (1969) may be cited, where the initial  $\text{Sr}^{87}/\text{Sr}^{86}$  ratios appear to be related to the Rb/Sr ratios, suggesting an age of 30-40 m.y. This has apparently resulted from a 30 to 40 m.y. delay between a fractionation event in the mantle and the time of extrusion at the surface. At any time in the future the Rb-Sr isochron age will always be in excess of the age of extrusion.

An intimate mixing of older sedimentary material with material of essentially zero age will produce a system which yields an apparent age corresponding to the time of deposition but will probably yield an anomalously high initial strontium ratio.

#### 2. Migration of Rubidium and Alkali Metasomatism

If a related group of whole rocks lost  $\text{Rb}^{87}$  during metamorphism, in amounts proportional to their initial Rb contents then an isochron with an



anomalous slope would result. The possibility of this being achieved is unlikely, since different rock-forming silicate minerals would likely lose Rb at different rates; the amounts lost by a particular whole rock being dependent on the mineralogical mode of the rock, unless one particular mineral contained most of the rubidium in the related group of whole rocks.

However, should metamorphism involve the metasomatic addition and removal of alkalis from a group of rocks in an uncorrelated manner, then the rocks would scatter about a zero isochron at the time of metamorphism. The degree of scatter exhibited by the rocks would be dependent upon the length of their previous history and their former Rb/Sr ratios. Such a process could conceivably produce a zero isochron with minimal scatter from a group of sediments which had a short crustal history prior to metamorphism or from sediments which had equilibrated with sea water strontium at the time of sedimentation.

### 3. Strontium Isotopic Migration and Mixing

Radiogenic and common strontium are normally located in different lattice sites in silicate minerals and it might be anticipated that they will behave differently under metamorphic conditions. With respect to the preferential loss of radiogenic strontium, the arguments developed above for rubidium loss are applicable. However, it is entirely feasible that large scale removal of radiogenic strontium by partial anatexis may in some instances be capable of producing a zero isochron. In the case of  $\text{Sr}^{87}$  redistribution, the amounts leaving and being gained by whole rock systems must be proportional to their contents relative to the average for the group of rocks (i.e. the axis of isochron rotation during redistribution) at the time of metamorphism, and the amounts gained must in some obscure manner be related to their pretransfer  $\text{Sr}^{87}$  contents. Neither of these processes would appear to be of potential importance.

Complete mixing of strontium isotopes between whole rock phases





is dependent upon the scale of Rb/Sr variation and can be treated in a similar manner to the post-formational metamorphic redistribution of strontium between minerals in a whole rock. If Rb/Sr variability occurs on a very local scale in granitic rocks, some degree of strontium isotopic mixing is to be expected, but if only on a regional scale would be rather unlikely. Such Sr isotopic mixing is most probable for a disequilibrium assemblage of sedimentary rocks.

### The Levang Gneiss Dome

Seven whole rock samples have been analyzed from the Levang gneiss dome, five of which are granite gneisses and two of which are granodiorite gneisses (see petrographic descriptions in Appendix A). Analytical data for the samples is presented in Table 10. The results have been plotted on a conventional Nicolaysen diagram in Fig 29 and are seen to define a  $1673 \pm 24$  m.y. isochron (one standard deviation). The isochron was fitted to the data points with the aid of an A.P.L. program written by H. Baadsgaard based on the method of least-squares fitting of a straight line of YORK (1966) and McINTYRE et al. (1966), which allows for non-uniform variance in the  $\text{Rb}^{87}/\text{Sr}^{86}$  ratios and incorporates prior estimates of the precision for both coordinates. The estimates of variance used are those of H. Baadsgaard: constant of variance in  $\text{Rb}^{87}/\text{Sr}^{86} = 2.551 \times 10^{-5}$ ;  $\text{VARY}_1 =$  variance in  $\text{Sr}^{87}/\text{Sr}^{86} = 2.2 \times 10^{-7}$ . Variance estimates for the single  $\text{Sr}^{84}$  'spiking' method currently in use have not yet been made, and work is presently in progress to do this.

The Levang gneiss dome appears to be composed of rocks formed in a previous orogenic cycle, which have been mobilized, but not homogenized with respect to strontium, during the 1150-1100 m.y. metamorphic episode. The 1673 m.y. apparent age most likely refers to the time of formation of the paragneisses comprising the gneiss dome. Sampling localities of the Levang





TABLE 10.

Rb/Sr Analytical Data for the Levang Gneiss Dome.

Sample No.	Rb(ppm)	Sr <sup>N</sup> (ppm)	Sr <sup>87rad.</sup> (ppm)	Rb <sup>87</sup> /Sr <sup>86</sup> atomic ratio	Sr <sup>87</sup> /Sr <sup>86</sup> atomic ratio
SN-68-161	88.5	293.1	0.484	0.8732	0.7169
SN-68-104	91.5	168.1	0.578	1.575	0.7352
SN-68-158	161.6	169.5	1.067	2.758	0.7643
SN-57	162.9	123.5	1.055	3.815	0.7873
SN-68-157	164.0	127.9	1.039	3.708	0.7830
SN-61	89.1	315.0	0.522	0.8177	0.7169
SN-68-105	159.3	129.0	1.025	3.571	0.7811

\* Sr<sup>N</sup> refers to normal strontium.



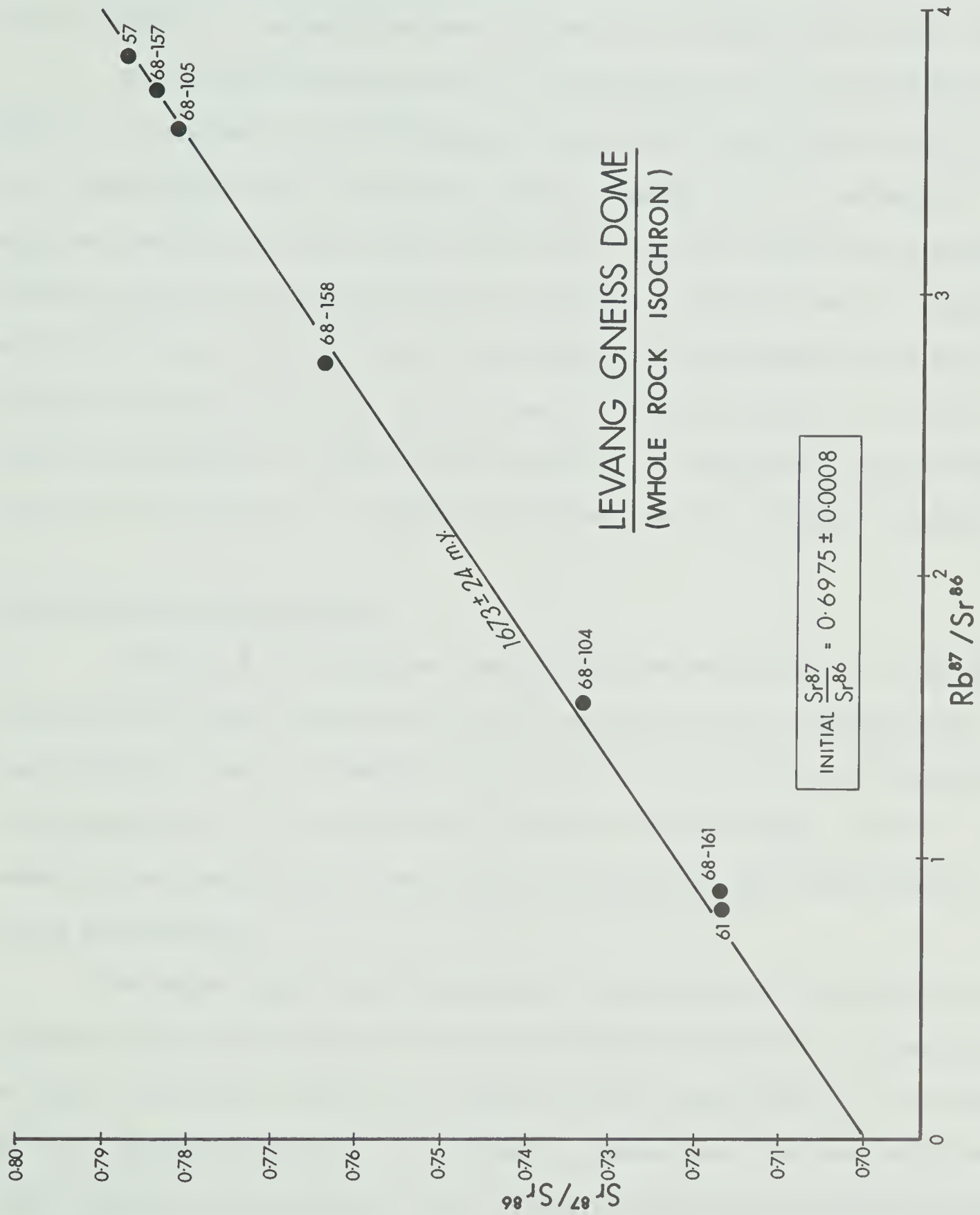


Fig. 29. Whole rock isochron for the Levang gneiss dome.



gneiss dome are separated by a minimum of approximately 1 Km and the gneisses at least show closed system behaviour on this scale, indicating that the size of the whole rock system as defined in the Introduction during the 1150-1100 m.y. metamorphism must obviously be a smaller scale than 1 Km.

The initial strontium ratio of approximately 0.7 is low and is in fact a little lower than the probable average mantle for 1700 m.y. ago (c.f. ARMSTRONG, 1968). It certainly does not appear that the sediments equilibrated with sea water upon deposition or had any significant previous curstal history. The Levang paragneiss dome most probably formed at approximately 1675 m.y., at which time the strontium isotope composition became uniform throughout the rocks by a process of strontium mixing or intense alkali metasomatism. The additional possibility of radiogenic strontium loss during partial melting (c.f. HEIER, 1964) must also be considered however.

#### The Hovdefjell Banded Gneiss

A sample of banded gneiss composed of alternating bands of fine-to medium-grained granite gneiss and biotite amphibolite was collected from near Hovdefjell, west of Vegårshei, approximately 1.5 Km from the Porsgrunn-Kristiansand fault. The sample was initially collected with a view to examining the possibility of small scale strontium isotope homogenization during metamorphism.

The banded gneiss sample measures 9 cms across and the relative proportions of the granite gneiss and biotite amphibolite bands is illustrated in Fig 30. The biotite amphibolite bands are each approximately 1 cm in width and are composed essentially of hornblende, plagioclase, biotite, quartz and a second amphibole which appears to be cummingtonite, whereas the granite gneiss bands are composed of quartz, K-feldspar, biotite and minor amounts of plagioclase and hornblende. Nine bands were sawn from the sample and analyzed as





TABLE 11.

Rb/Sr Analytical Data for the Hovdefjell Banded Gneiss

Sample No.	Rb (ppm)	Sr <sup>N</sup> (ppm)	Sr <sup>87rad.</sup> (ppm)	Rb <sup>87</sup> /Sr <sup>86</sup> atomic ratio	Sr <sup>87</sup> /Sr <sup>86</sup> atomic ratio
SN-77A	137.2	79.1	0.657	5.016	0.7888
SN-77B	116.6	127.4	0.796	2.648	0.7678
SN-77C	112.5	116.7	0.875	2.789	0.7806
SN-77D	120.8	120.4	0.894	2.902	0.7798
SN-77E	110.4	125.4	0.760	2.547	0.7659
SN-77F	123.8	81.8	0.676	4.381	0.7884
SN-77G	120.6	133.0	0.769	2.623	0.7630
SN-77H	133.1	148.3	0.973	2.596	0.7710
SN-77I	147.5	169.2	0.985	2.521	0.7634



# HOVDEFJELL BANDED GNEISS

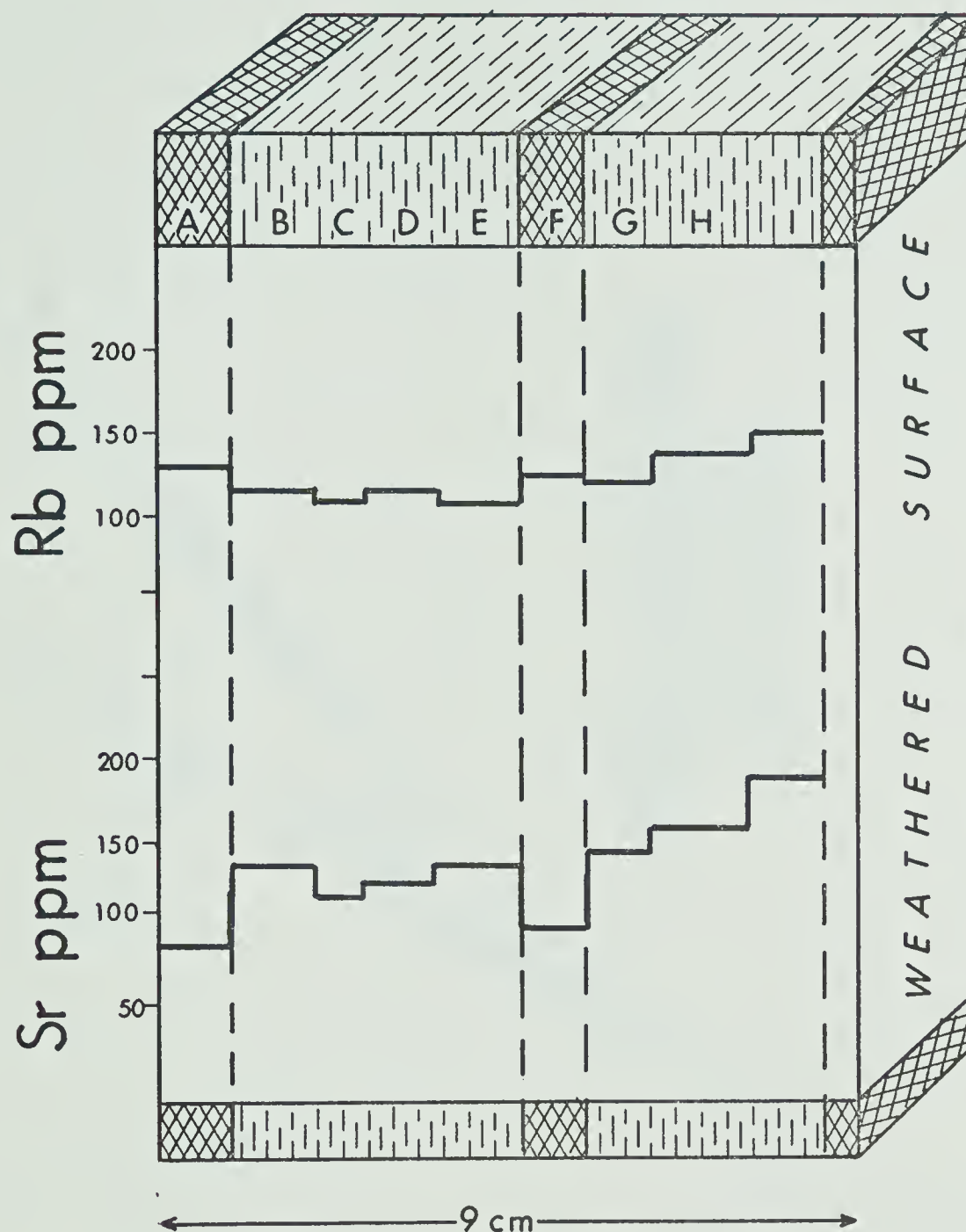


Fig.30. Schematic diagram of the Hovdefjell banded gneiss, showing the bands analysed and their Rb and Sr contents. The cross-hatched areas are biotite amphibolite and the remainder is granitic gneiss. See text for a description.



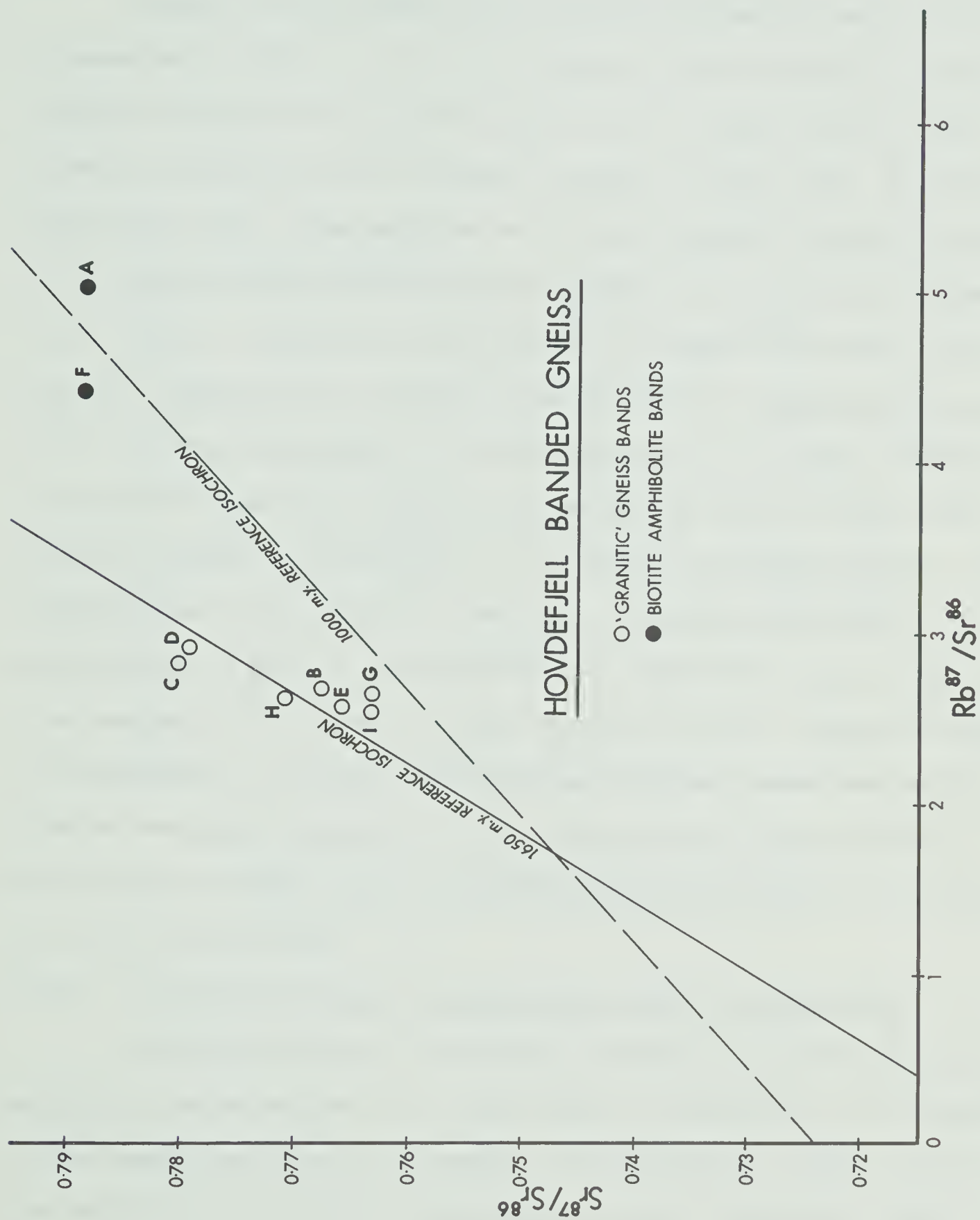


Fig. 31. Nicolaysen plot of the Hovdefjell banded gneiss samples.





shown in Fig 30; the weathered biotite amphibolite band on the right-hand side being discarded.

Results of the rubidium and strontium analyses for each of the bands is presented in Table 11. It is of interest to note the fairly constant rubidium concentration across the sample, but the sharp decline in the strontium concentration and therefore increase in Rb/Sr ratio, in the biotite amphibolite layers. The rubidium and strontium isotopic analyses for each of the samples plotted on a Nicolaysen diagram in Fig 31 are not colinear and do not define a consistent isochron within the assumed analytical error of the analyses; suggesting that complete strontium isotopic homogenization was not achieved during metamorphism. From consideration of this data, however, it is possible to make some deductions concerning the scale of whole rock behaviour during the metamorphism of the Hovdefjell banded gneisses. The interpretation of the results is basically dependent upon whether it is assumed that the granitic gneiss and biotite amphibolite layers were at no time homogenous with respect to their strontium isotopic composition prior to metamorphism, or whether they did actually become homogenized during a previous metamorphic episode. At the present time it is not possible to differentiate between these two possibilities and the data will be discussed for both of these cases.

#### CASE 1. No strontium isotopic homogenization prior to metamorphism

If strontium isotopic inhomogeneity between the granite gneiss and amphibolite bands existed at all times prior to metamorphism, an explanation of the present position of the samples on the Nicolaysen diagram requires that the initial ratio of the two lithologies were quite different. This is diagrammatically illustrated in Fig 32 for whole rock systems which formed  $T$  m.y. ago. At the time of metamorphism ( $t_m$ ) the granite gneiss samples lie on an isochron of slope  $(T - t_m)$  which has a higher projected initial ratio than the



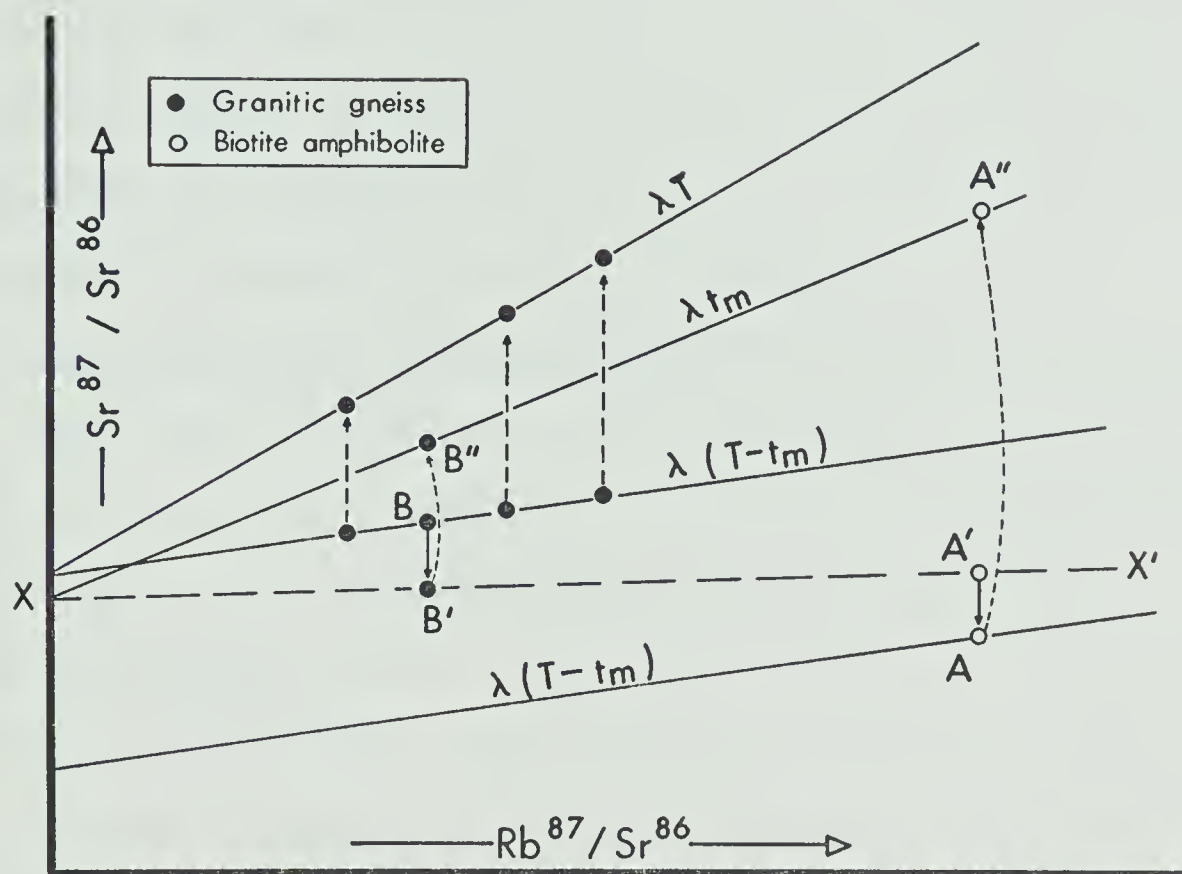


Fig.32. Nicolaysen diagram illustrating a possible evolution of radiogenic strontium in the Hovdefjell banded gneiss assuming that there was no homogenisation of strontium prior to the Sveconorwegian metamorphism.  $T$  is the time of initial formation of the banded gneisses and  $t_m$  is the time of the Sveconorwegian metamorphism.



biotite amphibolite isochron. If during metamorphism, strontium isotopic mixing took place between the biotite amphibolite bands and the first 1 cm or so of granite gneiss in contact with them (this would involve samples SN-77 A,B,E,F,G and I), then points A and B in Fig 32 would be rotated towards a zero isochron ( $XX^1$ ) and to the positions  $A^1$  and  $B^1$  respectively. Subsequent evolution of radiogenic strontium proportional to Rb/Sr for the samples would then move  $B^1$  to  $B^{11}$  and  $A^1$  to  $A^{11}$  onto an isochron of slope of  $t_m$ , somewhat less than the slope ( $T$ ) of the 'undisturbed' granitic gneiss isochron. This interpretation suggests that strontium isotopic mixing took place on the scale of only a few centimetres during metamorphism.

#### CASE 2. Strontium isotopic homogenization during an earlier metamorphism

This case is somewhat more complex than Case 1. However it is assumed, and it is only an assumption, that strontium isotope homogenization occurred between the biotite amphibolite and granitic gneiss during a metamorphism occurring approximately 1650 m.y. ago, and was partially re-established in the 1150-1100 m.y. metamorphism. Some isotopic mixing between samples A and B on the one hand and samples E,F and G on the other, or a preferential migration of radiogenic strontium between these bands, seems probable, because bands A and F have higher Rb/Sr ratios than B,E and G. In view of the fact that both A and B appear to have lost radiogenic strontium, it must be assumed that it was either removed from the total system or else is now located in C. The mechanism by which this might occur is not immediately apparent, however recent heating experiments on the Prosperous Lake granite by H. Baadsgaard (BAADSGAARD, pers. comm.) may have some bearing on the problem.

Baadsgaard found that the thermal migration of rubidium and strontium between the mineral phases in the granite was governed by the 'acceptor' phase rather than by diffusion rates from the 'donor' phase. The combined feldspars increased in radiogenic strontium and both biotite and muscovite lost radiogenic





strontium as phase changes occurred. Since band C contains an almost monomineralic band of K-feldspar it is possible that both bands A and B could lose radiogenic strontium relative to band C. However band I, which also has a high K-feldspar content, appears to have lost radiogenic strontium and there is no obvious mineralogical reason why the radiogenic Sr should be located in band H.

Undoubtedly Case 1 is the most tenable, but this does not necessarily imply that it is correct. Whichever mechanism was operative it is apparent that strontium isotopic homogenization took place over only a small distance during the 1150-1100 m.y. metamorphism. Such small scale redistribution of elements may appear suprising, but KROGH et al. (1967) have arrived at similar conclusions in a study on a banded gneiss from the Grenville Province of Ontario. Studies of a banded biotite-tremolite schist from the Swaziland system by ALLSOPP et al. (1968) however, suggest that complete metamorphic homogenization of strontium was achieved.

The present investigation lends support to the observation of CHINNER (1961), who noted abrupt changes in the ferrous/ferric iron ratios within finely banded gneisses, indicating that the size of a closed chemical system during high-grade regional metamorphism may be very small.

#### The Gabbros and Metagabbros

A wide scale pre-or syn-metamorphic emplacement of gabbroic rocks in the Bamble area involved the formation of chlorapatite veins at many localities, including Ødegaardens-verk. In an attempt to obtain an age of emplacement for these gabbroic rocks whole rock samples of coronite gabbro, metagabbro and gabbroic wall-rock of the Ødegaarden chlorapatite veins have been analyzed.

Analytical data for the whole rock samples are presented in Table 12 and the data has been plotted on a Nicolaysen diagram in Fig 33. A certain



TABLE 12.Rb/Sr Analytical Data for the Gabbros and Metagabbros

Sample No.	Rb(ppm)	Sr <sup>N</sup> (ppm)	Sr <sup>87rad.</sup> (ppm)	Rb <sup>87</sup> /Sr <sup>86</sup> atomic ratio	Sr <sup>87</sup> /Sr <sup>86</sup> atomic ratio
SN-35	34.16	37.22	0.138	2.655	0.7418
SN-27	28.90	87.85	0.121	0.9517	0.7181
SN-25	10.99	129.9	0.088	0.2447	0.7109
SN-41	14.70	263.9	0.0057	0.1611	0.7042
SN-28	24.55	388.3	0.00	0.1829	0.70222



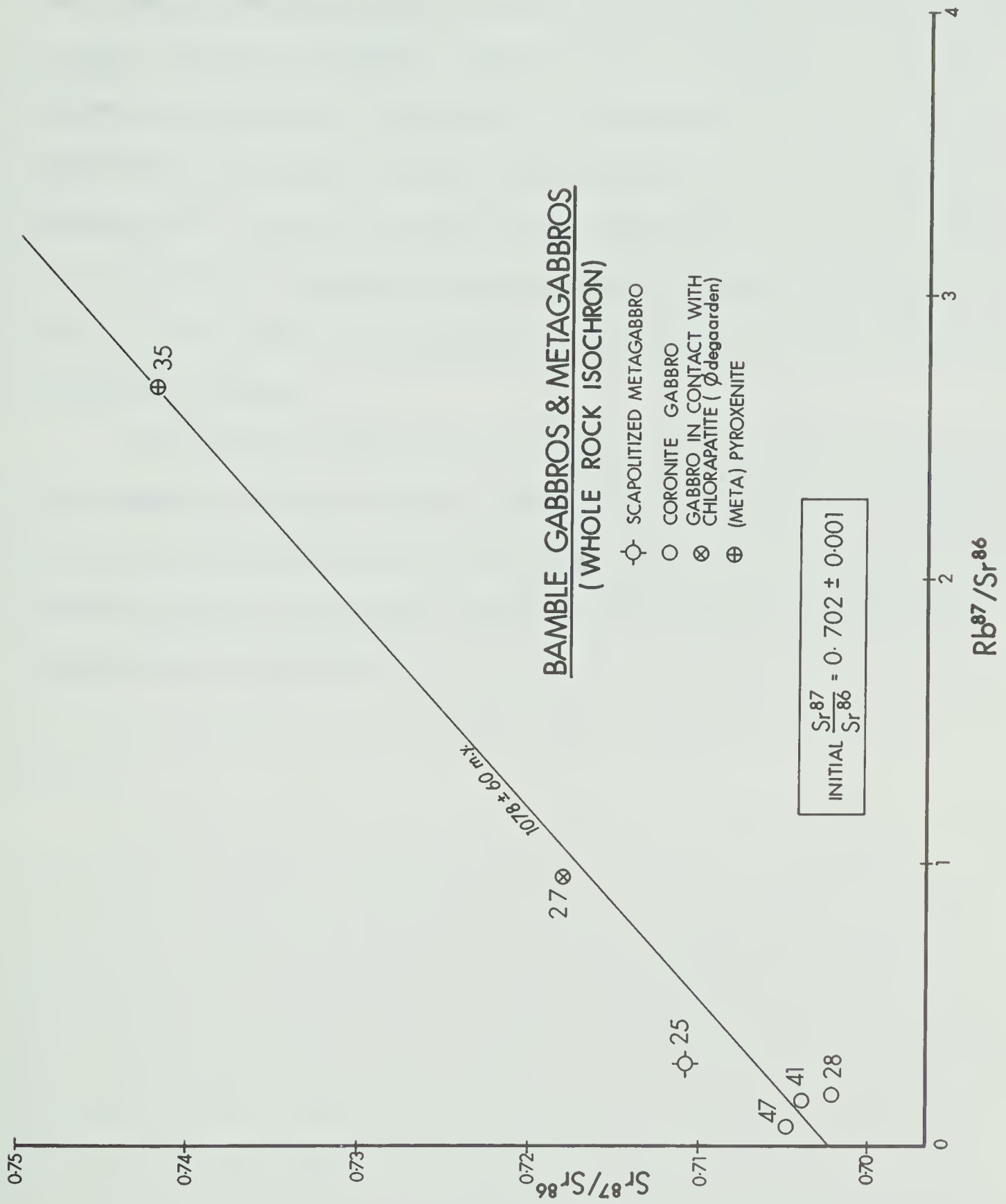


Fig. 33. Whole rock isochron plot for the gabbros.





amount of scatter is present and the points do not define a good isochron. An isochron fitted to all samples yields an apparent age of  $1045 \pm 81$  m.y. (one standard deviation), and if sample SN-25 is ignored an apparent age of  $1078 \pm 60$  m.y. is obtained. These results are somewhat at variance with estimates of the time of emplacement of the gabbros from U-Th-Pb dating. Sample SN-35 for example may have been subjected to a certain amount of alkali metasomatism. This would account for the abundance of secondary phlogopite in the rock and its apparent young age if the metasomatism occurred, say 100 m.y., or so after its emplacement. This problem will be further discussed in the next section.

The gabbroic rocks do not all appear to have remained closed systems since their emplacement and may in part have been subjected to a certain degree of rubidium metasomatism, and in the case of SN-25 some addition of radiogenic strontium may have been during conversion of the gabbro to Ødegaardite (hornblende plus scapolite).



## CHAPTER VII - TECTONIC HISTORY OF THE BAMBLE AREA

Introduction

Utilising the geochronological data obtained during the course of this thesis investigation and in addition, field and petrological observations made by numerous workers, an attempt will be made during the course of this Chapter to develop a tectonic history of the Bamble-sector of the Baltic Shield. Although the data available is still comparatively meagre, there is sufficient to provide at least a framework of the tectonic evolution of this portion of the Shield, which may serve as a guiding principle for further investigations.

The application of radiometric dating techniques to regional metamorphic terrains commonly results in apparent inconsistencies between the dating results and deductions based upon petrological observations. Such inconsistencies are more apparent than real and become progressively fewer in number as our understanding of metamorphism as a process and the behaviour of various parent-daughter systems under metamorphic conditions progresses.

The duration of metamorphic episodes and discrete metamorphic events within metamorphic episodes is a subject of considerable interest to geologists. Metamorphic events are usually identified from textural and mineralogical criteria and thus by means of careful and detailed petrographic observations it may prove possible to identify not only a number of events belonging to a single metamorphic episode, but also to infer something of the physico-chemical conditions at the time of the events. Although regional metamorphism may be considered as an predominantly thermal phenomenon, individual metamorphic reactions are not only a function of total pressure and temperature but also commonly of the fugacities of water, oxygen and carbon-dioxide and other components. The retention of daughter



products and the overall behaviour of parent-daughter systems during regional metamorphism primarily depends upon temperature, (although it is becoming increasingly apparent that other parameters may also affect their behaviour), therefore results of radiometric dating tend to provide a somewhat simplified picture of the metamorphic conditions. Variations of temperature during a metamorphic episode have on numerous occasions been inferred from textural and mineralogical criteria, prompting some workers to plot temperature-time graphs showing pronounced thermal maxima at the time of metamorphic events with distinct thermal minima separating these events (c.f. RAST, 1958; RAMSAY, 1963). If radiometric dating can in a particular instance apply some constraints upon the length of time available for a given metamorphic episode, it may be possible to discuss the feasibility of such temperature fluctuations during a metamorphic episode more objectively than has hitherto been the case.

In the remainder of this Chapter various aspects of the tectonic evolution of the Bamble area will be discussed sequentially, approximately relative to their positions within the tectonic cycle.

#### Provenance of the Bamble Metasediments

Rb-Sr whole rock dating has revealed the possibility of some metasedimentary rocks in the Bamble area being formed during an earlier, possibly the Svecofennian, orogenic cycle. Undoubtedly some metasedimentary rocks other than those presently exposed in the Levang gneiss dome, were formed during an earlier pre-Sveconorwegian orogenic cycle.

Zircons extracted from the Kjonnyøya para-amphibolite and the Arø metaconglomerate are unmistakeably detrital in nature, but do not exhibit overgrown zircon material as do the detrital zircons in the Levang gneiss dome. The apparent U-Pb age of 1400 to 1450 m.y. for these zircons must be considered as a minimum age and they may have even been derived from





Svecofennian rocks. However, it does suggest that the provenance of at least some of the Bamble metasediments was from a source in excess of 1400 m.y. old.

The most likely source region for the metasediments would be from the Telemark complex, consistent with the observation of MORTON (1969a) that Arø quartzites were derived from a source lying approximately to the northwest. Further work is obviously required on the metasedimentary rocks in various parts of the Bamble area to clarify their provenance.

#### Emplacement of Gabbroic and Associated Rocks

Basic plutonic activity within the Bamble-Sveconorwegian orogenic cycle involved the emplacement of basic igneous rocks varying from nepheline to quartz normative compositions. In the case of the Bjørdammen intrusion, a lower cumulate pyroxenite phase suggests that some degree of gravity differentiation was achieved and at Ødegaardens-verk the association of gabbro, albitite, and apatite may result from differentiation by a process of liquid immiscibility.

Field relationships and the mineralogy of the corona structures around olivine in the Bamble suite have led to the belief that the gabbroic rocks and their associated differentiates were emplaced slightly pre- or syn-metamorphically. This field evidence is quite indisputable and the Rb-Sr whole rock isochron apparent age of  $1078 \pm 60$  m.y., which is significantly less than estimates of the time of the thermal metamorphic maximum, is obviously indicative of post-intrusive open system behaviour.

An estimate of the time of the emplacement of the gabbroic and associated rocks at Ødegaardens-verk can be obtained from the apparent  $t_{207/206}$  age obtained on xenotime cogenetic with the chlorapatite and the apparent  $t_{207/206}$  age of 1190 m.y. obtained on a sphene associated with an albitite vein within the neighbouring meta-gabbro. These cannot be



shown to be significantly older than estimates of the thermal maximum of the metamorphism as derived from other sphene and zircon U-Pb concordia-discordia apparent ages and suggest an approximate contemporaneity between gabbro emplacement and the apparent metamorphic thermal maximum.

The departure from colinearity in the Rb-Sr whole rock isochron defined by the gabbroic rocks was shown to probably result from an alkali metasomatism in the neighbourhood of the Ødegaarden and Bjørdammen intrusives. An indication of the time of this metasomatic event may be derived from K-Ar results. Mg-rich amphiboles associated with the Ødegaarden gabbro (SN-88) and the Bjørdammen gabbro (SN-89, SN-35) have apparent ages of 1035, 1034 and 1012 m.y. respectively. Such amphibole compositions should supposedly have retained radiogenic argon from close to their time of formation, if the correlations concerning amphibole composition and argon retentivity made in Chapter IV are of general applicability. However, they may have been affected and possibly recrystallized by a metasomatic event at approximately 1030 m.y. At this time the whole rock gabbro isochron would be slightly positive and an introduction of rubidium could displace the points from the isochron. If such a metasomatism occurred at the time of intrusion, no amount of rubidium metasomatism alone would have displaced the points off a zero isochron. Evidence for an alkali metasomatism is derived from the Bjørdammen metapyroxenite which contains abundant secondary phlogopite. It is difficult to see why a pyroxenite phase should initially have had such a high alkali content.

The conclusions of O'NIONS et al. (1969) concerning the time of emplacement of the Ødegaarden apatite deposits cannot now be substantiated and it appears that the K-Ar apparent ages of amphiboles associated with the gabbros result from a parochial metasomatic event at approximately 1030 m.y.





Development of the Levang Gneiss Dome

The Levang gneiss dome was described earlier as consisting essentially of granitic gneiss with some interbanded biotite-granodiorite gneisses, biotite schists and amphibolites. Considering the lack of evidence to the contrary no inferences were made concerning the relative ages of the gneiss dome and the mantling rocks.

Rb-Sr whole rock isochron dating suggests that the gneisses comprising the Levang gneiss dome formed during an earlier orogenic cycle (the Svecofennian cycle) at  $1673 \pm 24$  m.y., and that the whole rock samples remained closed systems with respect to Rb and Sr during the later reheating event of the Sveconorwegian metamorphism. The low initial ratio does not suggest any prolonged previous history for the material. Many of the zircons contained within paragneisses of the Levang gneiss dome are apparently detrital in nature. Some of the zircons apparently were extensively modified during the Sveconorwegian metamorphism and together with the sphenes, give an apparent concordia age of 1160 m.y. Other zircons however showing less extensive evidence of metamorphic modification and lie approximately on a 1450 m.y. discordia. These results are obviously at variance with the whole rock Rb/Sr results and it seems that the present position of the detrital zircons on a 1400 m.y. discordia is a result of both metamorphic and possibly authigenic addition of zircon material together with episodic daughter loss during the Sveconorwegian orogeny. The actual history of these polycyclic zircons may be even more complex involving daughter loss during the Svecofennian orogeny also, with a superimposed pattern of continuous lead loss.

It is therefore concluded that the Levang gneiss dome resulted from a mobilization and reactivation of Svecofennian rocks during the Sveconorwegian orogeny into overlying and presumably younger material





formed during the Sveconorwegian orogenic cycle.

#### Formation of Metamorphic Pegmatites

Field relationships have shown the plagioclase pegmatites of the Bamble sector to be approximately syn-metamorphic and this is in part substantiated by the K-Ar apparent ages of coarse pegmatite biotites. The K-feldspar pegmatites of the Bamble sector however are post-kinematic and an estimate of their age provides a minimum age for the cessation of the folding movements. A U-Pb concordia age of 1100 m.y. obtained for various gravity fractions of zircon from the Ødegaarden pegmatite and an allanite from the Engevann pegmatite suggests that the folding of the area was complete by approximately 1100 m.y.

It was shown earlier that pelitic rocks in the Bamble region, at least, would be subjected to partial melting during the P-T conditions characterizing the reaction of muscovite + quartz to sillimanite + orthoclase (c.f. VON PLATEN, 1965). It is therefore possible that the K-feldspar pegmatites resulted from partial anatexis of metasedimentary rocks and may have been intruded at higher levels and lower temperatures if sufficient water was available.

#### The Duration of the Sveconorwegian Orogenic Cycle

From the apparent ages obtained for the gabbroic and associated rocks and the K-feldspar pegmatites, it is possible to impose some constraints on the duration of the folding episode in Bamble. The 1190 m.y. apparent age for the emplacement of the gabbroic rocks is considered to be an upper limit for the onset of folding, and the 1100 m.y. apparent age of the K-feldspar pegmatites provides a lower limit for the termination of the folding episode.

The time of deposition of the sedimentary predecessors of the



metasediments and the commencement of the Sveconorwegian orogenic cycle is not known with any degree of certainty, but was obviously prior to 1190 m.y. and subsequent to the Svecofennian orogeny. By approximately 1150 m.y. ago temperatures of around 700° C appear to have been attained and at that time large scale shear folding movements had commenced with the formation of NE-SW trending isoclinal folds. This folding also involved the reactivation of the underlying Svecofennian basement. Subsequent refolding along N-S axes in Eastern Bamble and the more complex series of folding in the Risør area appear to have been completed by 1100 m.y. During a length of time comparable to the duration of the Tertiary, the essential structural configuration at the level presently exposed in Bamble was imposed upon the area.

The latter stages of the orogenic cycle involved the uplift of the area and the consequent cooling down of the metamorphic belt.

#### Thermal History

The maximum temperature attained during the Sveconorwegian metamorphism in Bamble at around 1150 m.y. was probably of the order of 700° C. The length of time taken for this rise in temperature is not certain, but may be of comparable duration to the time the area took to cool down, if a simplistic model for the development of an orogenic belt is adopted. The essential metamorphic fabrics of the rocks as seen today were probably formed during a period of less than 90 m.y. During this length of time it does not seem possible that the area could cool down and heat up again to around 700° C to account for the two discrete high grade metamorphic events identified in the Risør area by STARMER (1969). If this length of time is not completely atypical of this structural level of a regional metamorphic belt, it does not seem that the complex temperature variations during metamorphic episodes proposed by some authors could possibly have existed.





It is felt that much simpler thermal histories existed in the majority of Precambrian metamorphic belts (there will always of course be exceptions) and that the temperature-time graph published by FYFE et al. (1958) showing a steady increase followed by a steady decline of temperature is an entirely acceptable model.

The Sveconorwegian metamorphism did not result in large scale strontium isotopic homogenization, at least in the situations investigated. Some potassium argon systems of high-Mg amphiboles and coarse-grained pegmatitic micas became closed shortly after the metamorphic maximum. Other more Fe-rich amphibole compositions and medium grained micas yield apparent K-Ar ages as low as 975 m.y. suggesting that the K-Ar systems were not closed until this time. These results have been interpreted in terms of a cooling history over a period of approximately 150 m.y., commensurate with uplift of the area, during which the temperature was reduced from around 700 °C to approximately 250 °C. Such a proposed long cooling history may be unacceptable to some geologists but cooling histories of similar duration have been reported for the Scottish Caledonides (HARPER, 1967a, MOORBATH, 1967) and the Yellowknife area (GREEN, 1968). The only other explanation is that a second metamorphic episode has occurred in all three situations some 150 m.y. after the first, causing differential updating of the parent-daughter systems.

#### Evolution of the Oslo Graben

The Oslo graben structure is now thought to swing parallel to the Skagerrak coastal region of South Norway in its southern portion. The Kristiansand-Porsgrunn fault is probably the northernmost boundary fault of the graben structure; the southernmost boundary fault lying off the Skagerrak coast.





The Oslo graben structure appears to have been initiated in Precambrian time possibly as part of the Sveconorwegian orogeny. Subsequent to the Sveconorwegian orogeny there appears to have been a period of comparative tectonic quiescence which persisted until Permian times. Activity associated with the Permian Igneous Province was at a maximum in the Oslo area and appears to decrease southwestwards. In the Bamble area it is represented by small Permian ore deposits and explosion breccias in Eastern Bamble and by NW-SE trending dykes across the whole Bamble region (although a Permian age for these is only assumed according to popular convention).

#### Summary

The tectonic evolution of the Bamble sector of the Baltic Shield has been long and complex. The area has been involved in two major Precambrian orogenic cycles and suffered the formation of a major graben structure in the late Palaeozoic.

The Sveconorwegian orogenic cycle was characterized by a metamorphic culmination over an interval of less than 90 m.y., during which time the essential structural and metamorphic character of the area was imposed. Some 150 m.y. elapsed before sufficient uplift and possibly decline in geothermal gradient resulted in the lowering of the temperature to around 250°C. Renewed accession of heat to the northeastern part of the area and renewed tectonic activity resulted in a series of events giving rise to the Oslo graben and the Permian Oslo Igneous Province.



## CHAPTER VIII - COMPARISONS WITH OTHER AREAS

Introduction

Multifarious attempts have been made to subdivide the Precambrian era on geochronological, biological and lithological bases. Biostratigraphic subdivisions of the Precambrian into periods such as Archaeozoic, Agnotozoic, Azoic and Proterozoic are now, with the exception of Proterozoic, little used. The retention of the term Proterozoic is somewhat unfortunate, since its duration cannot be precisely defined on the basis of the fossil record and the Proterozoic-Archaen, or Proterozoic-Azoic boundary is quite arbitrarily defined. Such arbitrariness is surely undesirable.

Stratigraphic subdivisions of the Precambrian are inherently difficult. Lithostratigraphic subdivisions may be parochially useful, but cannot be given any more than minimal significance in a Precambrian classificatory hierarchy. Likewise chronostratigraphic and biostratigraphic subdivisions and correlations require geochronological or biological proof of contemporaneity; evidence for which is frequently lacking.

Time classifications of the Precambrian are in many ways the most desirable. GOLDICH (1968) has proposed a subdivision of Precambrian time into 400 m.y. intervals, commencing at 600 m.y. and referred to consecutively as the alpha-Precambrian, beta-Precambrian through to theta-Precambrian; a scheme, however, which tends to obscure some of the most obvious features of Precambrian history. A case in point is the widely recognised Grenville orogeny in North America which appears to span the alpha-beta Precambrian interval of Goldich's classification. A more desirable time classification is therefore that of VINAGRAOV and TOUGARINOV (1961).

Time m.y.

600  $\pm$  50

1000  $\pm$  100

Upper Proterozoic



Time m.y.

1900  $\pm$  100

Lower Proterozoic

2700  $\pm$  150

Archean

3600  $\pm$  200

Katarchaen

This scheme has been modified by SEMENENKO et al. (1968) to exclude the meaningless Proterozoic, Archaen and Katarchaen terms:

<u>Megacycle</u>	<u>Time span</u>
Precambrian V	1200 to 550 m.y.
Precambrian IV	1700 to 1200 m.y.
Precambrian III	1700 to 2000 m.y.
Precambrian II	2000 to 2700 m.y.
Precambrian I	3500 to 2700 m.y.

The megacycle concept has distinct advantages as a time classification since the five cycles bracket the most widely recognised orogenic episodes and locally recognised orogenies can be superimposed on this scheme.

It is not the purpose of this Chapter to propose new subdivisions of the Precambrian, since additional contributions at this time can do no more than add to the existing confusion; rather the scheme of SEMENENKO et al. (loc.cit.) is adopted as being the presently most acceptable. Various attempts have been made to correlate Precambrian orogenic and anorogenic episodes; some of the more recent being those of SUTTON (1963), WELIN (1966), BOWES (1968) and BURWASH (1969). At this time we are concerned only with regions comparable to the Sveconorwegian zone, but it is necessary to comment upon the correlation of Precambrian orogenies in general. For example BURWASH (op.cit.) has based the duration of orogenies in the Canadian Shield on the mean value of apparent K-Ar ages and states "... the value of  $2\sigma$  is considered to be a better measure of the orogeny than the total range of values under one histogram peak." Such an approach





is both misleading and without foundation and by these means the Grenville orogeny is considered to extend from 1000 m.y. to approximately 880 m.y., a deduction which is obviously incompatible with the recent work of HARPER (1967b), KROGH and HURLEY (1968) and McINTIRE et al. (1967).

Inevitably, it must be asked what precisely is meant by an 'orogeny' before attempting to make world-wide correlations. An orogeny is the sum of structural changes accompanying mountain building, which may include, but does not necessarily imply accompanying metamorphism, metasomatism and magmatism. Since micas and some amphiboles probably do not retain argon until postorogenic uplift commences and temperatures fall below approximately 250°C, the final time of 'closure' of apparent K-Ar ages may well serve as a convenient, but not necessarily accurate, time to consider an orogenic episode complete.

The main purpose of this chapter is to compare the deduced geological history of the Bamble sector of the Sveconorwegian zone with other areas. Such comparisons are severely hampered by a complete lack of data in many areas and only K-Ar data in others; however it is possible to make some preliminary comparisons.

#### Comparisons Within Europe and Greenland

1. Sweden: Apparent K-Ar ages comparable to those of Bamble have been obtained from similar lithologies in southwest Sweden by MAGNUSSON (1960), POLKANOV and GERLING (1961) and WELIN and BLOMQUIST (1964), and have served to indicate an approximate contemporaneity of metamorphism and magmatism throughout the southern portion of the Baltic Shield. WELIN and BLOMQUIST (op.cit.) have reported uranium-lead ages of a number of pegmatic minerals (including euxinite, zircon and monazite) which give a concordia age of 930 m.y.; somewhat younger than the ages of pegmatites



dated in Bamble. It is tempting to speculate upon migration of thermal structures during metamorphism, but the presently available data does not really permit this. The Bamble region and the contiguous areas of south-west Sweden including the so-called Dalslandian and Pregothian complexes appear to have been affected by an orogeny between 1200 and 900 m.y. ago, which may conveniently be termed the Sveconorwegian orogeny of Precambrian V.

2. Ukrainian Shield: SEMENENKO et al. (1968) have proposed that the Sveconorwegian orogeny is contemporaneous with the Riphean folding in the Ukraine; reporting similar ages from the western slope of the Ukrainian Shield, which includes the well-known Valday series. A cycle of folding in the Black Sea region has apparently been dated by Semenenko and coworkers at 800-1000 m.y. This belt can be traced in the northwest part of the Baltic Shield to the edge of the Kola peninsular where it is represented by metamorphic rocks dated at 1000 m.y. in Kildin Island and formations dated at 890-1100 m.y. in the peninsulas of Srendi, Rybachi and Varanger. The age of the Timanian folding on the northeast side of the European platform has been dated at 1130 m.y. in the Chatlass series. Unfortunately the data are few and the dating methods employed are not mentioned by the above authors. It is therefore very difficult to say anything affirmative about the equivalence of the Black Sea, the Sveconorwegian and the Timanian orogenies.

3. France: LUTWEIN (1968) has reported apparent K-Ar ages of up to 1090 m.y. for amphiboles from the Amorian Massif in north-western France. He has suggested an age of  $1000 \pm 100$  m.y. for the Pentevrien orogeny.

4. Scotland: Evidence for an 1100 m.y. old event in Scotland is very meagre. However recent K-Ar and Rb/Sr age determinations on detrital micas and feldspars in the Torridonian sandstones (MOORBATH et al., 1967) suggests that at least part of the Torridonian source area was affected





by an 1100 m.y. event. The nature of this event (regional metamorphic or otherwise) is presently not certain. It would be premature to consider an extension of the Sveconorwegian orogeny into Scotland.

5. Greenland: Apparent ages of between 1000 and 1250 m.y. by K-Ar and Rb/Sr methods have been obtained from intrusive complexes from southern Greenland (BRIDGWATER, 1965; MOORBATH and PAULY, 1962; and MOORBATH et al., 1960). However it should be emphasized that these are all non-orogenic dates and cannot be correlated in a direct sense with the metamorphic dates from South Norway.

#### Comparisons with the Grenville Province

Considerably more information is available for the Grenville province of Eastern Canada than many parts of Europe. The Grenville province is composed largely of medium to high-grade metasedimentary and metavolcanic rocks extending northeastwards from the East coast of Georgian Bay (Lake Huron) to the Atlantic coast of Labrador. To the northwest the Grenville province is separated from the Superior province by a major fault or abrupt metamorphic transition, together known as the Grenville front. The results of an extensive K-Ar dating programme performed by the Geological Survey of Canada have been discussed by STOCKWELL (1964 and 1968) and BURWASH (1969). The mean of apparent K-Ar ages from the Grenville province is 945 m.y. and Burwash's estimate of the duration of the orogeny is from approximately 1000 m.y. to 880 m.y. Recently HARPER (1967b) has offered an interesting reinterpretation of the apparent K-Ar ages obtained in the Grenville province, proposing that the gradual increase in apparent K-Ar ages of micas from the St. Lawrence, in the southeast, (850 m.y.) to the Grenville front in the northwest, (1100 m.y.) is related to differential uplift and a consequent





cooling gradient. If this is the case, the Grenville orogeny obviously commenced prior to 1100 m.y. ago.

Whole rock Rb/Sr dating on the Grenville of S.E. Ontario by KROGH and HURLEY (1968) has provided further insight into the metamorphic history of the Grenville province. In the southeastern part of the Grenville province consistent isochron ages were obtained for metasedimentary and granitic material. For example an apparent age of  $1103 \pm 39$  m.y. was obtained for the Burleigh paragneiss dome and  $1284 \pm 41$  m.y. for the pre-metamorphic Blue Mountain nepheline syenite. Initial ratios for these rocks were low, in the range normally obtained for marbles and basalts, thus suggesting a short pre-Grenville history. Metasedimentary rocks along the Grenville front do not yield consistent isochron arrays and have high initial  $\text{Sr}^{87}/\text{Sr}^{86}$  ratios (0.725) which most probably results from an extensive pre-Grenville history. KROGH et al. (1967) studied the banded French River paragneiss of southern Ontario which yielded a whole rock isochron age of  $1622 \pm 70$  m.y. with whole rock-mineral isochron evidence for a disturbance between 900 m.y. and 1000 m.y.

There are obviously a number of close similarities between the Grenville province of Canada and at least the South Norwegian part of the Sveconorwegian zone. A contemporaneity of thermal events appears to have occurred within the two areas and it seems justifiable to consider the two regions parts of a contiguous N. Atlantic orogenic belt. The lack of a well defined equivalent to the Grenville orogeny in Scotland is surprising and it is possible that much evidence for it has been obliterated by extensive Caledonian metamorphism.



## SUMMARY AND CONCLUSIONS

The combined application of K-Ar, U-Th-Pb and Rb-Sr radiometric dating methods to the eastern part of the Bamble sector of the Baltic Shield, in South Norway, has made possible the definition of the nature and duration of what is now referred to as the Sveconorwegian orogeny. During this investigation, particular attention has been paid to the more fundamental behaviour of the three parent-daughter systems during high-grade regional metamorphic conditions.

K-Ar dating of micas and amphiboles has shown that the thermal maximum of the Sveconorwegian metamorphism in Bamble was attained in excess of approximately 1100 m.y. ago. As a generalization, coarse-grained pegmatitic biotites appear to have retained argon from higher temperatures than medium-grained micas, consistent with observations in other area. Apparent K-Ar ages of the amphiboles from various lithologies range from approximately 1100 m.y. to 975 m.y., and it would appear that the argon retentivities of some amphiboles is similar to medium-grained biotites, under conditions of slow cooling. Although amphiboles undoubtedly have higher activation energies for the liberation of radiogenic argon than do micas, it would appear that during cooling, the diffusion rate constant in high Fe-amphibole compositions, near the ferropargasite end-member, is enhanced. Such an enhancement may result from the high Fe-amphibole's ability to exchange OH with its external environment to lower temperatures than the high Mg-amphiboles. A process of Mg-blocking has been suggested for preventing the exchange of hydroxyl in amphiboles with higher Mg content. Other factors concerning the unit cell size and order-disorder relationships amongst Y-cations were not shown to be important. However more precise determinations of possible differences of ordering of Fe and information concerning ordering in the A sites would be useful. The apparent K-Ar ages of amphiboles are, therefore, interpreted in terms of a cooling history, where amphiboles near the pargasite end-member and coarse-grained pegmatitic





micas retained argon from considerably higher temperatures than amphiboles near the ferropargasite end-member and medium-grained biotites.

Zircons extracted from lithologies of the Levang gneiss dome appear to have had a complex evolutionary history. Most of the zircons have features suggestive of a detrital history. The apparent U-Pb concordia age of 1400-1450 m.y. for some of the zircons is intermediate between the time of the Sveconorwegian metamorphism and the Rb-Sr whole rock isochron age of the Levang gneiss dome and most likely results from superimposed lead-loss patterns and metamorphic and/or authigenic overgrowths of 'younger' zircon material. The 1160 m.y. apparent concordia U-Pb age for other zircons extracted from petrographically indistinguishable lithologies is comparable to independent estimates of the time of the thermal maximum of the Sveconorwegian metamorphic event and these zircons appear to have been in part recrystallized and 'isotopically reset' at this time. Some members of this zircon population show no evidence of a detrital history. The Th-Pb ages of the Levang gneiss dome zircons are not concordant; the degree of discordance being approximately related to their uranium plus equivalent thorium concentrations. Some of the discordancy patterns appear to require some degree of parent loss.

The sphenes sampled from the Levang gneiss dome and various pegmatitic lithologies are metamorphic minerals and provide an independent estimate of the time of the Sveconorwegian metamorphic maximum. Considering all the U-Th-Pb data together, 1150 to 1180 m.y. may be taken as a reasonable estimate for the culmination of the Sveconorwegian metamorphism.

The U-Pb age of approximately 1100 m.y. obtained for the post-kinematic Ødegaarden K-feldspar pegmatite zircons provides a lower time limit for the end of the Sveconorwegian folding episode. It would then seem that, within analytical error, the Sveconorwegian deformation occurred between approximately 1180 and 1100 m.y.





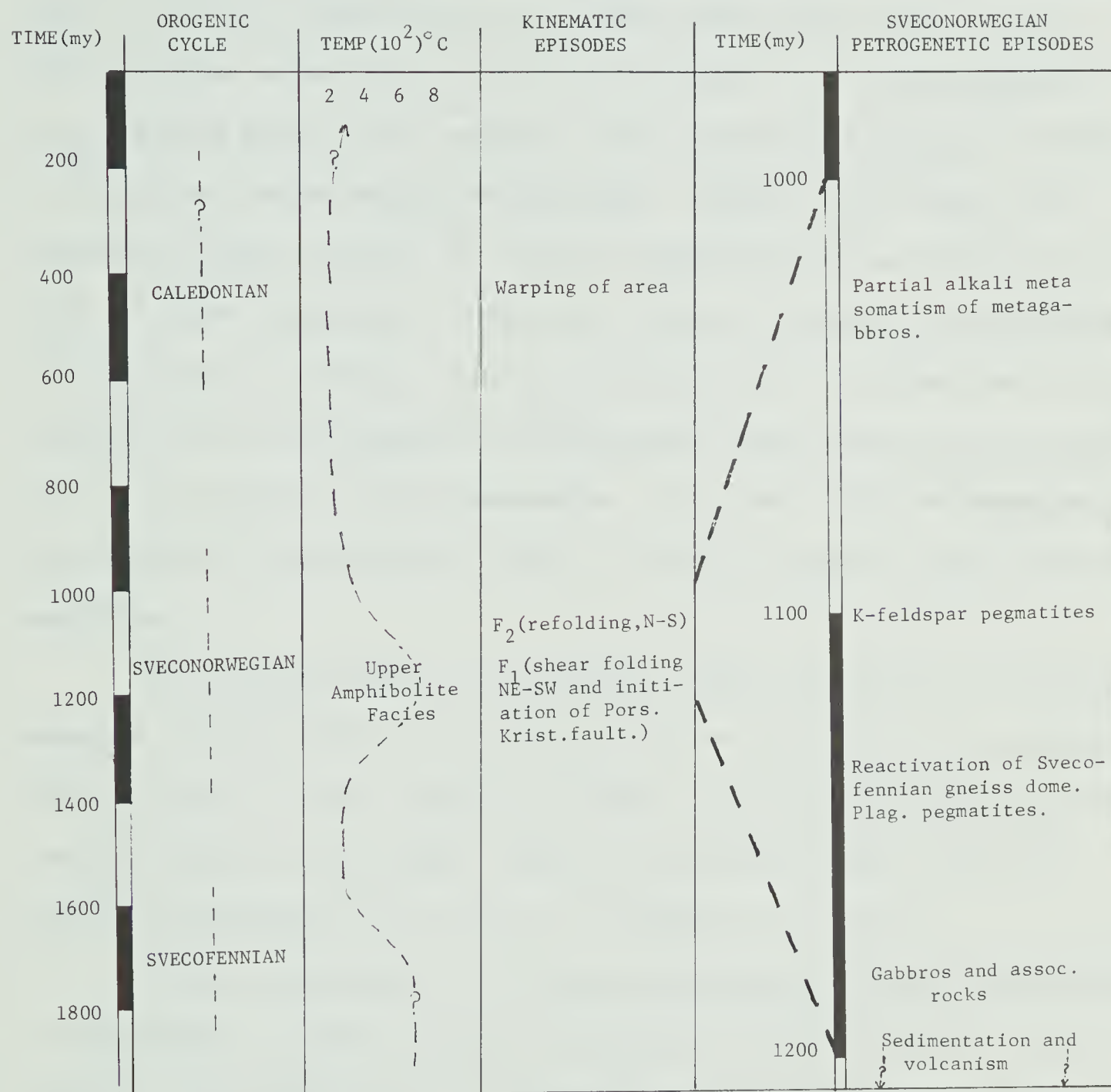


Fig. 37. Tectonic history of the Bamble - sector of the Baltic Shield. Note: The four folding events identified in the Risør area by STARMER (1969) have not been included on the diagram, since it is possible that they are a combination of both Sveconorwegian and Svecofennian folding episodes.



Rb-Sr whole rock isochron dating has demonstrated that rocks belonging to the Svecofennian orogenic cycle were remobilized during the Sveconorwegian orogeny. U-Pb apparent ages of sphenes and K-Ar apparent ages of micas and amphiboles in the Levang gneiss dome relate to the Sveconorwegian metamorphism. Whole rock samples, on the scale examined in the Levang gneiss dome, remained closed systems with respect to Rb and Sr during the Sveconorwegian metamorphism. However in the case of the Hovdefjell banded gneisses, Sr isotopic homogenization was effected on the scale of a few centimetres. Whole rock samples of gabbros and metagabbros do not produce a consistent isochron and the results are consistent with the contention that the Ødegaarden and Bjørdammen gabbros were in part affected by a post-intrusive alkali metasomatism. The time of this metasomatism may be estimated at approximately 1030 m.y. from K-Ar apparent ages of high Mg-amphiboles.

The tectonic history of the Bamble region has involved two quite separate orogenic cycles, and it is possible on the basis of the presently available data to infer something of their time separation and nature. The tectonic history of the Bamble sector of the Baltic Shield, as it is presently understood by the author, is summarised in Fig 37.

Much is obviously to be learned concerning the nature and duration of metamorphic episodes in regional metamorphic terrains, such as South Norway, by the application of radiometric dating methods, but any one particular method of radiometric dating is only capable of providing a part of this information. The application of another parent-daughter system to the rocks already studied, were it possible, would undoubtedly provide considerably more information concerning the tectonic history of this region and enhance our understanding of the other systems also.



## REFERENCES.

- ABBEY, S. and MAXWELL, J.A. (1960) Determination of potassium in micas. Chem. Can. 12, 37 - 41.
- ADDISON, C.C., ADDISON, W.E., NEAL, G.H. and SHARP, J.H. (1962) Amphiboles Pt.1. The oxidation of crocidolite. J. Chem. Pt.1, 1468.
- AHRENS, L.H. (1965) Some observations on the uranium and thorium distributions in accessory zircon from granitic rocks. Geochim. Cosmochim. Acta. 29, 711 - 716.
- ALDRICH, L.T. and WETHERILL, G.W. (1958) Geochronology by radioactive decay. Ann. Rev. Nucl. Sci. 8, 257 - 298.
- .....DAVIS, G.L., and JAMES, H.L. (1965) Ages of minerals from metamorphic and igneous rocks near Iron Mountain, Michigan. J. Pet. 6, 445-472.
- ALLEGRE, G.J. (1966) Methode de discussion geochronologique concordia generalisee. Application a la discussion des ages uranium-thorium-plomb discordants. Earth Plan. Sci. Letters. 2, 57-66.
- ALLSOP, H.L., ULRYCH, T.J. and NICOLAYSEN, L.O. (1968) Dating some significant events in the history of the Swaziland system by the Rb-Sr isochron method. Can. J. Earth Sci. 5, 605-621.
- ARMSTRONG, R.L. (1966) K-Ar dating of plutonic and volcanic rocks in orogenic belts. In. Potassium argon dating. Eds. O.A. Schaeffer and J. Zähringer. Springer-Verlag, New York.
- .....(1968) A model for the evolution of strontium and lead isotopes in a dynamic earth. Rev. Geophys. 6, 175-200.
- .....and HILLS, F.A. (1967) Rb-Sr and K-Ar geochronologic studies of mantled gneiss domes, Albion Range, south Idaho, U.S.A. Earth Plan. Sci. Letters. 3, 114-124.
- AZAROFF, L.F. and BUEGER, M.J. (1968) The powder method in X-ray crystallography. Mc Graw Hill, New York.





- BAADSGAARD, H. (1965) Geochronology. Medds. fra Dansk. Geol. Foren. 16, 1-48.
- .....and GODFREY, J. (1967) Geochronology of the Canadian Shield in northeastern Alberta. I. Andrew Lake area. Can. J. Earth Sci. 4, 541-563.
- BANCROFT, G.M., BURNS, R.G., and MADDOCK, A.G. (1967) Applications of the Mössbauer effect to silicate mineralogy. I. Iron silicates of known crystal structure. Geochim. Cosmochim. Acta. 31, 2219-2246.
- BANKS, P.O., and CAIN, J.A. (1969) Zircon ages of Precambrian granitic rocks, northeastern Wisconsin. J. Geol. 77, 208-220.
- BARTH, T.F.W. (1933) The large Precambrian intrusive bodies in the southern part of Norway. Rpt. 16, XVI. Int. Geol. Congr., Washington, 279-309.
- .....(1947) The nickeliferous Ireland-Evje amphibolite and its relations. Norges Geol. Unders. No. 168a.
- .....and REITAN, P.H. (1963) The Precambrian of Norway. In The Precambrian. Ed. K. Rankama. Interscience, London.
- BODART, D.E. (1968) On the paragenesis of albitites. Norsk. Geol. Tidss. 48, 269-280.
- BOWES, D.R. (1968) The absolute time scale in the subdivision of Precambrian rocks in Scotland. Geol. Fören. Förh. 90, 175-188.
- BRIDGWATER, D. (1965) Isotopic age determinations from south Greenland and their geological setting. Medd. om Grønland. Bd. 179, Nr. 4.
- BROCH, O.A. (1964) Age determinations of Norwegian minerals up to March 1964. Norges. Geol. Unders. 228, 84-113.
- BROEDEL, G.H. (1937) The structure of the gneiss domes near Baltimore, Maryland. Maryland Geol. Survey B, 149-188.



BRÜGGER, W.C. (1900) Norges geologi. Norge i det 19 aarhundrede.

Kristiania, Cammermeyer.

.....(1934) On several Archæan rocks from the south coast of Norway.

7. Nodular granites from the environs of Kragerø. Vid. Akad. Skr.

M-N. Kl. 193, No.8.

.....(1935) The south Norwegian hyperites and their metamorphism.

Vid. Akad. Mat. Nat. Kl. No. 2.

BUGGE, A. (1928) En forkastning i det syd-Norske grunnfjell. Norges Geol.

Unders. No. 95.

.....(1936) Kongsberg - Bamble formasjonen. Norges Geol. Unders. No. 146.

.....(1965) Iakttagelser fra rektangelbladet Kragerø og den store  
grunfjelltreksje. Norges Geol. Unders. Nr. 229, 115 pp.

BUGGE, J.A.W. (1943) Geological and petrological investigations in the  
Kongsberg-Bamble formation. Norges. Geol. Unders. No. 160.

BURNS, R.G., and STRENS, R.G.J. (1966) Infrared study of the Hydroxyl  
bands in clinoamphiboles. Science, 153, 890-892.

BURRELL, D.C. (1964) The geology of the country west of the Levang peninsula,  
south Norway. Unpublished Ph.D. thesis, University of Nottingham.

BURWASH, R.A. (1969) Comparative Precambrian geochronology of the North  
American, European and Siberian Shields. Can. J. Earth Sci. 6, 357-365.

BRANDT, S.B., and PERMINOV, A.V. (1968) P-T dependence of migration properties  
of lead under hydrothermal conditions. Geochem. Intern. 5, 614-617.

CATANZARO, E.J. (1963) Zircon ages in southwestern Minnesota. J. Geophys.  
Res. 68, 2045.

.....(1968) The interpretation of zircon ages. In Radiometric dating for  
geologists. Ed. E.I. Hamilton and R.M. Farquhar. Interscience, London.

CHINNER, G.A. (1961) Pelitic gneisses with varying ferrous/ferric ratios  
from Glen Clova, Angus, Scotland. J. Pet. I. 178-215.





- COLVILLE, P., ERNST, W.G. and GILBERT, M.C.(1966) Relationships between cell parameters and chemical compositions of monoclinic amphiboles. Amer. Min. 51, 1727-1754.
- COMPSTON, W. and JEFFEREY, P.M. (1961) Metamorphic chronology by the rubidium - strontium method. Ann. N.Y. Acad. Sci. 91, 185-191.
- CUMMING, G.L. (1969) A recalculation of the age of the solar system. Can. J. Earth Sci. 6, 719-736.
- DAMON, P.E. (1968) Potassium argon dating of igneous and metamorphic rocks with applications to the Basin ranges of Arizona and Sonora. In. Radiometric dating for geologists. Eds. E.I. Hamilton and R.M. Farquhar. Interscience, London.
- DAVIS, G.L., HART, S.R. and TILTON, G.R. (1968) Some effects of contact metamorphism on zircon ages. Earth Plan. Sci. Letters. 5, 27-34.
- .....TILTON, G.R. and WETHERILL, G.W.(1962) Mineral ages from the Appalachian province in North Carolina and Tennessee. J. Geophys. Res. 67, 1987-1996
- DEER, W.A., HOWIE, R.A. and ZUSSMAN, J. (1962) Rock forming minerals. Vol. 2. Chain silicates. Longmans, London.
- DICKINSON, D.R., DODSON, M.H., GASS, I.G. and REX, D.C.(1969) Correlation of initial  $\text{Sr}^{87}/\text{Sr}^{86}$  with Rb/Sr in some late Tertiary volcanic rocks from south Arabia. Earth Plan. Sci. Letters. 6, 84-90.
- DENISENKO, Y.A. (1965) Determination of the activation energy of argon. Geochem. Intern. 2, 74076.
- DUNCUMB, B.P., and REED, S.J.B. (1967) The calculation of stopping power and back-scatter effects in electron probe microanalysis. In. Quantitative electron probe microanalysis. Ed. K.F.J. Heinrich Nat. Bur. Stands. Spec. Pub. 198, 133-154.





- ELDERS, T. (1964) Geology of the Levang gneiss dome. Unpublished Ph.D. thesis, University of Durham.
- ELDERS, W.A. (1961) Geological and petrological studies in the Precambrian gneisses and granites of the southeast part of Aust-Agder, southern Norway. Unpublished Ph.D. thesis, University of Durham.
- .....(1963) On the form and mode of emplacement of the Herefoss granite Norges Geol. Unders. No. 214a.
- ELLIOT, R.B. (1966) The association of amphibolite and albitite, Kragerø, south Norway. Geol. Mag. 103, 1-7.
- ENGEL, A.E.J., and ENGEL, C.G. (1962) Hornblendes formed during progressive metamorphism of amphibolites, northwest Adirondack Mountains, New York. Bull. Geol. Soc. Am. 73, 1499.
- .....and HAVEN, R.G. (1964) Mineralogy of amphibolite interlayers in the gneiss complex, northwest Adirondack Mountains, New York. Jour. Geol. 72, 131.
- ERNST, W.G. (1968) Minerals, rocks and inorganic materials. I. Amphiboles. Springer-Verlag, New York.
- ESKOLA, P.E. (1949) The problem of mantled gneiss domes. Quart. J. Geol. Soc. Lond. 104, 461-476.
- EVANS, B.W. (1965) Applications of a reaction rate method to the breakdown equilibria of muscovite and muscovite plus quartz. Am. J. Sci. 263, 647-667.
- .....and GUIDOTTI, C.V. (1966) The sillimanite-potash feldspar isograd in western Maine, U.S.A. Contrib. Min. Pet. 12, 25-62,
- EVANS, H.T. JNR., APPLEMAN, D.E., and HADWERKER, D.J. (1963) The least-squares refinement of crystal unit cells with powder diffraction data by an automatic computer indexing method. A. Mtg. Am. Cryst. Ass., Cambridge, Mass., 1963. Program and Abstract, E-10, 42-43 (abs.).



EVERNDEN, J.F., CURTIS, G.H., KISTLER, R.W. and OBRADOVICH, J. (1960)

Argon diffusion in glauconite, microcline, sanidine, leucite and phlogopite. *Am. J. Sci.* 258B, 583.

FECHTIG, H., and KALBITZER, S. (1966) The diffusion of argon in potassium-bearing solids. In Potassium-argon dating. Ed. O.A. Schaeffer and J. Zahringer. Springer-Verlag, Berlin.

FLYNN, K.F., and GLENDENIN, L.E. (1959) Half life and beta spectrum of  $\text{Rb}^{87}$ . *Phys. Rev.* 116, 744-748.

FOSTER, M.D. (1960) Layer change relationships in dioctahedral and trioctahedral micas. *Am. Miner.* 45, 383-398.

FRITZ, J.S. and GARRALDA, B.B. (1962) Anion exchange separation of thorium using nitric acid. *Anal. Chem.* 34, 1387-89.

FRODESEN, S. (1968a) Coronas around olivine in a small gabbro intrusion, Bamble area, south Norway. *Norsk. Geol. Tidss.* 48, 201-206.

.....(1968b) Petrographical and chemical investigations of a Precambrian gabbro intrusion, Hiasen, Bamble area, south Norway. *Norsk. Geol. Tidss.* 48, 281-306.

GARLICK, G.D., and EPSTEIN, R.S. (1967) Oxygen isotope ratios in coexisting minerals of regionally metamorphosed rocks. *Geochim. Cosmochim. Acta.* 31, 181-214.

GATES, R.H. (1967) Amphibolites: syntectonic intrusives? *Am. J. Sci.* 265, 118-131.

GERLING, E.K., MOROZOVA, I.M., and KURBATOV, V.V. (1961) The retentivity of radiogenic argon in ground micas. *Ann. N.Y. Acad. Sci.* 91, 227-234.

.....LEVSKII, L.K., and MOROZOVA, I.M. (1963) On the diffusion of radiogenic argon from minerals. *Geochemistry.* 6, 551.

GERLING, E.K., KOL'TSOVA, T.V., PETROV, B.V. and ZULFIKAROVA, Z.K. (1965) On the suitability of amphiboles for age determination by the K-Ar





method. *Geochem. Intern.* 2, 148-154.

GHOSE, S. (1961) The crystal structure of cummingtonite. *Acta. Cryst.* 14, 622-627.

GJELSVIK, T. (1952) Metamorphosed dolerites in the gneiss area of Sunnmøre on the west coast of southern Norway. *Norsk. Geol. Tidss.* 30, 34-134.

GOLDICH, S.S. (1968) Geochronology of the Lake Superior region *Can. J. Earth Sci.* 715-724.

GOTTFRIED, D., JAFFE, H.W., and SENFTLE, F.E. (1959) Evaluation of the lead-alpha (LARSEN) method for determining ages of igneous rocks. *U.S. Geol. Surv. Bull.* 1097-a.

GREEN, D.C. (1968) Geology and geochronology of the Yellowknife area, Northwest Territories. Unpublished Ph.D. thesis, University of Alberta.

GREEN, D.H., and RINGWOOD, A.E. (1967) An experimental investigation of the gabbro to eclogite transformation and its petrological implications. *Geochim. Cosmochim. Acta.* 31, 767-834.

GUIDOTTI, C.V. (1963) Metamorphism of pelitic schists in the Byrant Pond quadrangle, Maine. *Amer. Min.* 48, 772-779.

HAMILTON, E.I. (1966) *Applied geochronology.* Academic Press, London.  
.....and FARQUHAR, R.M. (1968) *Radiometric dating for geologists.* Interscience, London.

HANSON, G.N., and GAST, P.W. (1967) Kinetic studies in contact metamorphic zones. *Geochim. Cosmochim. Acta.* 31, 1119-1154.

HARPER, C.T. (1967a) The geological interpretation of potassium-argon ages from the Scottish Caledonides. *Scott. J. Geol.* 3, 46-66.

.....(1967b) On the interpretation of K-Ar ages from Precambrian Shields and Phanerozoic orogens. *Earth Plan. Sci. Letters.* 3, 125-132.

HART, S.R. (1960) Some diffusion measurements relating to the K-Ar dating method. In: *variations in isotopic abundances of strontium, calcium,*





argon and related topics. Eighth-Ann. Prog. Rep. for 1960. U.S. Atom Energy  
Comm.

.....(1961) The use of hornblendes and pyroxenes for K-Ar dating. J. Geophys.  
Res. 66, 2995-3001.

.....(1964) The petrology and isotopic mineral age relations of a contact  
zone in the Front Range, Colorado Jour. Geol. 72, 493-525.

HEIER, K.S. (1964) Rb/Sr and  $Sr^{87}/Sr^{86}$  ratios in deep crustal material.  
Nature. 202, 477-478.

.....and TAYLOR, S.R. (1959) Distribution of Li, Na, K, Rb, Cs, Pb and Tl  
in southern Norwegian Precambrian alkali feldspars. Geochim. Cosmochim.  
Acta. 15, 284-304.

.....PALMER, P.D., and TAYLOR, S.R. (1967) Comment on the Pb distribution  
in southern Norwegian Precambrian alkali feldspars. Norsk. Geol. Tidss.  
47, 185-189.

HEINRICH, K.F.J. (1966) The electron microprobe. 296-377. Wiley, New York.

.....(1967) The absorption correction model for microprobe analysis.  
Trans. 2nd. Nat. Conf. Electron microprobe analysis. Boston, 1967.  
Publ. by Mass. Inst. Tech.

HOFSETH (1942) Geologiske undersøkelser ved Kragerø, Holleia og Troms.  
Norges Geol. Unders. No. 157.

HOLLAND, H.D., and GOTTFRIED, D. (1955) The effect of nuclear radiation  
on the structure of zircon. Acta. Cryst. 8, 291-301.

HODSON, C.A. (1964) The crystalline rocks of the Howard and Montgomery  
Counties: The geology of Howard and Montgomery Counties. Maryland  
Geol. Survey. 27-215.

HOLTEDAHN, O. (1945) Lecture to the Norsk Geologisk Forening, Oslo.  
Norsk. Geol. Tidss. 24, 150-161.



.....(1960) Geology of Norway. Norges Geol. Unders. Nr. 208.

HURLEY, P.M., HUGHES, H., PINSON JR., W.H., and FAIRBAIRN, H.W. (1962)

Radiogenic argon and strontium diffusion parameter in biotite at low temperatures obtained from Alpine Fault uplift in New Zealand. Geochim. Cosmochim. Acta. 26, 67-80.

JÄGER, E. (1966) Das alter von graniten und gneissen. Tsch. Min. Petr. Mitt. 11, 304-316.

KIRSTEN, T. (1966) Determination of radiogenic argon. In. Potassium argon dating. Eds. O.A. Schaeffer and J. Zahringer. Springer, Berlin.

KOSTYUK, E.A. and SOBOLEV, V.S. (1969). Paragenetic types of calciferous amphiboles of metamorphic rocks. Lithos. 2, 67-82.

KOTLOVSKAYA, T.V. (1964) Retention of radiogenic argon by hornblende. Geochem. Intern. 4, 812.

KOUVO, O., and TILTON, G.R. (1966) Mineral ages from the Finnish Precambrian. Jour. Geol. 74, 421-422.

KRATZ, K.O., GERLING, E.K., and LOBACH-ZHUCHENKO, S.B. (1968) The isotope geology of the Precambrian of the Baltic Shield. Can. J. Earth Sci. 5, 657-660.

KROGH, T.E., and HURLEY, P.M. (1968) Strontium isotope variation and whole rock isochron studies, Grenville Province of Ontario. J. Geophys. Res. 73, 7107-7125.

.....DAVIS, G.L., ALDRICH, L.T., HART, S.R. and STUEBER, A. (1967) Geological history of Grenville Province. Carn. Inst. Yearb. Geophys. Lab. 528-536.

KULP, J.L., and ECKLEMAN, W.R. (1957) Discordant U-Pb ages and mineral type. Amer. Miner. 42, 154-164.

.....and NEUMANN, H. (1961) Some potassium-argon ages from the Norwegian basement. Ann. N.Y. Acad. Sci. 91, 469-475.





- LANPHERE, M.A. and DALRYMPLE, G.B. (1967) K-Ar and Rb-Sr measurements on P-207, the U.S.G.S. interlaboratory standard muscovite. *Geochim. Cosmochim. Acta.* 31, 1091-1093.
- .....WASSERBURG, G.J., ALBEE, A.L. and TILTON, G.R. (1964) Redistribution of strontium and rubidium isotopes during metamorphism, World Beater complex, Penamint Range, California. In. Isotopic and cosmic chemistry. Eds. H. Craig, S. Miller and G.J. Wasserburg. North Holland Pub. Amsterdam.
- LEAKE, B.E. (1965) The relationship between composition of calciferous amphiboles and grade of metamorphism. In. Controls of metamorphism Eds. W.S. Pitcher and G.W. Flynn. Oliver and Boyd, London.
- LIPOVA, I.M. (1966) Mechanism of metamict mineral alteration. *Geokhimiya* 6, 729-733.
- .....KUZNETSOVA, G.A. and MAKAROV, Y.S. (1965) An investigation of the metamict state in zircons and cyrtolites. *Geochem. Intern.* 2, 513-525.
- LONG, L.E. (1964) Rb-Sr chronology of the Carn Chuinneag intrusion, Ross-Shire, Scotland. *J. Geophys. Res.* 69, 1589-1597.
- .....(1966) Isotope dilution analysis of common and radiogenic strontium using  $\text{Sr}^{84}$  - enriched spike. *Earth Plan. Sci. Letters.* 1, 289-292.
- LONG, J.V.P. (1968) Electron probe microanalysis. In. Physical methods in determinative mineralogy. Ed. J. Zussman. Acad. Press, London.
- LUNDGREN, L.W. (1966) Muscovite reactions and partial melting in southeastern Connecticut. *Jour. Pet.* 7, 421-453.
- LUTWEIN, F. (1968) Contribution a la connaissance du Precambrian recent en Europe occidentale et developpement geochronologique du Brioverien en Bretagne (France). *Can. J. Earth Sci.* 5, 673-682.





- MAGNUSSON, N.H. (1960) Age determinations of Swedish Precambrian rocks. Geol. Fören, Förh. Stockh. 82, 407-432.
- MAKAROV, E.S. and LIPOVA, I.M. (1962) An x-ray investigation of thorianites, uranothorianites and aldanites. Geochem. Intern. No. 7, 676-683.
- McINTYRE, G.A., BROOKS, C., COMPSTON, W., and TUREK, A. (1966) The statistical assessment of Rb/Sr isochrons. J. Geophys. Res. 71, 5459-5468.
- McINTYRE, R.M., YORK, D., and MOORHOUSE, W.W. (1967) Potassium argon age determinations in the Madoc-Bancroft area in the Grenville Province of the Canadian Shield. Can. J. Earth Sci. 4, 815-828.
- MICHOT, J., and PASTEELS, P. (1968) Etude geochronologique du domaine metamorphique du sud-ouest de la Norvege. Ann. Soc. Geol. Belg. 91, 93-110.
- MOORBATH, S. (1965) Isotopic dating of metamorphic rocks. In. Controls of metamorphism. Eds. Pitcher, W.S. and Flynn, G.W. Oliver and Boyd, London.
- .....(1967) Recent advances in the application and interpretation of radiometric age data. Earth Sci. Rev., 3, 111-133.
- .....and PAULY, H. (1962) Rubidium-strontium and lead isotope studies on intrusive rocks from Inuvigut, south Greenland. In Variations in isotopic abundance of strontium calcium and argon and related topics. 10th Ann. Prog. Rpt. for 1962. Mass. Inst. Tech.
- .....STEWART, A.D., LAWSON, D.E., and WILLIAMS, G. (1967) Geochronological studies on the Torridonian sediments of northwest Scotland. Scott. J. Geol. 3, 389-412.
- .....WEBSTER, R.K., and MORGAN, J.W. (1960) Absolute age determinations in southwest Greenland. Medd. on Grønland. Bd. 162. Nr. 9.



- .....and VOKES, F.M. (1963) Lead isotope abundance studies on galena occurrences in Norway. Norsk. Geol. Tidss. 43, 283-343.
- MORTON, R.D. (1960) The Ødegaarden phosphate deposits. Int. Geol. Cong. XXI Session Norden. In. Mineral occurrences in southern Norway. Ed. H. Neumann.
- .....(1961) Contributions to the mineralogy of Norway No. 9.  
On the occurrence of two rare phosphates in the Ødegaarden apatite mines. Bamble, South Norway. 1. A variety of woodhouseite.  
2. whitlockite. Norsk. Geol. Tidss. 41, 233-241.
- .....(1969a) Geological investigations in the Bamble sector of the Fennoscandian Shield, S. Norway. No. II. Metasediments and meta-pyroclastics (?) within the Precambrian metamorphic suite of the S. Norwegian Skaergaard. In press.
- .....(1969b) Graben structures in South Norway. in preparation.
- MORTON, R.D., BATEY, B.H., and O'NIONS, R.K. (1969) Geological investigations in the Bamble sector of the Fennoscandian Shield, S. Norway. I. The Geology of Eastern Bamble. in press.
- MUMPTON, F.A., and ROY, R. (1961) Hydrothermal stability studies of the zircon-thorite group. Geochim. Cosmochim. Acta. 21, 217-238.
- NAYLOR, R.S. (1969) Age and origin of the oliverian domes, central-western New Hampshire. Bull. Geol. Soc. Am. 80, 405-428.
- NICOLAYSEN, L.O. (1957) Solid diffusion in radioactive minerals and the measurement of absolute age. Geochim Cosmochim. Acta. 11, 41-59.
- NICOLAYSEN, L.O. (1961) Graphic interpretation of discordant age measurements on metamorphic rocks. Ann. N.Y. Acad. Sci. 91, 198-206.
- NIER, O.A. (1950) A redetermination of the relative abundance of the isotopes of carbon, nitrogen, oxygen, argon and potassium. Phys. Rev. 77, 789-793.





- NEUMANN, H. (1960) Apparent ages of Norwegian minerals and rocks. Norsk. Geol. Tidss. 40, 173-189.
- O'NIONS, R.K., MORTON, R.D., and BAADSGAARD, H. (1969) Potassium argon ages from the Bamble sector of the Fennoscandian Shield in South Norway. Norsk. Geol. Tidss. 49, 171-190.
- .....SMITH, D.G.W., BAADSGAARD, H., and MORTON R.D. (1969). Influence of chemical composition on argon retentivity in metamorphic calcic amphiboles from South Norway. Earth Plan. Sci. Letters. 5, 339-345.
- PETTERSON, M.J. (1964) The geology of the country around Sanida South Norway. Unpublished Ph.D. thesis, University of Nottingham.
- PHILPOTTS, A.R. (1967) Origin of certain iron-titanium oxide and apatite rocks. Econ. Geol. 62, 303-315.
- POLDERVAART, A. (1950) Statistical studies on zircons as a criterion in granitization. Nature. 16, 574-575.
- .....(1955) Zircons in rocks. I. Sedimentary rocks. Am. J. Sci. 253, 433-461.
- .....(1956) Zircons in rocks II. Igneous rocks. Am. J. Sci. 254, 521-554.
- POLKANOV, A.A., and GERLING, E.K. (1961) The Precambrian geochronology of the Baltic Shield. Ann. N.Y. Acad. Sci. 91, 492-499.
- RAMSAY, J.G. (1963) Structure and metamorphism of the Dalradian rocks of Scotland. In. The British Caledonides. Ed. M.R.W. Johnson and F.H. Stewart. Oliver and Boyd, Edinburgh.
- RAST, N. (1958) Metamorphic history of the Schichallion complex, Perthshire. Trans. R. Soc. Edinb. 63, 143.
- REED, S.J.B. (1965) Characteristic fluorescence corrections in electron probe microanalysis. Eds. Patee, Coslett and Engstrom. 3, 379. Academic Press, New York.





- REITAN, P. (1959) Structural control of small pegmatites in amphibolite, Rytterholmen, Kragerøfjord, Norway. *Norges. Geol. Tidss.* 39, 175.
- REYNOLDS, R.C., and FREDERICKSON, A.F. (1962) Corona development in Norwegian hyperites and their bearing upon the metamorphic facies concept. *Bull. Geol. Soc. Am.* 73, 59.
- RÖSLER, H.J., and PILOT, J. (1967) Zur alterbestimmung hydrothermaler lagerstätten mit hilfe der K-Ar methode. *Forst. Miner.* 45, 37-51.
- RYAN, M.J. (1966) Geology of the area around Ødegaardens-verk, South Norway. Unpublished Ph.D. thesis, University of Nottingham.
- SAXENA, S.K. (1966) Evolution of zircons in sedimentary and metamorphic rocks. *Sedimentology.* 6, 1-33.
- SCHAEFFER, O.A., and ZHRINGER, J. (1966) Potassium-argon dating. Springer-Verlag, New York.
- SELMER-OLSEN, R. (1950) Om forkastninger og oppbrotninger i Bamble formasjonen. *Norsk. Geol. Tidss.* 28, 171.
- SEMENENKO, N.P., SCHERBAK, A.P., VINAGADOV, A.P., TOUGARINOV, A.I., ELISEEVA, G.D., COTLOVSKAY, F.I., and DEMIDENKO, S.G. (1968) Geochronology of the Ukrainian Precambrian. *Can. J. Earth Sci.* 5, 661-672.
- SILVER, L.T. (1961) The relationship between radioactivity and discordance in zircons. *Nucl. Geophys. Nat. Acad. Sci.* 1075.
- .....and DEUTSCH, S. (1961) Uranium-lead method on zircons. *Ann. N.Y. Acad. Sci.* 91, 279-283.
- .....(1963) Uranium Lead isotopic variations in zircons. A case study. *Jour. Geol.* 71, 721-758.
- SMITHSON, S.B. (1963a) Granite studies. I.A. Gravity investigation of two Precambrian granites in South Norway. *Norges. Geol. Unders.* No. 219.
- .....(1963b) Granite studies II. The Precambrian Flå granite. *Norges. Geol. Unders.* No. 219.



- .....(1965) The nature of the granitic layer of the crust in the southern Norwegian Precambrian. Norsk. Geol. Tidss. 45, 113-134.
- STARMER, I.C. (1967) The geology of the Risør area, south Norway. Unpublished Ph.D. thesis, University of Nottingham.
- .....(1969) The migmatite complex of the Risør area, Aust. Agder, Norway. Norsk. Geol. Tidss. 49, 33-56.
- STEIGER, R.H. (1964) Dating of orogenic phases in the central Alps by K-Ar ages of hornblende. J. Geophys. Res. 69, 5407-5421.
- .....and WASSERBURG, G.J. (1966) Systematics of the  $Pb^{208}$  -  $Th^{232}$ ,  $Pb^{207}$  -  $U^{235}$ , and  $Pb^{206}$  -  $U^{238}$  systems. J. Geophys. Res. 71, 6065-6090.
- STOCKWELL, C.H. (1964) Fourth report on structural provinces, orogenics and time classification of rocks of the Canadian Precambrian Shield. In. Age determinations and geological studies. Geol. Surv. Can. Paper 64-112 Part II.
- .....(1968) Geochronology of stratified rocks of the Canadian Shield. Can. J. Earth Sci. 5, 693-698.
- STRENS, R.G.J. (1966) Infrared study of cation ordering and clustering in some (Fe, Mg) amphibole solid solutions. Chem. Comms. 519.
- SUTTON, J. (1963) Long term cycles in the evolution of the continents. Nature. 198, 731-735.
- TAUBENECK, W.H. (1957) Zircons in the metamorphic aureole of the Bald Mountain batholith, Elkhorn Mountains, northeastern Orogen. Bull. Geol. Soc. Am. 68, 1083.
- TILTON, G.R. (1960) Volume diffusion as a mechanism for discordant lead ages. J. Geophys. Res. 65, 2933-2945.
- .....Davis, G.L., WETHERILL, G.W., and ALDRICH, L.T. (1957) Isotopic ages of zircon from granites and pegmatites. Trans. Am. Geophys. Union. 38,





360-371.

.....and NICOLAYSEN, L.O. (1957) The use of monazites for age determination. *Geochim. Cosmochim. Acta.* II, 28-40.

.....PATTERSON, C., BROWN, H., INGRAM, M., HAYDEN, R., HESS, D., and LARSEN, E. (1965) Isotopic composition and distribution of lead, uranium and thorium in a Precambrian granite. *Bull. Geol. Soc. Am.* 66, 1131-1148.

.....and GRUNENFELDER, MH. (1968) Sphene: Uranium-lead ages. *Science.* 159, 1458-1461.

TOURET, J. (1962) Geological studies in the region Vegårshei-Gjerstad. *Norges. Geol. Unders.* 215, 120-139.

.....(1967) Les gneiss oeillets de la region de Vegårshei-Gjerstad (Norge meridionale). 7. Etude petrographique. *Norsk. Geol. Tidss.* 131-148.

WELIN, E. (1966) The absolute time scale and the classification of Precambrian rocks. *Geol. Fören. Förh. Stockh.* 88, 29.

.....and BLOMQVIST, W. (1964) Age measurements on radioactive minerals from Sweden. *Geol Fören . Förh. Stockh.* 86, 33.

WESTCOTT, M.R. (1966) Loss of argon in biotite in thermal metamorphism. *Nature*, 210, 83-84.

WETHERILL, G.W. (1956) Discordant uranium lead ages 1. *Trans. Am. Geophys. Union.* 37, 320-326.

.....(1963) Discordant uranium lead ages 2. Discordant ages resulting from diffusion of lead and uranium. *J. Geophys. Res.* 68, 2957-2956.

WHITTAKER, E.J.W. (1949) The structure of Bolivian crocidolite. *Acta. Cryst.* 312-317.

YORK, D. (1966) Least-squares fitting of a straight line. *Can. J. Earth Sci.* 44, 1079-1086.





- ZUSSMAN, J. (1968). X-ray diffraction. In physical methods in determinative mineralogy. Ed. J. Zussman. Academic Press, London
- .....(1968) The Precambrian metamorphic rocks around Lake Vegar (Aust Agder, southern Norway). Norges. Geol. Under. Nr. 257.
- TUREK, A. (1966) Rubidium-strontium studies in the Kalgoorlie-Norseman area, Western Australia. Unpublished Ph.D. thesis, Australian National University.
- TURNER, F.J. (1968) Metamorphic petrology. McGraw Hill, New York.
- TUTTLE, O.F., and BOWEN, N.L. (1958) Origin of granite in the light of experimental studies. Bull. Geol. Soc. Am. Mem. 47.
- VINAGRADOV, A.P., and TOUGARINOV, A.I. (1961) The geologic age of Precambrian rocks of the Ukrainian and Baltic Shields. Ann. N.Y. Acad. Sci. 91, 500-513.
- WASSERBURG, G.J. (1963) Diffusion processes in lead-uranium systems. J. Geophys. Res. 68, 4823-4846.
- WEBB, A.W., and McDOUGALL, I. (1968) The geochronology of igneous rocks of eastern Queensland. J. Geol. Soc. Aust. 15, 313-346.



APPENDIX A.DESCRIPTION AND LOCATION OF ANALYSED SPECIMENS

SN-36 Lat.  $58^{\circ}51'53''\text{N}$  Long.  $9^{\circ}20'58''\text{E}$

Medium-grained diopside bearing marble. Diopside (approx. 8%) occurs as 1 to 3 mm grains with occasional serpentine alteration. Calcite (average 1 mm) is the main constituent comprising approximately 84% of the mode. Idioblastic phlogopite crystals (approx. 7%) are unaltered. Magnetite and apatite make up about 1% of the rock.

The phlogopite concentrate was >95% with a slight calcite impurity.

SN-21 and SN-68-121 Lat.  $58^{\circ}56'55''\text{N}$  Long.  $9^{\circ}38'9''\text{E}$

A medium-grained, poorly foliated, garnet-biotite amphibolite occurring as discontinuous bands within a sequence of quartzites. Lepidoblastic hornblende (approx. 39%) is unaltered and varies in size between 1 and 3 mm.  $\text{An}_{30}$  plagioclase (approx. 25%) occurs as slightly sericitized, 2 to 3 mm sub-idioblastic grains. Almandine garnet porphyroblasts (approx. 9%) up to 5 mm contain numerous quartz inclusions (sieve structure). Biotite (approx. 13%) is unaltered and forms 1 to 3 mm grains. Minor amounts of xenoblastic quartz (5%), magnetite (7%) and apatite (2%) are also present.

The biotite concentrate was >99%. The hornblende concentrate contained <1% quartz.

SN-23 Lat.  $58^{\circ}57'17''\text{N}$  Long.  $9^{\circ}37'34''\text{E}$

A nodular sillimanite-biotite gneiss (nodular granite of Bugge, 1943). Quartz (approx. 63%) is xenoblastic and varies between 2 and 3 mm. Sub-idioblastic microcline (approx. 8%), 2 by 3 mm is slightly sericitized. Plagioclase (<1%) is subordinate and strongly sericitized (approx. 11%), muscovite





(approx. 12%) laths 0.5 to 1 mm occasionally exhibit some alteration to prehnite (?) along cleavages, whereas the biotite (approx. 5%) is partially or completely altered to chlorite. Xenoblastic pumpellyite (?) and magnetite make up about 1% of the rock.

The muscovite concentrate was >99%.

SN-20 Lat.  $58^{\circ}57'52''\text{N}$  Long.  $9^{\circ}34'33''\text{E}$

A medium-grained well-foliated biotite schist. The biotite (approx. 58%) is unaltered, idioblastic and between 1 and 3 mm in diameter. Xenoblastic quartz (approx. 20%) and  $\text{An}_{30}$  plagioclase (approx. 12%) are finer grained and interstitial. Magnetite (approx. 9%) and apatite (1%) together make up the remainder of the rock.

The biotite concentrate was 98%, containing plagioclase and magnetite impurities.

SN-10 Lat.  $58^{\circ}57'54''\text{N}$  Long.  $9^{\circ}28'27''\text{E}$

A medium-grained massive amphibolite occurring as boudins within granitic gneisses. Primary, sub-idioblastic to xenoblastic hypersthene (approx. 14%) is largely altered to 1 to 2 mm hornblende (approx. 36%), but a relict igneous texture is preserved.  $\text{An}_{32}$  plagioclase (approx. 41%) shows minor sericitization and has a cloudy appearance due to very fine magnetite inclusions. The remainder of the rock is composed of magnetite (approx. 7%), and apatite, quartz, chlorite and unaltered biotite together making up 3% of the rock. This rock was probably emplaced synkinematically as a norite and incompletely amphibolitized.

The biotite concentrate was 99%, containing quartz as impurity. The hornblende concentrate was 98%, containing plagioclase and quartz.





SN-11 Lat.  $58^{\circ}57'4''\text{N}$  Long.  $9^{\circ}28'27''\text{E}$

A garnetiferous granodiorite gneiss containing almandine porphyroblasts 1 cm in diameter sporadically distributed throughout the rock.  $\text{An}_{30-32}$  plagioclase (approx. 41%) is sericitized and sub-idioblastic in form. Sericite is approximately 14 modal per cent. Biotite grains (approx. 3%), with frayed margins, show partial and occasionally complete alteration to prochlorite (<1%). Xenoblastic quartz (approx. 41%) is 2 to 6 mm and minor amounts of unaltered muscovite (<1%) are also present.

The biotite concentrate was 98%, with chlorite impurity.

SN-73 Lat.  $58^{\circ}41'24''\text{N}$  Long.  $9^{\circ}12'52''\text{E}$

Medium-grained amphibolite occurring in a sequence of augen gneisses. The hornblende (approx. 51%) is lepidoblastic and 0.5 to 1 mm in length. The  $\text{An}_{32}$  plagioclase (approx. 35%) is slightly sericitized and biotite (approx. 10%) occurs as unaltered 0.5 to 1 mm grains. Minor amounts of magnetite (approx. 2%) and quartz (approx. 2%) are present.

The biotite concentrate was 99%, containing quartz impurity. The hornblende concentrate was 98%, containing plagioclase and quartz.

SN-79 Lat.  $58^{\circ}33'44''\text{N}$  Long.  $9^{\circ}35'33''\text{E}$

Stretched quartz pebble metaconglomerate. Pebbles are stretched in 'b' commonly exceed 10 cms in long dimension and are composed of xenoblastic, 3 to 5 mm quartz and 3 to 4 mm muscovite. The matrix is finer grained, and composed of unaltered 2 to 3 mm idioblastic muscovite, xenoblastic quartz and fibrous sillimanite. Small amounts of biotite are present but are strongly chloritized.

The muscovite concentrate was 98%, with 1% biotite and 1% quartz impurities.



SN-56 Lat.  $58^{\circ}49'45''\text{N}$  Long.  $9^{\circ}16'43''\text{E}$

A coarse-grained biotite quartzite within a sequence of granitic gneisses. Quartz (approx. 92%) is xenoblastic and up to 8 mm. Biotite (approx. 6%) forms 2 or 3 mm serrated plates, occasionally marginally altered to chlorite. Small amounts of muscovite (approx. 1%) and plagioclase (1%) are present.

The biotite concentrate was 99%, with chlorite impurity.

SN-75 Lat.  $58^{\circ}40'0''\text{N}$ . Long.  $9^{\circ}11'16''\text{E}$

K-feldspar augen gneiss. K-feldspar microperthite augen (approx. 15%) are up to 8 mm. The  $\text{An}_{22-24}$  plagioclase (approx. 42%) in the finer groundmass shows some alteration to sericite and occasionally micrographic intergrowth with quartz. Quartz (approx. 19%) is xenoblastic and interstitial. Hornblende (approx. 9%) and biotite (approx. 13%) are unaltered and between 1 and 2 mm. Apatite, magnetite and sphene make up approximately 2% of the rock.

The biotite concentrate was 99% and contained hornblende impurity.

SN-74 Lat.  $58^{\circ}41'24''\text{N}$ . Long.  $9^{\circ}12'52''\text{E}$

K-feldspar augen gneiss, same locality as SN-73. K-feldspar microperthite augen are approximately 5 mm by 1 cm. Microcline in the finer grained groundmass is 1 to 2 mm and the  $\text{An}_{30-32}$  plagioclase (approx. 27%) shows some alteration to sericite. K-feldspar is 23 modal% in toto. Quartz (approx. 32%) is xenoblastic and up to 8 mm. Biotite (approx. 7%) and hornblende (approx. 9%) are unaltered and 1 to 2 mm in diameter. Accessory apatite, magnetite and sphene make up the remaining 2% of the rock.

The biotite concentrate was 99% and contains quartz impurity. The hornblende concentrate is >98% and contained magnetite and <1% biotite impurities.





SN-78 Lat.  $58^{\circ}53'40''\text{N}$  Long.  $9^{\circ}45'33''\text{E}$

Sillimanite-biotite quartzite with well preserved cross-bedding structures. Quartz (approx. 71%) is xenoblastic and 1 to 1.5 mm. Biotite (approx. 19%) varies from 0.5 to 1 mm and shows minor alteration to prehnite and chlorite along cleavages. Plagioclase (approx. 4%) is almost completely sericitized. Muscovite (approx. 3%) is unaltered and 0.5 to 1 mm in diameter and sillimanite (approx. 2%) occurs sporadically as radiating fibrous masses. Rutile (<1%) is concentrated along cross-bedding structures.

The biotite concentrate was >99%.

SN-6 Lat.  $58^{\circ}56'42''\text{N}$ . Long.  $9^{\circ}40'8''\text{E}$

A medium-grained biotite granite gneiss. The rock is well-foliated consisting of sub-idioblastic, 1 mm k-feldspar microperthite (approx. 19%) xenoblastic 0.5 to 1 mm quartz (approx. 66%) and unaltered 1 to 1.5 mm biotite plates (approx. 13%). Plagioclase ( $\text{An}_{30}$ ) is present in minor amounts (approx. 1%). Hornblende, epidote and magnetite together make up about 1% of the rock.

The biotite concentrate was >99% and contained quartz impurity.

SN-68 Lat.  $58^{\circ}47'56''\text{N}$ . Long.  $9^{\circ}18'36''\text{E}$

A well foliated garnet-mica schist. Garnet porphyroblasts (approx. 3%) are 3 mm in diameter and contain numerous quartz and biotite inclusions. There is development of chlorite along cracks in the garnet. Sub-idioblastic microcline (approx. 15%) and  $\text{An}_{30-32}$  plagioclase (approx. 29%) vary between 1 and 1.5 mm, the plagioclase showing minor sericite alteration. Biotite (approx. 10%) is unaltered and forms 1 to 1.5 mm plates. Quartz (approx. 42%) is 1 mm, xenoblastic and exhibits undulose extinction resulting from cataclasis. Sillimanite and rutile together make up approximately 1% of the rock.





The biotite concentrate was >97% with quartz and garnet impurities.

SN-3 Lat.  $58^{\circ}58'2''\text{N}$ . Long.  $9^{\circ}33'28''\text{E}$

A garnet-biotite schist. The rock is well-foliated containing almandine porphyroblasts (approx. 2%) up to 3 mm with numerous quartz and magnetite inclusions.  $\text{An}_{30}$  plagioclase (approx. 34%) is sub-idioblastic, 1 to 1.5 mm, with some alteration to sericite (approx. 2%) along the cleavages. Quartz (approx. 36%) is xenoblastic and varies between 0.5 to 1 mm. Biotite (approx. 8%) is idioblastic and is altered to penninite along the cleavages in some instances. Occasionally biotite is completely replaced by penninite (approx. 13%) and magnetite (<1% total). Carbonate is present in small veinlets (approx. 5%).

The biotite concentrate was >97% with chlorite impurity.

SN-16 Lat.  $58^{\circ}56'25''\text{N}$ . Long.  $9^{\circ}33'28''\text{E}$

A medium-grained hornblende-biotite schist. A well-foliated rock containing 1 to 2 mm lepidoblastic hornblende (approx. 37%) and unaltered 1 to 2 mm biotite plates (approx. 20%). Quartz (approx. 19%) is xenoblastic and the plagioclase (approx. 22%) is partially sericitized and in the range  $\text{An}_{30-32}$ . Magnetite and graphite together make up approximately 2% of the rock.

The biotite concentrate was 99% containing plagioclase impurity.

The hornblende concentrate was >98% containing quartz and biotite impurities.

SN-40 Lat.  $58^{\circ}51'59''\text{N}$ . Long.  $9^{\circ}11'44''\text{E}$

A coarse-grained granite gneiss showing good foliation in hand specimen. Quartz is xenoblastic, between 6 mm and 1 cm and commonly shows strained extinction. Microcline microperthite is the dominant feldspar,



xenoblastic to sub-idioblastic and between 3 and 6 mm; minor amounts of plagioclase are strongly sericitized. Biotite occurs as corroded sub-idioblastic grains, varying between 1/2 and 1 mm., with some alteration to chlorite and prehnite.

The biotite concentrate was 99% with quartz impurity.

SN-54 Lat.  $58^{\circ}53'43''\text{N}$ . Long.  $9^{\circ}15'46''\text{E}$

Coarse-grained biotite granodiorite gneiss. The  $\text{An}_{27}$  plagioclase (approx. 59%) is xenoblastic and up to 8 mm. Quartz is xenoblastic (approx. 37%) and forms irregular masses up to 1 cm. Biotite plates (approx. 4%) have serrated margins and show some minor chlorite alteration.

The biotite concentrate was 98% containing quartz impurity.

SN-44 Lat.  $58^{\circ}54'35''\text{N}$ . Long.  $9^{\circ}23'39''\text{E}$

A medium-grained moderately well foliated granite gneiss. Xenoblastic to sub-idioblastic  $\text{An}_{15}$  plagioclase (approx. 34%) forms grains 3 mm in diameter and is partially sericitized (sericite approx. 3%). Microcline (approx. 5%) is xenoblastic, unaltered and forms 1 - 2 mm diameter grains. Quartz (approx. 49%) is xenoblastic and varies between 1 and 3 mm. Quartz commonly shows strained extinction. Biotite (approx. 7%) varies from 0.5 to 1 mm, has serrated margins and shows minor chlorite (<1%) alteration. Allanite and apatite make up approximately 2% of the rock.

The biotite concentrate was >97% pure with 2% chlorite and traces of K-feldspar impurities.

SN-76 Lat.  $58^{\circ}46'20''\text{N}$ . Long.  $8^{\circ}51'55''\text{E}$

A coarse-grained K-feldspar augen gneiss. K-feldspar microperthite augen are up to 2 cm in diameter. Microcline in the groundmass is subidioblastic, 0.5 to 1 mm, with sericite alteration. Quartz is 0.5 to 1 mm and





frequently exhibits undulose extinction. The small amount of plagioclase is almost completely altered to sericite. Biotite occurs in clusters and is between 0.5 to 1 mm. Marginal alteration of the biotite to chlorite is common. Accessory amounts of apatite, garnet and magnetite are present.

The biotite concentrate was 97% with 2% chlorite and 1% quartz impurities.

SN-2 Lat.  $58^{\circ}58'2''N$ . Long.  $9^{\circ}33'28''E$

A medium-grained amphibolite. Sub-idioblastic to xenoblastic  $An_{28}$  plagioclase (approx. 23%) is sub-idioblastic to xenoblastic with slight sericite alteration. Hornblende (approx. 63%) occurs as sub-idioblastic to idioblastic, inclusion-free grains between 1 and 2 mm diameter. Biotite (approx. 1%) forms approximately 0.5 mm crystals. Quartz (approx. 8%) is xenoblastic and 0.5 to 1 mm diameter. Magnetite (approx. 4%) and apatite (approx. 1%) and epidote (<1%) are present.

The hornblende concentrate was >98% with plagioclase and epidote impurities.

SN-9 Lat.  $58^{\circ}58'19''N$ . Long.  $9^{\circ}29'28''E$

A medium-grained amphibolite occurring as discontinuous bands in a series of granitic gneisses. Hornblende (approx. 62%) occurs as 2 to 3 mm unaltered lepidoblastic grains.  $An_{30-35}$  plagioclase (approx. 28%) is sub-idioblastic and in part altered to sericite. Minor quartz (approx. 5%), magnetite (approx. 4%), and apatite (approx. 1%) are present.

The hornblende concentrate was 98% with magnetite and quartz impurities.





SN-22 Lat.  $58^{\circ}56'43''\text{N}$ . Long.  $9^{\circ}37'42''\text{E}$

A medium-grained amphibolite. Lepidoblastic hornblende (approx. 68%) is up to 5 mm. Plagioclase (approx. 26%) is sub-idioblastic to xenoblastic and strongly sericitized. Minor amounts of 0.5 to 1 mm biotite (approx. 1%), apatite (1%), quartz (approx. 2%) and magnetite (approx. 3%) are present.

The hornblende concentrate was >97% with magnetite and plagioclase impurities.

SN-45 Lat.  $58^{\circ}54'35''\text{N}$ . Long.  $9^{\circ}23'38''\text{E}$

A medium-grained amphibolite. This rock possesses a poor foliation and contains unaltered lepidoblastic hornblende (approx. 70%), sub-idioblastic  $\text{An}_{30}$  plagioclase (approx. 27%) and 2 mm biotite plates (approx. 2%) with serrated margins. Quartz, magnetite and apatite together make up about 2% of the rock.

The hornblende concentrate was >99% containing biotite impurity.

SN-38 Lat.  $58^{\circ}52'12''\text{N}$ . Long.  $9^{\circ}21'37''\text{E}$

A medium-grained, poorly foliated amphibolite. The rock consists of 1 to 2 mm lepidoblastic hornblende (approx. 55%) and 1 to 2 mm sub-idioblastic  $\text{An}_{33}$  plagioclase (approx. 40%) together with minor amounts of xenoblastic quartz (approx. 2%) and biotite (approx. 1%). Sphene, apatite, ilmenite and epidote make up approximately 2% of the rock.

The hornblende concentrate was 98% with epidote and plagioclase impurities.

SN-70 Lat.  $58^{\circ}41'18''\text{N}$ . Long.  $9^{\circ}9'18''\text{E}$

A medium-grained hornblende-plagioclase gneiss. Lepidoblastic



hornblende (approx. 39%) is unaltered an up to 3 mm.  $An_{30}$ , sub-idioblastic plagioclase (approx. 44%), between 1 and 2 mm, is partially altered to sericite. Xenoblastic quartz (approx. 8%) varies between 0.5 and 1.5 mm. Relicts of augite (approx. 1%) are enclosed by hornblende. Minor amounts of biotite (approx. 2%) and apatite (approx. 1%) and magnetite (approx. 3%) and sphene (<1%) and epidote (<1%) are present.

The hornblende concentrate was 98% with epidote impurity.

SN-71 Lat.  $58^{\circ}41'18''N$  Long.  $9^{\circ}9'18''E$

A medium-grained metagabbro occurring as conformable bands in a predominantly metasedimentary sequence. Relict augite (approx. 33%) shows incipient alteration to chlorite along the cleavages and is partly converted to sub-idioblastic hornblende (approx. 22%). A palimpsest igneous texture persists.  $An_{32}$  plagioclase is anhedral (approx. 35%) and interstitial. Minor amounts of quartz (approx. 4%), magnetite (approx. 5%), and apatite are present. The rock is an incompletely amphibolitized pre - or synkinematic gabbro.

The hornblende concentrate was >98% containing 1% epidote and a trace of biotite as impurities.

SN-57 Lat.  $58^{\circ}49'55''N$  Long.  $9^{\circ}22'42''E$

A poorly foliated, igneous textured, gneissic granite. Subhedral K-feldspar microperthite (approx. 40%) up to 4 mm in diameter coexists with 3 to 4 mm sericitized albite (approx. 17%). Biotite plates (approx. 19%) is anhedral and up to 4 mm. Anhedral amphibole (approx. 19%) is compositionally near ferrohastingsite. Monazite and apatite together make up 1% of the rock.

The biotite concentrate contained 1% of chlorite, 1% of apatite and 1% of plagioclase.





SN-61 Lat.  $58^{\circ}48'13''\text{N}$  Long.  $9^{\circ}23'42''\text{E}$

Porphyroblastic granite gneiss. A poorly foliated rock consisting of  $\text{An}_{8-10}$  plagioclase (approx. 48%) as 5 mm porphyroblasts in part altered to sericite, together with sub-idioblastic to xenoblastic 1 to 3 mm microcline (approx. 7%). Quartz (approx. 29%) is xenoblastic. Hornblende (approx. 5%) and biotite (approx. 10%) are unaltered and between 1 and 3 mm in size. The hornblende contains some magnetite inclusions. Accessory apatite, monazite, orthite and zircon comprise about 1% of the rock.

The biotite concentrate was 99% with feldspar impurity. The hornblende concentrate was 99% with feldspar and monazite (?) impurities.

SN-59 Lat.  $58^{\circ}47'33''\text{N}$  Long.  $9^{\circ}22'58''\text{E}$

A poorly foliated granite gneiss. K-feldspar microperthite (approx. 23%) varies from 2 to 3 mm. Oligoclase (approx. 31%) varies from 1 to 2 mm and occasionally forms a micrographic intergrowth with quartz. Quartz (approx. 36%) is xenoblastic and 3 to 4 mm in diameter. Biotite (approx. 8%) forms 1 to 2 mm plates frequently with frayed margins. Sphene, magnetite and apatite together comprise 2% of the rock.

The biotite concentrate was 99% with traces of quartz and feldspar.

SN-26 Lat.  $58^{\circ}57'40''\text{N}$  Long.  $9^{\circ}33'43''\text{E}$

Medium-grained Ödegaardite (BRÖGGER 1934, 1935). A medium-grained metagabbro containing hornblende (approx. 42%) approaching pargasite in composition and between 1 and 4 mm. Original plagioclase has been completely altered to scapolite (approx. 54%). Occasional patchy pyroxene relicts (approx. 2%) are seen in some of the hornblendes. Sphene (approx. 1%) is idioblastic. Rutile and apatite comprise approximately 2% of the rock. The





conversion of plagioclase to scapolite appears to be later than that of augite to hornblende.

The hornblende concentrate was 98%, containing scapolite and pyroxene impurities.

SN-68-161 Lat.  $58^{\circ}48'12''$ N. Long.  $9^{\circ}24'53''$ E

Porphyroblastic granodiorite gneiss. The rock is for the most part composed of xenoblastic quartz (approx. 28%) up to 7.5 mm in diameter and  $An_{5-10}$  plagioclase porphyroblasts (30%). The plagioclase shows a moderate amount of sericitization. In addition approximately 3 modal % of microcline is present. Idioblastic to sub-idioblastic hornblende (approx. 18%) is unaltered and contains apatite inclusions. Laths of biotite (approx. 8%) are 2 to 3 mm in length, unaltered and contain inclusions of zircon, apatite and sphene. Accessory allanite, zircon, apatite, magnetite and sphene together make up about 2 to 3% of the mode.

SN-68-159 Lat.  $58^{\circ}47'33''$ N. Long  $9^{\circ}22'58''$ E

This sample was collected from the same rock mass as SN-59 and is petrographically indistinguishable. See the above description of SN-59.

SN-68-158 Lat.  $58^{\circ}48'54''$ N. Long.  $9^{\circ}21'44''$ E

A foliated granitic gneiss. This rock is composed of xenoblastic quartz (approx. 22%) up to 4 mm in diameter, xenoblastic to sub-idioblastic microcline (approx. 35%) up to 5 mm in diameter and slightly sericitized  $An_{10}$  plagioclase (approx. 28%). The ferromagnesian constituents include well-formed biotite laths (8%) averaging 1 to 2 mm and 2 to 3 mm hornblende (approx. 6%) grains. Apatite and zircon comprise the remainder of the rock.



SN-68-104 Lat.  $58^{\circ}50'18''\text{N}$ . Long.  $9^{\circ}24'32''\text{E}$

Granitic gneiss. The mode of the rock is actually closer to that of an adamellite. Xenoblastic quartz (approx. 20%) is 2 to 3 mm in diameter. Unaltered idiomorphic to sub-idiomorphic microcline microperthite up to 1 cm in length comprises approximately 20% of the mode. Sub-idiomorphic sodic plagioclase in the  $\text{An}_{5-10}$  range (approx. 20 modal %) shows slight marginal sericitization. Hornblende (approx. 18%) is sub-idiomorphic and biotite (approx. 13%) occurs as 1 to 3 mm laths. The remainder of the rock is made up of accessory amounts of allanite, apatite and sphene.

SN-68-105 Lat.  $58^{\circ}50'33''\text{N}$ . Long.  $9^{\circ}22'51''\text{E}$

A granitic gneiss. As above this rock is actually closer to an adamellite in the modal proportions of its constituents. Idiomorphic to sub-idiomorphic microcline (approx. 39 modal %) is unaltered.  $\text{An}_{8-10}$  plagioclase (approx. 21%) occurs as sub-idiomorphic grains up to 5 mm in length and which show slight marginal alteration to sericite. Xenoblastic quartz forms approximately 20% of the mode. Biotite laths (approx. 6%) are usually well-formed, but occasionally show marginal alteration to chlorite. The remainder of the mode is made up of hornblende (approx. 3%), chlorite and apatite.

SN-90 Lat.  $58^{\circ}54'54''\text{N}$ . Long.  $9^{\circ}31'30''\text{E}$

Diopside-plagioclase-sphene pegmatite, associated with the Langøy gabbro.

SN-91 Lat.  $58^{\circ}57'42''\text{N}$ . Long.  $9^{\circ}33'43''\text{E}$

Sphene associated with xenolithic patches of hornblende and plagioclase in the K-feldspar Ødegaarden pegmatite.





SN-92 Lat.  $58^{\circ}56'30''\text{N}$ . Long.  $9^{\circ}30'0''\text{E}$

Sphene from the rutile bearing Ringsjø albitite body.

SN-94 Lat.  $58^{\circ}57'40''\text{N}$ . Long.  $9^{\circ}32'43''\text{E}$

Xenotime enclosed in chlorapatite at Ödegaardens-verk apatite mines.

SN-96 Lat.  $58^{\circ}57'40''\text{N}$ . long.  $9^{\circ}33'43''\text{E}$

Sphene associated with hornblende and albitite in the Ödegaardens-verk Road Metal Quarry. See SN-59 above.

SN-89 Lat.  $58^{\circ}57'40''\text{N}$ . Long.  $9^{\circ}33'43''\text{E}$

Massive hornblende occurring as veins cutting Ödegaardite in the "Road Metal Quarry" adjacent to the Ödegaarden Apatit Gruber. Probably related to the formation of the apatite deposits.

The hornblende concentrate was >99%.

SN-30 Lat.  $58^{\circ}57'40''\text{N}$ . Long  $9^{\circ}33'43''\text{E}$

Phlogopite occurring as an outer zone to the chlorapatite in a productive vein at Ödegaarden Apatit Grubene.

The phlogopite concentrate was >99%.

SN-27 Lat.  $58^{\circ}57'40''\text{N}$ . Long.  $9^{\circ}33'43''\text{E}$

Wall-rock to the productive vein at Ödegaarden Apatit Grubene (sandrock of the miners). The rock is friable and is composed of patches of talc (approx. 18%) pseudomorphous after enstatite. A few relict patches of enstatite (approx. 5%) remain enclosed by talc.  $\text{An}_{20-26}$  plagioclase (approx. 56%) is commonly sericitized and may be converted to scapolite (approx. 8%). Phlogopite (approx. 5%) occurs as unaltered plates 1 to 3 mm in length. Euhedral apatite is abundant (approx. 6%), and some ilmenite is present (approx. 2%).





The phlogopite concentrate was 95% containing scapolite impurity.

SN-35 Lat.  $58^{\circ}56'26''\text{N}$ . Long.  $9^{\circ}25'40''\text{E}$

Coarse-grained metapyroxenite. Initial euhedral cumulate hypersthene (average 3 cms) in part replaced by hornblende. Hornblende (approx. 43%) is 1 to 2 mm and forms a patchy intergrowth with hypersthene (approx. 34%). Phlogopite (approx. 23%) is also secondary and forms unaltered 1 to 3 mm laths. Minor magnetite (1%) is present. A cumulate texture is preserved. Field relations suggest that this rock is part of a late-kinematic differentiated gabbro body.

The phlogopite concentrate was 99%, with hornblende impurity. The hornblende concentrate was 95% with hypersthene impurity.

SN-43 Lat.  $58^{\circ}54'35''\text{N}$ . Long.  $9^{\circ}23'39''\text{E}$

A concordant pegmatite body in granitic gneisses. Contains plagioclase and K-feldspar perthite up to 10 cms in diameter, and quartz. Biotite varies from 1 to 2 cms in diameter.

The biotite concentrate was taken from 2 cm books and was 99% pure.

SN-84 Lat.  $59^{\circ}1'22''\text{N}$ . Long.  $9^{\circ}32'55''\text{E}$

Discordant K-feldspar pegmatite body. The muscovite concentrate was taken from 10 cms books and was >99% pure.

SN-85 Lat.  $58^{\circ}56'38''\text{N}$ . Long.  $9^{\circ}25'16''\text{E}$

Concordant pegmatite body (Björdammen) containing quartz, oligoclase (var. aventurine) and biotite.

The biotite concentrate was taken from 1 cm books and was >99% pure.

SN-42 Lat.  $58^{\circ}54'0''\text{N}$ . Long.  $9^{\circ}23'6''\text{E}$

A concordant pegmatite body occurring within a sequence of amphibolites



and granitic gneisses. Contains quartz, andesine and biotite (1 cm).

The biotite concentrate was >99% pure.

SN-86 Lat.  $58^{\circ}56'10''\text{N}$ . Long.  $9^{\circ}28'20''\text{E}$

A coarse-grained cordierite-anthophyllite rock occurring in association with amphibolites. Consists of cordierite, anthophyllite (gedrite), quartz biotite and rutile. The biotite varies from 1 to 1.5 cms in diameter.

The biotite concentrate was >99% pure.

SN-12 Lat.  $58^{\circ}57'4''\text{N}$ . Long.  $9^{\circ}28'27''\text{E}$

Small concordant pegmatite occurring within a sequence of amphibolites and granitic gneisses (see SN-10 above). Consists of quartz, andesine and biotite (up to 2 cms).

The biotite concentrate from 2 cm books was >99% pure.

SN-81 Lat.  $58^{\circ}59'6''\text{N}$ . Long.  $9^{\circ}21'55''\text{E}$

Discordant pegmatite containing K-feldspar, quartz and biotite (books in excess of 20 cms). Metamict minerals such as orthite and fergusonite are present.

The biotite concentrate was >99% pure.

SN-87 Lat.  $58^{\circ}58'26''\text{N}$ . Long.  $9^{\circ}32'58''\text{E}$

A discordant pegmatite containing quartz, K-feldspar and biotite (2 cm books).

The biotite concentrate was >99% pure.



APPENDIX B.CHEMICAL PROCEDURES FOR K, RB, SR AND PB.

With the exception of the techniques used for U and Th which are described separately in Appendix C, the chemical procedures employed by the author are now in fairly standard usage in the University of Alberta laboratory.

Potassium

All potassium determinations were made gravimetrically by the double Abbey leach method (ABBEY, 1960) followed by the precipitation of  $\text{KB}(\text{C}_6\text{H}_5)_4$ .

A 0.25 gm. sample in the case of micas and a 1 gm. sample in the case of hornblende, is weighed into a cleaned (hot conc.  $\text{HNO}_3$ ) platinum dish. 3 mls. of distilled  $\text{H}_2\text{O}$  is used to moisten the sample and 3 mls. 1:1  $\text{H}_2\text{SO}_4$  (6 mls. for 1 gm. samples) and 5 mls. 48% HF (10 mls. for 1 gm. samples) are added. After evaporation to dryness  $\text{SO}_3$  is fumed off and the residue ignited for 1 hour on a Tyrrell burner. The residue is then moistened with distilled  $\text{H}_2\text{O}$  and transferred to a 20 ml. beaker. K is leached with water four times on a steam bath, filtering each time through a blue band paper. After the fourth leach the residue is transferred back to the platinum dish, 3 mls. 1:1  $\text{H}_2\text{SO}_4$  are added and the procedure is repeated.

(K, Rb, Cs)  $\text{B}(\text{C}_6\text{H}_5)_4$  is precipitated at 60 C from the combined leach solutions with  $\text{NaB}(\text{C}_6\text{H}_5)_4$  added dropwise. The precipitate is allowed to settle out for two hours at room temperature, filtered through a fine fritted glass filter, dried and weighed.

$$\% \text{K}_2\text{O} = \frac{\text{wt. KB}(\text{C}_6\text{H}_5)_4 \times 0.1314 \times 100}{\text{sample wt.}}$$





The  $K_2O$  figure above is corrected for coprecipitated Rb by the analysis of the precipitates for Rb by an X.R.F.S. procedure. The precipitate is mounted onto aluminum discs with a mixture of durafix + acetone and analyzed versus (K, Rb)  $B(C_6H_5)_4$  standards. In actual fact the conversion factor 0.134 is not strictly correct because of the presence of Rb, but additional correction is not normally necessary.  $Rb_2O$  was found to vary between 0.01 and 0.05 wt. % for micas analyzed by the author and was insignificant in the case of hornblendes.

#### Rubidium.

The procedure employed for the isotope dilution analysis of rubidium is procedurally similar to the method for potassium.

Preliminary Rb and Sr determinations are made on all samples by X.R.F.S.

An amount of sample is weighed out into a cleaned (hot conc.  $HNO_3$ ) platinum dish, to give approximately 15 to 20 ug of Rb, and moistened with a few mls. of demineralised water. 5 mls. of HF and 5 mls 1:1  $H_2SO_4$  (diluted with demineralised water) are added and the sample is evaporated to dryness.

At this stage approximately 20 ug of enriched  $Rb^{87}$  isotope dilutant in HCl is added to the sample (Rb spikes were made up individually and stored in parafilm wrapped beakers and the amounts are based on calibrations performed by H. Baadsgaard). The samples are again evaporated to dryness and ignited on a Meker burner. Rb is leached with 1 ml. of demineralised water and transferred to cleaned silica vials and stored for mass spectrometric analysis.

The blank for this procedure is less than 0.01 micrograms.

#### Strontium.

Strontium is determined by isotope dilution analysis using an enriched



$\text{Sr}^{84}$  spike.

A sample is weighed out to give approximately 20 ug of strontium (optimum amount to give an 86/84 ratio of 1.0 using 2 ug of  $\text{Sr}^{84}$  enriched spike) directly into a cleaned (hot 1:1 HCl) teflon beaker. A  $\text{Sr}^{84}$  spike (about 2 ug) is added directly to the sample and the spike container is rinsed with about 10 ml. 1:1  $\text{HNO}_3$ , 10 mls. of 48% HF is added and the sample evaporated to dryness under a positive pressure of filtered air. When dry, 5 mls. of 1:1  $\text{HNO}_3$  are added and the sample is again evaporated to dryness at which point 5 mls. of 2.5M HCl are added and again the sample is evaporated to dryness.

The sample is taken up in 1 to 2 mls. of 2.5N HCl and added to a prepared Dowex 50W-X8 column and eluted with 2.5M HCl. The 'Sr fraction' is collected, evaporated to dryness and stored for mass-spectrometric analysis.

The columns prepared by the author were 18 cms by 1 cm (i.d.) of Dowex 50W-X8 (200 to 400 mesh) cation exchange resin. The strontium fraction is eluted in the 72 to 80 mls. interval. Columns were cleaned with 6M HCl and resettled with demineralized water followed by 2.5M HCl for re-use.

The blank for this procedure is less than 0.02 micrograms.

#### Lead.

The procedure employed for the extraction and purification of lead samples was described in Chapter V and is essentially the method of TILTON et al. (1957). A brief account of the preparation of the reagents used will be given here.

All glassware used is cleaned in hot concentrated  $\text{HNO}_3$ , rinsed in triple distilled water and wrapped in 'parafilm' as necessary. Only triple distilled water is used in the preparation of reagents and for the extraction of lead.

Chloroform: Reagent grade chloroform is cleaned twice with approx-





imately 25 mls./litre of 3M HCl and washed approximately 20 times in 3D water and filtered through a cleaned glass wool plug.

Dithizone: A 0.01% stock solution in  $\text{CHCl}_3$  of diphenylthiocarbozone is made up and extracted for impurities with 3M HCl. This solution will extract 40 micrograms of lead per ml. The solution is diluted 1:5 with  $\text{CHCl}_3$  (8 micrograms of lead equivalent) for the final lead extraction.

Borax: A 10% solution of sodium tetraborate is extracted with dithizone and washed with cleaned chloroform until all the dithizone has been visibly removed. The solution is evaporated to a syrup under a positive overpressure and ignited to an anhydrous glass. The borax glass is carefully cracked out of the platinum dish and stored for use.

Potassium Cyanide: A 2% solution of KCN in 3%  $\text{NH}_3$  is made directly from Fishers reagent KCN (reported Pb = 0.0000%).

Ammonium Citrate: A 40% ammonium citrate solution (400 gms. / litre) is extracted with dithizone and washed with chloroform.

Ammonium hydroxide:  $\text{NH}_4\text{OH}$  is prepared by passing gaseous ammonia through 3D water.

Two sets of reagents were used for the lead extractions. The first set was prepared by Dr. H. Baadsgaard (July 1968), and the second set (February, 1969) by the author. A sample calculation of the probable reagent blank is given here.

#### Feb. 3rd. Pb BLANK.

Reagents used for the blank were as follows:-

Borax:= 10.36 gms.

Ammonium citrate (40%) = 100 ml.

2% KCN in 3%  $\text{NH}_3$  = 20 ml.





6N HCl = 12 ml.

3% NH<sub>3</sub> = 20 ml.

2% HNO<sub>3</sub> = 5 ml.

Added 1.8952 gms. of Pb<sup>206</sup> spike solution number 1.

The measured isotopic ratios were:

$$^{204}\text{Pb}/^{206}\text{Pb} = 0.000471 \pm 0.000016$$

$$^{207}\text{Pb}/^{206}\text{Pb} = 0.00782 \pm 0.00006$$

$$^{208}\text{Pb}/^{206}\text{Pb} = 0.01849 \pm 0.00009$$

i.e. <sup>204</sup>Pb:<sup>206</sup>Pb:<sup>207</sup>Pb:<sup>208</sup>Pb is

$$1:2123:16.6:39.25.$$

Assume all the Pb<sup>206</sup> is from the spike.

Therefore blank is

$$1: 0: 16.6 :39.25$$

Pb<sup>207</sup>/Pb<sup>206</sup> for modern lead is 0.8451, therefore blank becomes

$$1: 19.64 :16.6 :39.25$$

Amounts of spike added are:

$$^{204}\text{Pb} = 0$$

$$^{206}\text{Pb} = 27.502 \text{ ug}$$

$$^{207}\text{Pb} = 0.00284 \text{ ug}$$

$$^{208}\text{Pb} = 0.004169 \text{ ug}$$

$$\text{Therefore } \frac{^{208}\text{Pb}}{^{206}\text{Pb}} = \frac{\text{ug Pb}_{\text{blank}}^{208} + \text{ug Pb}_{\text{blank}}^{208}}{\text{ug Pb}_{\text{blank}}^{206} + \text{ug Pb}_{\text{spike}}^{206}}$$

Substituting the above values the total blank is calculated to be 0.979 micrograms assuming that the blank has a modern lead composition (1L20.2:17.05:40.05).

The blank for the July 1968 reagent set was slightly higher than this.



APPENDIX C.CHEMICAL PROCEDURES FOR URANIUM AND THORIUM.

Ion exchange procedures have proven to be extremely useful for the separation of the microgram quantities of elements used in radiometric dating. FRITZ and GARRALDA (1962) have shown that thorium is quantitatively retained in 6M  $\text{HNO}_3$  on Dowex 1-X8 anion exchange resin. Their data also suggests that the distribution coefficient of  $\text{UO}_2^{2+}$  may be sufficiently large for the separation of U and Th from the materials commonly used in radiometric age determinations. In order to evaluate this method a column was calibrated for U,Th,Ce and Ti directly and also for a zircon, sphene and monazite diluted with U and Th.

Column Characteristics.

Dowex 1-X8 (200 to 400 mesh) anion exchange resin, supplied in the  $\text{Cl}^-$  form, was converted to the  $\text{NO}_3^-$  form by decanting several times with 5M  $\text{HNO}_3$ . The resin was added as a slurry to a 12 mm. I.D column, fitted with a drip-capillary and a 250 ml. bulb, to a bedded height of 16 cms. The resin was washed with 5M  $\text{HNO}_3$  until the effluent gave a negative test with  $\text{AgNO}_3$ .

Column Calibration.

Before use the columns were washed with 20 mls. of 6M  $\text{HNO}_3$ . Calibrations were performed separately for U, Th, Ti and Ce, each of which were loaded to the column in 10 ml. of 6M  $\text{HNO}_3$  and eluted 3 ml. at a time. The methods employed for the semi-quantitative analysis of the column effluent were as follows:

1. Uranium was determined by the measurement of the absorbance at 425 m $\mu$  of the yellow peroxy-complex formed in an alkali medium.

2. Thorium was determined by the measurement of the absorbance at 410 m $\mu$  of the yellow thorium morinate complex formed at at pH of 3 (see



SANDELL, 1959).

3. Cerium was usually determined by precipitating the hydroxide and estimating its amount visually.

4. Titanium was determined colourimetrically by measuring the absorbance of the yellow peroxy-complex in acid media at 425 mμ.

Results of the column calibration for U, Th, Ce, and Ti are shown in Fig. 34. Samples of zircon, sphene, and monazite were fused, dissolved, diluted with U and Th, and also Ce in the case of the zircon and sphene samples, and added to the columns in 10 ml. solutions of 6M HNO<sub>3</sub>. The results of the elution with 6M HNO<sub>3</sub> were similar in each case and only zircon is shown as an example in Fig. 35. La, P, Y and Si etc. all have very small distribution coefficients and are present in the sample effluent.

#### Stripping of Thorium.

Since thorium does not 'breakthrough' until the columns have been eluted with more than 250 mls. of 6M HNO<sub>3</sub>, it is most convenient to strip it from the column after the elution of the uranium. The stripping efficiencies of 0.01M HNO<sub>3</sub>, 0.5M HNO<sub>3</sub>, 6N H<sub>2</sub>SO<sub>4</sub>, and 0.5M H<sub>2</sub>C<sub>2</sub>O<sub>4</sub> were examined. The stripping efficiencies of 0.01 and 0.5M HNO<sub>3</sub> were found to be approximately the same (Fig. 36.), but only 25 to 30 mls. of 0.5M H<sub>2</sub>C<sub>2</sub>O<sub>4</sub> and 6N H<sub>2</sub>SO<sub>4</sub> were required to remove thorium from the columns. 0.5M HNO<sub>3</sub> was finally selected for the stripping of thorium as it proved convenient to load U and Th as combined nitrates for mass spectrometry.

#### Sample Procedure.

All the HNO<sub>3</sub> used for the separation of U and Th from samples was redistilled reagent grade HNO<sub>3</sub> diluted only with triple distilled water.

Before use the six prepared columns were resettled and cleaned with





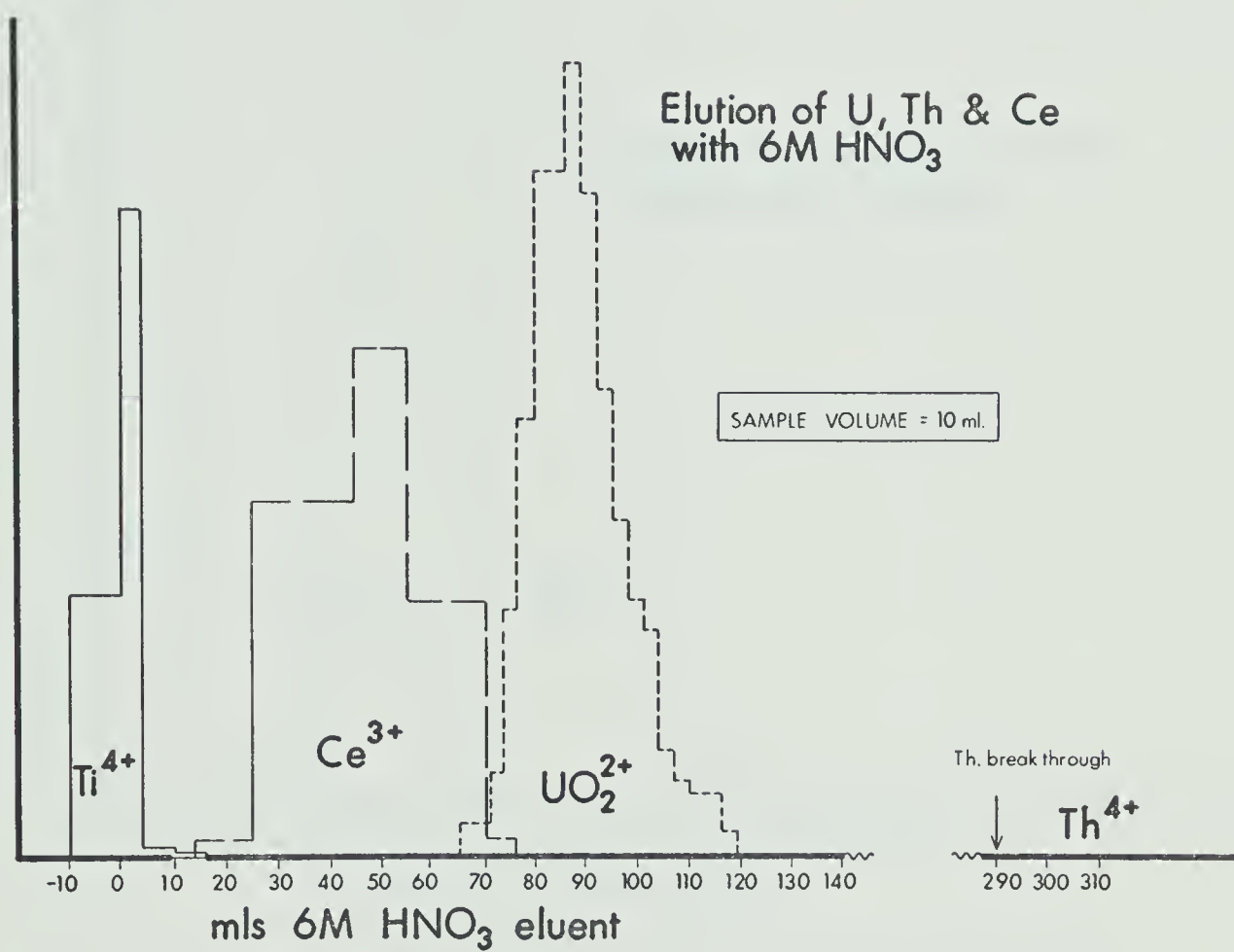


Fig.34. Calibration of a Dowex 1-X8 column for U,Th,Ce and Ti.



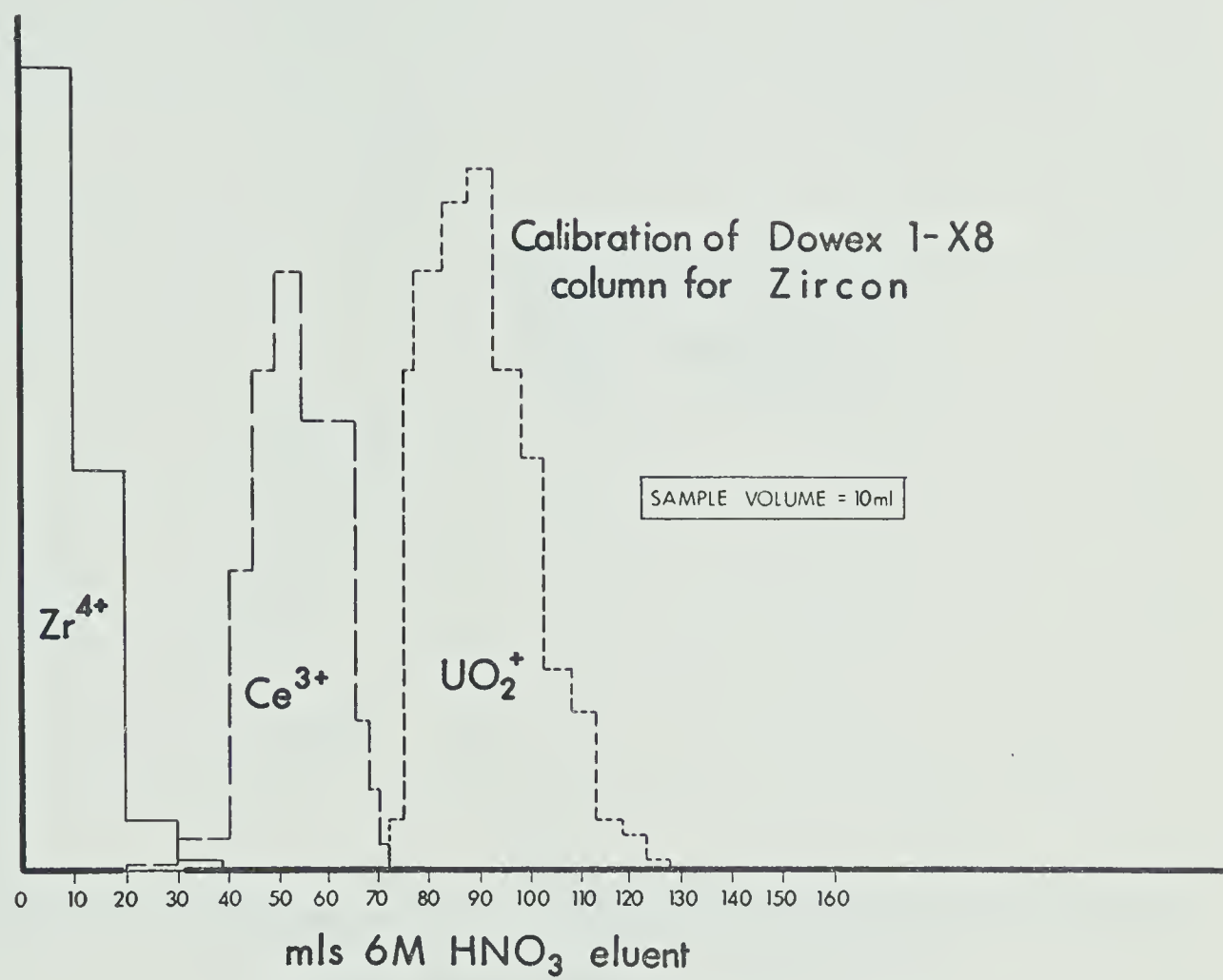


Fig.35. Calibration of a Dowex 1-X8 anion exchange column for zircon.



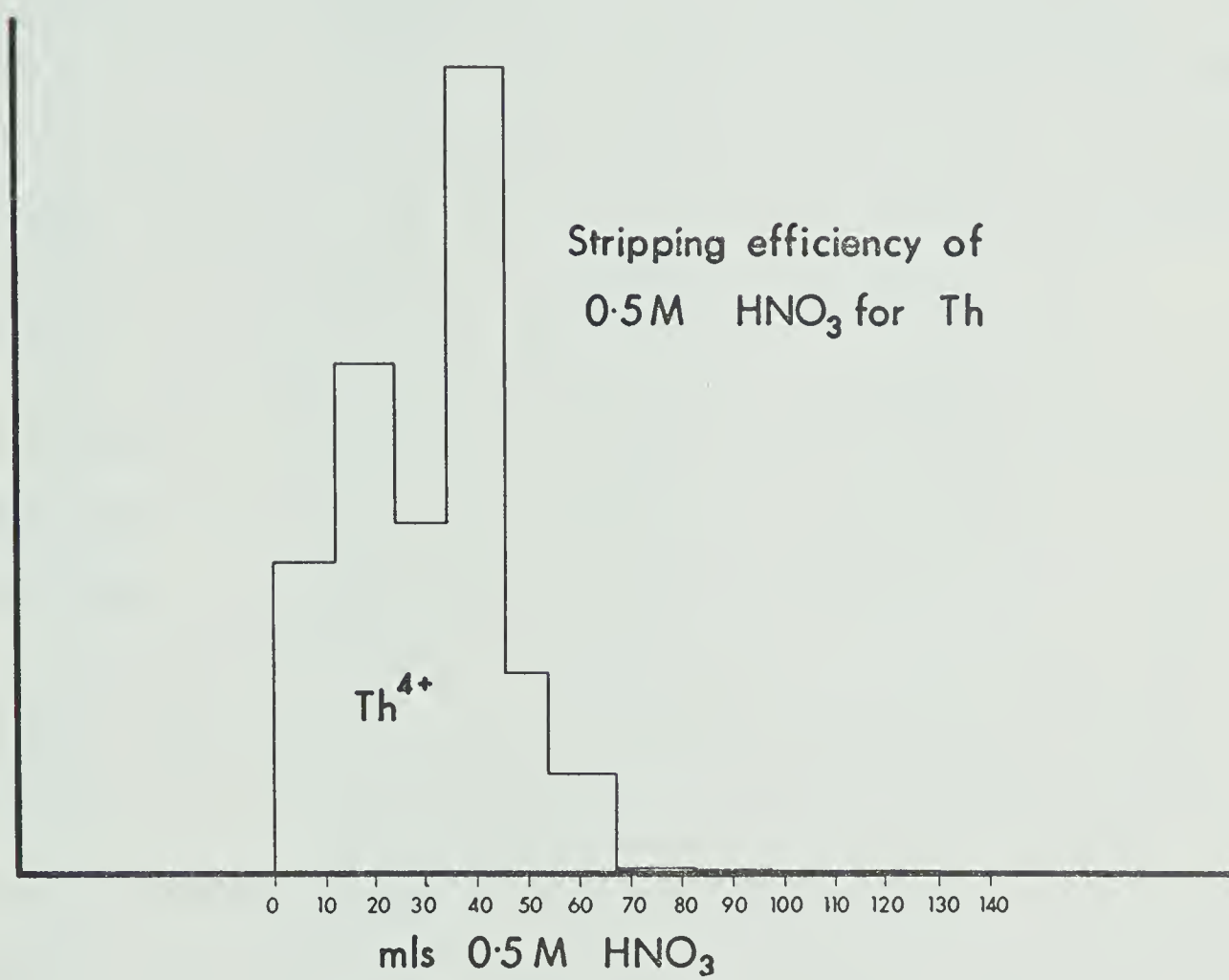


Fig.36. Stripping efficiency of 0.5M  $\text{HNO}_3$  for Th.





0.5M  $\text{HNO}_3$  and then washed with 40 ml. of 6M  $\text{HNO}_3$ .

Aliquots of sample solutions (in dilute  $\text{HCl}$ ) were pipetted directly into beakers containing the 10  $\mu\text{g}$  of  $\text{Th}^{230}$  and 20  $\mu\text{g}$  of  $\text{U}^{235}$  spike in amounts so that the measured  $\text{U}^{238}/\text{U}^{235}$  and  $\text{Th}^{232}/\text{Th}^{230}$  ratios would be approximately one. In the case of the allanite, xenotime and one of the sphenes, their unfavourable U and Th ratios necessitated the use of different aliquots for the determination of U and Th. U and Th were precipitated with  $\text{NH}_4\text{OH}$  as hydroxides together with the  $\text{R}_2\text{O}_3$  from the combined sample and spike solutions. The samples were centrifuged in specially cleaned (conc.  $\text{HNO}_3$ ) 50 ml. graduated centrifuge tubes, the supernate discarded and the precipitate redissolved in 10 ml. 6N  $\text{HNO}_3$ . In the case of some sphene samples  $\text{SiO}_2$  was co-precipitated with the hydroxides and could not be redissolved, in which case the solution was either centrifuged to remove the silica or else evaporated to dryness and U, Th, etc. leached with 6M  $\text{HNO}_3$ . The sample solutions were added directly to the columns and washed into the resin with 2 ml. of 6M  $\text{HNO}_3$  then eluted with more 6M  $\text{HNO}_3$ . The 70 to 110 ml. fraction of the eluent containing the uranium was collected and a further 80 to 90 ml. of 6M  $\text{HNO}_3$  added to the columns. Thorium was finally stripped from the columns by resettling with approximately 40 ml. of 0.5M  $\text{HNO}_3$ . The two solutions were evaporated to dryness and recombined for mass spectrometry.

The blank for this procedure was undetectable within the error of measurement in the case of thorium and approximately 0.005  $\mu\text{g}$  per sample in the case of uranium.

The above procedure developed for the combined separation of U and Th has the obvious advantages of high yields, purity of sample and simplicity of operation. With a certain amount of modification the method could probably be adopted for whole rock samples.



APPENDIX D.AMPHIBOLE X-RAY DATA

The following is a list of observed d-spacings for the analyzed amphiboles together with the calculated d-spacings for each reflection assuming the given cell parameters. The asterisks indicate the reflections accepted in the last cycle of the least-squares refinement program.

SN-2.

<u>2<math>\theta</math></u>	<u>d<sub>obs</sub></u>	<u>d<sub>calc</sub></u>	<u>(hkl)</u>
10.43	8.474*	8.463	(110)
26.27	3.390*	3.388	(150)
27.22	3.273	3.289	(240)
30.32	2.945*	2.945	(151)
31.92	2.801	2.821	(330)
32.94	2.717	2.724	(331)
34.62	2.589*	2.588	(241)
35.14	2.552*	2.553	(260)
37.79	2.379	2.393	(400)
41.62	2.168	2.181	(261)
44.83	2.020*	2.020	(222)
48.13	1.889	1.884	(242)
60.33	1.533	1.530	(1,11,1)
63.78	1.458	1.457	(173)
64.86	1.436	1.439	(661)
68.70	1.365*	1.365	(641)
74.03	1.279*	1.279	(750)

$$a = 9.850 \pm 0.004 \text{ \AA}$$

$$b = 18.110 \pm 0.008 \text{ \AA}$$

$$c = 5.296 \pm 0.005 \text{ \AA}$$

$$\beta = 103^{\circ} 37' \pm 4'$$

$$V = 918.2 \pm 0.09 \text{ \AA}^3$$

$$a \cdot \sin \beta = 9.574 \text{ \AA}$$



SN-45.

<u>2<math>\theta</math></u>	<u>d<sub>obs</sub></u>	<u>d<sub>calc</sub></u>	<u>(hkl)</u>
10.43	8.474	8.418	(110)
14.28	6.197	5.115	(001)
17.31	5.119*	5.115	(001)
19.59	4.528*	4.525	(040)
21.06	4.215*	4.219	(220)
26.25	3.392*	3.389	(041)
27.21	3.275*	3.278	(240)
28.57	3.112*	3.112	( <u>3</u> 10)
30.29	2.948*	2.949	(151)
31.88	2.805*	2.806	(330)
32.68	2.738*	2.738	( <u>3</u> 31)
33.01	2.711*	2.710	(151)
34.52	2.596*	2.598	(061)
35.07	2.557*	2.557	(002)
37.75	2.381	2.385	(350)
38.41	2.342*	2.343	( <u>3</u> 51)
41.71	2.164*	2.164	(261)
44.09	2.052	2.043	(202)
44.91	2.017*	2.017	(351)
48.07	1.891*	1.891	(510)
50.32	1.812	1.810	(0,10,0)
55.68	1.649*	1.650	(4,6,1)
58.21	1.584	1.585	(600)
60.16	1.537*	1.536	( <u>6</u> 02)
64.79	1.438*	1.438	(2,12,0)
68.66	1.366*	1.365	( <u>1</u> ,7,3)
72.08	1.309*	1.309	( <u>1</u> 14)

$$a = 9.842 \pm 0.002 \text{ \AA}$$

$$b = 18.10 \pm 0.004 \text{ \AA}$$

$$c = 5.294 \pm 0.001 \text{ \AA}$$

$$\beta = 104^{\circ} 57' \pm 2'$$

$$V = 911.18 \pm 0.20 \text{ \AA}^3$$

$$a \cdot \sin \beta = 9.511 \text{ \AA}$$





SN-88.

<u>2<math>\theta</math></u>	<u>d<sub>obs</sub></u>	<u>d<sub>calc</sub></u>	<u>(hkl)</u>
10.44	8.466	8.414	(110)
12.46	7.098		
19.62	4.509*	4.509	(040)
21.14	4.199*	4.207	(220)
27.22	3.273*	3.275	(240)
28.56	3.123*	3.122	(310)
30.32	2.945*	2.949	( $\bar{1}$ 51)
31.88	2.805*	2.805	(330)
32.70	2.736*	2.732	( $\bar{3}$ 31)
33.00	2.712*		(151)
33.42	2.679	2.712	(151)
41.68	2.165*	2.165	(261)
44.87	2.018*	2.019	(351)
48.10	1.890*	1.891	(510)
55.65	1.650	1.650	( $\bar{2}$ ,10,1)
58.16	1.585*	1.585	(600)
61.54	1.506	1.506	( $\bar{4}$ 43)
61.70	1.502*	1.502	(551)
64.74	1.439	1.438	( $\bar{6}$ 61)

$$a = 9.836 \pm 0.002 \text{ \AA}$$

$$b = 18.072 \pm 0.015 \text{ \AA}$$

$$c = 5.316 \pm 0.001 \text{ \AA}$$

$$\beta = 104^{\circ} 50' \pm 2'$$

$$V = 913.5 \pm 0.01 \text{ \AA}^3$$

$$a \cdot \sin \beta = 9.509 \text{ \AA}$$



SN-35.

<u>2<math>\theta</math></u>	<u>d<sub>obs</sub></u>	<u>d<sub>calc</sub></u>	<u>(hkl)</u>
10.46	8.457*	8.427	(110)
26.34	3.383	3.384	(131)
27.26	3.271*	3.276	(240)
30.60	2.921	2.940	(221)
31.99	2.800	2.808	(330)
33.10	2.706*	2.707	(151)
34.62	2.591*	2.594	(061)
35.14	2.554	2.547	( $\bar{2}$ 00)
37.86	2.376	2.382	(400)
41.83	2.160*	2.162	(261)
44.26	2.047*	2.046	(202)
44.94	2.017*	2.017	(351)
48.19	1.889*	1.895	(510)
50.45	1.809*	1.809	(441)
59.49	1.554	1.555	(133)
61.73	1.503	1.502	(551)
64.06	1.454	1.454	( $\bar{1}$ 73)
64.99	1.435*	1.434	(2,12,0)
68.98	1.361	1.361	(0,8,3)
70.53	1.335	1.335	(263)
72.27	1.307	1.307	( $\bar{3}$ 14)

$$a = 9.864 \pm 0.016 \text{ \AA}$$

$$b = 18.049 \pm 0.010 \text{ \AA}$$

$$c = 5.302 \pm 0.002 \text{ \AA}$$

$$\beta = 104^{\circ}58' \pm 5'$$

$$V = 911.8 \text{ \AA}^3$$

$$a \cdot \sin \beta = 9.533 \text{ \AA}$$



SN-71.

<u>2<math>\theta</math></u>	<u>d<sub>obs</sub></u>	<u>d<sub>calc</sub></u>	<u>(hkl)</u>
9.75	9.064*	9.051	(020)
10.41	9.491*	8.474	(110)
27.15	3.282*	3.291	(240)
28.48	3.131*	3.148	(310)
30.23	2.954*	2.954	( $\bar{1}$ 51)
32.90	2.720*	2.720	( $\bar{3}$ 31)
41.54	2.172	2.159	( $\bar{1}$ 52)
44.73	2.024	2.018	(401)
58.21	1.584	1.578	(422)
61.56	1.505	1.506	(481)
63.53	1.463*	1.463	(3,11,0)

$$a = 9.834 \pm 0.019 \text{ \AA}$$

$$b = 18.102 \pm 0.014 \text{ \AA}$$

$$c = 5.387 \pm 0.027 \text{ \AA}$$

$$\beta = 102^\circ 48'$$

$$V = 935.2 \text{ \AA}^3$$

$$a \cdot \sin \beta = 9.593 \text{ \AA}$$





SN-61.

<u>2<math>\theta</math></u>	<u>d<sub>obs</sub></u>	<u>d<sub>calc</sub></u>	<u>(hkl)</u>
10.42	8.482*	8.468	(020)
18.54	4.782*	4.790	(200)
26.27	3.390*	3.388	(150)
27.04	3.295*	3.290	(240)
30.21	2.956*	2.956	( $\bar{1}$ 51)
31.67	2.723*	2.822	(330)
32.86	2.723	2.724	(151)
34.27	2.614	2.606	(061)
35.94	2.496*	2.497	( $\bar{1}$ 70)
38.15	2.357	2.357	( $\bar{3}$ 51)
41.46	2.176*	2.176	(261)
44.63	2.029*	2.029	( $\bar{4}$ 02)
55.34	1.659*	1.659	(511)
59.73	1.547	1.547	( $\bar{6}$ 41)
64.30	1.448	1.449	(0,12,1)
68.36	1.371*	1.371	(083)

$$a = 9.896 \pm 0.004 \text{ \AA}$$

$$b = 18.108 \pm 0.007 \text{ \AA}$$

$$c = 5.339 \pm 0.002 \text{ \AA}$$

$$\beta = 104^{\circ} 31' \pm 2'$$

$$V = 926.4 \pm 0.4 \text{ \AA}^3$$

$$a \cdot \sin \beta = 9.581 \text{ \AA}$$



SN-89.

<u>2<math>\theta</math></u>	<u>d<sub>obs</sub></u>	<u>d<sub>calc</sub></u>	<u>(hkl)</u>
10.42	8.482*		
20.99	4.229*	4.300	(220)
26.22	3.396*	3.385	(150)
27.12	3.285*	3.287	(240)
28.47	3.132*	3.142	(310)
30.27	2.950	2.952	( $\bar{1}$ 51)
31.80	2.812*	2.820	(330)
32.98	2.714*	2.714	( $\bar{3}$ 31)
37.68	2.385	2.385	( $\bar{4}$ 01)
44.76	2.023	2.015	(401)
47.89	1.898	1.903	(510)
50.18	1.817*	1.815	( $\bar{1}$ 91)
57.99	1.589*	1.589	(403)

$$a = 9.812 \pm 0.005 \text{ \AA}$$

$$b = 18.093 \pm 0.010 \text{ \AA}$$

$$c = 5.380 \pm 0.006 \text{ \AA}$$

$$\beta = 102^{\circ} 45' \pm 8'$$

$$V = 931.5 \pm 0.02 \text{ \AA}^3$$

$$a \cdot \sin \beta = 9.572 \text{ \AA}$$



SN-74.

<u>2<math>\theta</math></u>	<u>d<sub>obs</sub></u>	<u>d<sub>calc</sub></u>	<u>(hkl)</u>
10.74	8.499*	8.473	(110)
18.51	4.790*	4.787	(200)
19.48	4.553*	4.551	(040)
24.85	3.580	3.677	( $\bar{2}$ 21)
27.00	3.300*	3.298	(240)
27.99	3.185	3.143	(310)
30.21	2.956*	2.954	( $\bar{1}$ 51)
31.65	2.825*	2.824	(330)
34.95	2.565*	2.563	(260)
38.15	2.357	2.345	( $\bar{3}$ 51)
38.98	2.309	2.312	(112)
41.42	2.178*	2.179	(261)
44.55	2.032*	2.033	(351)
58.93	1.566*	1.566	(402)
62.53	1.476*	1.476	(372)
64.25	1.449*	1.449	(4,10,0)
65.58	1.422*	1.422	( $\bar{5}$ 33)

$$a = 9.874 \pm 0.005 \text{ \AA}$$

$$b = 18.205 \pm 0.007 \text{ \AA}$$

$$c = 5.271 \pm 0.003 \text{ \AA}$$

$$\beta = 104^{\circ} 11' \pm 1'$$

$$V = 918.7 \text{ \AA}^3$$

$$a \cdot \sin \beta = 9.573 \text{ \AA}$$





SN-10.

<u>2<math>\theta</math></u>	<u>d<sub>obs</sub></u>	<u>d<sub>calc</sub></u>	<u>(hkl)</u>
10.40	8.499*	8.463	(110)
27.32	3.262	3.296	(240)
28.45	3.134*	3.139	(310)
30.27	2.950*	2.950	(221)
31.70	2.820*	2.821	(330)
32.89	2.721*	2.720	(151)
34.97	2.564*	2.561	(260)
37.57	2.392*	2.390	(400)
41.53	2.173	2.171	(132)
44.04	2.054*	2.054	(280)
44.85	2.019*	2.020	( $\bar{4}$ 02)
45.95	1.973*	1.972	( $\bar{4}$ 22)
47.83	1.900*	1.900	(510)
55.50	1.654*	1.655	( $\bar{4}$ 81)
61.00	1.518	1.517	( $\bar{6}$ 22)
64.40	1.446	1.446	( $\bar{6}$ 61)
68.92	1.361	1.361	(313)
71.60	1.317*	1.317	( $\bar{7}$ 51)

$$a = 9.884 \pm 0.003 \text{ \AA}$$

$$b = 18.201 \pm 0.010 \text{ \AA}$$

$$c = 5.283 \pm 0.006 \text{ \AA}$$

$$\beta = 104^{\circ} 43' \pm 3'$$

$$V = 919.4 \text{ \AA}^3$$

$$a \cdot \sin \beta = 9.5607 \text{ \AA}$$



SN-16.

<u>2<math>\theta</math></u>	<u>d<sub>obs</sub></u>	<u>d<sub>calc</sub></u>	<u>(hkl)</u>
10.43	8.474*	8.480	(110)
26.23	3.395	3.396	(041)
27.16	3.280	3.294	(240)
28.48	3.131	3.137	(201)
30.28	2.949*	2.951	( $\bar{1}$ 51)
31.78	2.813	2.827	(330)
32.91	2.719*	2.720	(151)
34.42	2.603*	2.603	(061)
35.06	2.557*	2.556	(260)
35.28	2.542*	2.542	( $\bar{2}$ 02)
37.62	2.389	2.398	(350)
41.60	2.169	2.175	(261)
44.78	2.022*	2.022	( $\bar{4}$ 02)
47.92	1.892	1.887	( $\bar{4}$ 61)
50.12	1.819	1.823	(441)
58.01	1.588	1.585	( $\bar{1}$ 53)
59.38	1.555	1.556	(391)
60.78	1.523	1.527	(282)
62.93	1.476	1.475	( $\bar{2}$ ,10,2)
64.56	1.442	1.440	( $\bar{2}$ ,12,0)
71.96	1.311*	1.311	( $\bar{2}$ ,2,4)

$$a = 9.909 \text{ \AA}$$

$$b = 18.118 \text{ \AA}$$

$$c = 5.301 \text{ \AA}$$

$$\beta = 104^{\circ} 27' \pm 5'$$

$$V = 921.6 \pm 0.9 \text{ \AA}^3$$

$$a \cdot \sin \beta = 9.602 \text{ \AA}$$



SN-38.

<u>2<math>\theta</math></u>	<u>d<sub>obs</sub></u>	<u>d<sub>calc</sub></u>	<u>(hkl)</u>
10.38	8.515	8.454	(110)
18.73	4.734	4.778	(200)
19.55	4.537*	4.534	(040)
26.18	3.401	3.403	(041)
27.12	3.285*	3.289	(240)
28.43	3.137*	3.137	(310)
30.24	2.953*	2.950	(221)
31.72	2.819*	2.818	(330)
32.50	2.753*	2.755	( $\bar{3}$ 31)
32.88	2.722*	2.719	(151)
34.40	2.605	2.607	(061)
37.54	2.394*	2.393	( $\bar{3}$ 50)
38.22	2.347	2.340	( $\bar{4}$ 21)
41.58	2.170*	2.171	(261)
44.77	2.023	2.024	(351)
47.83	1.900*	1.901	(510)
50.07	1.820	1.822	(530)
55.48	1.655	1.655	( $\bar{4}$ 81)
57.84	1.593	1.593	(600)
58.86	1.568	1.568	(2,10,1)
64.42	1.445*	1.444	(4,10,0)
68.51	1.368*	1.368	(083)

$$a = 9.899 \pm 0.010 \text{ \AA}$$

$$b = 18.135 \pm 0.009 \text{ \AA}$$

$$c = 5.333 \pm 0.005 \text{ \AA}$$

$$\beta = 105^{\circ} 8' \pm 6'$$

$$V = 924.4 \pm 0.88 \text{ \AA}^3$$

$$a \cdot \sin \beta = 9.557 \text{ \AA}$$





SN-26.

<u>2<math>\theta</math></u>	<u>d<sub>obs</sub></u>	<u>d<sub>calc</sub></u>	<u>(hkl)</u>
10.46	8.457*	8.424	(110)
19.62	4.521*	4.518	(040)
27.19	3.277*	3.277	(240)
28.52	3.127*	3.181	(201)
30.14	2.963	2.947	( $\bar{1}$ 51)
31.86	2.806*	2.808	(330)
32.61	2.744*	2.740	(151)
33.04	2.709*	2.709	( $\bar{3}$ 31)
34.50	2.598*	2.609	(061)
35.14	2.552*	2.545	( $\bar{2}$ 02)
37.72	2.383	2.385	(350)
47.99	1.894*	1.894	(510)
50.16	1.817	1.812	(312)
58.08	1.582	1.587	(600)
64.64	1.441*	1.441	( $\bar{5}$ 72)

$$a = 9.772 \pm 0.007 \text{ \AA}$$

$$b = 18.07 \pm 0.03 \text{ \AA}$$

$$c = 5.364 \pm 0.02 \text{ \AA}$$

$$\beta = 103^{\circ} 0.5' \pm 9'$$

$$V = 923.2 \pm 0.03 \text{ \AA}^3$$

$$a \cdot \sin \beta = 9.518 \text{ \AA}$$



SN-73.

<u>2<math>\theta</math></u>	<u>d<sub>obs</sub></u>	<u>d<sub>calc</sub></u>	<u>(hkl)</u>
10.40	8.499	8.438	(110)
18.62	4.759*	4.765	(200)
19.52	4.544*	4.540	(040)
26.22	3.396*	3.394	(150)
27.10	3.288*	3.287	(240)
28.49	3.130*	3.129	(310)
30.29	2.948*	2.953	( $\bar{1}$ 51)
31.79	2.812*	2.813	(330)
34.39	2.606*	2.606	( $\bar{1}$ 12)
38.32	2.347*	2.349	( $\bar{3}$ 51)
41.82	2.158*	2.158	(132)
44.79	2.022*	2.022	( $\bar{4}$ 02)
47.95	1.896*	1.896	(510)
50.18	1.816	1.816	(0,10,0)
57.99	1.589	1.588	(600)
61.30	1.511*	1.510	( $\bar{4}$ 82)
64.56	1.442*	1.442	(2,12,0)

$$a = 9.873 \pm 0.004 \text{ \AA}$$

$$b = 18.161 \pm 0.006 \text{ \AA}$$

$$c = 5.266 \pm 0.002 \text{ \AA}$$

$$\beta = 105^{\circ} 10' \pm 3'$$

$$V = 911.4 \pm 0.5 \text{ \AA}^3$$

$$a \cdot \sin \beta = 9.527 \text{ \AA}$$



SN-22.

<u>2<math>\theta</math></u>	<u>d<sub>obs</sub></u>	<u>d<sub>calc</sub></u>	<u>(hkl)</u>
17.43	5.088*	5.087	(130)
26.26	3.394	3.393	(131)
27.24	3.274*	3.274	(240)
28.58	3.123	3.123	(310)
30.22	2.957*	2.960	( $\bar{1}$ 51)
33.07	2.709*	2.712	(151)
34.49	2.600*	2.602	(061)
35.11	2.556*	2.562	(241)
41.75	2.164*	2.163	(261)
44.97	2.061	2.061	(351)
45.32	2.001*	2.001	(370)
48.23	1.887*	1.887	( $\bar{4}$ 61)
50.40	1.811	1.814	(530)
64.90	1.437	1.438	(4,10,0)

$$a = 9.875 \pm 0.007 \text{ \AA}$$

$$b = 18.07 \pm 0.02 \text{ \AA}$$

$$c = 5.355 \pm 0.02 \text{ \AA}$$

$$\beta = 105^{\circ} 29' \pm 5'$$

$$V = 920.9 \text{ \AA}^3$$

$$a \cdot \sin \beta = 9.516 \text{ \AA}$$





SN-70.

<u>2<math>\theta</math></u>	<u>d<sub>obs</sub></u>	<u>d<sub>calc</sub></u>	<u>(hkl)</u>
10.43	8.481*	8.478	(110)
18.48	4.800*	4.795	(200)
19.57	4.536*	4.534	(040)
27.10	3.290*	3.295	(240)
28.48	3.134*	3.134	(201)
31.81	2.813*	2.826	(330)
33.45	2.679	2.723	(151)
34.40	2.607*	2.607	(061)
34.91	2.571	2.575	(002)
39.45	2.384	2.295	( $\bar{3}$ 12)
55.50	1.655	1.656	( $\bar{4}$ 81)
66.46	1.407	1.410	(621)

$$a = 9.918 \pm 0.035 \text{ \AA}$$

$$b = 18.136 \pm 0.027 \text{ \AA}$$

$$c = 5.326 \pm 0.040 \text{ \AA}$$

$$\beta = 104^{\circ} 46' \pm 38'$$

$$V = 926.6 \pm 0.06 \text{ \AA}^3$$

$$a \cdot \sin \beta = 9.589 \text{ \AA}$$



SN-21.

<u>2<math>\theta</math></u>	<u>d<sub>obs</sub></u>	<u>d<sub>calc</sub></u>	<u>(hkl)</u>
10.46	8.450	8.410	(110)
26.24	3.393	3.382	(150)
27.20	3.276*	3.276	(240)
28.62	3.116*	3.119	(310)
30.34	2.944*	2.944	( $\bar{1}$ 51)
31.88	2.805*	2.804	(330)
32.98	2.714	2.699	(151)
34.40	2.605	2.600	( $\bar{1}$ 12)
41.86	2.156*	2.156	(261)
50.38	1.810*	1.809	(0,10,0)
64.83	1.437*	1.437	(2,12,0)

$$a = 9.847 \pm 0.012 \text{ \AA}$$

$$b = 18.093 \pm 0.002 \text{ \AA}$$

$$c = 5.255 \pm 0.005 \text{ \AA}$$

$$\beta = 105^{\circ} 16' \pm 4'$$

$$V = 903.2 \pm 0.01 \text{ \AA}^3$$

$$a \cdot \sin \beta = 9.497 \text{ \AA}$$



APPENDIX E.COMPUTATIONS.

In this Appendix a brief description of the computations necessary for the calculation of apparent ages and mineralogical date is given.

1. Potassium-Argon:

The following constants are used in the calculations.

$$\lambda_K = 0.585 \times 10^{-10} \text{ yr}^{-1}$$

$$\lambda_\beta = 4.72 \times 10^{-10} \text{ yr}^{-1}$$

$$\text{ppm Ar}^{40} = 1.7846 \times 10^3 \times \text{cc Ar}^{40}/\text{gm. (S.T.P.)}$$

Spike composition:

$$\text{Ar}^{36}/\text{Ar}^{38} = 0.000105, \quad \text{Ar}^{40}/\text{Ar}^{38} = 0.00354$$

All argon isotope ratios were calculated directly from chart data, extrapolating the values to the time of inlet.

The measured argon isotopes (peak height x scale factor) are corrected as follows for contaminant air argon:

	40 :38 :36	measured argon isotopes
minus	<u>40 :38 :36</u>	residual argon (peak height x factor)
	40 :38 :36	sample + air + spike argon

Each value is now multiplied by the mass discrimination factors obtained from the measurement of air argon.

The air argon correction can now be performed as follows assuming all  $\text{Ar}^{38}$  is from the spike:

	40	:38 :36	
minus	<u>38x0.00354: 0</u>	<u>:38x0.000105</u>	subtract 36 spike argon
	40	:38 :36	





$\frac{36 \times 295.5}{40} : 0 : 36$  subtract air argon  
 $: 38 : 0$  Radiogenic argon +  $\text{Ar}^{38}$  spike.

Then,

$$\text{Ar}^{40} \text{ ppm} = \frac{\text{Ar}^{40}}{\text{Ar}^{38}} \times \frac{\text{cc Ar}^{38} \text{ spike (S.T.P.)} \times 10^3 \times 1.7846}{\text{sample weight}}$$

The age may then be calculated from the  $\frac{\text{Ar}^{40}}{\text{K}^{40}}$  ratio.

In practice however, the age was usually read from prepared tables of  $\text{Ar}^{40}/\text{K}^{40}$  ratios and their corresponding ages using the decay constants given above, or else calculated together with the precision error of the apparent age and the total uncertainty in the apparent age, taking into consideration errors in decay constants, with the use of the Fortran IV program KARG. KARG was written by the author and is based on the error equations given by KIRSTEN (1966).

## 2. Uranium-Thorium-Lead.

2a. Uranium: Spike composition: 99.972%  $\text{U}^{235}$

The  $\text{U}^{235}/\text{U}^{238}$  ratio of  $781 \pm 13$  ratio measured by the author does not agree with the Oak Ridge National Laboratory  $\text{U}^{235}/\text{U}^{238}$  ratio of 398.6. The former value was used for all calculations.

Since the blank for uranium is negligible then,

$$\left(\frac{\text{U}^{238}}{\text{U}^{235}}\right)_{\text{meas}} \times \frac{238}{235} = \frac{\mu\text{g U}_{\text{sample}}^{238} + \mu\text{g U}_{\text{spike}}^{238}}{\mu\text{g U}_{\text{sample}}^{235} + \mu\text{g U}_{\text{spike}}^{235}} \quad (1)$$

For natural uranium,

$$\frac{\text{U}^{238}}{\text{U}^{235}} = 137.8 \quad (2)$$



From (1) and (2),

$$\mu\text{g U}^{238}_{\text{sample}} = \frac{238}{235} (\text{U}^{238}/\text{U}^{235})_{\text{meas}} \cdot (\mu\text{g U}^{235}_{\text{spike}}) - \mu\text{g U}^{238}_{\text{spike}}$$

$$1 - (\text{U}^{238}/\text{U}^{235})_{\text{meas}}/137.8$$

The amount of  $\text{U}^{235}$  can be found from (2).

## 2b. Thorium:

Spike composition: 92.04%  $\text{Th}^{230}$ . The composition measured by the author is essentially identical to the Oak Ridge value of , and this has been used in all calculations.

$$(\text{Th}^{232}/\text{Th}^{230})_{\text{meas}} \times \frac{232}{230} = \frac{\mu\text{g Th}^{232}_{\text{sample}} + \mu\text{g Th}^{232}_{\text{spike}}}{230}$$

$$\therefore \mu\text{g Th}^{232}_{\text{sample}} = [(\text{Th}^{232}/\text{Th}^{230})_{\text{meas}} \cdot \frac{232}{230} \cdot \mu\text{g Th}^{230}_{\text{spike}}] - \mu\text{g Th}^{232}_{\text{spike}}$$

## 2c. Lead:

Spike compositions:

$\text{Pb}^{206}$  spike: 99.975%  $\text{Pb}^{206}$ , 0.01%  $\text{Pb}^{207}$ , 0.015%  $\text{Pb}^{208}$

$\text{Pb}^{208}$  spike: 99.73%  $\text{Pb}^{208}$ , 0.05%  $\text{Pb}^{207}$ , 0.22%  $\text{Pb}^{206}$ , <0.1%  $\text{Pb}^{204}$

The measured isotope ratios both in a direct measurement of the samples lead isotope ratios (I.R.) and the ratios with an added isotope dilutant (I.D.) have to be corrected for blank lead (see Appendix B) and common lead in the mineral.

Setting  $\text{Pb}^{204} = 1$ , and subtracting approximate common lead ratios, from I.R. analysis.

204 :206 :207 :208 I.R. analysis

204 :206 :207 :208 common lead

:206 :207 :208 radiogenic lead (corrected)



Then,

$$\mu\text{g Pb}^{208}_{\text{rad}} = \mu\text{g Pb}^{206}_{\text{rad}} \times \frac{208}{206} (\text{Pb}^{208}/\text{Pb}^{206})_{\text{I.R.}} \text{ corr} \quad (1)$$

In the same manner for the I.D. isotope analysis,

204 : 206 : 207 : 208      I.D. analysis

204 : 206 : 207 : 208      common lead

: 206 : 207 : 208      radiogenic + spike lead (corrected)

Then,

$$\mu\text{g Pb}^{206}_{\text{rad}} = \frac{206}{208} (\text{Pb}^{206}/\text{Pb}^{208})_{\text{I.D.}} \text{ corr} [\mu\text{g Pb}^{208}_{\text{rad}} + \mu\text{g Pb}^{208}_{\text{spike}}] - \mu\text{g Pb}^{206}_{\text{spike}} \quad (2)$$

Now substituting (1) and (2),

$$\mu\text{g Pb}^{206}_{\text{rad}} = \frac{\frac{206}{208} (\text{Pb}^{206}/\text{Pb}^{208})_{\text{I.D.}} \text{ corr} \times \mu\text{g Pb}^{208}_{\text{spike}} - \mu\text{g Pb}^{206}_{\text{spike}}}{1 - (\text{Pb}^{206}/\text{Pb}^{208})_{\text{I.D.}} \text{ corr} \times (\text{Pb}^{208}/\text{Pb}^{206})_{\text{I.D.}} \text{ corr}} \quad (3)$$

From the above, the amount of radiogenic  $\text{Pb}^{206}$  is calculated for the I.R. aliquot. The amount of contaminant lead is calculated from the following relationships.

$$\frac{206}{204} (\text{Pb}^{206}/\text{Pb}^{204})_{\text{I.R.}} = \frac{\mu\text{g Pb}^{206}_{\text{rad}} + \mu\text{g Pb}^{206}_{\text{com}} + \mu\text{g Pb}^{206}_{\text{blank}}}{\mu\text{g Pb}^{204}_{\text{com}} + \mu\text{g Pb}^{204}_{\text{blank}}} \quad (4)$$

where 'com' refers to common lead.

$$\text{and } \mu\text{g Pb}^{206}_{\text{com}} = \mu\text{g Pb}^{204}_{\text{com}} \times \frac{206}{204} (\text{Pb}^{206}/\text{Pb}^{204})_{\text{com}} \quad (5)$$

Substituting (5) in (4);

$$\mu\text{g Pb}^{204}_{\text{com}} = \frac{(\mu\text{g Pb}^{206}_{\text{rad}} \times \mu\text{g Pb}^{206}_{\text{bl}}) - (\mu\text{g Pb}^{204}_{\text{bl}} \times \frac{206}{204} [\text{Pb}^{206}/\text{Pb}^{204}]_{\text{I.R.}})}{\frac{206}{204} (\text{Pb}^{206}/\text{Pb}^{204})_{\text{I.R.}} - \frac{206}{204} (\text{Pb}^{206}/\text{Pb}^{204})_{\text{com}}}$$





The total contaminant lead is:

$$\begin{array}{ll} 204 : 206 : 208 & \text{blank lead} \\ x(204 : 206 : 208) & \text{common lead} \\ 204 : 206 : 208 & \text{contaminant lead} \end{array}$$

where x is  $\mu\text{g Pb}_{\text{common}}^{204} / \mu\text{g Pb}_{\text{blank}}^{204}$ .

The calculations are now repeated twice more, using the new value obtained above for the contaminant lead.

After three iterations the amounts of  $\text{Pb}^{208}$  and  $\text{Pb}^{207}$  are found from:

$$g \text{ Pb}_{\text{rad}}^{208} = g \text{ Pb}_{\text{rad}}^{206} \times \frac{208}{206} (\text{Pb}^{208}/\text{Pb}^{206})_{\text{corr I.R.}}$$

$$g \text{ Pb}_{\text{rad}}^{207} = g \text{ Pb}_{\text{rad}}^{206} \times \frac{207}{206} (\text{Pb}^{207}/\text{Pb}^{206})_{\text{corr I.R.}}$$

One can also calculate amounts of  $\text{Pb}^{208}$  and  $\text{Pb}^{207}$  from the corrected I.D. ratios, but these are not mutually independent from the values above.

Ages can now be calculated using the following decay constants:

$$\begin{array}{l} \lambda_{238} = 1.54 \times 10^{-10} \text{yr}^{-1} \\ \lambda_{235} = 9.72 \times 10^{-10} \text{yr}^{-1} \\ \lambda_{232} = 4.99 \times 10^{-11} \text{yr}^{-1} \end{array}$$

In practice most of the calculations in this thesis were performed using an A.P.L. program (UPBCOMP) written by H. Baadsgaard. One particular advantage of the program is the selection of new common lead values appropriate to the  $\text{Pb}^{207}/\text{Pb}^{206}$  ratio for each iteration.

Common lead values were selected from a matrix of values calculated by the Russell-Farquhar-Cumming model using the following values:

$$\begin{array}{l} a_o = 9.50 \\ b_o = 10.36 \\ c_o = 29.49 \end{array}$$



$$V_o = 0.0654$$

$$W_o = 38.21$$

$$t_o = 4.56 \times 10^9$$

### 3. Rubidium-Strontium.

Both rubidium and strontium are determined by isotope dilution analysis, using  $\text{Rb}^{87}$  and  $\text{Sr}^{84}$  enriched isotope dilutants respectively.

#### 3a. Rubidium:

$$\begin{aligned} \text{Rubidium spike composition: } 99.19\% \text{ Rb}^{87} \\ \frac{87}{85} \cdot (87/85)_{\text{meas}} = \frac{\mu\text{g Rb}^{87}_{\text{spike}} + \mu\text{g Rb}^{87}_{\text{sample}}}{\mu\text{g Rb}^{85}_{\text{spike}} + \mu\text{g Rb}^{85}_{\text{sample}}} \end{aligned} \quad (1)$$

$$\text{Since } \mu\text{g Rb}^{85}_{\text{sample}} = 2.541 \times \mu\text{g Rb}^{87}_{\text{sample}} \quad (2)$$

the amount of  $\text{Rb}^{87}$  in the sample is calculated from

$$\begin{aligned} \mu\text{g Rb}^{87}_{\text{sample}} = \frac{\mu\text{g Rb}^{87}_{\text{spike}} + \frac{87}{85} \times (87/85)_{\text{meas}} \times \mu\text{g Rb}^{85}_{\text{spike}}}{(87/85 [87/85]_{\text{meas}} \times 2.541) - 1} \end{aligned} \quad (3)$$

The amount of  $\text{Rb}^{85}$  in the sample and hence the total Rb can be calculated from (2).

#### 3b. Strontium:

Using an enriched  $\text{Sr}^{84}$  spike it is only necessary to perform a single isotope dilution analysis. Mass Discrimination can be calculated from this analysis after the method of LONG (1966).

Since the proportions of  $\text{Sr}^{84}:\text{Sr}^{86}:\text{Sr}^{88}$  in common strontium are constant and strontium contributions from the blank will be in the same proportions, the amount of fractionation is dependent on the difference between the masses.

$$R_{86}^{88} = \frac{F_s^{88} S + F_n^{88} N}{F_s^{86} S + F_n^{86} N} \quad (1)$$



$$R_{84}^{88} = \frac{F_s^{88} S + F_n^{88} N}{F_s^{84} S + F_n^{84} N} \quad (2)$$

where  $R_{86}^{88}$ ,  $R_{84}^{88} = \text{Sr}^{88}/\text{Sr}^{86}$  and  $\text{Sr}^{88}/\text{Sr}^{84}$  atom ratios (R) in the spike-sample mixture,  $F_n^{86}$ ,  $F_s^{84}$ , etc. = fractional abundances (F) of  $\text{Sr}^{86}$  in common strontium,  $\text{Sr}^{84}$  in the spike etc. S, N = moles of spike and common strontium, respectively.

Substituting (1) in (2):

$$R_{84}^{88} = \frac{R_{86}^{88} \cdot A}{R_{86}^{88} C - B} \quad (3)$$

where  $A = F_s^{88} \cdot F_n^{86} - F_n^{88} \cdot F_s^{86}$ ,  $B = F_s^{84} \cdot F_n^{88} - F_n^{84} \cdot F_s^{88}$ ,  
 $C = F_s^{84} \cdot F_n^{86} - F_n^{84} \cdot F_s^{86}$

Let  $\alpha$  be the factor by which the time  $R_{84}^{88}$  is multiplied due to fractionation. That is:

$$R_{o84}^{88} = \alpha R_{84t}^{88} \quad (4)$$

where o = observed, t = time (corrected ratios)

Similarly

$$R_{o84}^{88} = 1/2(\alpha+1) R_{86}^{88} R_t \quad (5)$$

By substitution of equation 4 and 5 and solving for  $\alpha$ .

$$\alpha = \frac{R_{o84}^{88} (2C R_{o86}^{88} - B)}{2A R_{o86}^{88} + B R_{o84}^{88}} \quad (6)$$

$R_{84}^{88}$  is then corrected by (4) and other isotope ratios are corrected proportional to the mass differences. KROGH and HURLEY (1968) have given methods mathematically equivalent to the above.

The amounts of normal and radiogenic strontium are now calculable from the corrected ratios.

Strontium spike composition: 82.24%  $\text{Sr}^{84}$ , 3.71%  $\text{Sr}^{86}$ , 1.56%  $\text{Sr}^{87}$ , 12.49%  $\text{Sr}^{88}$ .





Let N be the amount of normal strontium, then:

$$\frac{86}{84} \frac{(96/84)_{\text{corr}}}{\text{meas}} = \frac{\mu\text{g Sr}_{\text{sp}}^{86} + 0.828 \text{ 3N}}{\mu\text{g Sr}_{\text{sp}}^{84} + 0.0967\text{N}} \quad (7)$$

from which the amount of normal strontium (N) is calculated. It can also be calculated from an analogous isotope balance equation to (7) written for  $(88/84)_{\text{corr}}$ .  
meas

$$\frac{87}{86} \frac{(87/86)_{\text{corr}}}{\text{meas}} = \frac{\mu\text{g Sr}_{\text{sp}}^{87} + \mu\text{g Sr}_{\text{n}}^{87} + \mu\text{g Sr}_{\text{rad}}^{87}}{\mu\text{g Sr}_{\text{sp}}^{86} + \mu\text{g Sr}_{\text{n}}^{86}} \quad (8)$$

Since  $\mu\text{g Sr}_{\text{n}}^{86}$  and  $\text{Sr}_{\text{n}}^{87}$  and  $\text{Sr}_{\text{spike}}^{87}$  are known, the amount of radiogenic strontium ( $\text{Sr}_{\text{rad}}^{87}$ ) can be found.

The ages may then be calculated using the following decay constant for  $\text{Rb}^{87}$ .

$$\lambda = 1.39 \times 10^{-11} \text{ yr}^{-1}$$

In practice the above computations were performed using an A.P.L. program (RBSRCOMP) written by H. Baadsgaard, details of which are obtainable from the Department of Geology, University of Alberta.

#### 4. Least Squares Fitting of Rb-Sr Isochrons.

The closed system evolution of radiogenic strontium is described by the following equation:

$$(\text{Sr}^{87}/\text{Sr}^{86})_t = (\text{Sr}^{87}/\text{Sr}^{86})_o + (\text{Rb}^{87}/\text{Sr}^{86}) \cdot (e^{\lambda t} - 1) \quad (1)$$

which is the equation of a straight line of the form  $y = a + bx$ , where

$$y = (\text{Sr}^{87}/\text{Sr}^{86})_t; a = (\text{Sr}^{87}/\text{Sr}^{86})_o; x = \frac{\text{Rb}^{87}}{\text{Sr}^{86}} \text{ and } b = e^{\lambda t} - 1.$$

If a given point lies exactly on this line then:

$$y_i - (a + bx_i) = 0 \quad (2)$$



However, the right - hand side of (2) will be greater than or less than zero, proportional to the degree of displacement of the data point away from the line. This residual amount will be referred to as R.

A sum of squares function may be set up as follows (McINTIRE et al. 1966):

$$f(U) = \frac{\sum_{i=1}^n (y_i - a - bx_i)^2}{\text{var}(R)} \quad (3)$$

where

$$\text{var}(R) = \text{var}(y_i) + b^2 \text{var}(x_i) = \frac{1}{w_i}$$

Then (3) becomes:

$$f(U) = \sum_{i=1}^n w_i (y_i - a - bx_i)^2 \quad (4)$$

The treatment of McINTIRE et al. (op.cit.) allows for nonuniform variance in  $\text{Rb}^{87}/\text{Sr}^{86}$  and incorporates prior estimates of the precision in both coordinates. Some methods by which the estimates of the variance may be calculated have been given by TUREK (1966). Estimates for the constant of variance in 'x' and the variance in 'y' used for the fitting of isochrons to the Levang gneiss dome and the gabbros were based on the double spiking procedure formerly in use in this laboratory and new variance estimates for the single  $\text{Sr}^{84}$  spiking procedure currently in use have not been made.

The above function (4) is minimised by setting up a least - squares cubic equation (see YORK, 1966) and solving for 'a' and 'b' by an iterative method from an initial estimate of 'b'.

An A.P.L. program (RBSRISOCHRON) written by H. Baadsgaard, based upon the York and McIntire treatments was used for the least - squares fitting of isochrons to the Rb-Sr data from the Levang gneiss dome and the gabbros. In addition to 'a' (initial  $\text{Sr}^{87}/\text{Sr}^{86}$ ) and 'b' ( $e^{\lambda t} - 1$ ), the program also



calculates the mean square weighted deviates for the data, which is given by  $(f(U)/n-2)$ . Theoretically if all the data points fit the isochron within the variance estimates, then the MSWD will be less than one, thus obviating the need for rigorous estimates of variance if inferences concerning open system behaviour or otherwise are to be made.

### 5. Monoclinic Lattice Parameters.

Since the following relationship holds for monoclinic systems (see AZAROFF and BUERGER, 1958, or ZUSSMAN, 1968);

$$\frac{1}{d_{hkl}^2} = \frac{h^2}{a^2 \sin^2 \beta} + \frac{l^2}{c^2 \sin^2 \beta} + \frac{2hl \cos \beta}{ac \sin^2 \beta} + \frac{k^2}{b^2} \quad (1)$$

$$\text{or } \sin^2 \theta = \alpha A + \gamma B + \delta C + \Sigma \sqrt{AC \cdot \cos \beta} \quad (2)$$

where

$$\alpha = h^2, \gamma = k^2, \delta = l^2 \text{ and } \Sigma = 2hl$$

$$\text{and } A = \frac{\lambda^2}{4a^2 \sin^2 \beta}, B = \frac{\lambda^2}{4b^2}, C = \frac{\lambda^2}{4c^2 \sin^2 \beta}$$

It is possible to write an equation for each reflection:

$$\begin{aligned} \alpha_1 A + \gamma_1 B + \delta_1 C + \Sigma_1 \sqrt{AC} \cdot \cos \beta &= \sin^2 \theta_1 \\ \text{to } \alpha_i A + \gamma_i B + \delta_i C + \Sigma \sqrt{AC} \cdot \cos \beta &= \sin^2 \theta_i \end{aligned} \quad (3)$$

For the  $i$  th. reflection:

$$\alpha_i A + \gamma_i B + \delta_i C + \Sigma \sqrt{AC} \cdot \cos \beta - \sin^2 \theta_i = \Delta_i$$

where  $\Delta_i$  results from the measurement errors in the d-specings.

A least - squares solution may now be applied in order to minimise  $\Delta_i$ , such that:

$$\sum_{i=0}^i \Delta_i^2 = \text{minimum}$$





This is achieved by setting the following partial derivations to zero,

$$\frac{\delta \Sigma \Delta_i^2}{\delta A} = \frac{\delta \Sigma \Delta_i^2}{\delta B} = \frac{\delta \Sigma \Delta_i^2}{\delta C} = \frac{\delta \Sigma \Delta_i^2}{\delta (\sqrt{AC} \cdot \cos \beta)} = 0$$

from which four normal equations may be obtained by summing from 0 to 1.

In practice this is carried out [w.r.t. (3) above] by multiplying all equations by their  $\alpha$ 's and adding, all by their  $\beta$ 's and adding, etc. This results in the following four normal equations which may be solved for A, B, C and  $\sqrt{AC} \cdot \cos \beta$  and eventually, a, b, c, and  $\beta$ ,

$$\Sigma \alpha_i \sin^2 \theta_i = A \Sigma \alpha_i^2 + B \Sigma \alpha_i \gamma_i + C \Sigma \alpha_i \gamma_i + \sqrt{AC} \cdot \cos \beta \Sigma \alpha_i \epsilon_i.$$

$$\Sigma \gamma_i \sin^2 \theta_i = A \Sigma \alpha_i \gamma_i + B \Sigma \gamma_i^2 + C \Sigma \gamma_i \delta_i + \sqrt{AC} \cdot \cos \beta \Sigma \epsilon_i \gamma_i.$$

$$\Sigma \delta_i \sin^2 \theta_i = A \Sigma \alpha_i \delta_i + B \Sigma \gamma_i \delta_i + C \Sigma \delta_i^2 + \sqrt{AC} \cdot \cos \beta \Sigma \epsilon_i \delta_i.$$

$$\Sigma \epsilon_i \sin^2 \theta_i = A \Sigma \alpha_i \epsilon_i + B \Sigma \gamma_i \epsilon_i + C \Sigma \epsilon_i \delta_i + \sqrt{AC} \cdot \cos \beta \Sigma \epsilon_i^2.$$

In practice the equations were solved by a least - squares unit cell refinement programme, employing variable indexing options, written by EVANS, APPLEMAN and HANDWERKER (1963). The normal equations are solved by the square root method for symmetrical coefficient matrices.

## 6. Correction of Microprobe Data.

Corrections are applied to the apparent element concentrations for the atomic number effect, mass absorption and fluorescence as follows.

### 6a. Atomic number correction.

The ratio of X-ray intensity in the sample to X-ray intensity in the standard (KA) is related to the 'stopping power' and back-scattering coefficients as follows: (after DUNCUMB and REED, 1967).



$$K_A = C_A \cdot \frac{R_{AB}}{R_A} \cdot \frac{\bar{S}_A}{\bar{S}_{AB}} \quad (1)$$

where  $K_A = \frac{\text{X-ray intensity in sample}}{\text{X-ray intensity in standard}}$

$C_A$  = concentration of element in standard

$R_{AB}$  = back-scattering coefficient for sample (AB)

$R_A$  = back-scattering coefficient for standard (A)

$\bar{S}_A$  = mean stopping power in standard

$\bar{S}_{AB}$  = mean stopping power in sample

#### 1) Stopping Power:

$$S = \text{const.} \cdot \frac{Z}{A} \cdot \frac{1}{E} \quad (n \cdot 1.166 \bar{E}/J)$$

where  $\bar{E} = 1/2(E_o + E_t)$

$E_o$  = beam voltage

$E_k$  = critical excitation voltage in ev

Mean  $\bar{S}$ (stopping power) =  $\sum C_i S_i$

$C_i$  = concentration of  $i$  th. element.

$J$  values determined from tables given by Duncumb and Reed.

The constant and  $\frac{1}{E}$  cancel when the sample is compared with a standard.

#### 2) Back Scatter Coefficient R:

Values for  $R$  are interpolated from tables given by DUNCUMB and REED

(op.cit.) for  $R$  versus  $\frac{1}{\mu} = \frac{E_k}{E_o}$  and  $Z$  (atomic number).

#### 6b. Absorption Correction.

The absorption correction applied is essentially that given by

LONG (1967);



$$f(X) = \frac{\text{emergent intensity}}{\text{generated intensity}}$$

$$f(X) = \frac{F(X)}{F(0)} = \frac{1 + h}{\left(1 + \frac{\chi}{\sigma_c}\right) \left(1 + h \left[1 + \frac{\chi}{\sigma_c}\right]\right)} \quad (2)$$

where  $\sigma_c = \frac{4.5 \times 10^5}{E_o^{1.65} - E_c^{1.65}} \quad (\text{Lenard coefficient})$

$E_o$  = beam voltage in Kev

$E_c$  = critical excitation voltage in Kev

$h = 1.2 A/Z^2$  (averaged for specimen)

$\chi = (\mu/\rho) \operatorname{cosec} \theta$

where  $\mu$  = linear absorption coefficient

$\rho$  = density

$\mu/\rho$  = mass absorption coefficient

$\theta$  = take-off angle (52.5 for A.R.L. E.M.X.)

#### 6c. The Fluorescence Correction.

Castaing originally derived a formula for K-K fluorescence in 1951 (CASTAING, 1951), which has been modified to include L-L and L-K fluorescence and K-L fluorescence (REED, 1965),

$$\frac{I_f}{I_a} = 0.5 P_{ij} \cdot \frac{C_B r_A^{-1}}{r_A} \cdot W_k(B) \cdot \frac{A}{B} \cdot (U_B^{-1}/U_A^{-1})^{1.67} \frac{\mu_B^A}{\mu_B} (\ln [1 + x/x] [1 + y/y]) \quad (3)$$

where  $I_f$  = fluorescence intensity

$I_A$  = intensity of primary radiation from element A

$C_B$  = mass concentration of element B

$r_A$  = K-absorption edge jump ratio of element A

$W_k(B)$  = K-shell fluorescence yield of element B





A and B = atomic weights of elements A and B

$\mu_B^A$  = mass absorption coefficient of element A for K(B) radiation.

$\mu_B$  = mass absorption coefficient for specimen for K(B) radiation.

$x = (\mu_A / \mu_B) \operatorname{cosec} \theta$

$y = \sigma / \mu_B$

$\mu_A$  = mass absorption coefficient for K(A) radiation

$\sigma$  = Lenard coefficient

$\theta$  = take-off angle

$P_{ij}$  = factor for excitation of j radiation by i

Note  $P_{KK} = P_{LL} = 1$

$P_{KL} = 0.24$

$P_{LK} = 4.2$

The formula has been further simplified by Reed by substituting:

$$J(A) = 0.5 P_{ij} (R_A - 1 / R_A) \cdot W(B) \cdot \frac{A}{B} \quad (4)$$

where  $J(A)$  is determined from tables.

The formula now becomes:

$$\gamma = \frac{I_f}{I_A} = C_B J(A) [(U_B - 1) / (U_A - 1)]^{1.67} \cdot \frac{\mu_B^A}{\mu_B} \cdot [\ln(1+x)/x + \ln(1+y)/y] \quad (5)$$

where  $U = \text{overvoltage ratio} = \frac{E_o}{E_k} = \frac{\text{incident (KV)}}{\text{critical excitation (KV)}}$

All computations were actually performed using an APL program (PROBEDATA) written by D.G.W. Smith and M.L. Tomlinson. Details are obtainable from the Department of Geology, University of Alberta.



Composition of Standards used for Microprobe Analyses.

	EP/S12-1	EP/S12-2	EP/S6-13	Ep/S12-4
	Biotite	Biotite	Pyroxene	Garnet
SiO <sub>2</sub>	34.4	38.62	53.80	30.00
TiO <sub>2</sub>	3.05	2.29	0.10	0.08
Al <sub>2</sub> O <sub>3</sub>	13.30	10.72	1.30	22.00
Fe <sub>2</sub> O <sub>3</sub>	4.60	1.80	0.80	0.75
FeO	26.00	16.51	3.90	21.36
MnO	0.38	0.95	0.20	0.50
MgO	4.60	14.01	15.10	11.53
CaO	0.02	0.02	2.42	4.20
Na <sub>2</sub> O	0.16	0.69	0.50	
K <sub>2</sub> O	9.20	9.20		
P <sub>2</sub> O <sub>5</sub>	0.05			0.04
H <sub>2</sub> O <sup>+</sup>	3.60	2.66		0.14
Rb <sub>2</sub> O	0.06	0.03		
Ba	0.18	0.11		
F	0.65	3.3		
Cl	0.05			

Operating Conditions of Microprobe.

Take off angle = 52.5 degrees.

Operating voltage = 15 KV.

Emission current = 200 microamps.

Beam current = 0.1 microamp.



## 7. Structural Formulae.

All structural formulae for the amphiboles analysed in this study were calculated on the basis of 23 oxygens. A Fortran IV program (MINFORM), written by the author calculates structural formulae on the basis of O or O+OH+F+Cl. A subroutine calculates the mean cation radii of  $M_2$  assuming ordered and disordered structures and estimates the wt. % of  $H_2O$  for amphiboles when calculated on the basis of 23 oxygens.









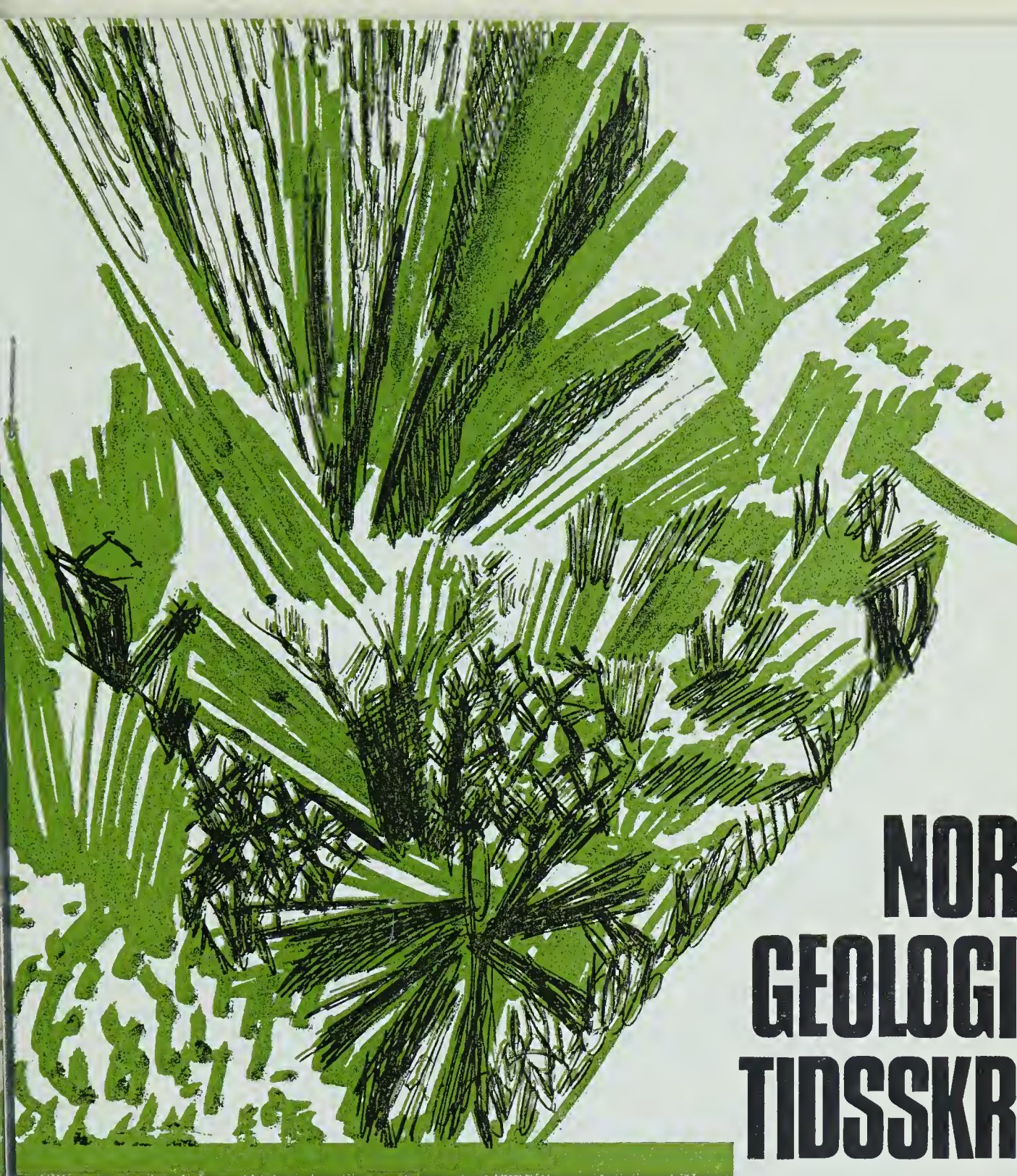












# NORSK GEOLOGISK TIDSSKRIFT

O'Nions, R. K., Morton, R. D. & Baadsgaard, H.

*Potassium argon ages from the Bamble sector of the  
Fennoscandian shield in South Norway*

Volume 49 · 1969 Number 2

Universitetsforlaget

**REPRINT**





# Norsk Geologisk Tidsskrift

*A Norwegian journal of geology issued under the auspices of  
the Norwegian Geological Society*

---

## EDITOR

Professor GUNNAR HENNINGSMOEN, Geologisk Museum, Sars gate 1, Oslo 5, Norway.

## EDITORIAL COMMITTEE

Docent B. G. ANDERSEN, Professor T. F. W. BARTH, Professor J. A. W. BUGGE,  
Professor A. HEINTZ, and Professor T. STRAND.

## PUBLISHER

UNIVERSITETSFORLAGET, P. O. Box 307, Blindern, Oslo 3, Norway. American office: P. O.  
Box 142, Boston, Massachusetts 02113, U. S. A.

## SUBSCRIPTIONS

*Members* of the Norwegian Geological Society who have paid their annual subscription (N. Kr. 25.-) receive the journal free from Universitetsforlaget. Membership subscriptions, changes of address, and communications from members concerning the journal should be sent to the Treasurer, Norsk Geologisk Forening, Geologisk Museum, Sars Gate 1, Oslo 5, Norway.

*Non-members* of the Norwegian Geological Society should send their orders to Universitetsforlaget. The subscription price per volume (four issues) including postage, is as follows:

Norway: N. kr. 45. - postgiro 15530.

Denmark: D. kr. 45. - postgiro 14954.

Sweden: S. kr. 33. - postgiro 44337.

U. S. A. and Canada: \$ 7.50, P. O. Box 142,  
Boston, Mass. 02113, U. S. A.

Single issues, at a price of N. kr. 12. -, \$ 2.00, can also be ordered.

# POTASSIUM-ARGON AGES FROM THE BAMBLE SECTOR OF THE FENNOSCANDIAN SHIELD IN SOUTH NORWAY

R. K. O'NIONS, R. D. MORTON & H. BAADSGAARD

*Department of Geology, University of Alberta, Canada*

O'NIONS, R. K., MORTON, R. D. & BAADSGAARD, H.: Potassium-argon ages from the Bamble sector of the Fennoscandian Shield in South Norway. *Norsk Geologisk Tidsskrift*, Vol. 49, pp. 171-190. Oslo 1969. Systematic K-Ar dating has been carried out on micas and amphiboles from upper amphibolite facies rocks in the Bamble sector of the Fennoscandian Shield in South Norway. Interpretation of fifty-one new K-Ar ages is made in terms of a cooling history. A spread of apparent ages from 1125 ( $\pm 30$ ) m.y. to 975 ( $\pm 30$ ) m.y. is related to differing argon retentivities of the dated minerals. Apparent ages of amphiboles cover the whole time span. Selection of amphiboles of appropriate composition and micas of appropriate grain size has made possible the definition of the thermal maximum of a regional metamorphic event at  $\sim 1100$  m.y. Medium-grained biotites from metasediments and metavolcanics range from  $\sim 1040$  m.y. to  $\sim 970$  m.y. Apparent ages of micas from concordant plagioclase pegmatites suggest they are broadly synkinematic. Emplacement of late-kinematic gabbroic rocks and associated apatite deposits (Ödegårdens Verk) at  $\sim 1040$  m.y. is suggested by apparent ages of Mg-rich amphiboles and phlogopites. Coarse-grained micas from discordant K-feldspar pegmatites at Ödegården are thought to yield ages near the true age of the pegmatites i.e.  $\sim 1000$  m.y.

## CONTENTS

Abstract .....	171
Introduction .....	171
Analytical methods and errors .....	173
Previous age determinations .....	175
Argon diffusion in micas and amphibole .....	176
Interpretation of mica apparent ages .....	178
Interpretation of amphibole apparent ages .....	180
Summary and conclusions .....	181
Acknowledgements .....	182
Appendix: description and location of analysed specimens ....	182
References .....	189

## INTRODUCTION

Sufficient radiometric age determinations have now been carried out in the Fennoscandian Shield (or Baltic Shield) to make a zonal subdivision possible. Polkanov & Gerling (1961) and Kratz, Gerling & Lobach-Zhuchenko (1968) have subdivided the Shield into three zones: a Saamo-Karelian zone (3600 m. y. to 1900 m. y.) corresponding to the Karelides in the eastern part of

the Shield; a Sveco-Fennian zone (2300 m. y. to 1650 m. y.) corresponding to the Svecofennides of the central and western part of the Shield; and a Sveco-Norwegian zone (1200 m. y. to 900 m. y.) in the southern part of the Shield consisting of Pregothian, Gothian, Dalslandian, and Telemark complexes. The present paper is concerned with the interpretation of fifty-one new potassium-argon age determinations in the Sveco-Norwegian zone from the Bamble sector of the Fennoscandian Shield in South Norway.

Various aspects of the geology of the region have been studied by a number of workers. Bugge (1943) has published a regional description of the whole Kongsberg-Bamble portion of the Shield in South Norway, which has been enlarged upon and modified in subsequent publications by Barth & Dons (1960), Barth & Reitan (1963) and Bugge (1965). More recently a systematic survey of the Bamble-Risør region was initiated by one of us (R.D.M.) at the University of Nottingham. Investigations by Morton, Batey & O'Nions (1968) in Eastern Bamble, and unpublished work of Burrell (1964) and Petterson (1964) in the Levang district, Ryan (1966) in the Ödegårdens verk district, and Starmer (1967) in the Risør district, have provided the basis for the collection of specimens in the present geochronological studies.

The extent and distribution of some of the salient geological features of the area under consideration are presented in Fig. 1. To the east of the area the Precambrian basement is overlain by sediments of Cambro-Silurian age and the northern boundary is demarcated by the Porsgrunn-Kristiansand Fault, often loosely referred to as the 'Great Friction Breccia'. The region is occupied by a series of high-grade metasediments and metavolcanics, whose mineral assemblages are diagnostic of the sillimanite-almandine-orthoclase subfacies of the almandine amphibolite facies. Emplaced within the metasediments and metavolcanics are synkinematic and late-kinematic granites and gabbroic rocks. Granite occurs principally as the synkinematic Levang granite; the better known late-kinematic Grimstad and Herefoss granites being southwest of the area. The gabbroic rocks include norite, olivine norite, gabbro and olivine gabbro (collectively termed 'hyperites' by Scandinavian geologists), many of which show corona development. Field studies indicate that there are probably two phases of gabbro emplacement and that the famous chlorapatite deposits at Ödegårdens verk are associated with the late-kinematic phase. Pegmatites are ubiquitous throughout the area and appear to belong to two groups. The older group is predominantly concordant plagioclase pegmatites whereas the younger group is predominantly discordant K-feldspar pegmatites. In the Ödegårdens verk district Bugge (1965) notes that the apatite deposits are younger than the concordant plagioclase pegmatites, but are cut by K-feldspar pegmatites. Locally within the area, presumably where reduced  $P_{H_2O}$  conditions existed, assemblages diagnostic of the hornblende granulite facies occur, but no regional P-T variation in the form of isograds has as yet been identifiable. Outside the present area in the Arendal district, granulite facies rocks with charnockitic and enderbitic affinities are developed (the so-called 'arendalites')

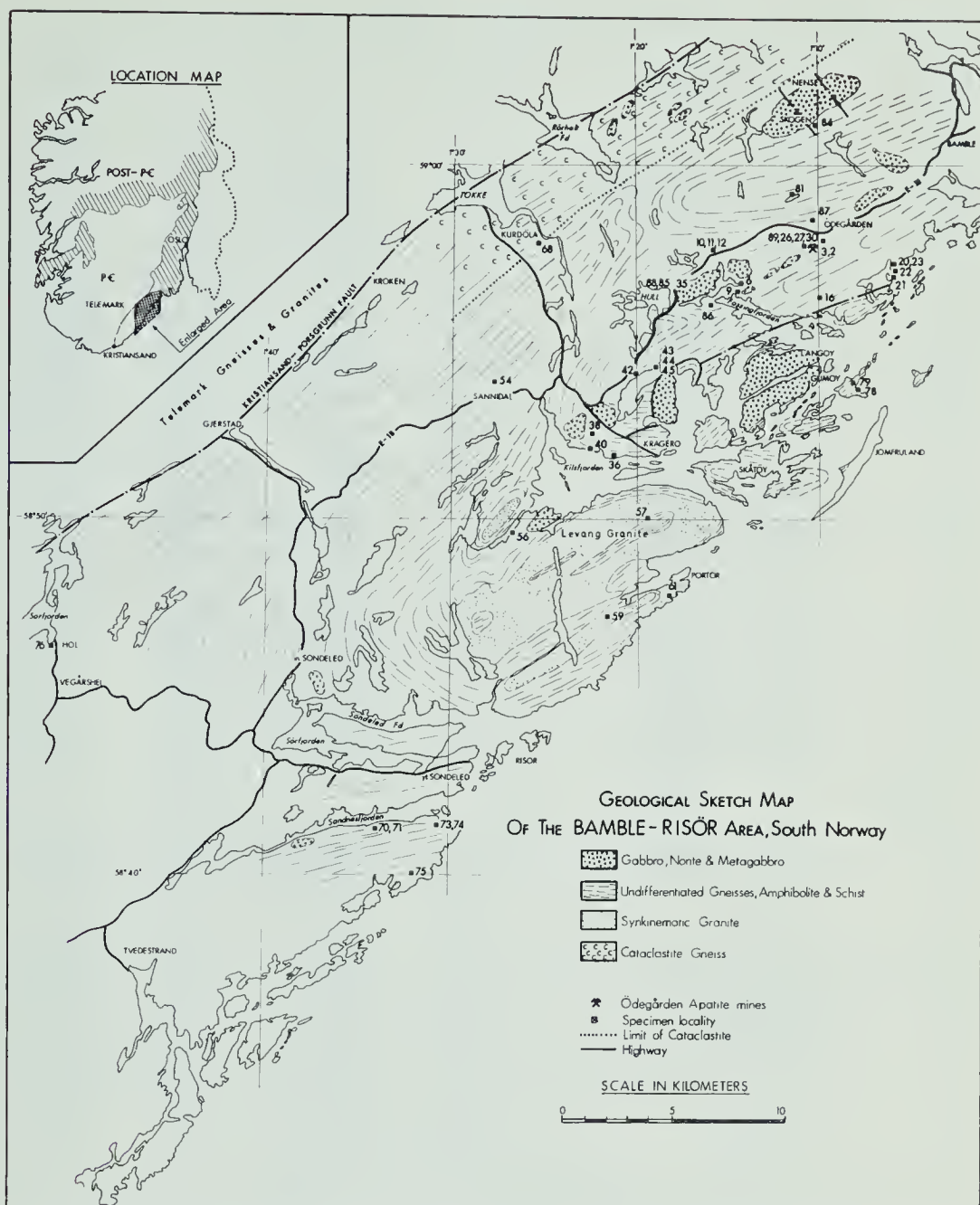


Fig. 1. Geological sketch map of the Bamble-Risør area indicating location of analyzed samples. Note: longitude is west of Oslo (Oslo meridian  $10^{\circ}43'22.5''$  east of Greenwich).

and appear to extend locally to the Vegårshei-Gjerstad area (Touret 1962, 1967).

The apparent ages reported here are all mica and hornblende mineral ages from rocks representative of the above phases.

#### ANALYTICAL METHODS AND ERRORS

All samples were crushed to  $-60 + 120$  mesh, and minerals were separated by conventional magnetic and heavy liquid techniques. Estimates of biotite and hornblende sample purity are given in the Appendix.



Table 1. Apparent K-Ar ages of metasediments and metavolcanics

Number	Sample*	K <sup>40</sup> ppm.	Ar <sup>40</sup> /K <sup>40</sup>	% rad. Ar <sup>40</sup>	App. age m.y.
<i>Micas</i>					
SN-36	Marble (P)	9.50	0.09092	99.6	1038 ± 16
SN-21	Biotite amphibolite (B)	6.83	0.08020	99.2	1030 ± 16
SN-23	Nodular sillimanite gneiss (M)	11.05	0.08008	98.9	1029 ± 16
SN-20	Biotite schist (B)	8.96	0.07982	99.6	1027 ± 16
SN-10	Orthoamphibolite (B)	8.52	0.07977	99.4	1026 ± 16
SN-73	Amphibolite (B)	7.64	0.07816	99.9	1010 ± 16
SN-11	Granite gneiss (B)	9.28	0.07776	99.8	1006 ± 15
SN-79	Metaconglomerate (M)	10.53	0.07761	98.8	1005 ± 15
SN-56	Quartzite (B)	8.85	0.07769	99.9	1005 ± 16
SN-74	Augen gneiss (B)	7.46	0.07712	99.6	1000 ± 16
SN-75	Augen gneiss (B)	8.42	0.07651	99.1	993 ± 15
SN-78	Quartzite (B)	9.21	0.07646	99.7	993 ± 15
SN-6	Graphitic gneiss (B)	8.79	0.07622	99.6	991 ± 15
SN-68	Garnet-biotite schist (B)	9.29	0.07581	99.6	986 ± 15
SN-3	Biotite schist (B)	8.01	0.07575	99.5	986 ± 15
SN-16	Graphitic schist (B)	8.51	0.07520	99.9	980 ± 15
SN-40	Biotite gneiss (B)	7.84	0.07469	99.3	975 ± 15
SN-54	Biotite gneiss (B)	7.36	0.07385	99.7	966 ± 15
SN-44	Granite gneiss (B)	7.95	0.06950	98.7	921 ± 14
SN-76	Augen gneiss (B)	6.86	0.06355	98.9	860 ± 14
<i>Amphiboles</i>					
SN-2	Amphibolite	0.59	0.08839	98.8	1110 ± 34
SN-9	Garnet amphibolite	0.60	0.08788	99.7	1105 ± 33
SN-10	Orthoamphibolite	1.64	0.08661	99.8	1093 ± 33
SN-22	Amphibolite	0.56	0.08492	97.9	1077 ± 33
SN-45	Amphibolite	0.65	0.08224	90.7	1050 ± 32
SN-16	Graphitic schist	1.35	0.08218	99.7	1050 ± 32
SN-21	Amphibolite	0.61	0.08193	92.4	1047 ± 32
SN-73	Amphibolite	1.02	0.08177	98.9	1046 ± 32
SN-38	Amphibolite	1.35	0.07913	95.5	1020 ± 31
SN-74	Augen gneiss	1.88	0.07728	98.9	1001 ± 31
SN-70	Amphibolite	0.96	0.07652	99.2	994 ± 31
SN-71	Metagabbro	0.76	0.07419	90.5	970 ± 30

\* B = Biotite; M = Muscovite; P = Phlogopite

Potassium determinations of both the micas and amphiboles were made by precipitation of potassium tetraphenylboron. This method has been employed for potassium determinations of micas for a number of years at the University of Alberta, and duplicate determinations yield a standard deviation of 1 % (see Lanphere & Dalrymple 1967). In order to assess the precision of the method for low-potassium minerals, nine replicate determinations were performed over a period of a few months on the hornblende SN-88, which yielded a mean value of 0.52 % K<sub>2</sub>O and a standard deviation of 2.8 %. It may be expected that amphiboles with higher K<sub>2</sub>O contents will be more precise.

Argon was extracted from samples using a flux-fusion technique similar

Table 2. Apparent K-Ar ages of gabbros, granites and pegmatites

Number	Sample*	K <sup>40</sup> ppm.	<sup>40</sup> Ar/K <sup>40</sup>	<sup>o</sup> <sub>o</sub> rad. Ar <sup>40</sup>	App. age m.y.
<i>Levang synkinematic 'granite'</i>					
SN-57	Foliated Granite (B)	6.48	0.07729	99.9	1001 ± 15
SN-61	Porphyritic granite (B)	7.62	0.07586	99.7	987 ± 15
SN-59	Gneissic granite (B)	8.59	0.07528	99.5	981 ± 15
SN-61	Porphyritic granite (H)	1.76	0.08285	94.3	1056 ± 32
<i>Ödegården apatite mines</i>					
SN-26	Ödegårdite (H)	0.47	0.08887	98.5	1114 ± 32
SN-89	Hornblende (massive)	0.82	0.08057	98.3	1034 ± 32
SN-30	Phlogopite (apatite vein)	8.23	0.08043	92.3	1033 ± 16
SN-27	Wall rock (P)	7.64	0.07894	99.3	1020 ± 16
<i>Late-kinematic gabbro</i>					
SN-35	Pyroxenite (H)	0.54	0.07830	97.6	1012 ± 31
SN-88	Massive hornblende	0.53	0.08065	96.1	1035 ± 32
SN-35	Pyroxenite (P)	7.91	0.07582	99.2	987 ± 15
<i>Pegmatites and coarse-grained metavolcanics</i>					
SN-43	Plagioclase pegmatite (B)	8.65	0.08871	96.5	1112 ± 17
SN-84	K-feldspar pegmatite (M)	10.38	0.08641	94.7	1091 ± 17
SN-85	Plagioclase pegmatite (B)	8.36	0.08452	96.2	1073 ± 16
SN-42	Plagioclase pegmatite (B)	8.23	0.08390	95.3	1067 ± 16
SN-86	Cordierite-anthophyllite rock (B)	8.26	0.08374	94.2	1065 ± 16
SN-12	Plagioclase pegmatite (B)	9.65	0.08120	93.3	1040 ± 16
SN-81	K-feldspar pegmatite (B)	9.39	0.07893	91.3	1017 ± 16
SN-87	K-feldspar pegmatite (B)	9.61	0.07790	94.9	1008 ± 16

\* B = Biotite; H = Hornblende; M = Muscovite, P = Phlogopite

to that described by Goldich et al. (1961) and measured dynamically on a modified A.E.I. MS-10 mass spectrometer. The precision of duplicate argon determinations in this procedure is about 1 % (Baadsgaard 1965).

Ages were calculated using the following constants:

$$\begin{aligned}\lambda_e &= 0.585 \cdot 10^{-10} \text{yr.}^{-1} \\ \lambda_B &= 4.72 \cdot 10^{-10} \text{yr.}^{-1} \\ K^{40}/K &= 0.0119 \text{ atomic per cent.}\end{aligned}$$

Analytical errors were calculated using a standard deviation of 1 % for Ar<sup>40</sup> and K<sup>40</sup> determinations of biotites and a standard deviation of 1 % and 3 % for Ar<sup>40</sup> and K<sup>40</sup> determinations respectively of amphiboles. Calculated errors and apparent ages are presented in Tables 1 and 2. The total uncertainty in the apparent ages, taking uncertainties in the values of the decay constants into consideration, is approximately ± 60 m. y. and ± 80 m. y. for biotites and amphiboles respectively.

## PREVIOUS AGE DETERMINATIONS

Previous radiometric age determinations from South Norway published by Neumann (1960), Kulp & Neumann (1961), Polkanov & Gerling (op. cit.) and Broch (1964) have been principally concerned with K-Ar ages of micas and

have served to define a metamorphic event between 1100 m. y. and 900 m. y. Within the area forming the subject of this paper, only one previous K-Ar age and one U-Pb age have been reported. Kulp & Neumann (1961) obtained an apparent age of 1080 m. y. for phlogopite from a productive vein at the Ödegården apatite mines, in reasonable agreement with 1033 m. y. obtained on a similar sample (SN-30) in this work. The major discrepancy would appear to lie in the potassium determination (see Pinson 1961, Lanphere & Dalrymple 1967). Kulp & Ecklemann (1957) report a  $\text{Pb}^{206}/\text{Pb}^{207}$  age of 940 m. y. and a  $\text{Th}^{232}/\text{Pb}^{208}$  age of 980 m. y. for a euxinite sample from the Kalstad pegmatite near Kragerö. Broch (1964) has summarized all age determinations carried out on Norwegian rocks up to 1964; however, it should be noted that the K-Ar analyses carried out by Russian workers are 5 % to 6 % higher than ages calculated using presently accepted decay constants. Age determinations in the Risør-Arendal area range from 1345 m. y. to 828 m. y. with a pronounced histogrammic maximum at 900 m. y. This maximum was termed the 'Sveconorwegian Regeneration Period' by Magnusson (1960).

## ARGON DIFFUSION IN MICAS AND AMPHIBOLES

It is becoming increasingly more apparent that K-Ar ages from regional metamorphic terranes do not relate to any specific geological event, but are 'cooling' ages related to the time at which specific minerals became closed systems to the diffusion of radiogenic argon during post-metamorphic uplift and cooling (Armstrong 1966, Armstrong & Hills 1967, Harper 1967a, 1967b, 1968, and Moorbath 1967). Since the time of 'closure' of different potassium-bearing minerals is related to the argon diffusion characteristics of that mineral, some of the pertinent features of argon diffusion in micas and hornblendes will be briefly reviewed.

The diffusion coefficient of radiogenic argon is empirically related to the activation energy by the following relationships:

$$D_t = D_0 \exp (-E/RT) \dots\dots\dots (1)$$

$$\text{or: } D_t/a^2 = D_0/a^2 \exp (-E/RT) \dots\dots\dots (2)$$

where  $D_t$  = diffusion coefficient at some temperature  $T$

$D_0$  = constant.

$a$  = effective radius of sphere of argon diffusion.

$E$  = activation energy.

$R$  = gas constant.

$T$  = absolute temperature.

The effective radius of the sphere of argon diffusion may vary from mineral to mineral and is not always a known quantity; thus the diffusion parameter  $D/a^2$  of (2) is the most useful (Hart 1960). Fechtig & Kalbitzer (1966) and Moorbath (1967) have recently reviewed the more reliable determinations of  $D$  or  $D/a^2$  and  $E$  for a number of minerals.



Experimentally determined activation energies for biotite range from 33 kcal./mole to 86 kcal./mole. Gerling et. al. (1963) report activation energies of 33, 48 and 69 kcal./mole for a biotite, each related to energetically different reservoirs of argon in the mineral. The low activation energies probably result from non-volume, low temperature diffusion of loosely bound argon in structural defects. Reported activation energies for muscovite, on the other hand, are slightly higher, ranging from 56 kcal./mole to 83 kcal./mole. Denisenko (1965) found three distinct activation energies for the liberation of argon from muscovite, 38, 72 and 83 kcal./mole. It is interesting to note that geological estimates of diffusion parameters and activation energies are lower than experimental values. For example Hurley et. al. (1962) give a geological estimate of  $E = 27$  kcal./mole for a biotite and Wescott (1966) estimates  $E = 40$  kcal./mole also for a biotite. Higher experimentally determined values of  $E$  may result from a violation of boundary conditions regarding the amount of radiogenic argon present at the time of the experiment (Fechtig & Kalbitzer 1966).

The actual temperatures at which minerals become closed systems to the diffusion of radiogenic argon is not certain, but is probably around  $200^{\circ}$  to  $300^{\circ}$  C for muscovite and  $150^{\circ}$  to  $200^{\circ}$  C for biotite. There does appear to be a qualitative agreement between experimental studies concerning the probable relative 'closure' temperatures of micas and field studies. Harper (1967a) found muscovite from the Scottish Caledonides to be consistently 10 m. y. older than coexisting biotites.

Comparatively few reliable determinations of  $E$  and  $D/a^2$  have been made for amphiboles. Gerling et al. (1965) report activation energies ranging from 110 kcal./mole to over 200 kcal./mole for five amphiboles ranging in composition from riebeckite to pargasite and note an inverse correlation between increasing total iron content and decreasing experimental activation energy. Investigations by Hart (1961 and 1964) and Steiger (1964) indicate that amphiboles may frequently yield older apparent ages than coexisting micas, as may be expected from the determined activation energies.

From equation (2) it can be seen that the diffusion constant is dependent upon the radius of the sphere of argon diffusion and potentially may exert considerable control on the argon diffusion characteristics of a mineral. For amphiboles, Hart (1960) has shown the effective radius of the diffusion sphere to be less than 30 microns in the case of hornblende, less than the physical grain size of material normally considered. Studies of micas of variable grain size by Hart (1964) and Rösler & Pilot (1967) indicate that, up to a limit, the actual physical grain size influences the retentivity of the mica, coarse-grained micas being more retentive than fine-grained micas.

Argon liberation from minerals may be controlled by different factors during cooling from the temperature of crystallization and during reheating, as noted by Harper (1967a). During cooling, argon diffusion will be controlled by the diffusion rate ( $D/a^2$ ) and since this parameter is very sensitive to temperature change in the range of activation energies under consideration,

there may be only 50° to 100° C between the temperature at which argon is quantitatively retained in the lattice and the temperature at which argon will diffuse through the lattice. Conversely during updating, the activation energy for argon diffusion will be the controlling step as the temperature increases. Thus, in an area undergoing epeirogenesis and slow cooling it may be possible for some amphiboles (if  $D/a^2$  is high enough) to lose argon at low temperatures and yield apparent ages similar to those for coexisting micas. Data of O'Nions et al. (1968) suggest that this is the case for amphiboles near the ferropargasite end-member. Upon reheating, such amphiboles with higher activation energies than micas, would require higher temperatures than micas for argon to surmount the potential barrier and diffuse out of the lattice.

### INTERPRETATION OF MICA APPARENT AGES

The foregoing discussion shows that the apparent ages of the micas are related to the time at which they became closed systems to the diffusion of radiogenic argon upon post-metamorphic uplift and cooling, or in the terms of Armstrong (1966), passed through the 'metamorphic veil'.

The apparant ages of medium-grained micas from metasediments and metavolcanics range from 966 m. y. to 1038 m. y. and are graphically represented in Fig. 2 in terms of a numerical frequency diagram. As only two medium-grained muscovite samples have been dated, it is not possible to draw any conclusions concerning their argon retentivity relative to biotite. The spread in biotite apparent ages is outside of experimental error and must be related to geological parameters. Consideration of Fig. 1 does not reveal any logical geographical variation of apparent ages and it is unlikely that the spread can be related to thermal gradients at the time of cooling (cf. Harper 1967b). Since all samples were crushed to -60+120 mesh, grain size effects are difficult to evaluate, however since the grain size of the original metasediments and metavolcanics are fairly uniform, it is doubtful if the spread of apparent ages can be attributed entirely to grain size effects. It may be expected that departures from an ideal trioctahedral composition (see Foster 1960) together with polytypic variations could influence the retentivity of the biotites. Gerling, Morozova & Kurbatov (1961) have demonstrated the effect of structural changes on the argon retentivity of micas.

Coarse-grained pegmatitic muscovites and biotites are as a group older than their enclosing metasediments and metavolcanics. They range in age from 1112 m. y. to 1008 m. y. and their distribution is indicated in Fig. 2. Grain size and compositional factors alone cannot explain the distribution of apparent ages, for the most coarse-grained sample (SN-81) was in excess of 10 cm in diameter and considerably younger (1008 m. y.) than other more fine-grained samples. Field relations have indicated two phases of pegmatite formation; an older group of mainly concordant plagioclase pegmatites and a younger group of mainly K-feldspar pegmatites, which

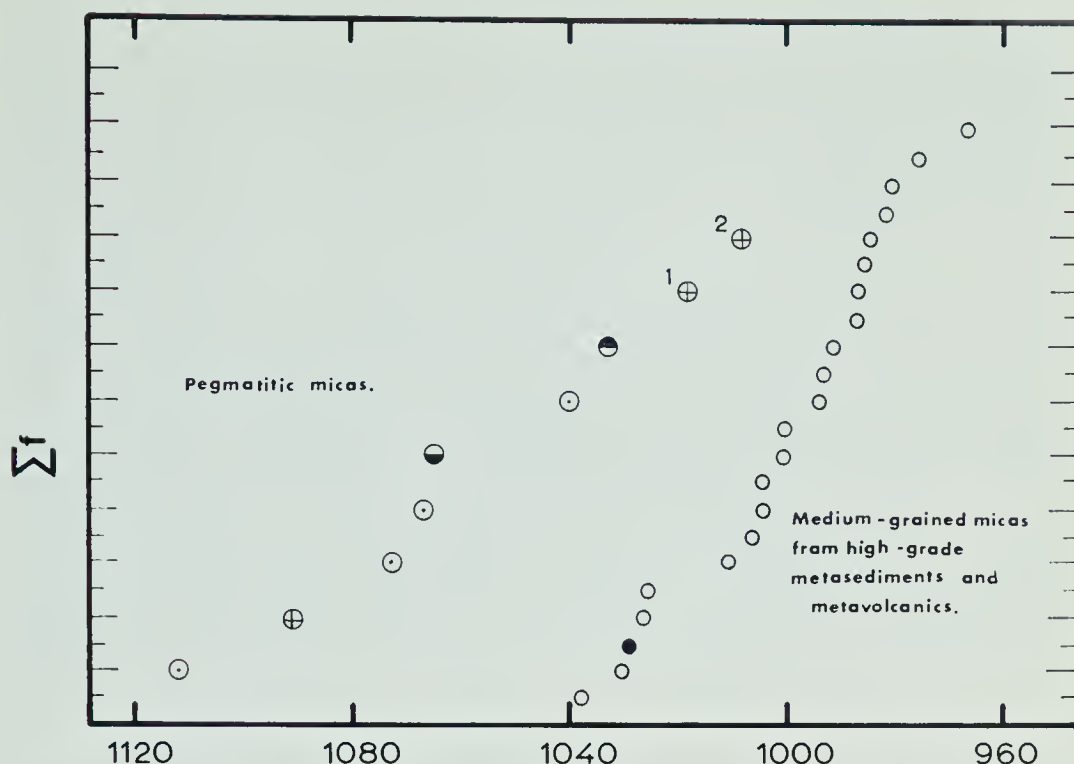


Fig. 2. Cumulative frequency distribution of mica apparent ages. Small circles: medium-grained biotites (open circles) and muscovite (solid circle) from upper amphibolite facies metasedimentary and metavolcanic rocks. Dotted circles: coarse-grained biotites from concordant plagioclase pegmatites. Crossed circles: micas from discordant K-feldspar pegmatites (1 and 2 seen to be younger than the apatite deposits of Ödegårdens Verk; see Fig. 3). Upper half-solid circles: biotite from cordierite-anthophyllite rock (included with the pegmatites in view of its coarse grain size). Lower half-solid circles: phlogopite associated with chloroapatite at Ödegården Apatite Mines.

appear to be younger than the Ödegårdens Verk apatite deposits. The two young K-feldspar pegmatites, SN-81 and SN-87, 1017 m. y. and 1008 m. y. respectively, must be expected to be near their true ages, in view of their coarse grain size and the fact that medium-grained biotites in metasediments and metavolcanics had already started to retain radiogenic argon. The plagioclase pegmatites and the K-feldspar pegmatite SN-84 are thought to belong to an older broadly synkinematic group.

The apparent age of SN-44 of 921 m. y. does not fit in the general scheme of apparent ages. It would appear to have been affected by a later thermal event. Southwestwards in the Arendal-Kristiansand district post-kinematic granites (eg. Herefoss granite) have yielded apparent ages around 860 m. y. However, field studies around Kragerö have not as yet revealed a possible cause for the updating of SN-44.

It would appear that the thermal maximum of the metamorphism (650° to 700° C) was in excess of 1112 m. y., and that by 975 m. y., uplift had been sufficient to cool the area to 150° to 200° C.



## INTERPRETATION OF AMPHIBOLE APPARENT AGES

Recent studies by Steiger (1964), Hart (1964) and Baadsgaard & Godfrey (1967) indicate the greater argon retentivity of amphiboles relative to micas. In the present study, amphiboles have been analysed from gneisses, amphiboles, synkinematic granitic and gabbroic rocks, and late-kinematic gabbroic rocks and associated veins. Amphibole apparent ages from metasediments, metavolcanics and synkinematic granitic and gabbroic rocks cover the same time span as the micas (Fig. 3). It is likely that the activation energies for diffusion of radiogenic argon in all the amphiboles are higher than for micas (Gerling et. al. 1965). Thus in some of the amphiboles the diffusion constants must have been sufficiently high to allow diffusion of argon down to comparatively low temperatures. Electron microprobe analysis of the above amphiboles by O'Nions et. al. (1968) has shown that the amphiboles are variable in composition from near the ferropargasite end-member to near the pargasite end-member and that the amphibole apparent ages decrease systematically from the Mg-rich compositions to Fe-rich compositions. There-

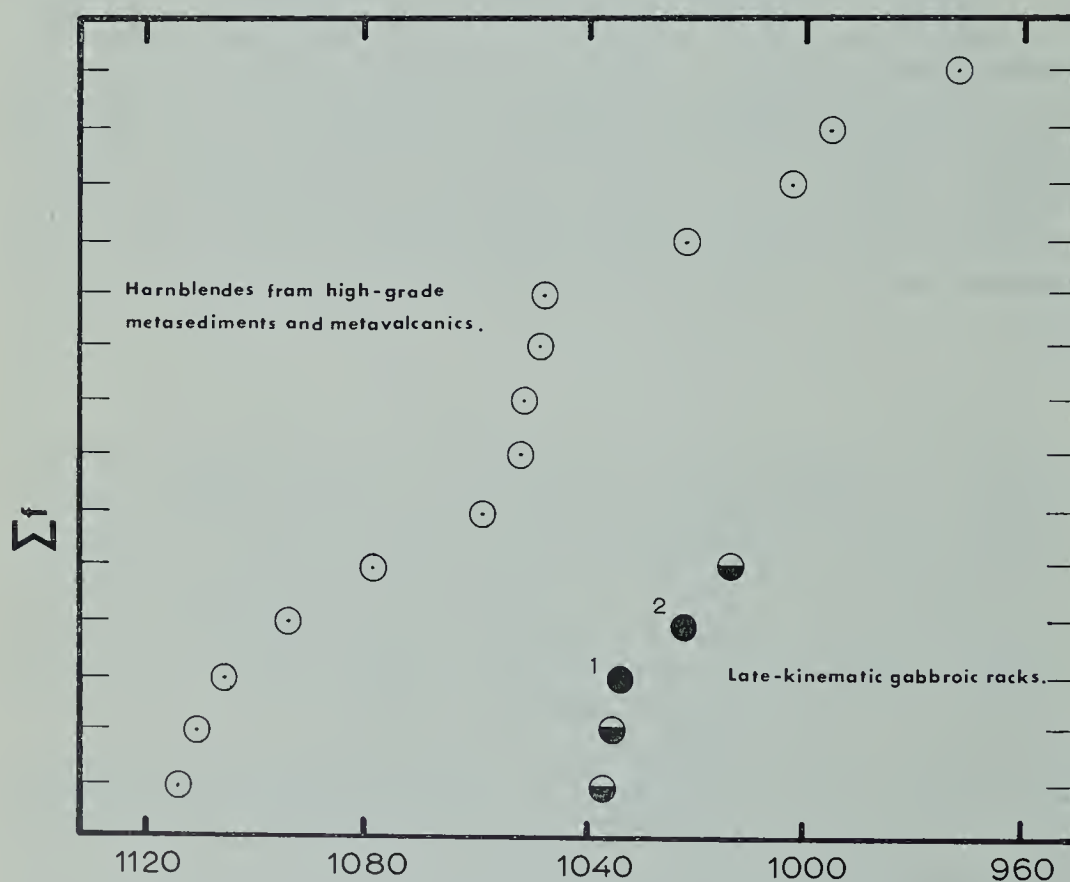


Fig. 3. Cumulative frequency distribution of amphibole apparent ages from upper amphibolite facies metasedimentary and metavolcanic rocks together with apparent ages of late kinematic gabbroic rocks. Dotted circles: hornblendes from upper amphibolite facies rocks. Solid circles: coarse-grained phlogopite from chlorapatite vein (1) and medium-grained phlogopite from wall rock (2) at Ödegården Apatite Mines. Lower half-solid circles: amphiboles associated with late-kinematic gabbroic rocks.

fore in amphiboles of appropriate composition the activation energy may be sufficiently low and the diffusion constant sufficiently high for argon to diffuse out of the lattice to quite low temperatures. Conversely, under such conditions of slow cooling, only those amphiboles of appropriate composition may be expected to yield older apparent ages approximating to the time of the thermal maximum of the metamorphic event.

Amphiboles associated with late-kinematic gabbroic intrusions, SN-88, SN-89, SN-35 have apparent ages of 1034, 1035 and 1012 m. y., respectively (Fig. 3). Analyses (O'Nions et. al. 1968) indicate that they are all Mg-rich and probably very retentive. Coarse-grained phlogopite from a productive apatite vein at Ödegårdens verk (SN-30) and medium-grained phlogopite from the wall rock (SN-27) have apparent ages of 1020 m. y., respectively. If any of these samples had crystallized much before  $\sim 1035$  m. y. they would be expected to yield older apparent ages. The Ödegården apatite deposits appear to be related to a late-kinematic phase of gabbroic intrusion around 1035 m. y. and to be intermediate in age between the synkinematic pegmatites and K-feldspar pegmatites formed at approximately 1010 m. y.

## SUMMARY AND CONCLUSIONS

Individual episodes of a metamorphic event are not usually distinguishable by potassium-argon methods in Precambrian metamorphic belts. However, by careful selection of appropriate material, information can be gained as to the probable cooling duration of the metamorphic belt in addition to late and post-kinematic igneous episodes.

Within the Bamble area, K-Ar apparent ages of coarse-grained pegmatites and Mg-rich amphiboles suggest that the thermal maximum of the metamorphic event was attained at about 1110 m. y. At this time epeirogenic cooling commenced and by 975 m. y. the region had cooled to around  $150^{\circ}$  to  $200^{\circ}$  C; i. e. some 150 m. y. elapsed before uplift was essentially complete. Cooling intervals of a similar magnitude have been reported for the Scottish Caledonides by Harper (1967a) and Moorbath (1967). In the Western Alps Steiger (1964) found hornblende apparent K-Ar ages in excess of 45 m. y., some 30 m. y. older than the 16-21 m. y. Rb/Sr apparent ages of micas reported by Jager (1962). This suggests a cooling interval of 30 m. y. The much faster rate of uplift in the Western Alps compared with South Norway and the Scottish Caledonides, indicate a fundamental difference in the type of metamorphic belt, a point which has been emphasized by Sutton (1965) and Zwart (1967).

In summary, the main metamorphic episode in the Bamble region at approximately 1100 m. y. involved the emplacement of the Levang granite and numerous gabbroic bodies and the formation of plagioclase pegmatites by local anatexis. Subsequently, at approximately 1040 m. y., a second phase of gabbroic emplacement occurred with the emplacement of associated chlorapatite veins. Finally, at approximately 1000 m. y., in the Ödegårdens

verk district the K-feldspar pegmatites, which are seen to cut the apatite deposits, were intruded. By 975 m. y. the area had cooled and the metamorphic event was essentially complete. Elsewhere in South Norway post-kinematic granites were emplaced at about 860 m. y.

## ACKNOWLEDGEMENTS

This work was supported by grants from the National Research Council of Canada and from Norges Almenvitenskapelige Forskningsråd. One of the authors (R.K.O.) acknowledges financial assistance received during the tenure of a National Research Council Studentship. The authors wish to thank Dr. I. C. Starmer for information concerning field relations within the Risör area.

*Department of Geology,  
The University of Alberta,  
Edmonton, Canada  
3rd October 1968*

## APPENDIX: DESCRIPTION AND LOCATION OF ANALYSED SPECIMENS

SN-36 Lat.  $58^{\circ}51'53''$ N Long.  $9^{\circ}20'58''$ E

Medium-grained diopside-bearing marble. Diopside (approx. 8 %) occurs as 1 to 3 mm. grains with occasional serpentine alteration. Calcite (average 1 mm.) is the main constituent comprising approximately 84 % of the mode. Idioblastic phlogopite crystals (approx. 7 %) are unaltered. Magnetite and apatite make up about 1 % of the rock.

The phlogopite concentrate was  $> 95$  % with a slight calcite impurity.

SN-21 Lat.  $58^{\circ}56'55''$ N Long.  $9^{\circ}38'9''$ E

A medium-grained, poorly foliated, garnet-biotite amphibolite occurring as discontinuous bands within a sequence of quartzites. Lepidoblastic hornblende (approx. 39 %) is unaltered and varies in size between 1 and 3 mm.  $An_{30}$  plagioclase (approx. 25 %) occurs as slightly sericitized, 2 to 3 mm. subidioblastic grains. Almandine garnet porphyroblasts (approx. 9 %) up to 5 mm contain numerous quartz inclusions (sieve structure). Biotite (approx. 13 %) is unaltered and forms 1 to 3 mm. grains. Minor amounts of xenoblastic quartz (5 %), magnetite (7 %) and apatite (2 %) are also present.

The biotite concentrate was  $> 99$  %. The hornblende concentrate contained  $< 1$  % quartz.

SN-23 Lat.  $58^{\circ}57'17''$ N Long.  $9^{\circ}37'34''$ E

A nodular sillimanite-biotite gneiss (nodular granite of Bugge, 1943). Quartz (approx. 63 %) is xenoblastic and varies between 2 and 3 mm. Sub-idioblastic microcline (approx. 8 %), 2 by 3 mm. is slightly sericitized. Plagioclase ( $< 1$  %) is subordinate and strongly sericitized (approx. 11 %), muscovite (approx. 12 %) laths 0.5 to 1 mm. occasionally exhibit some alteration to prehnite (?) along cleavages, whereas the biotite (approx. 5 %) is partially or completely altered to chlorite. Xenoblastic pumpellyite (?) and magnetite make up about 1 % of the rock.

The muscovite concentrate was  $> 99$  %.



SN-20 Lat. 58°57'52"N Long. 9°37'33"E

A medium-grained well-foliated biotite schist. The biotite (approx. 58 %) is unaltered, idioblastic and between 1 and 3 mm. in diameter. Xenoblastic quartz (approx. 20 %) and An<sub>30</sub> plagioclase (approx. 12 %) are finer grained and interstitial. Magnetite (approx. 9 %) and apatite (1 %) together make up the remainder of the rock.

The biotite concentrate was 98 %, containing plagioclase and magnetite impurities.

SN-10 Lat. 58°57'54"N Long. 9°28'27"E

A medium-grained massive amphibolite occurring as boudins within granitic gneisses. Primary, sub-idioblastic to xenoblastic hypersthene (approx. 14 %) is largely altered to 1 to 2 mm. hornblende (approx. 36 %), but a relict igneous texture is preserved. An<sub>32</sub> plagioclase (approx. 41 %) shows minor sericitization and has a cloudy appearance due to very fine magnetite inclusions. The remainder of the rock is composed of magnetite (approx. 7 %), and apatite, quartz, chlorite and unaltered biotite together making up 3 % of the rock. This rock was probably emplaced synkinematically as a norite and incompletely amphibolitized.

The biotite concentrate was 99 %, containing quartz as impurity. The hornblende concentrate was 98 %, containing plagioclase and quartz.

SN-11 Lat. 58°57'4"N Long. 9°28'27"E

A garnetiferous granodiorite gneiss containing almandine porphyroblasts 1 cm. in diameter sporadically distributed throughout the rock. An<sub>30-32</sub> plagioclase (approx. 41 %) is sericitized and sub-idioblastic in form. Sericite is approximately 14 modal per cent. Biotite grains (approx. 3 %), with frayed margins, show partial and occasionally complete alteration to prochlorite (< 1 %). Xenoblastic quartz (approx. 41 %) is 2 to 6 mm. and minor amounts of unaltered muscovite (< 1 %) are also present.

The biotite concentrate was > 98 %, with chlorite impurity.

SN-73 Lat. 58°41'24"N Long. 9°12'52"E

Medium-grained amphibolite occurring in a sequence of augen gneisses. The hornblende (approx. 51 %) is lepidoblastic and 0.5 to 1 mm. in length. The An<sub>32</sub> plagioclase (approx. 35 %) is slightly sericitized and biotite (approx. 10 %) occurs as unaltered 0.5 to 1 mm. grains. Minor amounts of magnetite (approx. 2 %) and quartz (approx. 2 %) are present.

The biotite concentrate was 99 %, containing quartz impurity. The hornblende concentrate was 98 %, containing plagioclase and quartz.

SN-79 Lat. 58°33'44"N Long. 9°35'33"E

Stretched quartz pebble metaconglomerate. Pebbles are stretched in 'b', commonly exceed 10 cms. in length, and are composed of xenoblastic, 3 to 5 mm. quartz and 3 to 4 mm. muscovite. The matrix is finer grained, and composed of unaltered 2 to 3 mm. idioblastic muscovite, xenoblastic quartz and fibrous sillimanite. Small amounts of biotite are present but are strongly chloritized.

The muscovite concentrate was 98 %, with 1 % biotite and 1 % quartz impurities.

SN-56 Lat. 58°49'45"N Long. 9°16'43"E

A coarse-grained biotite quartzite within a sequence of granitic gneisses. Quartz (approx. 92 %) is xenoblastic and up to 8 mm. Biotite (approx. 6 %) forms 2 or 3 mm. serrated plates, occasionally marginally altered to chlorite. Small amounts of muscovite (approx. 1 %) and plagioclase (1 %) are present.

The biotite concentrate was 99 %, with chlorite impurity.

SN-75 Lat. 58°40'0"N Long. 9°11'16"E

K-feldspar augen gneiss. K-feldspar microperthite augen (approx. 15 %) are up to 8

mm. The  $An_{22-24}$  plagioclase (approx. 42 %) in the finer groundmass shows some alteration to sericite and occasionally micrographic intergrowth with quartz. Quartz (approx. 19 %) is xenoblastic and interstitial. Hornblende (approx. 9 %) and biotite (approx. 13 %) are unaltered and between 1 and 2 mm. Apatite, magnetite and sphene make up approximately 2 % of the rock.

The biotite concentrate was 99 % and contained hornblende impurity.

SN-74 Lat.  $58^{\circ}41'24''N$  Long.  $9^{\circ}12'52''E$

K-feldspar augen gneiss, same locality as SN-73. K-feldspar microperthite augen are approximately 5 mm. by 1 cm. Microcline in the finer grained groundmass is 1 to 2 mm. and the  $An_{30-32}$  plagioclase (approx. 27 %) shows some alteration to sericite. K-feldspar is 23 modal % in toto. Quartz (approx. 32 %) is xenoblastic and up to 8 mm. Biotite (approx. 7 %) and hornblende (approx. 9 %) are unaltered and 1 to 2 mm. in diameter. Accessory apatite, magnetite and sphene make up the remaining 2 % of the rock.

The biotite concentrate was 99 % and contains quartz impurity. The hornblende concentrate is  $> 98$  % and contained magnetite and  $< 1$  % biotite impurities.

SN-78 Lat.  $58^{\circ}53'40''N$  Long.  $9^{\circ}45'33''E$

Sillimanite-biotite quartzite with well-preserved cross-bedding structures. Quartz (approx. 71 %) is xenoblastic and 1 to 1.5 mm. Biotite (approx. 19 %) varies from 0.5 to 1 mm. and shows minor alteration to prehnite and chlorite along cleavages. Plagioclase (approx. 4 %) is almost completely sericitized. Muscovite (approx. 3 %) is unaltered and 0.5 to 1 mm. in diameter, and sillimanite (approx. 2 %) occurs sporadically as radiating fibrous masses. Rutile ( $< 1$  %) is concentrated along cross-bedding structures.

The biotite concentrate was  $> 99$  %.

SN-6 Lat.  $58^{\circ}56'42''N$  Long.  $9^{\circ}40'8''E$

A medium-grained biotite granite gneiss. The rock is well-foliated consisting of sub-idioblastic, 1 mm. K-feldspar microperthite (approx. 19 %) xenoblastic 0.5 to 1 mm quartz (approx. 66 %) and unaltered 1 to 1.5 mm. biotite plates (approx. 13 %). Plagioclase ( $An_{30}$ ) is present in minor amounts (approx. 1 %). Hornblende, epidote and magnetite together make up about 1 % of the rock.

The biotite concentrate was  $> 99$  % and contained quartz impurity.

SN-68 Lat.  $58^{\circ}57'56''N$  Long.  $9^{\circ}18'36''E$

A well-foliated garnet-mica schist. Garnet porphyroblasts (approx. 3 %) are 3 mm. in diameter and contain numerous quartz and biotite inclusions. There is development of chlorite along cracks in the garnet. Sub-idioblastic microcline (approx. 15 %) and  $An_{30-32}$  plagioclase (approx. 29 %) vary between 1 and 1.5 mm., the plagioclase showing minor sericite alteration. Biotite (approx. 10 %) is unaltered and forms 1 to 1.5 mm. plates. Quartz (approx. 42 %) is 1 mm., xenoblastic and exhibits undulose extinction resulting from cataclasis. Sillimanite and rutile together make up approximately 1 % of the rock.

The biotite concentrate was  $> 97$  % with quartz and garnet impurities.

SN-3 Lat.  $58^{\circ}58'2''N$  Long.  $9^{\circ}33'28''E$

A garnet-biotite schist. The rock is well-foliated containing almandine porphyroblasts (approx. 2 %) up to 3 mm. with numerous quartz and magnetite inclusions.  $An_{30}$  plagioclase (approx. 34 %) is sub-idioblastic, 1 to 1.5 mm., with some alteration to sericite (approx. 2 %) along the cleavages. Quartz (approx. 36 %) is xenoblastic and varies between 0.5 to 1 mm. Biotite (approx. 8 %) is idioblastic and is altered to peninite along the cleavages in some instances. Occasionally biotite is completely replaced

by penninite (approx. 13 %) and magnetite (< 1 % total). Carbonate is present in small veinlets (approx. 5 %).

The biotite concentrate was > 97 % with chlorite impurity.

SN-16 Lat. 58°56'25"N Long. 9°33'28"E

A medium-grained hornblende-biotite schist. A well-foliated rock containing 1 to 2 mm. lepidoblastic hornblende (approx. 37 %) and unaltered 1 to 2 mm. biotite plates (approx. 20 %). Quartz (approx. 19 %) is xenoblastic and the plagioclase (approx. 22 %) is partially sericitized and in the range An 30 to 32. Magnetite and graphite together make up approximately 2 % of the rock.

The biotite concentrate was 99 % containing plagioclase impurity. The hornblende concentrate was > 98 % containing quartz and biotite impurities.

SN-40 Lat. 58°51'59"N Long. 9°11'44"E

A coarse-grained granite gneiss showing good foliation in hand-specimen. Quartz is xenoblastic, between 6 mm. and 1 cm. and commonly shows strained extinction. Microcline microperthite is the dominant feldspar, xenoblastic to subidioblastic and between 3 and 6 mm.; minor amounts of plagioclase are strongly sericitized. Biotite occurs as corroded subidioblastic grains, varying between 1/2 and 1 mm., with some alteration to chlorite and prehnite.

The biotite concentrate was 99 % with quartz impurity.

SN-54 Lat. 58°53'43"N Long. 9°15'46"E

Coarse-grained biotite granodiorite gneiss. The An<sub>27</sub> plagioclase (approx. 59 %) is xenoblastic and up to 8 mm. Quartz is xenoblastic (approx. 37 %) and forms irregular masses up to 1 cm. Biotite plates (approx. 4 %) have serrated margins and show some minor chlorite alteration.

The biotite concentrate was 98 % containing quartz impurity.

SN-44 Lat. 58°54'35"N Long. 9°23'39"E

A medium-grained moderately well-foliated granite gneiss. Xenoblastic to subidioblastic. An 15 plagioclase (approx. 34 %) forms grains 3 mm. in diameter and is partially sericitized (sericite approx. 3 %). Microcline (approx. 5 %) is xenoblastic, unaltered and forms 1–2 mm. diameter grains. Quartz (approx. 49 %) is xenoblastic and varies between 1 and 3 mm. Quartz commonly shows strained extinction. Biotite (approx. 7 %) varies from 0.5 to 1 mm., has serrated margins and shows minor chlorite (< 1 %) alteration. Allanite and apatite make up approximately 2 % of the rock.

The biotite concentrate was > 97 % pure with 2 % chlorite and traces of K-feldspar impurities.

SN-76 Lat. 58°46'20"N Long. 8°51'55"E

A coarse-grained K-feldspar augen gneiss. K-feldspar microperthite augen are up to 2 cm. in diameter. Microcline in the groundmass is subidioblastic, 0.5 to 1 mm., with sericite alteration. Quartz is 0.5 to 1 mm. and frequently exhibits undulose extinction. The small amount of plagioclase is almost completely altered to sericite. Biotite occurs in clusters and is between 0.5 to 1 mm. Marginal alteration of the biotite to chlorite is common. Accessory amounts of apatite, garnet and magnetite are present.

The biotite concentrate was 97 % with 2 % chlorite and 1 % quartz impurities.

SN-2 Lat. 58°58'2"N Long. 9°33'28"E

A medium-grained amphibolite. Subidioblastic to xenoblastic An<sub>28</sub> plagioclase (approx. 23 %) is subidioblastic to xenoblastic with slight sericite alteration. Hornblende (approx. 63 %) occurs as subidioblastic to idioblastic, inclusion-free grains between 1



and 2 mm. diameter. Biotite (approx. 1 %) forms approximately 0.5 mm. crystals. Quartz (approx. 8 %) is xenoblastic and 0.5 to 1 mm. diameter. Magnetite (approx. 4 %) and apatite (approx. 1 %) and epidote ( $< 1$  %) are present.

The hornblende concentrate was 98 % with plagioclase and epidote impurities.

SN-9 Lat.  $58^{\circ}56'19''\text{N}$  Long.  $9^{\circ}29'28''\text{E}$

A medium-grained amphibolite occurring as discontinuous bands in a series of granitic gneisses. Hornblende (approx. 62 %) occurs as 2 to 3 mm. unaltered lepidoblastic grains. An 30-35 plagioclase (approx. 28 %) is subidioblastic and in part altered to sericite. Minor quartz (approx. 5 %), magnetite (approx. 4 %), and apatite (approx. 1 %) are present.

The hornblende concentrate was  $> 98$  % with magnetite and quartz impurities.

SN-22 Lat.  $58^{\circ}56'43''\text{N}$  Long.  $9^{\circ}37'42''\text{E}$

A medium-grained amphibolite. Lepidoblastic hornblende (approx. 68 %) is up to 5 mm. Plagioclase (approx. 25 %) is sub-idioblastic to xenoblastic and strongly sericitized. Minor amounts of 0.5 to 1 mm. biotite (approx. 1 %), apatite (1 %), quartz (approx. 2 %) and magnetite (approx. 3 %) are present.

The hornblende concentrate was 97 % with magnetite and plagioclase impurities.

SN-45 Lat.  $58^{\circ}54'35''\text{N}$  Long.  $9^{\circ}23'38''\text{E}$

A medium-grained amphibolite. This rock possesses a poor foliation and contains unaltered lepidoblastic hornblende (approx. 70 %), sub-idioblastic An<sub>30</sub> plagioclase (approx. 27 %), and 2 mm. biotite plates (approx. 2 %) with serrated margins. Quartz, magnetite and apatite together make up about 2 % of the rock.

The hornblende concentrate was  $> 99$  % containing biotite impurity.

SN-38 Lat.  $58^{\circ}52'12''\text{N}$  Long.  $9^{\circ}21'37''\text{E}$

A medium-grained, poorly foliated amphibolite. The rock consists of 1 to 2 mm. lepidoblastic hornblende (approx. 55 %) and 1 to 2 mm. subidioblastic An<sub>33</sub> plagioclase (approx. 40 %) together with minor amounts of xenoblastic quartz (approx. 2 %) and biotite (approx. 1 %). Sphene, apatite, ilmenite and epidote make up approximately 2 % of the rock.

The hornblende concentrate was 98 % with epidote and plagioclase impurities.

SN-70 Lat.  $58^{\circ}41'18''\text{N}$  Long.  $9^{\circ}9'18''\text{E}$

A medium-grained hornblende-plagioclase gneiss. Lepidoblastic hornblende (approx. 39 %) is unaltered and up to 3 mm. An<sub>30</sub>, sub-idioblastic plagioclase (approx. 44 %), between 1 and 2 mm., is partially altered to sericite. Xenoblastic quartz (approx. 8 %) varies between 0.5 and 1.5 mm. Relicts of augite (approx. 1 %) are enclosed by hornblende. Minor amounts of biotite (approx. 2 %) and apatite (approx. 1 %) and magnetite (approx. 3 %) and sphene ( $< 1$  %) and epidote ( $< 1$  %) are present.

The hornblende concentrate was 98 % with epidote impurity.

SN-71 Lat.  $58^{\circ}41'18''\text{N}$  Long.  $9^{\circ}9'18''\text{E}$

A medium-grained metagabbro occurring as conformable bands in a predominantly metasedimentary sequence. Relict augite (approx. 33 %) shows incipient alteration to chlorite along the cleavages and is partly converted to sub-idioblastic hornblende (approx. 22 %). A palimpsest igneous texture persists. An<sub>32</sub> plagioclase is anhedral (approx. 35 %) and interstitial. Minor amounts of quartz (approx. 4 %), magnetite (approx. 5 %), and apatite are present. The rock is an incompletely amphibolitized pre- or synkinematic gabbro.

The hornblende concentrate was  $> 98$  % containing 1 % epidote and a trace of biotite as impurities.

SN-57 Lat. 58°49'55"N Long. 9°22'42"E

A poorly, foliated, igneous textured, gneissic granite. Subhedral K-feldspar microperthite (approx. 40 %) up to 4 mm. in diameter coexists with 3 to 4 mm. sericitized albite (approx. 17 %). Biotite plates (approx. 5 %) have serrated margins and abundant zircon inclusions. Quartz (approx. 36 %) is anhedral and up to 4 mm. Anhedral amphibole (approx. 19 %) is compositionally near ferrohastingsite. Monazite and apatite together make up 1 % of the rock.

The biotite concentrate contained 1 % of chlorite, 1 % of apatite, and 1 % of plagioclase.

SN-61 Lat. 58°48'13"N Long. 9°23'42"E

Porphyroblastic granite gneiss. A poorly foliated rock consisting of Ans-10 plagioclase (approx. 48 %) as 5 mm. porphyroblasts in altered to sericite, together with sub-idioblastic to xenoblastic 1 to 3 mm. microcline (approx. 7 %). Quartz (approx. 29 %) is xenoblastic. Hornblende (approx. 5 %) and biotite (approx. 10 %) are unaltered and between 1 and 3 mm. in size. The hornblende contains some magnetite inclusions. Accessory apatite, monazite, orthite and zircon comprise about 1 % of the rock.

The biotite concentrate was 99 % with feldspar impurity. The hornblende concentrate was 99 % with feldspar and monazite (?) impurities.

SN-59 Lat. 58°47'33"N Long. 9°22'58"E

A poorly foliated granite gneiss. K-feldspar microperthite (approx. 23 %) varies from 2 to 3 mm. Oligoclase (approx. 31 %) varies from 1 to 2 mm. and occasionally forms a micrographic intergrowth with quartz. Quartz (approx. 36 %) is xenoblastic and 3 to 4 mm. in diameter. Biotite (approx. 8 %) forms 1 to 2 mm. plates frequently with frayed margins. Sphene, magnetite and apatite together comprise 2 % of the rock.

The biotite concentrate was 99 % with traces of quartz and feldspar.

SN-26 Lat. 58°57'40"N Long. 9°33'43"E

Medium-grained Ödegaardite (Brögger 1934, 1935). A medium-grained metagabbro containing hornblende (approx. 42 %) approaching pargasite in composition and between 1 and 4 mm. Original plagioclase has been completely altered to scapolite (approx. 54 %). Occasional patchy pyroxene relicts (approx. 2 %) are seen in some of the hornblendes. Sphene (approx. 1 %) is idioblastic. Rutile and apatite comprise approximately 2 % of the rock. The conversion of plagioclase to scapolite appears to be later than that of augite to hornblende.

The hornblende concentrate was 98 %, containing scapolite and pyroxene impurities.

SN-89 Lat. 58°57'40"N Long. 9°33'43"E

Massive hornblende occurring as veins cutting Ödegårdite in the 'Road Metal Quarry' adjacent to the Ödegården Apatit Gruber. Probably related to the formation of the apatite deposits.

The hornblende concentrate was > 99 %.

SN-30 Lat. 58°57'40"N Long. 9°33'43"E

Phlogopite occurring as an outer zone to the chlorapatite in a productive vein at Ödegården Apatit Gruber.

The phlogopite concentrate was > 99 %.

SN-27 Lat. 58°57'40"N Long. 9°33'43"E

Wall-rock to the productive vein at Ödegården Apatit Gruber (sandrock of the miners). The rock is friable and is composed of patches of talc (approx. 18 %) pseudomorphous after enstatite. A few relict patches of enstatite (approx. 5 %) remain en-

closed by talc. An 20-25 plagioclase (approx. 56 %) is commonly sericitized and may be converted to sapolite (approx. 8 %). Phlogopite (approx. 5 %) occurs as unaltered plates 1 to 3 mm. in length. Euhedral apatite is abundant (approx. 6 %), and some ilmenite is present (approx. 2 %).

The phlogopite concentrate was 95 % containing scapolite impurity.

SN-35 Lat. 58°56'26"N Long. 9°25'40"E

Coarse-grained metapyroxenite. Initial euhedral cumulate hypersthene (average 3 cms.) in part replaced by hornblende. Hornblende (approx. 43 %) is 1 to 2 mm. and forms a patchy intergrowth with hypersthene (approx. 34 %). Phlogopite (approx. 23 %) is also secondary and forms unaltered 1 to 3 mm. laths. Minor magnetite (1 %) is present. A cumulate texture is preserved. Field relations suggest that this rock is part of a late-kinematic differentiated gabbro body.

The phlogopite concentrate was 99 %, with hornblende impurity. The hornblende concentrate was 95 % with hypersthene impurity.

SN-43 Lat. 59°54'35"N Long. 9°23'39"E

A concordant pegmatite body in granitic gneiss. Contains plagioclase and K-feldspar perthite up to 10 cms. in diameter, and quartz. Biotite varies from 1 to 2 cms. in diameter.

The biotite concentrate was taken from 2 cm. books and was 99 % pure.

SN-84 Lat. 59°1'22"N Long. 9°32'55"E

Discordant K-feldspar pegmatite body. The muscovite concentrate was taken from 10 cms. books and was > 99 % pure.

SN-85 Lat. 58°56'38"N Long. 9°25'16"E

Concordant pegmatite body (Bjordammen) containing quartz, oligoclase (var. aventurine) and biotite.

The biotite concentrate was taken from 1 cm. books and was > 99 % pure.

SN-42 Lat. 58°54'0"N Long. 9°23'6"E

A concordant pegmatite body occurring within a sequence of amphibolites and granitic gneisses. Contains quartz, andesine and biotite (1 cm.).

The biotite concentrate was > 99 % pure.

SN-86 Lat. 58°56'10"N Long. 9°28'20"E

A coarse-grained cordierite-anthophyllite rock occurring in association with amphibolites. Consists of cordierite, anthophyllite (gedrite), quartz biotite and rutile. The biotite varies from 1 to 1.5 cms. in diameter.

The biotite concentrate was > 99 % pure.

SN-12 Lat. 58°57'4"N Long. 9°28'27"E

Small concordant pegmatite occurring within a sequence of amphibolites and granitic gneisses (see SN-10 above). Consists of quartz, andesine and biotite (up to 2 cms.).

The biotite concentrate from 2 cm. books was > 99 % pure.

SN-81 Lat. 58°59'6"N Long. 9°21'55"E

Discordant pegmatite containing K-feldspar, quartz biotite (books in excess of 20 cms.). Metamict minerals such as orthite and Fergusonite are present.

The biotite concentrate was > 99 % pure.

SN-87 Lat. 58°58'26"N Long. 9°32'58"E

A discordant pegmatite containing quartz, K-feldspar and biotite (2 cm. books).

The biotite concentrate was > 99 % pure.



## REFERENCES

- ARMSTRONG, R. L. 1966: K-Ar dating of plutonic and volcanic rocks in orogenic belts. In SCHAEFFER, O. A. & ZÄHRINGER, J. (Eds.) *Potassium-Argon Dating*. Springer, Berlin-Heidelberg-Göttingen.
- ARMSTRONG, R. L. & HILLS, F. A. 1967: Rb-Sr and K-Ar geochronologic studies of mantled gneis domes, Albion Range, Southern Idaho, U.S.A. *Earth & Planetary Science Letters*, 3, 114-124.
- BAADSGAARD, H. 1965: Geochronology. *Meddel. fra Dansk Geol. For.* 16, No. 1, 48 pp.
- BAADSGAARD, H. & GODFREY, J. D. 1967: Geochronology of the Canadian Shield in North-eastern Alberta. I. Andrew Lake Area, *Can. J. Earth Sci.* 4, 541-563.
- BARTH, T. F. W. & DONS, J. A. 1960: Precambrian of Southern Norway. In HOLTEDAHN, O. (Ed.) *Geology of Norway (Norges Geol. Undersök.* 208), 6-67.
- BARTH, T. F. W. & REITAN, D. H. 1963: The Precambrian of Norway. In RANKAMA, K. (Ed.) *The Precambrian, Vol. I*. Interscience, New York-London-Sydney.
- BROCH, O. A. 1964: Age determinations of Norwegian minerals up to March, 1964. *Norges Geol. Undersök.* 228, 84-113.
- BRÖGGER, W. C. 1934: On several Archäan rocks from the south coast of Norway. I. Nodular granites from the environs of Kragerö. *Skr. Norske Vidensk.-Akad., I Mat.-naturv. Kl.*, 1933, no. 8.
- BRÖGGER, W. C. 1935: On several Archäan rocks from the south coast of Norway. II. The south Norwegian hyperites and their metamorphism. *Skr. Norske Vidensk.-Akad., I. Mat.-naturv. Kl.*, 1934, No. 1.
- BUGGE, A. 1965: Iakttagelser fra rektangelbladet Kragerö og den store grunnfjellsbreksje. *Norges Geol. Undersök.* 229, 115 pp.
- BUGGE, J. A. W. 1943: Geological and petrological investigations in the Kongsberg-Bamble formation. *Norges Geol. Undersök.* 160, 149 pp.
- BURRELL, D. C. 1964: The geology of the country west of Levang peninsula, South Norway. *Unpublished Ph.D. thesis, University of Nottingham*.
- DENISENKO, Y. A. 1965: Determination of the activation energy of argon. *Geochem. Intern.* 2, 74-76.
- FECHTIG, H. & KALBITZER, S. 1966: The diffusion of argon in potassium-bearing solids. In SCHAEFFER, O. A. & ZÄHRINGER, J. (Eds.) *Potassium-Argon Dating*. Springer, Berlin-Heidelberg-Göttingen.
- FOSTER, M. D. 1960: Layer change relations in dioctahedral and trioctahedral micas. *Amer. Miner.* 45, 383-398.
- GERLING, E. K., KOLTSOVA, T. V., PETROV, B. V. & ZULFIRKAROVA, Z. K. 1965: On the suitability of amphiboles for age determination by the K-Ar method. *Geochem. Intern.* 2, 148-154.
- GERLING, E. K., LEVSKII, L. K. & MOROZOVA, I. M. 1963: On the diffusion of radiogenic argon from minerals. *Geochemistry* 6, 551-555.
- GERLING, E. K., MOROZOVA, I. M. & KURBATOV, V. V. 1961: The retentivity of radiogenic argon in ground micas. *Ann. N.Y. Acad. Sci.* 91, 227-234.
- GOLDICH, S. S., NIER, R., BAADSGAARD, H., HOFFMAN, J. H. & KRUEGER, H. W. 1961: *The Precambrian Geology and Geochronology of Minnesota*. Univ. of Minnesota Press, Minneapolis, Minnesota.
- HARPER, C. T. 1967a: The geological interpretation of potassium-argon ages from the Scottish Caledonides. *Scott. Jour. Geol.* 3, 46-66.
- HARPER, C. T. 1967b: On the interpretation of K-Ar ages from Precambrian Shield and Phanerozoic orogens. *Earth Planetary Sci. Letters* 3, 125-132.
- HARPER, C. T. 1968: Isotopic ages from the Appalachians and their tectonic significance. *Canad. Jour. Earth Sci.* 5, 49-60.
- HART, S. R. 1960: Some diffusion measurements relating to the K-Ar dating method. *Mass. Inst. Technol. Prog. Rep.* 8, 161-166.

- HART, S. R. 1961: The use of hornblendes and pyroxenes for K-Ar dating. *Jour. Geophys. Res.* 66, 2995-3001.
- HART, S. R. 1964: The petrology and isotopic mineral age relations of a contact zone in the Front Range, Colorado. *Jour. Geol.* 72, 493-525.
- HURLEY, P. M., HUGHS, H., PINSON, W. H., JR. & FAIRBAIRN, H. W. 1962: Radiogenic argon and strontium diffusion parameter in biotite at low temperatures obtained from Alpine Fault uplift in New Zealand. *Geochim. et Cosmochim. Acta* 26, 67-80.
- JAGER, E. 1962: Rb-Sr age determinations on micas and total rocks from the Alps. *J. Geophys. Res.* 67, 5293-5306.
- KRATZ, K. O., GERLING, E. K. & LOBACH-ZHUCHENKO, S. B. 1968: The isotope geology of the Precambrian of the Baltic Shield. *Canad. J. Earth Sci.* 5, 657-660.
- KULP, J. L. & ECKLEMAN, W. R. 1957: Discordant U-Pb ages and mineral type. *Amer. Miner.* 42, 154-164.
- KULP, J. L. & NEUMANN, H. 1961: Some potassium-argon ages from the Norwegian basement. *Ann. N.Y. Acad. Sci.* 91, 469-475.
- LANPHERE, M. A. & DALRYMPLE, G. B. 1967: K-Ar and Rb-Sr measurements on P-207, the U.S.G.S. interlaboratory standard muscovite. *Geochim. et Cosmochim. Acta* 31, 1091-1093.
- MAGNUSSON, N. H. 1960: Age determinations of Swedish Precambrian rocks. *Geol. Fören. Stockholm Förh.* 82, 407-432.
- MOORBATH, S. 1967: Recent advances in the application and interpretation of radiometric age data. *Earth Sci. Rev.* 3, 111-133.
- MORTON, R. D., BATEY, B. H. & O'NIONS, R. K. 1968: Geological investigations in the Bamble sector of the Fennoscandian Shield, South Norway (*In preparation*).
- NEUMANN, H. 1960: Apparent ages of Norwegian minerals and rocks. *Norsk Geol. Tidsskr.* 40, 173-189.
- O'NIONS, R. K., SMITH, D. G. W., BAADSGAARD, H. & MORTON, R. D. 1968: Influence of chemical composition on the argon retentivity of metamorphic calcic amphiboles from South Norway *Earth & Planetary Science Letters*, *in press*.
- PETTERSSON, M. J. 1964: The geology of the country around Sannidal, South Norway. *Unpublished Ph.D. thesis, University of Nottingham*.
- PINSON, H. W. 1961: The potassium argon method. The problem of potassium analysis. *Ann. N.Y. Acad. Sci.* 91, 221-224.
- POLKANOV, A. A. & GERLING, E. K. 1961: The Precambrian geochronology of the Baltic Shield. *Ann. N.Y. Acad. Sci.* 91, 492-499.
- RÖSLER, H. J. & PILOT, J. 1967: Zur Alterbestimmung hydrothermalen Lagerstätten mit Hilfe der K-Ar Methode. *Fortschr. Mineralogie* 45, 37-51.
- RYAN, M. J. 1966: Geology of the area around Ödegårdens-verk, South Norway. *Unpublished Ph.D. thesis, University of Nottingham*.
- STARMER, I. C. 1967: Geology of the Risør area, South Norway. *Unpublished Ph.D. thesis, University of Nottingham*.
- STEIGER, R. H. 1964: Dating of orogenic phases in the central Alps by K-Ar ages of hornblende. *Jour. Geophys. Res.* 69, 5407-5421.
- SUTTON, J. 1965: Some recent advances in our understanding of the controls of metamorphism. In PITCHER, W. S. & FLINN, G. W. (eds.) *Controls of Metamorphism*. Oliver & Boyd, Edinburgh.
- WESCOTT, M. R. 1966: Loss of argon in biotite in thermal metamorphism. *Nature* 210, 83-84.
- TOURET, J. 1962: Geological studies in the region Vegårshei-Gjerstad. *Norges Geol. Undersök.* 215, 120-139.
- TOURET, J. 1967: Les gneiss ocellés de la région de Vegårshei-Gjerstad (Norvège Méridionale) 1. Etude pétrographique. *Norsk Geol. Tidsskr.* 47, 131-148.
- ZWART, H. J. 1967: The duality of orogenic belts. *Geologie en Mijnbouw* 8, 283-309.

# Instructions to Authors

Manuscripts should be sent to the Editor. The author's permanent and temporary addresses must be given. Accepted manuscripts will not be returned until printed, and the author is requested to retain a complete copy of the manuscript. Authors will receive one set of proofs which should be read carefully and returned promptly to Universitetsforlaget. The author will be charged for changes against the manuscript made by him in the proof. Fifty reprints are sent free of charge to an author. In cases of multiple authorship, 75 reprints are sent to the team. Reprints in addition to those supplied free should be ordered when the first proofs are returned to Universitetsforlaget.

## MANUSCRIPT

The manuscript must be typewritten (carbon copy not acceptable) on one side of standard-sized paper, double spaced, with an ample margin. The text must be clear and concise, and written preferably in English; however, Norwegian, Danish, Swedish, French, or German may be used. Manuscripts should be arranged in the following order: (1) Informative but brief title. (2) Author's name. (3) A short abstract, always in English, starting with a repetition of 2 and 1 and a translation in parentheses of non-English titles. (4) The main text. Use three or fewer grades of headings. Instead of footnotes, insert paragraphs which can be composed in smaller type or use parentheses. Indicate in the left-hand margin the places for the insertion of Figures and Tables. All halftones will be printed at their proper place in the text. The words 'Fig.' ('Figs.') and 'Table' (unabbreviated) are to be capitalized. (5) List of references conforming with the examples given below. Abbreviations used should be consistent: necessary editorial changes will be made according to the *Suggestions to Authors of the Reports of the United States Geological Survey* (5th ed., 1958). (6) The author's professional postal address and a dating of the manuscript. (7) Figure captions on a separate sheet. Add an English caption below captions in other languages. (8) Tables, if any, with captions, numbered with arabic numerals.

## ILLUSTRATIONS

Illustrations should be reducible to a maximum size of  $11.8 \times 19.8$  cm or less. If not adjustable to the entire width of the type area, 11.8 cm, they must be considerably narrower. Line drawings (maps, sections, etc.) may occasionally be allowed to extend into the inner margin of the page by an additional 2.7 cm. Drawings are to be in black Indian ink. Letters should not be smaller than 1 mm after reduction for reproduction. Photographs should be clear, sharply contrasted, and printed on white paper with glossy finish. Figures may be composed of several units (designated A, B, C, etc.) and mounted in such a way that each unit after reduction is separated by a space at least 1 mm broad. All units should be similar in tone. Illustrations should generally be termed Figures (not Plates) even if occasionally covering an entire page. All Figures should be marked with the author's name and the Figure number. Do not attach captions to the Figures. When not obvious, the top and bottom of Figures, and their scale, should be indicated.

## REFERENCES

- BARTH, T. F. W. 1962: *Theoretical Petrology*, 2nd ed., 416 pp. John Wiley & Sons, Inc., New York.
- BJØRLYKKE, H. & SVINNDAL, S. 1960. The carbonatite and per-alkaline rocks of the Fen area. Mining and exploration work. In HOLTEDAHN, O. (ed.) *Geology of Norway, Norges Geol. Unders.* 208, 105–110. Oslo.
- ESKOLA, P. 1920: Mineral facies of rocks. *Norsk Geol. Tidsskr.* 6, 143–194. Kristiania [Oslo].
- STØRMER, L. 1944: On the relationship and phylogeny of fossil and recent Arachnomorpha. *Skr. Norske Vidensk.-Akad. i Oslo, Mat.-naturv. Kl.*, 1944 no. 5, 158 pp. Oslo.



# Norsk Geologisk Tidsskrift

VOLUME 49 NUMBER 2



## INNHold — CONTENTS

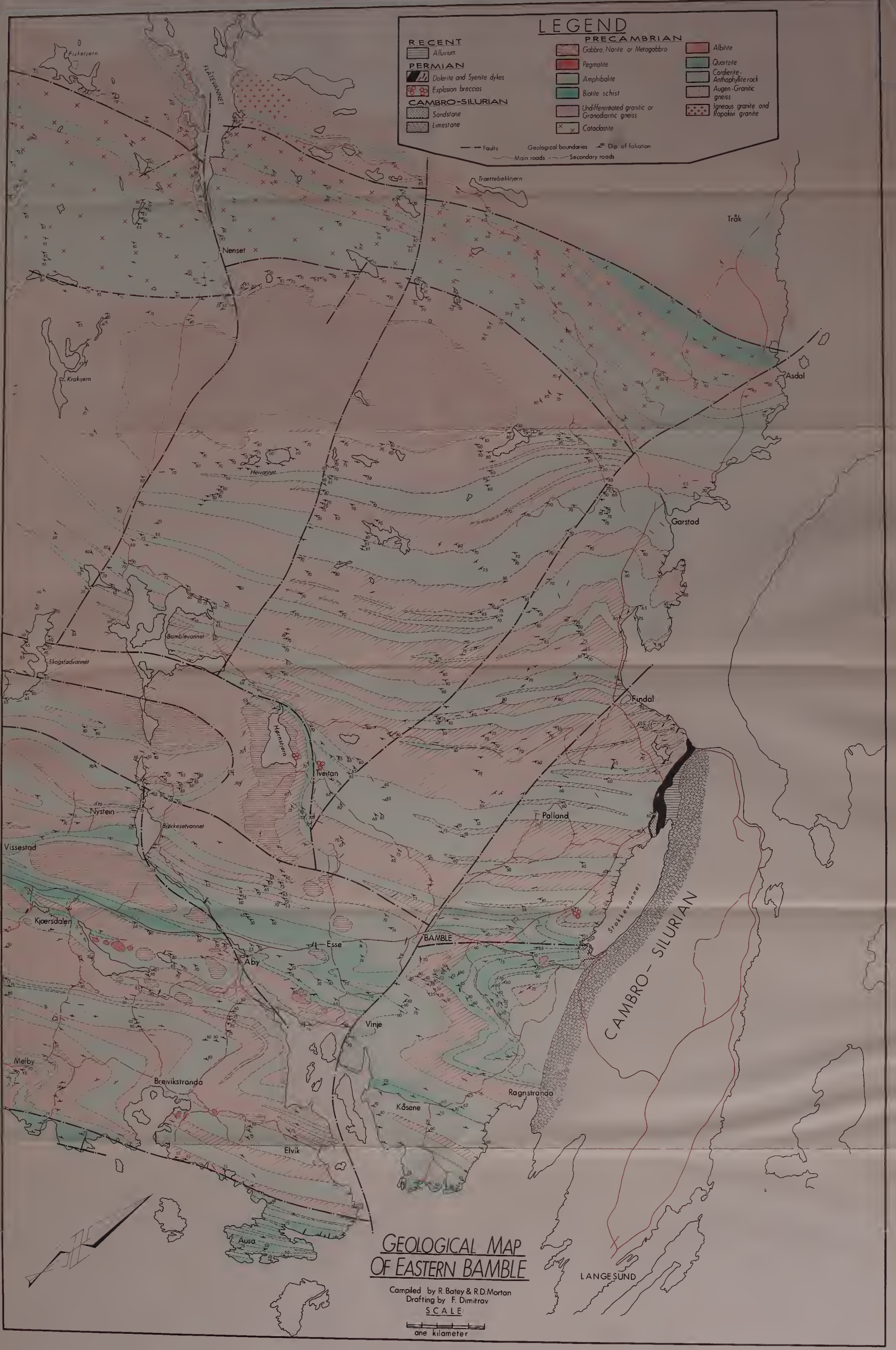
### AVHANDLINGER — PAPERS

Müller, G. & Wurm, F.: <i>Die Gesteine der Inselgruppe Randøy — Fogn. Beiträge zur Metamorphose und zum Aufbau der Kambrosilurischen Gesteine des Stavanger-Gebietes I</i> ..	97
Dons, J. A.: <i>Interrupted creation of nepheline syenite pegmatite dikes in the Langesundsfjord Area, S. Norway</i> ..	145
Hasan, Zia-Ul: <i>Petrology of the soda-minette dikes from Håöya, Langesundsfjord, S. Norway</i> .. .. .	159
O'Nions, R. K., Morton, R. D. & Baadsgarad, H.: <i>Potassium-argon ages from the Bamble sector of the Fennoscandian shield in South Norway</i> .. .. .	171
GÆA NORVEGICA .. .. .	191

Issued June 1969









**B29933**